NUMERICAL SIMULATIONS OF FLUID-STRUCTURE INTERACTION IN BIOLOGICAL AIRWAYS VALIDATED WITH *EX-VIVO* LUNGS

A Thesis
Presented in Partial Fulfilment of the Requirements for the
Degree of Master of Science
with a
Major in Mechanical Engineering
in the
College of Graduate Studies
University of Idaho

By
Sally M. Mei

Major Professor: Tao Xing, Ph.D.
Committee Members: Gordon Murdoch, Ph.D., Gabriel Potirniche, Ph.D.
Department Administrator: Steven Beyerlein, Ph.D.

December 2018

AUTHORIZATION TO SUBMIT THESIS

The thesis of Sally M. Mei, submitted for the degree of Master of Science with a major in Mechanical Engineering and titled “NUMERICAL SIMULATIONS OF FLUID-STRUCTURE INTERACTION IN BIOLOGICAL AIRWAYS VALIDATED WITH *EX-VIVO* LUNGS,” has been reviewed in final form. Permission, as indicated by the signatures and dates below, is now granted to submit final copies to the College of Graduate Studies for approval.

Major Professor:	______________________________ Tao Xing, Ph.D.	Date: ____________
Committee Members:	______________________________ Gordon Murdoch, Ph.D.	Date: ____________
	______________________________ Gabriel Potirniche, Ph.D.	Date: ____________
Department Administrator:	______________________________ Steven Beyerlein, Ph.D.	Date: ____________

ABSTRACT

Understanding fluid and structure interactions in biological airways is essential for explaining the physics of gas exchange that governs air flow in human and animal lungs. However, a limited number of studies are available due to the challenges of modeling and lack of experimental data. This study bridges the knowledge gap through Fluid-Structure Interaction (FSI) simulations combined with mechanical tissue testing. FSI is a coupling between two classic simulation methods: Computational Fluid Dynamics (CFD) and Finite Element Analysis (FEA). FSI is especially popular among researchers performing biomedical and biomechanical studies, due to the complex, dynamic geometries. In the case of human lungs, the geometry of respiratory tract is extremely complex. To accurately model the behavior of the lower respiratory tract, smaller portions of the respiratory system: the trachea and two generations of connecting bronchi (part of the upper airway) were specially chosen for this research. Couple case studies have been used to prove the validity of the human lung FSI simulation results. The case studies included a quasi-2D “square balloon” FSI simulation and a 3D balloon FSI simulation. In addition, tensile tests were conducted to obtain material properties of porcine tissue for the lung FSI simulation. Material properties were determined with curve fitting of porcine tissue in axial and circumferential directions to further enhance the accuracy of the human lung FSI model. Conclusions from each case study, experimental testing, and human lung FSI are provided and serve to advance the interdisciplinary study of respiration kinetics.

ACKNOWLEDGEMENTS

First and for most, I would like to acknowledge my major professor, Dr. Tao Xing, and my committee members, Dr. Gabriel Potirniche and Dr. Gordon Murdoch for their support and mentorship throughout my Master's degree. Each provided guidance and knowledge in their field of study; which allowed me to learn, grow, and expand my knowledge over the course of my degree. My degree would not have been possible without their wealth of knowledge and patience.

Next, I would like to acknowledge Dr. Nathan Schiele and Sophia Theodossiou, in the department of Biological Engineering at the university, for their support and expertise in biological material testing. Dr. Rabijit Dutta, post-doctoral researcher, for his technical expertise in performing experiments with ventilators and CFD knowledge.

I would also like to thank all the faculty and staff members in the Mechanical Engineering department at the university. Without their day to day support, my degree would have been challenging to achieve. For the staff that helped me with my paperwork and computer issue; and to all the faculty members simply asks how things are going or tells "When I was your age I only had…" stories have all supported me in more ways than one.

Then I would like to acknowledge all my friends, colleagues, and family that have helped and supported me throughout my degree. I would like to especially thank Alex Olson and Ahmad Abdel-Azim. Alex has help me with more things than I can count. From debugging code, providing industry experience and insights, to being the go-to person to bounce ideas off of and provide sanity checks. Ahmad for his help and expertise in CFD programs which have saved me many times throughout my degree.

Lastly, I would like to acknowledge Pullman Regional Hospital for providing an anonymous CT scan of a patient to generate the lung geometry for the upper airway simulation and Percussionaire Corporation for providing me with necessary resources to complete my research.

DEDICATION

I would like to dedicate this work to the Mei family. Without the support and cultivation from my family, I would never have become the person I am today. I am truly grateful to have a family that encourages me to always do my best, supports my decisions, and most importantly, inspires me to learn and apply the knowledge to better myself and others.

TABLE OF CONTENTS

AUTHORIZATION TO SUBMIT THESIS ii

ABSTRACT iii

ACKNOWLEDGEMENTS iv

DEDICATION v

TABLE OF CONTENTS vi

LIST OF FIGURES x

LIST OF TABLES xv

NOMENCLATURE xvii

Chapter 1: LITERATURE REVIEW 1

- 1.1 Introduction 1
- 1.2 Background 2
  - 1.2.1 Respiratory System 2
  - 1.2.2 Fluid Structure Interaction 3
- 1.3 Geometry for Simulations 4
- 1.4 Fluid-Structure Interaction Simulations 5
- 1.5 Material Testing 5
- 1.6 Limitations 6
- 1.7 Conclusion 6

Chapter 2: THE QUANDARY OF COMPRESSIBILITY 8

- 2.1 Incompressibility, Compressibility, and Artificial Compressibility 8
- 2.2 2D Square Balloon Geometry 8
- 2.3 Methods 9
  - 2.3.1 Mesh 10
  - 2.3.2 Boundary Conditions 12

2.3.3 Material Properties 16
2.3.4 Convergence Settings 17
2.4 Results 20
2.4.1 Pressure Comparison 20
2.4.2 Ideal Gas Law 21
2.4.3 Pressure Contour Comparison 24
2.4.4 Velocity Magnitude Contour Comparison 27
2.4.5 Velocity Vector and Structural Deformation Contour 31
2.4.6 Solution Verification 33
2.5 Conclusion 36
Chapter 3: THREE-DIMENSIONAL BALLOON EXPANSION 37
3.1 Three-Dimensional Balloon Motivation 37
3.2 3D Balloon Geometry 38
3.3 3D Balloon Methods 38
3.3.1 Mesh 39
3.3.2 Boundary Conditions 41
3.3.3 Material Properties 45
3.3.4 Convergence Settings 46
3.4 Results 48
3.4.1 3D Balloon – Structural Region 48
3.4.2 3D Balloon – Fluid Region 56
3.5 Conclusion 66
Chapter 4: PORCINE TRACHEAL MATERIAL PROPERTIES 67
4.1 Porcine Material Property Characterization 67
4.2 Phase 1: Lab Experiments – Uniaxial Tensile Testing of Porcine Trachea 68

4.2.1 Specimen Sample Preparation 69

4.2.2 Uniaxial Tensile Testing – Post Processing and Results 72

4.3 Phase 2: Curve Fitting – Hyperelastic Material Model 82

4.3.1 Ogden Material Model 83

4.3.2 MATLAB Curve Fitting Toolbox 84

4.4 Phase 3: Single Element Model 88

4.4.1 Geometry, Mesh, Boundary Conditions, and Material 88

4.5 Conclusion 91

Chapter 5: FSI HUMAN UPPER AIRWAY SIMULATION 92

5.1 Human Airways 92

5.2 Lung Geometry 93

5.3 Lung FSI Methods 95

5.3.1 Mesh 95

5.3.2 Boundary Conditions 98

5.3.3 Material Properties 101

5.3.4 Convergence Settings 101

5.4 Results 103

5.4.1 Human Lung Model – Structural Region 103

5.4.2 Human Lung Model – Fluid Region 121

5.5 Conclusion 132

Chapter 6: CONCLUSIONS AND FUTURE RESEARCH 134

6.1 Summary and Conclusions 134

6.2 Potential Future Research 135

6.2.1 3D Balloon 135

6.2.2 Tensile Testing and Curve Fitting 136

6.2.3 FSI Human Lung 137

REFERENCES 139

APPENDIX A – Chapter 2: The Quandary of Compressibility 142

APPENDIX B – Chapter 3: Three-Dimensional Balloon Expansion 157

APPENDIX C – Chapter 4: Porcine Tracheal Material Properties 181

APPENDIX D – Chapter 5: FSI Human Upper Airway Simulation 192

LIST OF FIGURES

Figure 1.1: Respiratory system by *J. Ladyof Hats* [7]. 3
Figure 1.2: FSI coupling flow chart for simulations 4
Figure 2.1: Geometry of literature square balloon 9
Figure 2.2: ANSYS Workbench layout for running a SC analysis 10
Figure 2.3: Square Balloon – Simulation 1 fluid mesh 11
Figure 2.4: Square Balloon – Simulation 1 structural mesh 12
Figure 2.5: Square Balloon – Boundary conditions 12
Figure 2.6: Square Balloon – Additional boundary conditions for quasi-2D simulation 13
Figure 2.7: Square Balloon – Velocity inlet profile 13
Figure 2.8: Square Balloon – Mesh scale information for Simulation 1 from Fluent 15
Figure 2.9: Square Balloon – All fluid pressures plotted on a logarithmic scale 20
Figure 2.10: Square Balloon – Fluid pressure comparison. Values from *Bogaers et al.* [10] where regenerated using *A. Rohatgi.* [15]'s program. 21
Figure 2.11: Square Balloon – Pressure divided by density curve, values obtained from Simulation 1. 23
Figure 2.12: Square Balloon – Comparing Ideal Gas Pressure with literature and case study pressures 24
Figure 2.13: Square Balloon – Fluid pressure and structural stress for Simulation 1 at t = 0.5 second 25
Figure 2.14: Square Balloon – Fluid pressure and structural stress for Simulation 1 at t = 1 second 25
Figure 2.15: Square Balloon – Fluid pressure and structural stress for Simulation 1 at t = 5 seconds 26
Figure 2.16: Square Balloon – Fluid pressure and structural stress for Simulation 1 at t = 9 seconds 26
Figure 2.17: Square Balloon – Fluid pressure (kPa) contour plot at t = 15 seconds from *Küttler et al.* [9] 27
Figure 2.18: Square Balloon – Fluid velocity magnitude and structural strain for Simulation 1 at t = 0.5 second 28

Figure 2.19: Square Balloon – Fluid velocity magnitude and structural strain for Simulation 1 at t = 1 second 28
Figure 2.20: Square Balloon – Fluid velocity magnitude and structural strain for Simulation 1 at t = 5 seconds 29
Figure 2.21: Square Balloon – Fluid velocity magnitude and structural strain for Simulation 1 at t = 9 seconds 29
Figure 2.22: Square Balloon – Velocity (m/s) contour plot at t = 15 seconds from *Küttler et al.* [9] 30
Figure 2.23: Square Balloon – Velocity (m/s) contour plot at t = 10 seconds from *Bogaers et al.* [10] 30
Figure 2.24: Square Balloon – Fluid velocity vector and structural deformation for Simulation 1 at t = 0.5 second 31
Figure 2.25: Square Balloon – Fluid velocity vector and structural deformation for Simulation 1 at t = 1 second 32
Figure 2.26: Square Balloon – Fluid velocity vector and structural deformation for Simulation 1 at t = 5 seconds 32
Figure 2.27: Square Balloon – Fluid velocity vector and structural deformation for Simulation 1 at t = 9 seconds 33
Figure 3.1: Section view of 3D Balloon geometry. 38
Figure 3.2: 3D Balloon fluid mesh, side view 40
Figure 3.3: 3D Balloon solid mesh, side view 40
Figure 3.4: 3D Oscillating balloon 41
Figure 3.5: Boundary condition of 3D Balloon 42
Figure 3.6: Velocity profile for the 3D Balloon 43
Figure 3.7: Mesh scale information of 3D Balloon from ANSYS Fluent 44
Figure 3.8: 3D Balloon – von Mises stress at six different times 49
Figure 3.9: 3D Balloon – Rotated isometric view of von Mises stress, t = 2.5 seconds 50
Figure 3.10: 3D Balloon – Cylindrical pressure vessel stress orientation 51
Figure 3.11: 3D Balloon – Equivalent strain from the same six times as the stresses 52
Figure 3.12: 3D Balloon – Stress-strain curve from simulation 53
Figure 3.13: 3D Balloon – Displacement from six different times 54

Figure 3.14: 3D Balloon – Deformation with time 55

Figure 3.15: 3D Balloon – Behavior of air flow in balloon 56

Figure 3.16: 3D Balloon – Velocity contour of fluid region at six different times................. 58

Figure 3.17: 3D Balloon – Velocity magnitude at t = 0.5 second. (a) 3D isosurface (range between -0.55 and 0.3), (b) horizontal slice, (c) vertical slice, and (d) velocity and time of flow 59

Figure 3.18: 3D Balloon – Velocity magnitude at t = 0.7 seconds. (a) 3D isosurface (range between -0.55 and 0.3), (b) horizontal slice, (c) vertical slice, and (d) velocity and time of flow 60

Figure 3.19: 3D Balloon – Velocity magnitude at t = 1 second. (a) 3D isosurface (range between -0.55 and 0.3), (b) horizontal slice, (c) vertical slice, and (d) velocity and time of flow 61

Figure 3.20: 3D Balloon – Velocity magnitude at t = 1.5 seconds. (a) 3D isosurface (range between -0.55 and 0.3), (b) horizontal slice, (c) vertical slice, and (d) velocity and time of flow 62

Figure 3.21: 3D Balloon – Velocity magnitude at t = 2.5 seconds. (a) 3D isosurface (range between -0.55 and 0.3), (b) horizontal slice, (c) vertical slice, and (d) velocity and time of flow 63

Figure 3.22: 3D Balloon – Pressure contour and velocity vector at t = 1 second.................... 64

Figure 3.23: 3D Balloon – Pressure contour and velocity vector at t = 1.5 seconds 64

Figure 3.24: 3D Balloon – Velocity (a) and Pressure (b) curve from simulation.................... 65

Figure 4.1: Tensile Testing – Material curve fitting and verification approach 68

Figure 4.2: Axial samples 70

Figure 4.3: Circumferential samples.. 70

Figure 4.4: Tensile Testing – Example of locational measurements from carina.................... 70

Figure 4.5: Mini-Instron load frame... 71

Figure 4.6: Mounted specimen... 71

Figure 4.7: Ideal data – Force-Displacement curve of an axial test... 73

Figure 4.8: Ideal data – Stress-Strain curve of an axial test... 74

Figure 4.9: Ideal data – Stress-Stretch curve of an axial test... 74

Figure 4.10: Extra trimming required – Force-Displacement curve of an axial test................ 75

Figure 4.11: Extra trimming required – Stress-Strain curve of an axial testing 75
Figure 4.12: Tensile Testing – Flow chart of data trimming for MATLAB code 76
Figure 4.13: Tensile Testing – Graphed slope values, graph created in MATLAB R2016a, x axis is Strain, ε (mm/mm), y axis is Stress, σ (MPa) 77
Figure 4.14: All axial data from tensile testing.. 78
Figure 4.15: Stress-Stretch curve, figure obtained from *Lally et al.* [12] 79
Figure 4.16: Stress-Stretch curve of the axial direction. 79
Figure 4.17: All circumferential data from tensile testing 80
Figure 4.18: Stress-Stretch curve, figure obtained from *Trabelsi et al.* [11] 81
Figure 4.19: Stress-Stretch curve of circumferential data.. 81
Figure 4.20: Stress-Strain regions 82
Figure 4.21: Ogden Model curve fit on axial data 85
Figure 4.22: Ogden model curve fit for circumferential data 87
Figure 4.23: Boundary conditions for SEM simulation 88
Figure 4.24: Axial – single element simulation results... 90
Figure 4.25: Circumferential – single element simulation results 90
Figure 5.1: 3D Slicer [43, 44] generated human lung geometry... 93
Figure 5.2: Fluid geometry for human lung model 94
Figure 5.3: Structural geometry for human lung model.. 95
Figure 5.4: Human Lung – Fluid region mesh: (a) Isometric view of mesh, (b) upper trachea, (c) lower left bronchi, and (d) lower right bronchi. 97
Figure 5.5: Human Lung – Structural region mesh: (a) Isometric view of mesh, (b) upper trachea, (c) lower left bronchi, and (d) lower right bronchi. 98
Figure 5.6: Human Lung Model – Boundary condition.. 99
Figure 5.7: Human Lung Model – Prescribed PCV velocity 100
Figure 5.8: Human Lung – Reference for the selected time steps. 104
Figure 5.9: von Mises Stress of the Human Lung model.. 109
Figure 5.10: Time series plot of maximum stress for human lung model 110
Figure 5.11: Equivalent Strains of the human lung model.. 115
Figure 5.12: Displacements of the human lung model 121
Figure 5.13: Velocity Magnitude contour plots for human lung model 126

Figure 5.14: Fluid pressure contour plots for human lung model 132

LIST OF TABLES

Table 2.1: Square Balloon – Mesh settings for all fluid and structural regions 10
Table 2.2: Square Balloon – Mesh properties for the fluid and structural regions 11
Table 2.3: Square Balloon – Smooth re-meshing settings for all simulations 14
Table 2.4: Square Balloon – Re-meshing mesh parameters for various simulations.............. 15
Table 2.5: Square Balloon – Dynamic Mesh Zones 16
Table 2.6: Square Balloon – Material properties obtained from *Küttler et al.* [9] and *Bogaers et al.* [10] for simulations 16
Table 2.7: Square Balloon – Material properties for the fluid and structural regions 17
Table 2.8: Square Balloon – Fluid region main convergence settings.................................... 17
Table 2.9: Square Balloon – SC Data Transfer settings 18
Table 2.10: Square Balloon – Fluid region simulation settings.. 19
Table 2.11: Square Balloon – Structural region simulation settings....................................... 19
Table 2.12: Square Balloon – System coupling settings.. 19
Table 2.13: Square Balloon – Convergence values obtained from pressure data 33
Table 2.14: For Square Balloon – Types of convergences for CFD 34
Table 2.15: Square Balloon – Mesh refinement table... 35
Table 2.16: Square Balloon – Values for convergence study results...................................... 35
Table 2.17: Square Balloon – Uncertainty estimation results.. 35
Table 3.1: 3D Balloon – Mesh settings for all fluid and structural regions 39
Table 3.2: 3D Balloon – Mesh properties for the fluid and structural regions 39
Table 3.3: 3D Balloon – Smooth re-meshing settings 44
Table 3.4: 3D Balloon – Re-meshing mesh parameters... 45
Table 3.5: 3D Balloon – Dynamic Mesh Zone settings... 45
Table 3.6: 3D Balloon – Material properties for the fluid and structural regions................... 46
Table 3.7: 3D Balloon – Fluid region main convergence settings.. 47
Table 3.8: 3D Balloon – SC Data Transfer settings.. 47
Table 3.9: 3D Balloon – Simulation settings for the three modules 48
Table 4.1: Tensile Testing – Length of porcine trachea used in tests 69
Table 4.2: Tensile Testing – Preliminary material properties of porcine trachea 72
Table 4.3: 2nd Order Ogden material constants for the axial direction. 84

Table 4.4: Fit Option settings for axial curve fit in MATLAB 85
Table 4.5: 2^{nd} Order Ogden material constants for the circumferential direction.................... 86
Table 4.6: Starting values of the constants for the circumferential direction 87
Table 4.7: BCs for SEM.. 89
Table 5.1: Mesh settings for lung geometry.. 96
Table 5.2: Human Lung – Mesh properties for the fluid and structural regions...................... 96
Table 5.3: Human Lung Model – Material properties for the fluid and structural regions ... 101
Table 5.4: Human Lung Model – Fluid region main convergence settings........................... 102
Table 5.5: Human Lung Model – SC Data Transfer settings... 102
Table 5.6: Human Lung – Simulation settings for the three modules 103

NOMENCLATURE

AC – Artificial Compressibility
BCs – Boundary Conditions
BR – Breath Rate
CFD – Computational Fluid Dynamics
Cp – Specific Heat
CT – Computer Tomography
DMZ – Dynamic Mesh Zone
E – Elastic Modulus
FEA – Finite Element Analysis
FS – Factor of Safety
FSI – Fluid-Structure Interaction
G, G – Shear Modulus, Lung generations
HFPV – High Frequency Percussive Ventilation
K – Bulk Modulus
LES – Large Eddy Simulation
M – Molecular Weight
m – Mass
n – Number of Moles
P – Pressure
PCV – Pressure Controlled Ventilation
RE – Generalized Richardson Extrapolation
Re – Reynolds Number
SC – System Coupling
SEM – Single Element Model
SES – Single Element Simulation
STL – Stereolithography
T – Temperature
u – Velocity
V – Volume
γ – Diffusion coefficient

ε – Strain

κ – Thermal Conductivity

λ – Stretch

μ – Dynamic Viscosity

υ – Kinematic Viscosity, Poisson’s Ratio

ρ – Density

σ – Stress

Chapter 1: LITERATURE REVIEW

1.1 Introduction

Mechanical ventilation is used as a life support treatment when patients are unable to breathe effectively on their own. Various types of ventilators are used in the medical field. The focus of this study will be on pressure-controlled ventilation (PCV), with respect to the physical properties governing the movement of gas. Research has been done to quantify the effectiveness between PCV and other ventilators, such as high-frequency percussive ventilation (HFPV) in terms of gas exchange. *Dutta et al.* [1] experimentally determined HFPV provides better results in terms of gas exchange; based on nitrogen washout times. *Lucangelo et al*. [2] have also conducted experiments to quantify HFPV's improvement in gas exchange compared to PCV. On the other hand, numerical simulations have also been conducted to better visualize the effects of air flow in the lung. *Lambert et al.* [3] and *Calay et al*. [4] have conducted computational fluid dynamics (CFD) simulations of the lungs, using a large eddy simulation (LES) and prescribed normal, as well as exercising breathing conditions to their models, respectively. *Xia et al.* [5] have performed a fluid structure interaction (FSI) simulation in a part of the lung airway tree with various wall thicknesses and Reynold's numbers (Re). *Malvè et al.* [6] have also conducted an FSI simulation comparing normal breathing rate and mechanical ventilator flow in the trachea. However, an FSI simulation of more than just the trachea has never been directly in terms of numerical simulations. Some research has been conducted to show the difference either experimentally or through CFD. However, mechanical stresses on the lung walls themselves are equally as important. Reason being, the lung walls themselves are delicate in nature, inflammation can cause tissue damage to the walls. As stated previously, this study is aimed to quantify PCV through FSI; showing the differences in terms of the fluid pressure exerted on the tracheal walls and the respective stresses that are exerted on the internal walls of the airway.

Many researchers have conducted FSI simulations for various situations, such as turbines, pumps, and biomechanics. FSI does not have to be between the two classic simulation methods: CFD and Finite Element Analysis (FEA). For example, FSI can be between thermal (heat transfer) or acoustics and solid mechanics; these simulations are also called Multiphysics simulations. For this study, the classical coupling between: CFD and FEA is employed. FSI takes into account both the fluid flow and the structural behaviors of systems. These simulations allow researchers to visualize the various situations that cannot be experimentally or analytically performed. FSI is especially popular among biomedical and biomechanical studies, due to the complex, dynamic geometries. In addition, these complex situations are difficult and time consuming to accurately measure. Therefore, a validated numerical simulation is generally favored. In the case of human lungs, the geometry of the lower respiratory tract is intricate. This research is focused on simulating deformation and fluid flow field from the human trachea down to the 3rd generation of the human lung. In addition, couple case studies have been used to prove the validity of the human lung FSI simulation results.

1.2 Background

The focus of the study is to perform an FSI simulation for the lower respiratory tract. The first step would be to understand where in the respiratory tract the study and model is focused on and effectively represents. Second, would be to understand how an FSI simulation is performed.

1.2.1 Respiratory System

The human respiratory system is divided into two regions: the upper respiratory tract and the lower respiratory tract. Shown in Figure 1.1, the parts that are above the cricoid cartilage, which is a part of the larynx, is in the upper respiratory tract, everything else below is in the lower respiratory tract. The lower respiratory tract consists of the trachea, bronchi, bronchioles, and the left and right lungs containing the alveoli. The focus of this research will be in the lower respiratory airway tract, specifically the trachea, main bronchi, and bronchi.

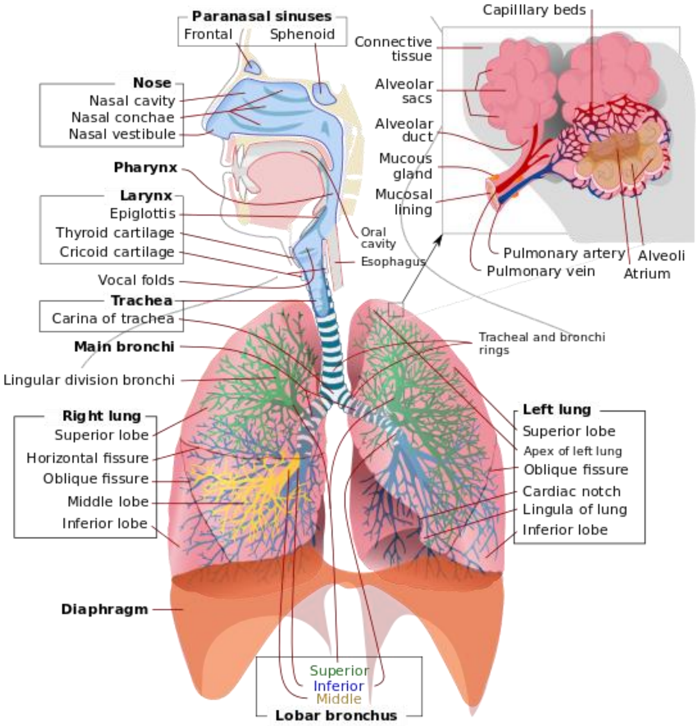

Figure 1.1: Respiratory system by *J. Ladyof Hats* [7].

Note: each bifurcation is also referred as a “generation”, or just “G”. For example, the trachea is G1. The region of interest is also part of what researchers would call the upper airway. The upper airway is from the trachea (G1) down to the seventh generation (G7). As stated previously, the focus will be the trachea, main bronchi, and bronchi; which is G1 through G4.

1.2.2 Fluid Structure Interaction

This FSI study is a coupling between two classic simulation methods: CFD and FEA. FSI takes into account both the fluid flow and structural behaviors of systems. FSI has not been a dominating simulation method, mainly because of the scarcity of powerful computers. However, in the recent years of technological improvement, FSI simulations are not as time costly as before. In addition, most researchers’ focus is either in CFD or FEA. There are several reasons for the popularity of CFD and FEA over FSI. First, most researchers’ focuses are either in the fluid mechanics or solid mechanics field. Though in reality, the fluid and the solid closely interact with each other in most situations. Second, FSI is also difficult to converge if the geometry, flow field or, solid behavior is too complex. Combining these two reasons, results in costly simulations and possible inaccurate results.

Generally, an FSI simulation works through a portioned approach. Meaning, the fluid solver is separate from the solid mechanics solver, and the two are connected with a “coupling system”. The governing equations for the fluid solver will be solved and the results will be fed into the solid system solver. Once the solid mechanics system is solved, its output will become the fluid mechanic’s new input. This cycle repeats until either the set convergence is achieved or if the number of iterations are met, then the program moves onto the next time step.

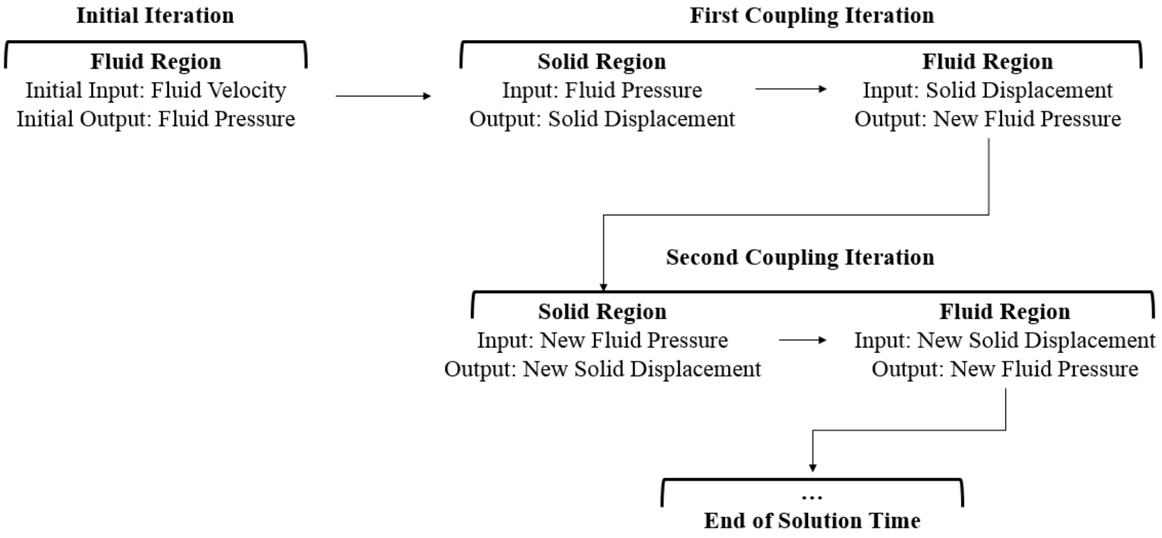

Figure 1.2: FSI coupling flow chart for simulations

Shown in Figure 1.2 is the FSI coupling logic for the simulations conducted in this study. Note, not all FSI simulations will always have these as inputs and output. The input and outputs are dependent upon the study and the specific conditional parameters employed.

1.3 Geometry for Simulations

To run any kind of numerical simulation such as CFD, FEA, or FSI, geometry for the models must exist or else the geometry would have to be created. For the first two case studies, the quasi-2D balloon and 3D balloon, the geometries were modeled in SolidWorks 2017. For the human lung simulation, the geometry was created from a program called 3D Slicer. The human lung geometry was created from a series of computerized tomography (CT) scans using 3D Slicer, and saved as a stereolithography (STL) file. Other methods, as *Kitaoka et al.* [8] used, is an algorithm to generate the airway tree. Though this method can generate the geometry to a fine detail, it is not as realistic as a geometry generated from a CT scan, especially in three dimensions. Other researchers such as *Xia et al.* [5], *Malvè et al.*[6], and many others have relied on generating the lung geometry from CT scans for geometry accuracy.

1.4 Fluid-Structure Interaction Simulations

A couple of FSI validation case studies were simulated before applying the method to the human lung FSI simulation. The first case is a quasi-2D square balloon simulation. This simulation was first purposed by *Küttler et al.* [9]. The simulation was originally used as a test for an in-house FSI code. For this study, ANSYS was used to perform the same case study and results are then compared to *Küttler et al.* [9] and *Bogaers et al.* [10].

Another case study is a 3D balloon simulation. The boundary conditions (BCs) used in this simulation are applied to the lung geometry since the simulations themselves are similar in nature. The author was not able to find a journal paper that conducted the same study, however the results are reasonable with the given BCs.

Lastly for the human lung simulation, several researchers have previously conducted rudimentary FSI simulations. However, direct comparisons cannot be made due to the difference in material properties and BCs used. General comparisons and conclusions are made in the chapter. For example, *Malvè et al.* [6] simulated a human lung geometry of a 70 year old healthy man. The geometry was created from a series of CT scans, with normal and ventilation BCs prescribed in the simulation. The material applied to the lung was obtained from literature; based on tensile testing of human tracheas. However, the material values *Malvè et al.* [6] used were from *Trabelsi et al.* [11]; whose studies were based on previously frozen tissues. Whereas, this project applies experimental “fresh” *ex vivo* porcine tracheal properties.

1.5 Material Testing

Uniaxial tensile testing was performed to obtain material properties for the lung simulation. The tensile tests of the porcine tissue were performed using a mini-Instron. Afterwards, the data was curve fitted using the hyperelastic Ogden Material model. Other researchers have done similar testing; *Lally et al.* [12], *Shi et al.* [13], *Teng, et al.* [14], and *Trabelsi et al.* [11] have all conducted various types of tensile testing on porcine specimens. However, the techniques, both in terms of testing and curve fitting, used by the various researchers are different than what was done in this current study. Please refer to Chapter 4 for additional details.

1.6 Limitations

Many researchers have conducted various forms of simulations and experimentation on the airway. However, limitations of the conducted studies still exist. While material tensile testing has been conducted by several researchers, one of the most common hyperelastic models was not utilized: the Ogden model. Another instance would be simulating simple geometries such as a balloon simulation. FEA simulations have been conducted for balloon stents. However, a simple FSI simulation of a 3D balloon inflating has never been previously reported done before. Though the solid mechanics of the balloon is easy to visualize, the fluid flow is more complicated. A simple study like a 3D balloon is a good simulation to commence with prior to advancing on to something that is of greater complexity in geometry such as a human airway and lung. Lastly, FSI study of the human lung has some minor limitations as well. *Malvè et al.* [6] conducted FSI simulations to compare the structural differences between normal breathing and PCV. However, the focus was only on the trachea, while the other regions below, such as the bronchi, were neglected in *Malvè et al.* [6] simulation.

1.7 Conclusion

This study aims to further bridge the knowledge gap through FSI simulations and mechanical tissue testing. From existing studies certain methods and results were drawn upon for guidance. However, the current research also has its own unique methods for comparison. For example, using a commercial simulation program, ANSYS was used instead of in-house codes. Using an existing commercial program ensures the BCs and various setups can be consistent regardless of user. In addition, incorporating another curve fitting model will further diversify existing material databases just as *Trabelsi et al.*[11] and *Lally et al.*[12] have done with Neo-Hookean and Moony-Rivlin, respectively. Lastly, adding one more way of simulating an anatomically accurate lung geometry, provides further advancements in both simulation and experimental research. By comparing results that may validate results from *Dutta et al.* [1] and *Lucangelo et al.* [2], or possibly comparing simulation results with *Malvè et al.* [6]. Throughout this study, conclusions in each chapter are drawn and built upon with the next. By combining the results from each chapter, it creates a unique approach in simulating the human lung behavior under certain ventilation conditions. The main objective of the study is to develop an FSI model for the human lung. The FSI model will incorporate tissue properties obtained from tensile testing, as well as a prescribed realistic PCV ventilator flow condition for increased modeling accuracy.

Chapter 2: THE QUANDARY OF COMPRESSIBILITY

2.1 Incompressibility, Compressibility, and Artificial Compressibility

Incompressible flow, also known as isochoric flow, is when the volume is constant throughout the fluid flow. The only way to maintain a constant volume, is if the material density is constant. Which means for a compressible flow, the volume/density is changing throughout the fluid flow. The change in density is caused by the change in pressure. Both forms of compressibility can be found in real-world physics: water (incompressible) and air (compressible). While the third form, artificial compressibility (AC), is mathematically in between incompressible and compressible. By adding a constant to the governing continuity equation, it relaxes the constraints of the conservation law. AC can only be mathematically proven and implemented.

Küttler et al. [9] was the first to pose the incompressible dilemma. In summary, incompressible flows along with highly deformable structures cannot be solved with simple alternating FSI iterations. An obvious case is where incompressible gas is going into an enclosed surface, such as a balloon. *Küttler et al.* [9] proposed several different approaches to solve the dilemma. Later, *Bogaers et al.* [10] used the same case study for an AC FSI simulation. In *Bogaers et al.* [10], the Dirichlet Artificial Compressibility is when a relaxation source term is added to the fluid continuity equation. This allows the continuity equation to relax and converge. However, this is not a direct reflection of the behavior in the balloon. Therefore, in this case study of the square balloon, actual compressibility will be used. This means, instead of treating the fluid region as incompressible air, the fluid is going to be an ideal gas allowing compressibility to happen within the square balloon.

For this case study, the simulation was run with three different mesh sizes: 1× , 2×, and 4×. The 1× (Simulation 3) is the original mesh size that both *Küttler et al.* [9] and *Bogaers et al.* [10] used. While the 2× and 4× mesh sizes are mesh refinements for validating the results.

2.2 2D Square Balloon Geometry

In order to compare the results with *Küttler et al.* [9] and *Bogaers et al.* [10], the square balloon geometry and the location of the pressure measurement are the same, as shown in Figure 2.1. The simulation was run using ANSYS 19.1 with the System Coupling (SC) module, as well as the Fluent and Transient Structural modules. However, due to a limitation of the ANSYS program, to perform a SC simulation, the geometry must be in 3D. Therefore, to accommodate the limitation, yet retain a geometry close to the literature geometry as much as possible, a thickness of 1 (mm) was added.

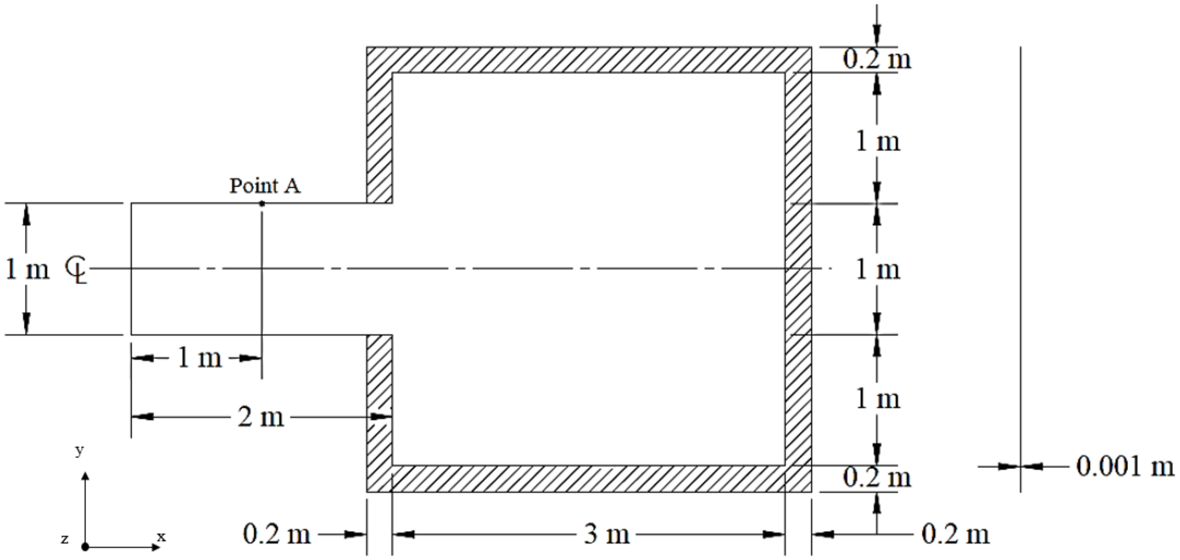

Figure 2.1: Geometry of literature square balloon

The geometry was modeled using SolidWorks 2017, a solid modeling program, as two separate regions. The structural region, hatched area, creates the outer boundary of the square balloon. The fluid region, non-hatched area, is the inner region of the balloon with an inlet.

2.3 Methods

The methods for this case study are divided into several sections: Mesh, Boundary Conditions, Material Properties, and Convergence Settings. The study has three different mesh sizes for the fluid and solid regions. Each simulation is labeled by their corresponding mesh refinements: 1×, 2×, and 4×. Other than the mesh refinements, the other settings, such as materials and convergence tolerance, are the same and they are summarized in the subsections below. Three FSI simulations each with a different mesh refinement. The mesh refinements are later used for an error and uncertainty analysis for the fluid region.

ANSYS uses existing analytical systems along with the SC module to perform FSI analyses. For this simulation, ANSYS Fluent and ANSYS Transient Structural are the main analytical systems, which are coupled using the SC module.

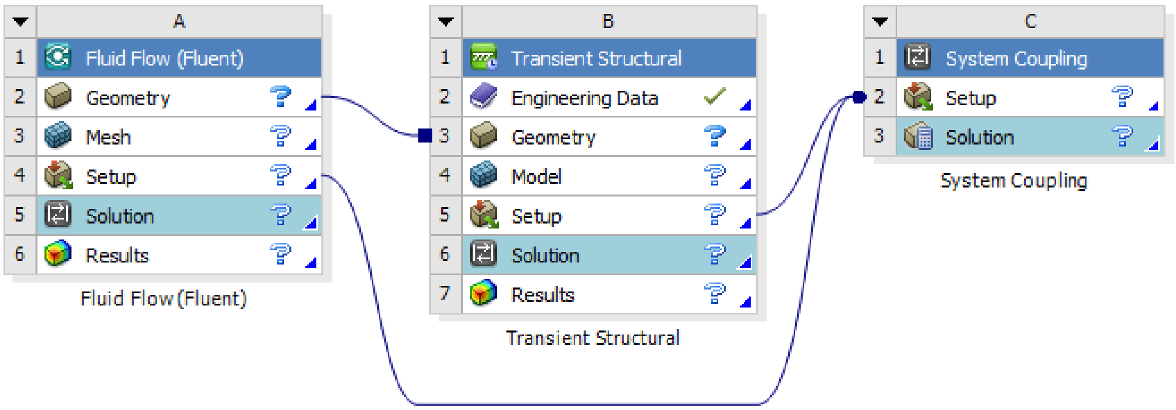

Figure 2.2: ANSYS Workbench layout for running a SC analysis

In Figure 2.2 it is shown how the “Geometry” for Fluent and Transient Structural are linked, and this signifies that the two systems are using the same geometry. Then, the “Setup” from both systems are linked with the SC “Setup”. Various settings such as convergence tolerances, material selection, and boundary conditions must be defined inside Fluent and Transient Structural. ANSYS requires the simulation time, step size, number of steps to be defined in both systems in addition to what is set in the SC module. It is worth noting that inputs in SC, will override inputs in Fluent and Transient Structural.

2.3.1 Mesh

Using the meshing program in ANSYS Fluent and ANSYS Transient Structural, three different size meshes were used to validate the results with each other as well as with *Küttler et al.* [9] and *Bogaers et al.* [10]. The general mesh settings and properties for the fluid and structural regions are summarized in the following tables. Table 2.1 summarizes the general mesh settings for both the fluid and structural regions.

Table 2.1: Square Balloon – Mesh settings for all fluid and structural regions

Mesh Settings	
Element Order	Linear
Size Function	Uniform
Relevance Center	Coarse
Smoothing	Medium

Generally, to capture the behavior of the fluid, the element sizes are smaller and tend to have more elements, in comparison to the solid region. In this case study, since the fluid and structural region are separate regions and use different analytical systems, the mesh sizes will be different. The fluid region will have more elements and smaller element sizes in comparison to the structural region.

Table 2.2: Square Balloon – Mesh properties for the fluid and structural regions

		Fluid Region	
Simulation	Mesh Refinement	Number of Elements	Element Size
1	4×	17,600	0.025 (m)
2	2×	4,400	0.050 (m)
3	1×	1,100	0.100 (m)
		Structural Region	
Simulation	Mesh Refinement	Number of Elements	Element Size
1	4×	944	0.050 (m)
2	2×	236	0.100 (m)
3	1×	59	0.200 (m)

Using the settings in Table 2.1 and Table 2.2 the mesh for Simulation 1 are shown below.

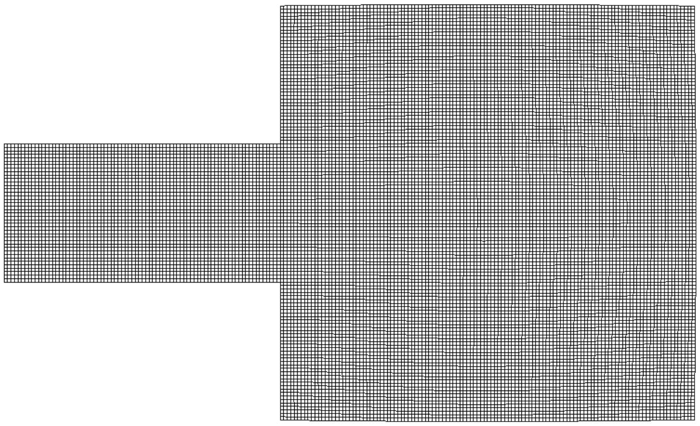

Figure 2.3: Square Balloon – Simulation 1 fluid mesh

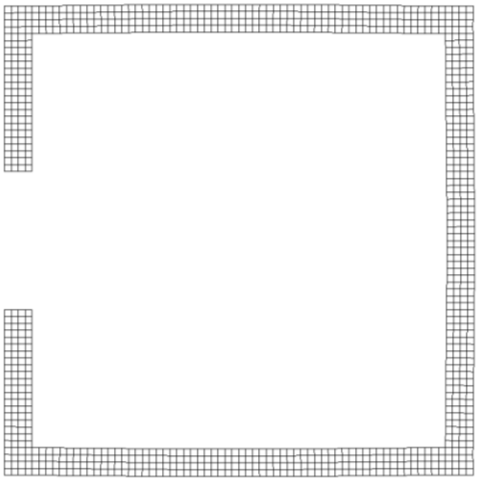

Figure 2.4: Square Balloon – Simulation 1 structural mesh

The other two meshes and simulation results for Simulation 2 and Simulation 3, are shown in Appendix A – Chapter 2: The Quandary of Compressibility.

2.3.2 Boundary Conditions

The BCs shown in Figure 2.5, are the same BCs that *Küttler et al.* [9] and *Bogaers et al.* [10] provided. However, for a quasi-2D simulation, the elements are free to move in the Z direction. Therefore, a “Frictionless Support” was added to the structural region on both sides of the square balloon. By adding a “Frictionless Support”, it constrains the elements in the Z direction, but still allows movement in the X and the Y direction. Similarly, a “Wall Symmetry” BC was added to the fluid region in the Z direction as well; for the same reason as stated for the structural region. These additional BCs are shown in Figure 2.6.

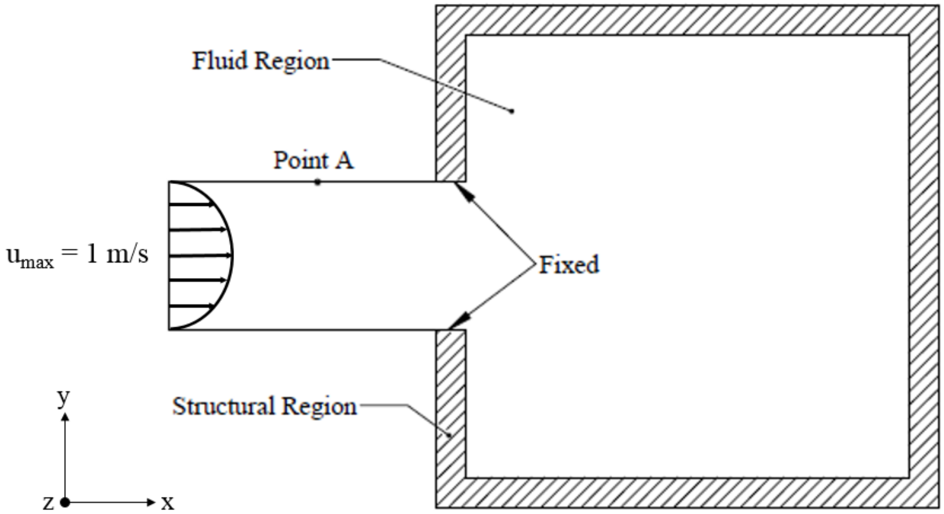

Figure 2.5: Square Balloon – Boundary conditions

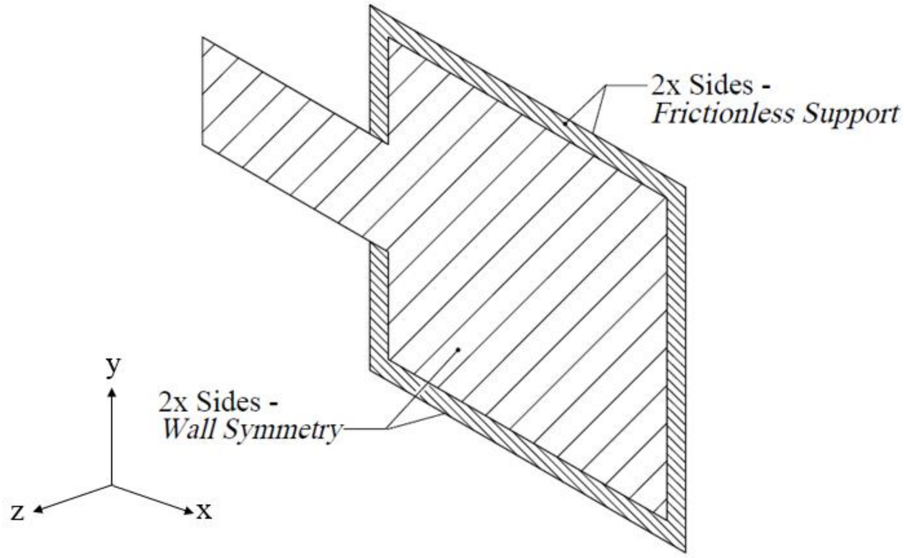

Figure 2.6: Square Balloon – Additional boundary conditions for quasi-2D simulation

As shown at the inlet in Figure 2.5, the maximum velocity inlet is 1 (m/s). However, the prescribed velocity is not a uniform, constant velocity profile. The profile used in the literature is shown in Figure 2.7. The maximum velocity, u_{max}, from 0 to 1 second is a sinusoidal curve defined by equation (2.1):

$$u_{\max} = \frac{\sin(\pi(t+\frac{3}{2}))+1}{2} \ . \tag{2.1}$$

Subsequently after the first second, the velocity is then constant at 1 (m/s).

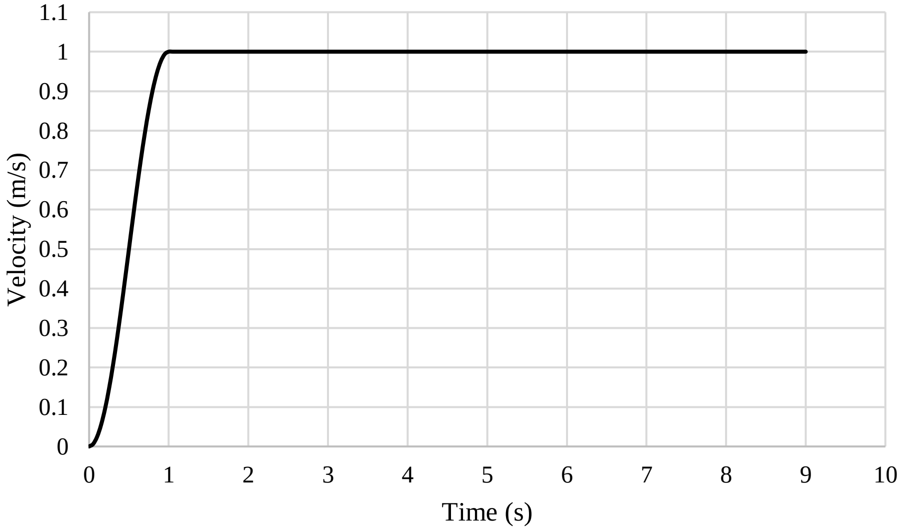

Figure 2.7: Square Balloon – Velocity inlet profile

As stated by *Bogaers et al.* [10], the reason to have a sinusoidal profile in the beginning is to avoid pressure oscillations. Pressure oscillations can occur if there is a rapid influx of pressure in a short amount of time. Once the pressure inside the square balloon stabilizes, a constant velocity can then be applied for the remainder of the simulation time. The same logic for the velocity profiles applies to the 3D balloon, in Chapter 3 as well.

The Re for this case study is 6.22 which makes the flow a laminar flow. Please reference Material Properties section for kinematic viscosity (υ) value. For the flow to be turbulent, Re must be 4000 or greater.

$$\mathrm{Re} = \frac{\rho u L}{\mu} = \frac{uL}{\upsilon} = 6.22 \tag{2.2}$$

where ρ is density, u is velocity, L is the characteristic dimension, in this case the diameter, μ is the dynamic viscosity, and υ is the kinematic viscosity.

In this quasi-2D simulation, a moving boundary was used in the fluid region. A dynamic mesh moves with the fluid such that the elements re-meshes after every iteration. Simulations with dynamic meshes are used to avoid negative volume, unwanted distortion in the elements, or for most cases a boundary in motion. For these FSI simulations, both smoothing and re-meshing dynamic mesh methods were used.

Table 2.3: Square Balloon – Smooth re-meshing settings for all simulations

Smoothing	
Diffusion	-
Diffusion Function	Boundary-distance
Diffusion Parameter	2

Smooth re-meshing methods include: Spring/Laplace/Boundary Layer, Diffusion, and Linearly Elastic Solid. For the square balloon case, the diffusion method was chosen. The mesh for the diffusion-based smoothing is governed by the diffusion equation

$$\nabla \cdot (\gamma \nabla \vec{u}) = 0 \tag{2.3}$$

Since the diffusion equation is velocity based, $\vec{u}$, and the diffusion coefficient, γ, is based on boundary motion. It would be appropriate to use this smoothing method for this prescribed velocity, moving boundary simulation.

Table 2.4: Square Balloon – Re-meshing mesh parameters for various simulations

Re-meshing Parameter			
	Simulation 1	Simulation 2	Simulation 3
Minimum Length Scale (m)	0.0075	0.0107	0.0151
Maximum Length Scale (m)	0.038	0.0760	0.1518
Maximum Cell Skewness	0.7	0.7	0.7
Maximum Face Skewness	0.7	0.7	0.7
Size Re-meshing Interval	1	1	1

The re-meshing method in the simulations will re-mesh every interval. The trigger for the program to re-mesh are the threshold values given in Table 2.4. The mesh must stay between the given thresholds after every iteration. To set the values for re-meshing method, the Minimum Length Scale (m) value must be smaller than the value provided. Similarly, for the Maximum Length Scale (m) the value must be larger than the value given. The Maximum Cell and Face Skewness dictates how warped the elements can be. Provided in Figure 2.8 are values calculated from Fluent for Simulation 1.

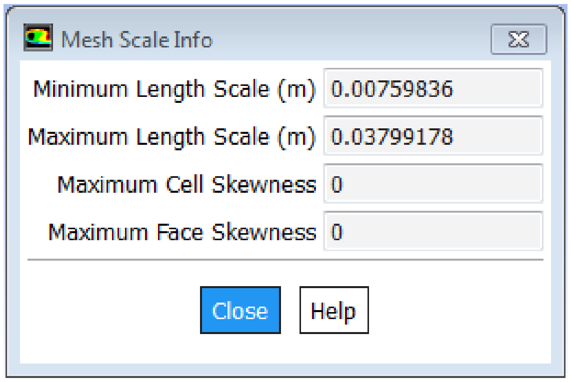

Minimum Length Scale (m) 0.00759836
Maximum Length Scale (m) 0.03799178
Maximum Cell Skewness 0
Maximum Face Skewness 0

Figure 2.8: Square Balloon – Mesh scale information for Simulation 1 from Fluent

As shown in the above figure, there are no skewness in the elements. However, the re-mesh parameters are allowing skewness to occur. Allowing for skewness in the elements will eliminate unnecessary re-meshing during the simulation. Since the other parameters are already restricting.

Lastly, with the Smoothing and Re-meshing parameters set, the Dynamic Mesh Zones (DMZ) will need to be set. The DMZs are what Fluent uses to map the fluid region(s) to the

FSI surface(s) in the solid region. DMZ also allows for the dynamic meshing to actually occur. For this case, there are two zones: the "Interior" and "Wall".

Table 2.5: Square Balloon – Dynamic Mesh Zones

Dynamic Mesh Zones	
Zone Names	*Type*
Interior	Deforming
Wall	System Coupling

The "Interior" is set to "Deforming", the elements will deform and move as needed to accommodate the change in the fluid. "Wall" is set to "System Coupling", this BC is where Fluent will transfer the information to the structural module, where the FSI surface will receive the information, and perform its computation.

2.3.3 Material Properties

Material properties used for square balloon simulations are taken from literature. The material properties are not of any specific material. The properties, shown in Table 2.6, used are unique to the incompressible dilemma simulation of the square balloon.

Table 2.6: Square Balloon – Material properties obtained from *Küttler et al.* [9] and *Bogaers et al.* [10] for simulations

Material Properties	**Fluid Region**	**Structural Region**
Density, ρ (kg/m^3)	1.1	1000
Kinematic Viscosity, υ (kg/m-s)	0.1606	-
Elastic Modulus, E (MPa)	-	0.7
Poisson's Ratio, υ	-	0.45

The material properties listed, closely resembles that of air in the fluid region. While the structural region's properties, based on the density, closely resemble that of water. The elastic modulus value is near negligible in terms of real-world properties.

Küttler et al. [9] and *Bogaers et al.* [10] used the material properties list above for their incompressible and artificial compressibility simulations, respectively. For the compressibility case studies, the ideal gas law will be implemented; thus having the following values.

Table 2.7: Square Balloon – Material properties for the fluid and structural regions

Fluid Material Properties	**Parameters**	**Value**
Density, ρ (kg/m^3)	Ideal-gas	-
Specific Heat, *Cp* (J/kg-K)	Constant	1006.43
Thermal Conductivity, κ (W/m-K)	Constant	0.0242
Dynamic Viscosity, μ (kg/m-s)	Constant	0.1606
Molecular Weight, *M* (kg/kmol)	Constant	28.966
Solid Material Properties	**Parameters**	**Value**
Density, ρ (kg/m^3)	-	1000
Isotropic Elasticity	-	-
	Young's Modulus, *E* (Pa)	7.0E+05
	Poisson's Ratio υ	0.45
	Bulk Modulus, *K* (Pa)	2.333E+06
	Shear Modulus, *G* (Pa)	2.414E+05

The structural region in the simulation is simpler. The structural properties are the same as *Küttler et al.* [9] and *Bogaers et al.* [10] in their simulations. The linear elastic structural properties allow the balloon walls to move with less resistance, but still provide the needed structure to push back on the fluid.

2.3.4 Convergence Settings

To ensure the results comply with real world physics, the convergence settings provide the solver guidelines of when the results are satisfactory. Fluid behavior tends to be more complex therefore, most of the convergence settings are for the fluid region. In ANSYS Fluent, the Solution Methods are left at default. The Residual Convergence values are changed to such that the iterative error has negligible effect on the results.

Table 2.8: Square Balloon – Fluid region main convergence settings

Solution Methods	
Scheme	SIMPLE
Gradient	Least Squares Cell Based
Pressure	Second Order

Continuation of Table 2.8	
Density	Second Order Upwind
Momentum	Second Order Upwind
Energy	Second Order Upwind
Transient Formulation	First Order Implicit
Residual Convergence	
Continuity	1e-05
x-velocity	1e-05
y-velocity	1e-05
z-velocity	1e-05
Energy	1e-06

Table 2.9 has the convergence settings for the SC. The convergence criteria for data transfers are defaulted to RMS Convergence Target = 0.005. The convergence settings for the SC are independent of the fluid and structural systems.

Table 2.9: Square Balloon – SC Data Transfer settings

Data Transfer 1		**Data Transfer 2**	
Source:	Fluent	Source:	Transient Structural
Region:	Wall-fff_solid 1	Region:	Fluid Solid Interface
Variable:	Force	Variable:	Displacement
Target:	Transient Structural	Target:	Fluent
Region:	Fluid Solid Interface	Region:	Wall-fff_solid 1
Variable:	Force	Variable:	Displacement

Data transfer between structural and fluid is completed the in SC. The defined source/target variable and regions are the participants in the FSI simulation. As shown above, Data Transfer 1 is between the “Force” generated by the pressure in fluid to the “FSI” region (the surface that interfaces the structural wall and fluid wall). While Data Transfer 2 is from the structure to the fluid. The displacement from the “FSI” region of the solid is then fed back to the “wall” of the fluid, providing the ‘new’ displacement. Shown in Table 2.10 are the simulation settings for the fluid region.

Table 2.10: Square Balloon – Fluid region simulation settings

	Simulation 1	Simulation 2	Simulation 3
Simulation Time (s)	9	9	9
Time Step Size (s)	0.0125	0.025	0.05
Number of Time Steps	720	360	180
Max Number of Iterations	40	40	40

Shown in Table 2.11 are the simulation settings for the structural region. Large deflection is specified to be ‘on’. The general rule for large deflections is when there are slender structures or large deflection, strain, and rotation. In these case studies, there are large deformation due to the high pressure from the fluid region. Hence, the large deflection function must be turned on.

Table 2.11: Square Balloon – Structural region simulation settings

Structural Region			
	Simulation 1	Simulation 2	Simulation 3
Time/Step End time (s)	9	9	9
Time Step (s)	0.0125	0.025	0.05
Large Deflection	On	On	On

Table 2.12 specifies the time settings for the SC. It is important to note that even though the SC settings will override the fluid and structural settings; the step size and end times must still match the structural values. If the values do not match each other, the simulation will not run.

Table 2.12: Square Balloon – System coupling settings

System Coupling Time Settings			
	Simulation 1	Simulation 2	Simulation 3
End Time (s)	9	9	9
Step Size (s)	0.0125	0.025	0.05
Minimum Iterations	1	1	1
Maximum Iterations	25	25	25

When running an FSI simulation in ANSYS, the SC settings will override the structural and fluid simulation settings. However, for consistency, the settings for the fluid and structural regions should also be inputted before running the simulation. The step size for each simulation is different. Simulation 1 and 2 are used for the error and uncertainty analysis. Therefore, the reducing method for the grid and step sizes are to remain consistent between simulations, each with a reduction of 2.

2.4 Results

2.4.1 Pressure Comparison

Both *Küttler et al.* [9] and *Bogaers et al.* [10] recorded the fluid pressure results at point A (shown in Figure 2.5). For comparison to the literature pressures, all the case studies' fluid pressure have also been recorded at the same location (Point A) and compared.

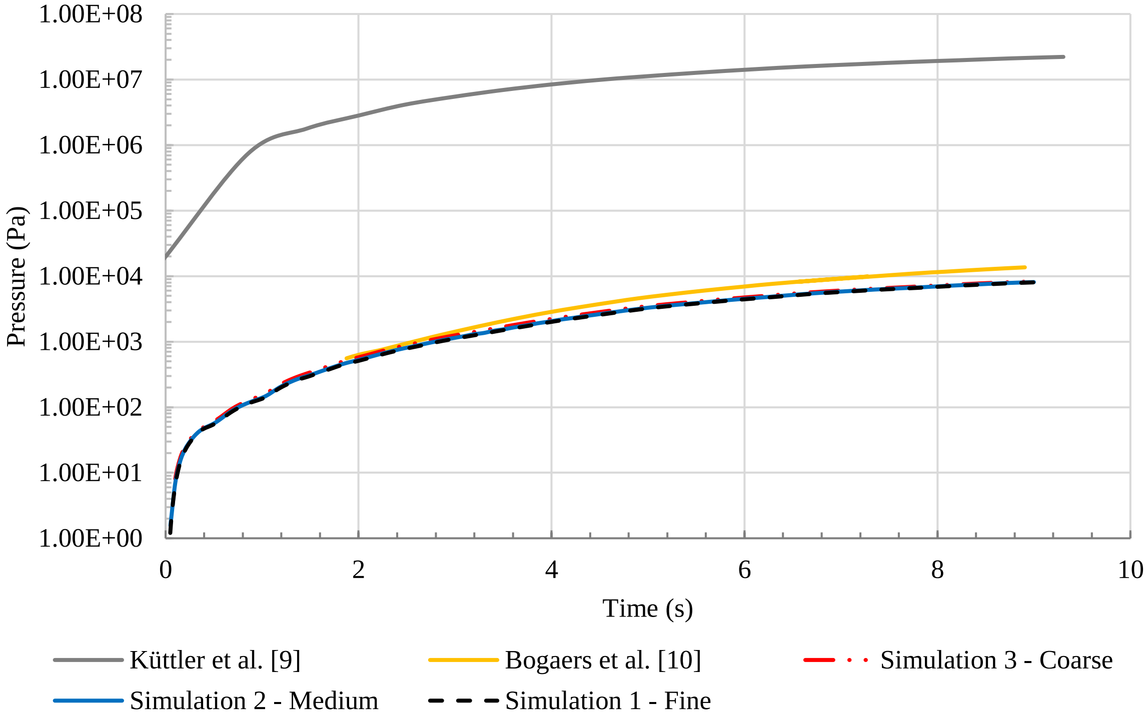

Figure 2.9: Square Balloon – All fluid pressures plotted on a logarithmic scale

As shown in Figure 2.9, the fluid pressure record from *Küttler et al.* [9] is significantly further away from the ANSYS simulations as well as from *Bogaers et al.* [10] . Therefore, the focus of the analysis will be performed with the ANSYS case studies and the pressure values from *Bogaers et al.* [10].

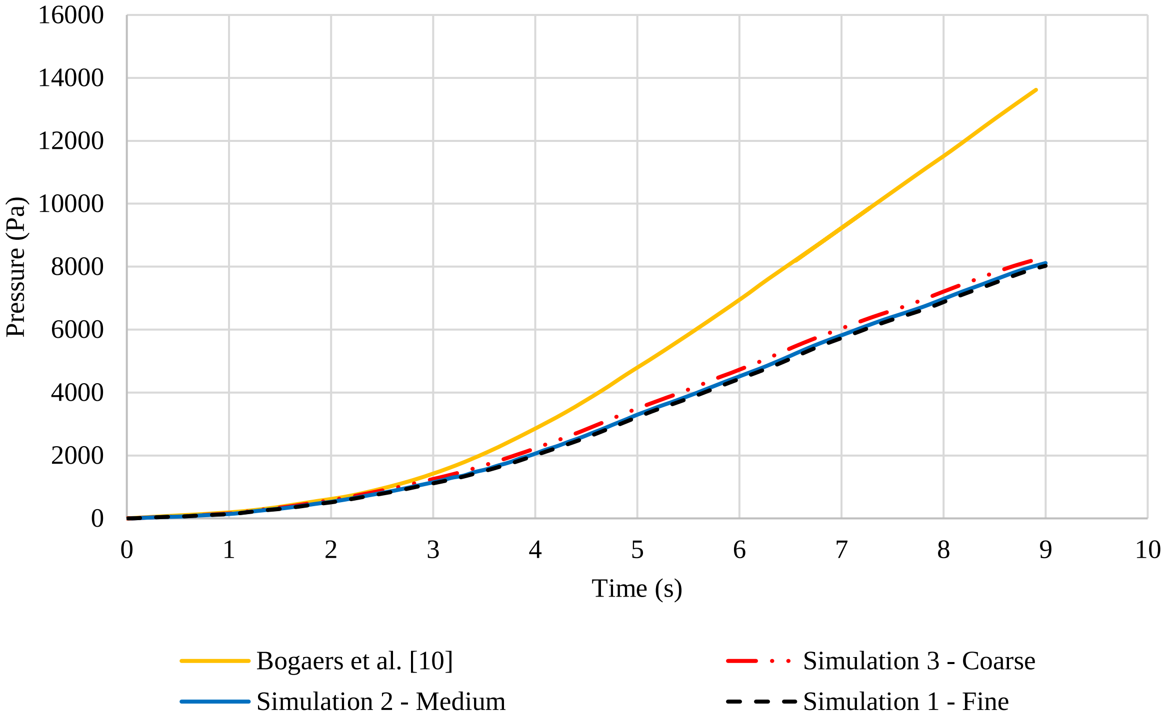

Figure 2.10: Square Balloon – Fluid pressure comparison. Values from *Bogaers et al.* [10] where regenerated using *A. Rohatgi.* [15]'s program.

The pressures shown Figure 2.10, show that the fluid pressure between the ANSYS simulations and *Bogaers et al.* [10] are different from each other. The maximum pressure difference is at t = 9 seconds; where the difference in pressure is about 5,600 (Pa). The cause in the variation can be from numerous different variables. Such as, differences in the simulation programs and in-house code versus ANSYS, or the differences between a pure 2D simulation with a quasi-2D simulation with ANSYS.

2.4.2 Ideal Gas Law

As shown, the pressure results between AC and the case studies are fairly significant. To ensure that the ANSYS simulations are satisfying real world physics the ideal gas law can be applied as an analytical check. Using the idea gas law and density values obtained from the simulation, an 'ideal gas pressure' curve will be created and compared to Figure 2.10. The new curve will show what the idealistic ideal gas pressure is at and then the results will be compared.

In order to apply the ideal gas equation, it is assumed the square balloon is a fully enclosed surface, the fluid is an ideal gas, the balloon is at room temperature, and is in atmospheric pressure. (Note, the solid region is not considered in the ideal gas calculations). To ensure the density values obtained from the simulation is valid, a calculated ideal gas law value is used to compare with ANSYS's prediction, shown in Figure 2.11.

The general form of the ideal gas law is:

$$PV = n\Re T \tag{2.4}$$

Where, P is the pressure of the gas, V is the volume of the gas, n is the number of moles, $\Re$ is the universal gas constant, and T is the absolute temperature of the gas. In addition, knowing that

$$n = \frac{m}{M} \tag{2.5}$$

where m is the mass of the gas and M is the molar mass of the gas. As well as,

$$\rho = \frac{m}{V} \tag{2.6}$$

where m is the mass of the gas and V is the volume of the gas. We then get an alternative form of equation (2.4):

$$P = \rho RT \tag{2.7}$$

where P is the pressure of the gas, ρ is the density, R is the specific gas constant, and T is the temperature.

Knowing the constants and dividing ρ over in equation (2.7) we can graph a Pressure/Density plot.

$$\frac{P}{\rho} = RT \tag{2.8}$$

In order to calculate R, the following constants are used:

$$\Re = 8.31445\left(\frac{Pa \cdot m^3}{mol \cdot K}\right) \text{ and } M_{Air} = 28.966\left(\frac{g}{mol}\right).$$

$$R = \frac{\Re}{M_{Air}} = 0.2870\left(\frac{Pa \cdot m^3}{g \cdot K}\right) \tag{2.9}$$

Lastly, the temperature, T is 300 (K), resulting in:

$$R \cdot T = 86.1\left(\frac{Pa \cdot m^3}{g}\right). \tag{2.10}$$

From equation (2.10), the values of pressure over density from ANSYS should be at a constant 86.1 (Pa-m^3/g).

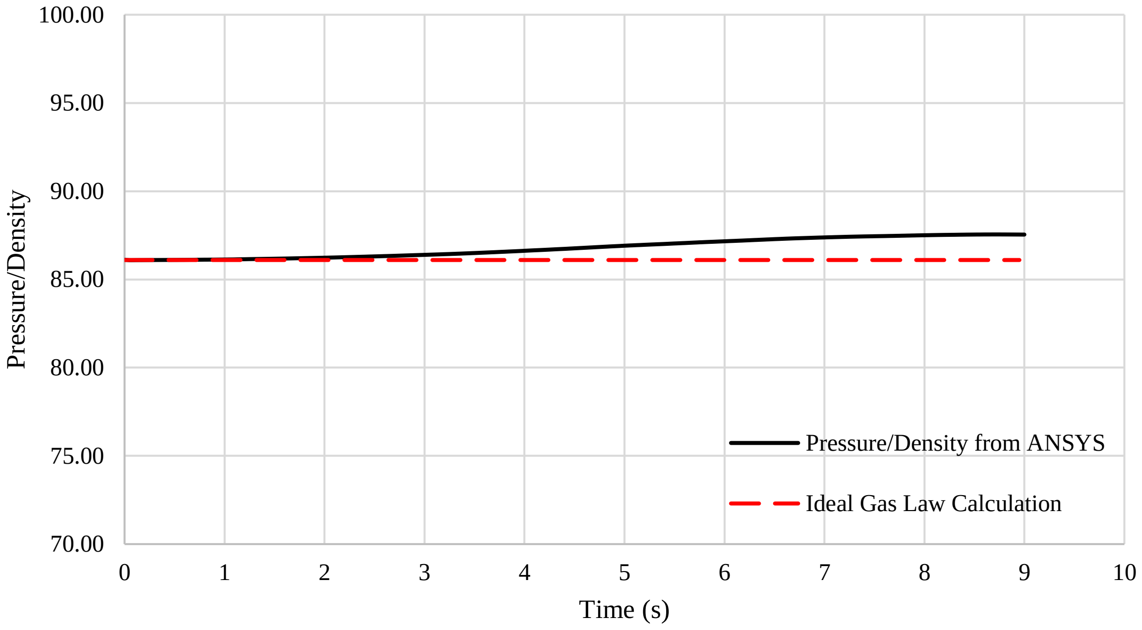

Figure 2.11: Square Balloon – Pressure divided by density curve, values obtained from Simulation 1.

Based on Figure 2.11, the calculated constant and the data obtained from ANSYS are close to each other. The slight variation may be caused by a numerical error in the simulation. Overall the curve is constant and is comparable to the calculated constant: 86.1 (Pa-m^3/g).

After showing that the density from the ANSYS simulation is plausible, we can use the density values and equation (2.7) to create the ideal gas pressure curve to overlay on Figure 2.10 to see where the “idealistic pressure” is supposed to be at with the made assumptions.

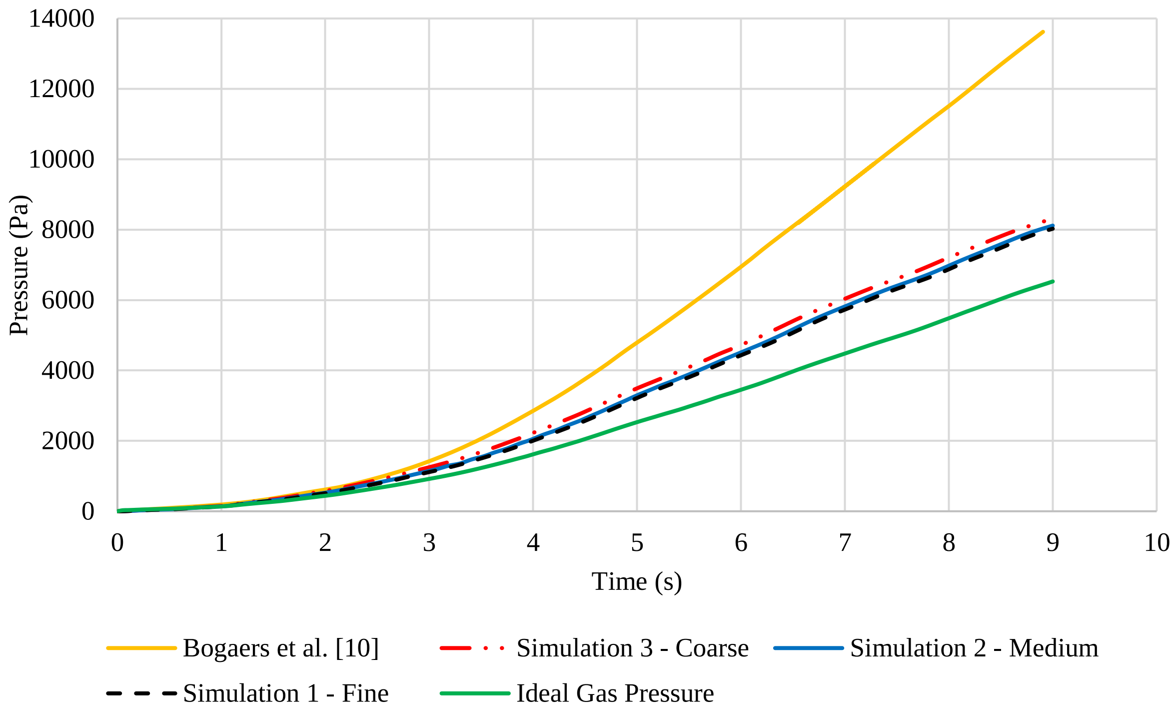

Figure 2.12: Square Balloon – Comparing Ideal Gas Pressure with literature and case study pressures

Looking at Figure 2.12, the ideal gas pressure is slightly lower that the simulated pressures. This is likely due to the force from the solid region elastically pushing back on the fluid. As specified in the assumptions above, the solid region was not considered for the ideal gas calculation. The difference in pressure between Simulation 1 and the ideal gas equation is about 1,500 (Pa). As shown in the graph, the finer the mesh the better the results. The difference in pressure is not too much, if the mesh grid were to be refined more, the difference in pressure would be even smaller.

2.4.3 Pressure Contour Comparison

Küttler et al. [9] provided a pressure contour plot of the square balloon at t = 15 seconds. Though the case study simulations only go up to t = 9 seconds, general conclusion between contours plots can still be made. Provided are four different time steps of fluid pressure with their associated stress contours overlaid with each other. All contour plots were created using Tecplot 360 EX 2017 R2.

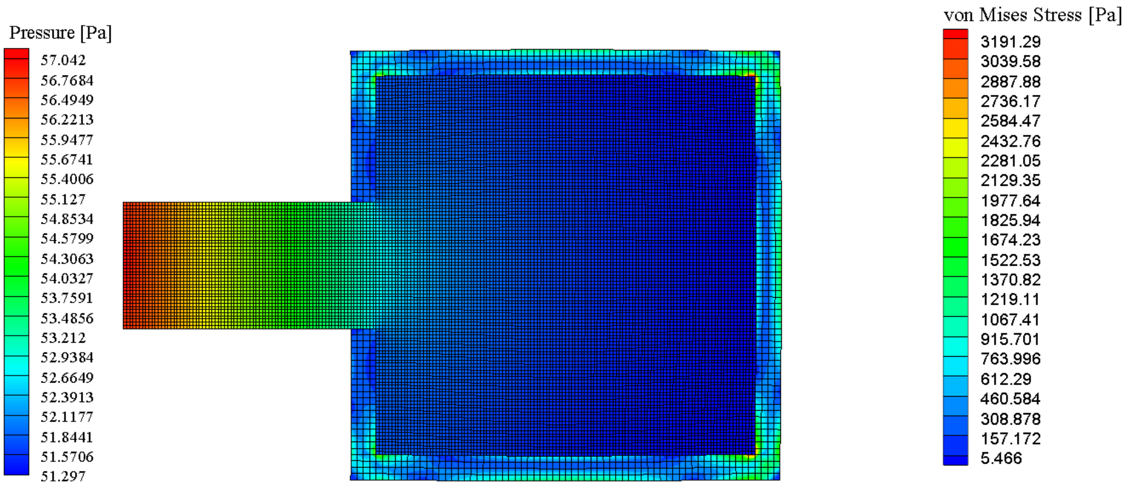

Figure 2.13: Square Balloon – Fluid pressure and structural stress for Simulation 1 at t = 0.5 second

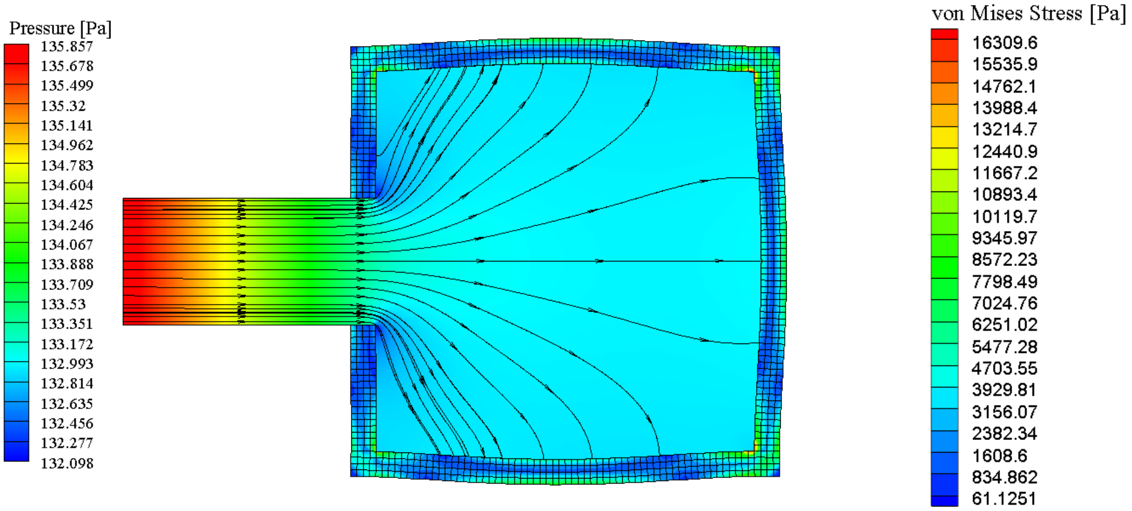

Figure 2.14: Square Balloon – Fluid pressure and structural stress for Simulation 1 at t = 1 second

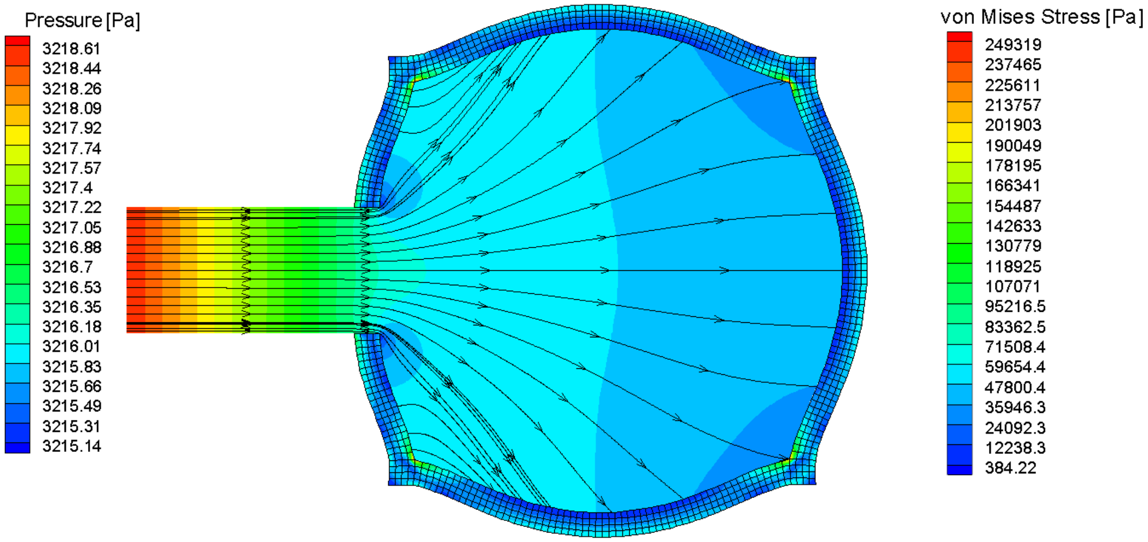

Figure 2.15: Square Balloon – Fluid pressure and structural stress for Simulation 1 at t = 5 seconds

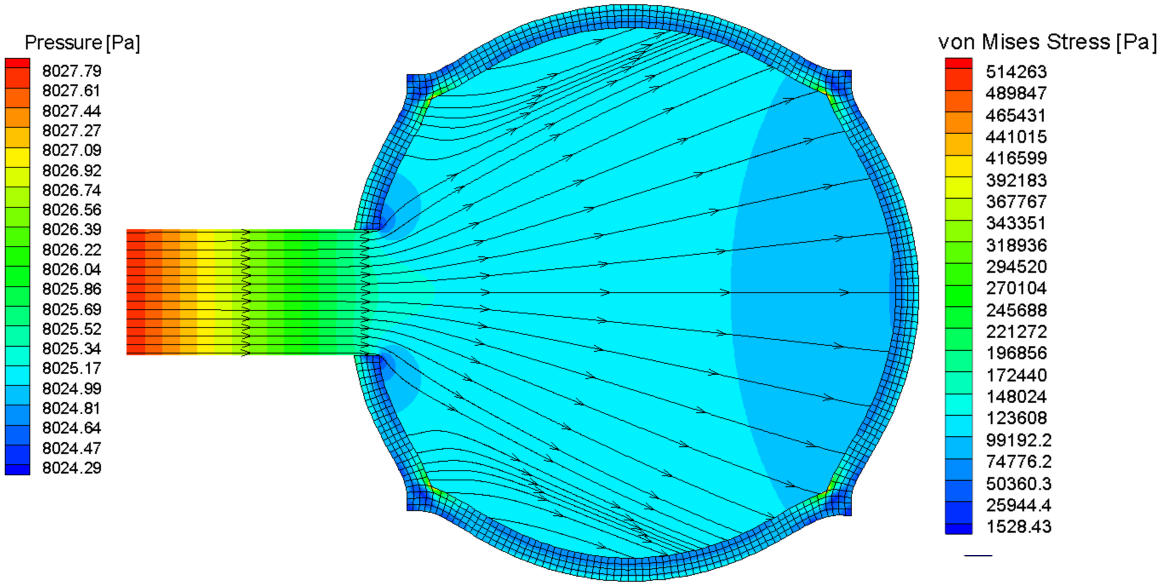

Figure 2.16: Square Balloon – Fluid pressure and structural stress for Simulation 1 at t = 9 seconds

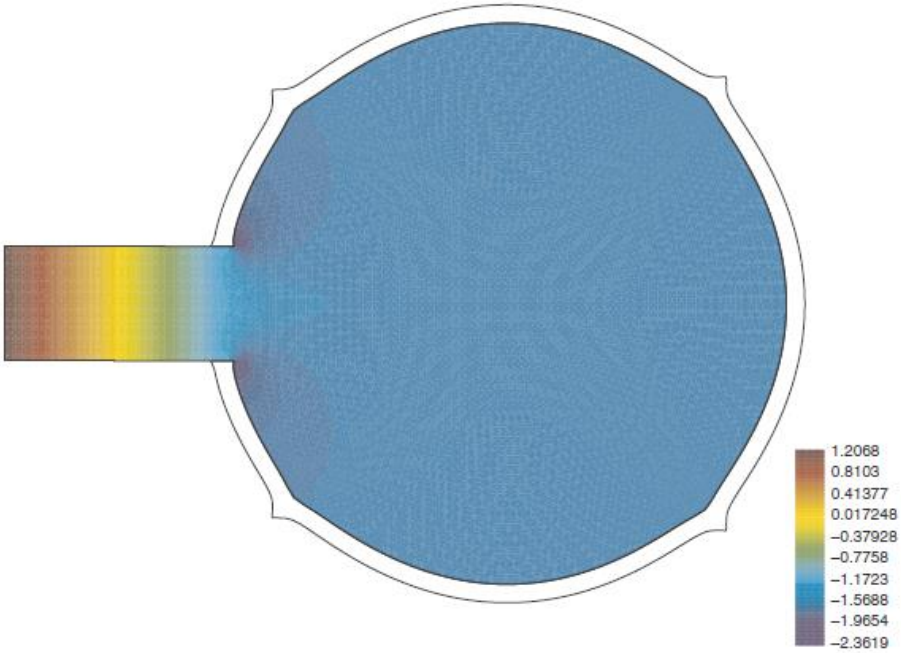

Figure 2.17: Square Balloon – Fluid pressure (kPa) contour plot at t = 15 seconds from *Küttler et al.* [9]

Comparing Figure 2.16 and Figure 2.17, the last time step of the simulations, we can see that the deformed shape is very similar. The pressure contours are very close as well. The difference between the case studies, are about 4,000 (Pa). However, considering *Küttler et al.* [9] is at t = 15 seconds and Simulation 1 is at t = 9 seconds; it can be said that if the pressures where at the same t the values would be close.

In addition to the pressure contour, the figures also show the von Mises stresses at the respective time steps as well. As shown, the maximum stresses are occurring at the corners of the balloon where the fluid is pushing at a stress concentration point. It can be observed that the stresses between the four figures, started out in the four corners and as the balloon expands, the stresses slowly equalize on each side.

2.4.4 Velocity Magnitude Contour Comparison

Both *Küttler et al.* [9] and *Bogaers et al.* [10] provided velocity contours plots for their last time step. Similarly, four different time steps including the last time step are provided for comparison. Velocity magnitude figures are also overlaid with the equivalent strains at their respective time step.

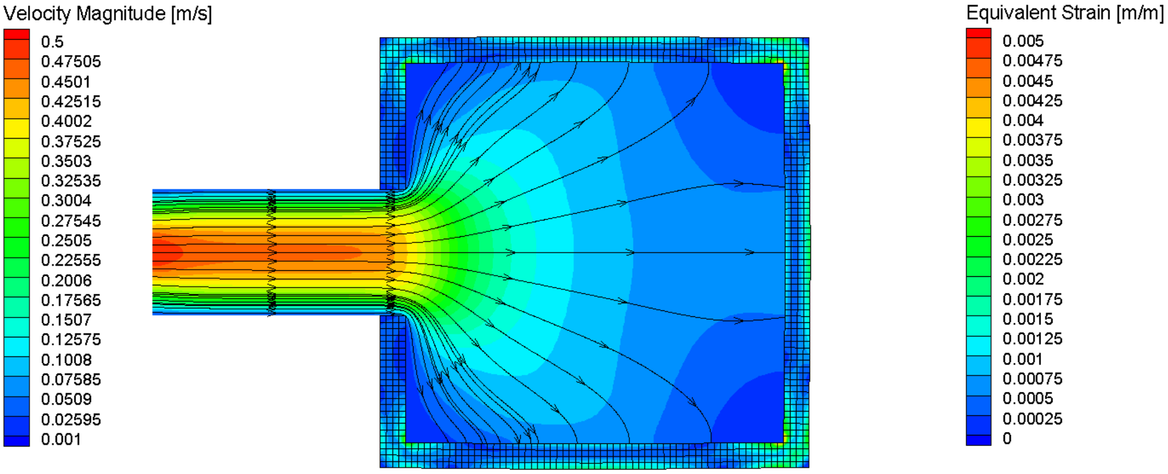

Figure 2.18: Square Balloon – Fluid velocity magnitude and structural strain for Simulation 1 at t = 0.5 second

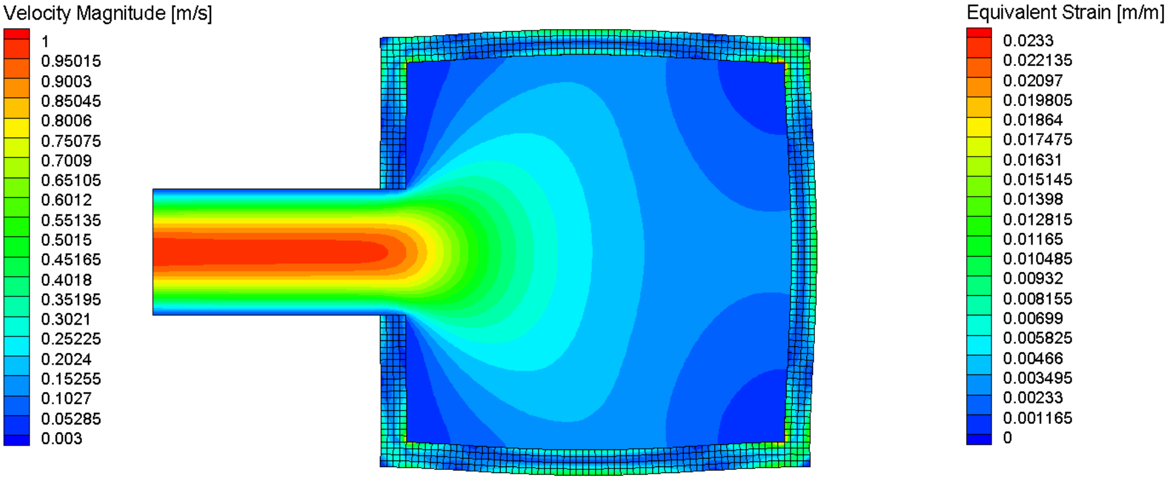

Figure 2.19: Square Balloon – Fluid velocity magnitude and structural strain for Simulation 1 at t = 1 second

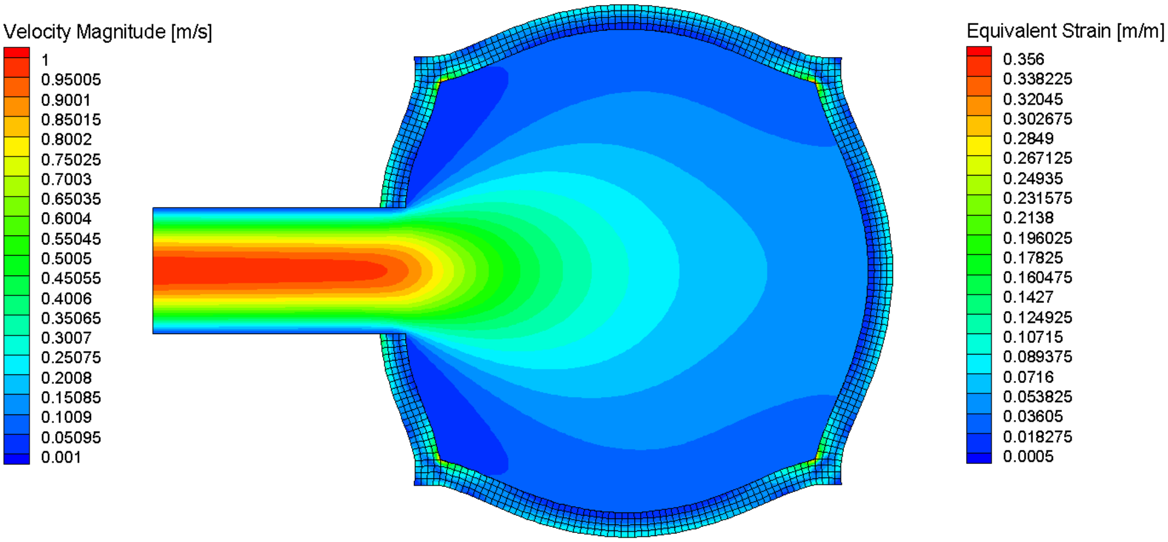

Figure 2.20: Square Balloon – Fluid velocity magnitude and structural strain for Simulation 1 at t = 5 seconds

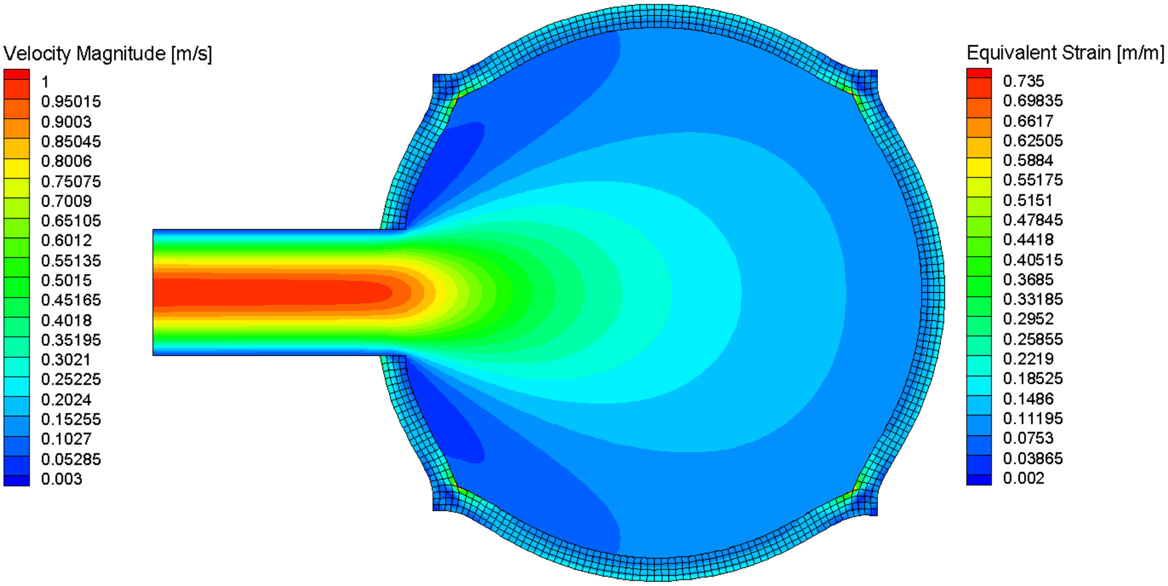

Figure 2.21: Square Balloon – Fluid velocity magnitude and structural strain for Simulation 1 at t = 9 seconds

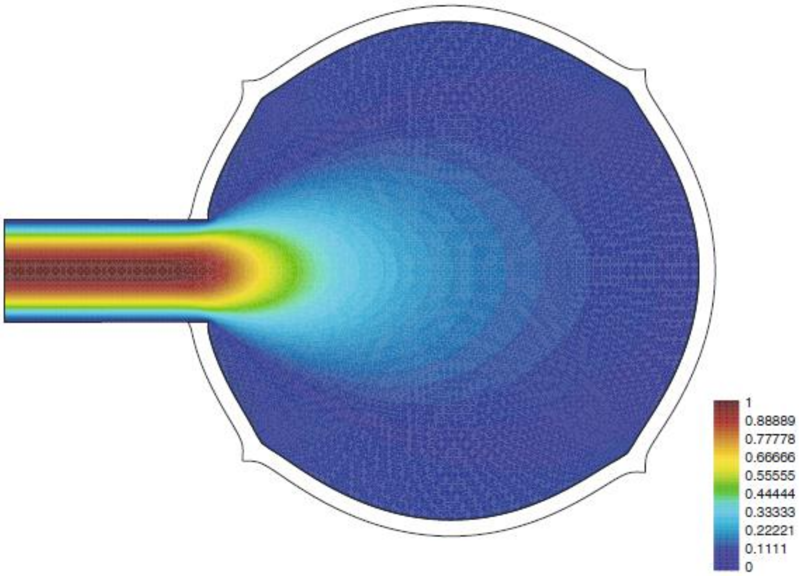

Figure 2.22: Square Balloon – Velocity (m/s) contour plot at t = 15 seconds from *Küttler et al.* [9]

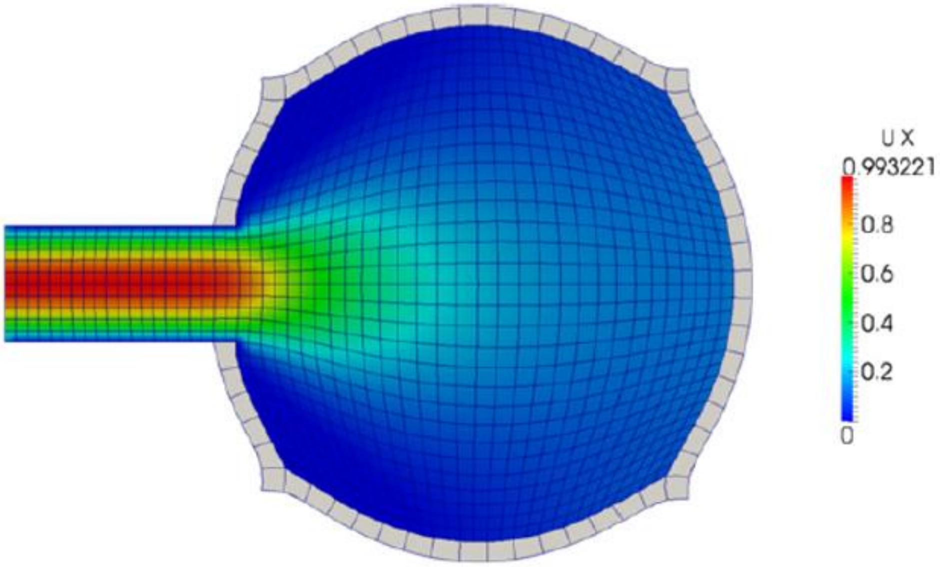

Figure 2.23: Square Balloon – Velocity (m/s) contour plot at t = 10 seconds from *Bogaers et al.* [10]

Comparing Figures 2.21-2.23, one can see that the velocities are almost the same in all three figures. Accordingly, the deformed shapes are similar to each other as well. From this, it can be concluded that the velocities applied and the behavior of the velocity contours agree with each other.

Similar to before, in addition to the velocity contour, the figures also show the Equivalent Strain at the respective time steps as well. The highest strains are occurring at the corners of the balloon where the fluid is pushing on the stress concentration points. It should be noted that the strain between the four figures, started out in the four corners and as the balloon expands, the strain slowly equilibrates on each side of the balloon.

2.4.5 Velocity Vector and Structural Deformation Contour

Provided below are the velocity vectors and solid deformation contour plots for the four time steps. The velocity vectors show the general flow direction and magnitude of the fluid. While the deformation for the solid region shows the amount the balloon deformed from the original position.

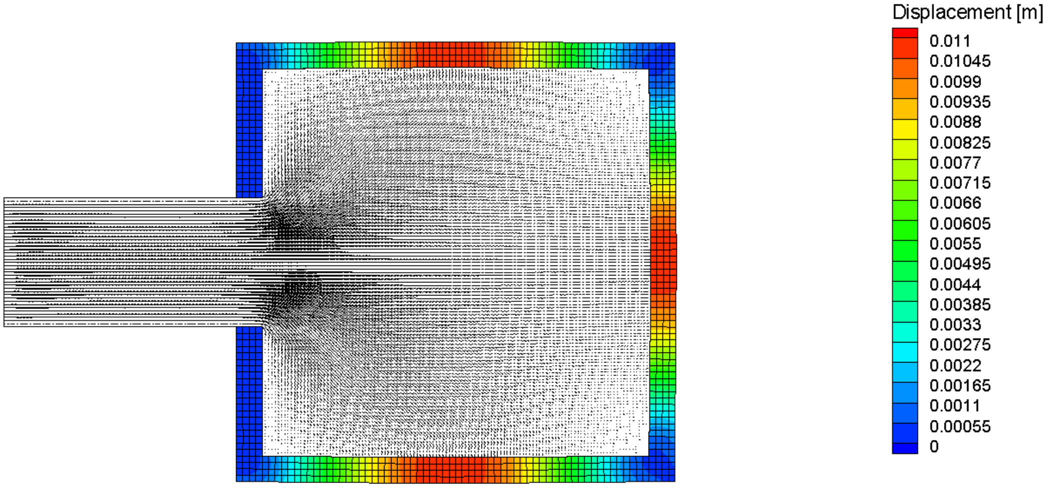

Figure 2.24: Square Balloon – Fluid velocity vector and structural deformation for Simulation 1 at t = 0.5 second

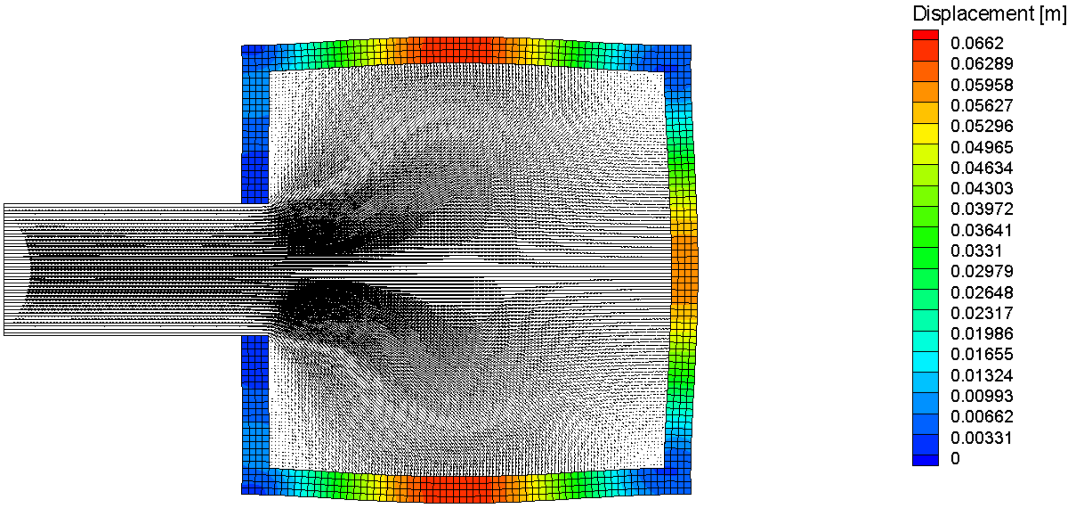

Figure 2.25: Square Balloon – Fluid velocity vector and structural deformation for Simulation 1 at t = 1 second

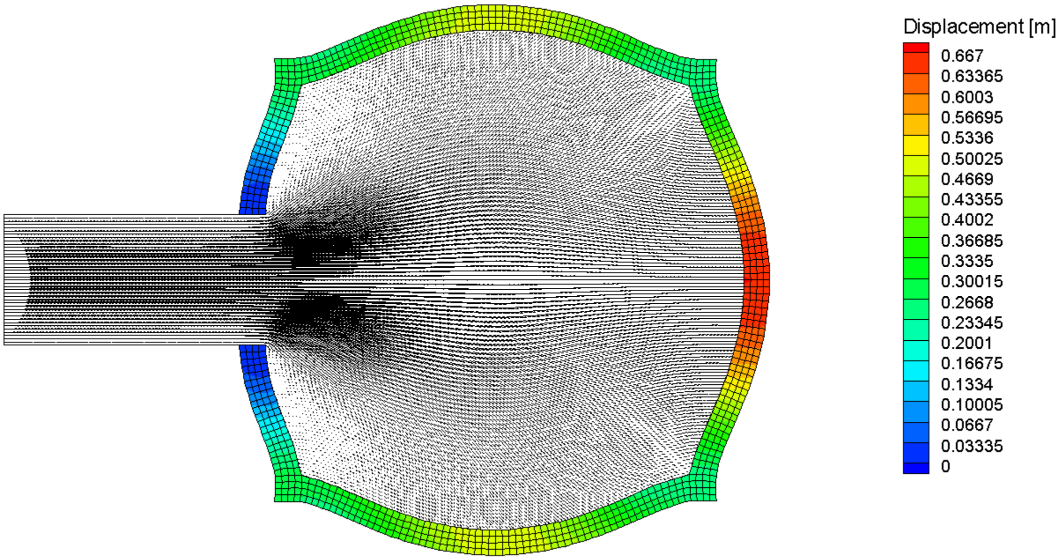

Figure 2.26: Square Balloon – Fluid velocity vector and structural deformation for Simulation 1 at t = 5 seconds

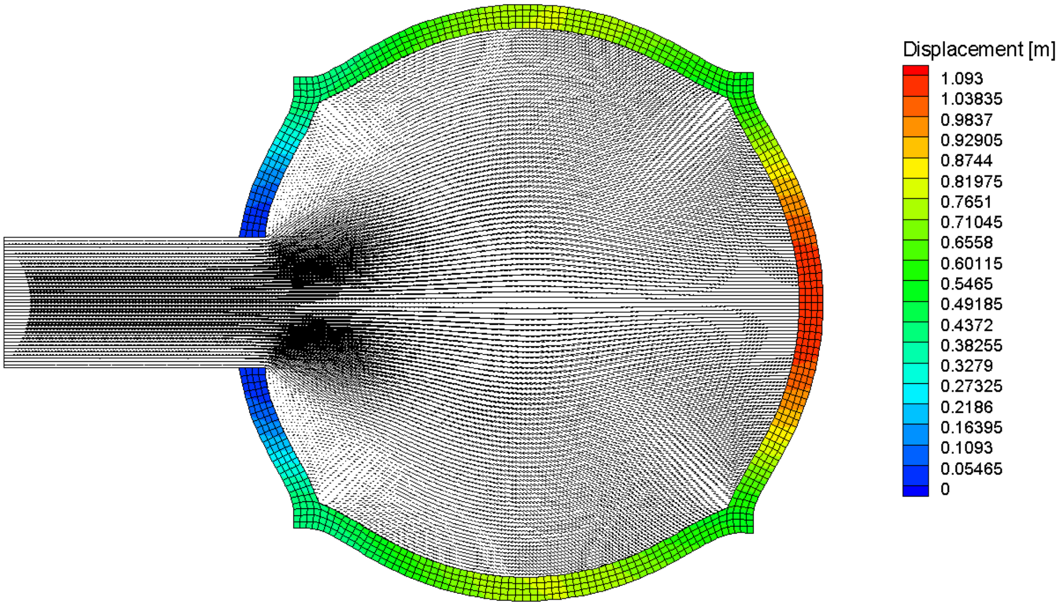

Figure 2.27: Square Balloon – Fluid velocity vector and structural deformation for Simulation 1 at t = 9 seconds

Based on Figure 2.27, the maximum deformation of the square balloon is 1.09 (m). Which means, in t = 9 seconds, the balloon grew by about 1/3 of its original size.

2.4.6 Solution Verification

A convergence study for the fluid region was performed to determine the type of convergence and the accuracy of the simulations. Convergence studies requires a minimum of three (m = 3) solutions to evaluate convergence. For this analysis, the pressures at t = 9 seconds in each simulation were used to evaluate the convergence.

Table 2.13: Square Balloon – Convergence values obtained from pressure data

Convergence Values		
1	Fine Mesh	S_1 = 8,026.53 (Pa)
2	Medium Mesh	S_2 = 8,114.43 (Pa)
3	Coarse Mesh	S_3 = 8,316.28 (Pa)

There are four types of convergence that a set of solutions can provide. The type of convergence is dictated by the *R* value.

Table 2.14: For Square Balloon – Types of convergences for CFD

Monotonic Convergence	$0 < R < 1$
Oscillatory Convergence	$R < 0$; $\lvert R\rvert < 1$
Oscillatory Divergence	$R < 0$; $\lvert R\rvert > 1$
Monotonic Divergence	$R > 1$

To calculate the R value, we need ε_{21} and ε_{32}.

$$\varepsilon_{21} = S_2 - S_1 \tag{2.11}$$

$$\varepsilon_{32} = S_3 - S_2 \tag{2.12}$$

$$R = \frac{\varepsilon_{21}}{\varepsilon_{32}} \tag{2.13}$$

ε_{21} and ε_{32} are the difference between the pressures (S_1, S_2, S_3). With the give equations, $\varepsilon_{21}, \varepsilon_{32}$, and the R value can be calculated and then used to determine what type of convergence (Table 2.14) was achieved. For this case, based on the R value, monotonic convergence was achieved.

The next step is to determine the observed order of accuracy, P_{RE}. The generalized Richardson extrapolation (RE) is used when the exact solution is unknown. However, with three numerical solutions and three different mesh sizes, the observed order of accuracy can be calculated. To calculate P_{RE}, $\varepsilon_{21}, \varepsilon_{32}$, and grid refinement ratio (r), will be used.

$$r = \frac{\Delta x_2}{\Delta x_1} = \frac{\Delta x_3}{\Delta x_2} \tag{2.14}$$

$$P_{RE} = \frac{\ln\left(\dfrac{\varepsilon_{32}}{\varepsilon_{31}}\right)}{\ln(r)} \tag{2.15}$$

r is the ratio between the meshes sizes. The mesh refinement between simulations must be consistent. For the square balloon case, the mesh sizes were refined by a factor of 2: x_1 is 4, x_2 is 2, and x_1 is 1.

Table 2.15: Square Balloon – Mesh refinement table

Simulation	**Mesh**	**Term**	**Element Size**
1	Fine Mesh	Δx_1	0.025 (m)
2	Medium Mesh	Δx_2	0.050 (m)
3	Coarse Mesh	Δx_3	0.100 (m)

Using information from Table 2.15 and equations (2.14) and (2.15), we obtain the values for *r* and P_{RE}, shown in Table 2.16 below. The error estimate, δ_{RE}, over or under predicts the comparisons between the pressures by a certain percentage.

$$\delta_{RE} = \frac{\varepsilon_{21}}{r^{P_{RE}} - 1} \tag{2.16}$$

Table 2.16: Square Balloon – Values for convergence study results

	S_1	S_2	S_3	ε_{21}	ε_{32}	R	r	P_{RE}	δ_{RE}
1, 2, 3	8,026.53	8,114.43	8,316.28	87.9	201.85	0.435	2	1.199	67.79

Next, using the values provided in Table 2.16, the uncertainty estimates can be calculated for the monotonic solution using the Factor of Safety (FS) method. The details of the FS method is described in *Xing et al.* [16] and [17]. In summary, the FS method has several constants: FS_0, FS_1, and FS_2. P_{th} is the theoretical order of accuracy, for this simulation, a second order upwind scheme was used. So the theoretical order is $P_{th} = 2$. Using the constants and P_{th}, the final form of the FS method is equation (2.18).

$$P = \frac{P_{RE}}{P_{th}} \tag{2.17}$$

$$U_{FS} = FS(P)\left|\delta_{RE}\right| = \left(2.45 - 0.85P\right)\left|\delta_{RE}\right| \tag{2.18}$$

For $0 < P < 1$

Using the Table 2.14 and equation (2.18) the results in Table 2.17 are obtained.

Table 2.17: Square Balloon – Uncertainty estimation results

	P	U_{FS} (%S_1)	Convergence Study
1, 2, 3	0.599	1.64%	Monotonic Convergence

For this study, the grid sizes converged monotonically, with a very small grid with an uncertainty of 1.64%S_1, based on the results from the FS method.

2.5 Conclusion

The square balloon case study consists of three grid sizes for the fluid and the solid regions. Each time the mesh size is refined, the step size would also proportionally decrease due to the nature of a transient analysis. The results where then compared to *Küttler et al.* [9] and *Bogaers et al.* [10] with several different parameters: pressure at Point A, pressure contour plots, and velocity contour plots. For pressure comparison at Point A, *Küttler et al.* [9] was not compared due to the offset of their pressure data. However, comparing the pressures of the three simulations with *Bogaers et al.* [10], indicated that the pressures are relatively close to each other. After calculating what is to be the analytical pressure (ideal gas pressure) for the fluid, the simulations achieved a more acceptable degree of accuracy. Furthermore, based on the convergence study and the FS method from *Xing et al.* [16] and [17], the square balloon pressures are producing results that have a low percentage of uncertainty. This demonstrates the simulation done in ANSYS SC, has a better accuracy than *Küttler et al.* [9] and *Bogaers et al.* [10]. Lastly, the comparisons between the pressure and velocity contour, the ANSYS simulations and literature plots agree with each other with respect to the general deformed shape and the pressure values obtained from their respective simulations. After comparing the results of the pressure curves and contours plots; it can be concluded that AC is a good starting point for complex simulations but the results would not be realistic. Based on the ANSYS simulations, the results are more realistic, but not perfect. Though ANSYS results are not perfect, it more closely resembles that observed in reality. For this quasi-2D balloon case, it is near impossible to conduct an experimental study, but the calculations backs up the simulation results pretty well. Therefore, the simulation results are believable enough such that the square balloon FSI setup can be used in other FSI studies.

Chapter 3: THREE-DIMENSIONAL BALLOON EXPANSION

3.1 Three-Dimensional Balloon Motivation

Numerical simulations have gained popularity in the recent decades due to the increase in availability of computational power. What would have taken months or years now can take as little as a week, a few days, or even a few hours. However, even with today's computational power, accurately simulating a simple 3D balloon geometry, is still quite challenging. Many researchers including *Chua et al.* [18], *Gervaso et al.* [19], *Zahedmanesh et al.* [20], and *Wang et al.* [21] have all conducted FEA simulations for stents in human arteries. The geometry of a stent, typically starts as a collapsed, cylindrical mesh around a tethered deflated balloon, known as a catheter. Once located, the balloon inflates, the cylindrical mesh will expand. Once the stent is in place the balloon deflates, and the catheter is then retrieved.

In addition, to the research conducted by *Chua et al.* [18], *Gervaso et al.* [19], *Zahedmanesh et al.* [20], and *Wang et al.* [21], other researchers have also done FEA simulations. For example, *Holzapfel et al.*[22] conducted FEA simulations for arteries and *Liu et al.* [23] conducted a thermal FSI simulation of a balloon. Many researchers have run FEA simulations of an enclosed balloon, in one way or another. Not many have done an interaction that uses fluid, such as air and structural material like rubber in an enclosed boundary. Many researchers have modeled various types of complex balloon geometries with FEA, such as a balloon attached to a stent or simulations of arteries and thermal FSI. However, a situation involving a region with fluid and a structural region, such as biological simulations, FEA is only half of the equation. For a study such as a lung simulation; where the entire respiratory lobes are expanding it is desirable to have expanding lobes when air flow is prescribed. Such simulation requires an FSI simulation, that takes into account both the fluid and structure near simultaneously. Therefore as a first step in simulating the fluid and structure coupling, would be to inflate a regular shaped balloon, as shown in Figure 3.1. An FSI simulation of a simple 3D balloon, has not been simulated that the author is able to find. The goal of this simulation is to provide a proof of concept for inflating a 3D balloon, without having to spend an abundant amount of computational resources.

3.2 3D Balloon Geometry

The balloon simulation was run using ANSYS 19.1 with the SC module, along with the Fluent and Transient Structural modules. The geometry was modeled using SolidWorks 2017 as two separate regions. The balloon geometry has a uniform geometry as shown in Figure 3.1, the ‘x’ direction is formed by revolving the geometry about the ‘z’ axis.

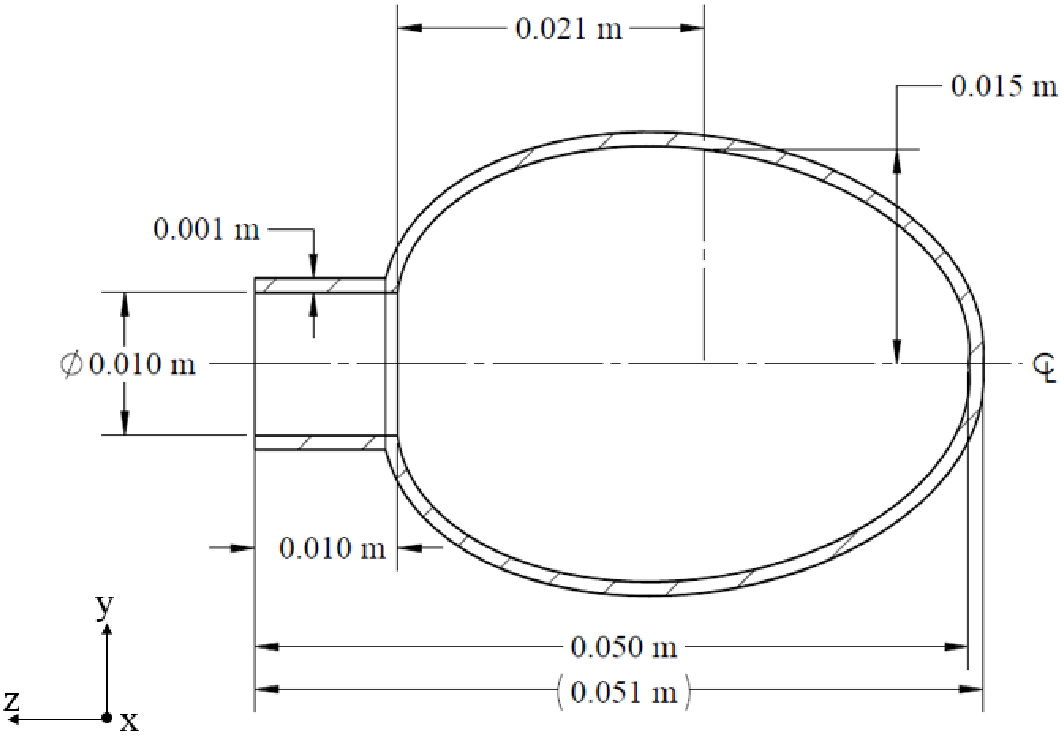

Figure 3.1: Section view of 3D Balloon geometry.

The structural region, hatched area, creates the outer boundary of the balloon. The fluid region, non-hatched area, is the inner region of the balloon with an inlet.

3.3 3D Balloon Methods

The methods for this case study are divided into several sections: Mesh, Boundary Conditions, Material Properties, and Convergence Settings. For this simulation only one mesh size was used, this simulation is a stepping stone for the real lung geometry simulation (Chapter 5), refer to Chapters 5 and 6 for additional details. ANSYS uses existing analytical systems along with the SC module to perform FSI analyses. For this simulation, ANSYS

Fluent and Transient Structural are the main analytical systems, which are coupled using the SC module (shown in Chapter 2, Figure 2.2).

3.3.1 Mesh

As stated earlier, only one mesh size was used for this case study. Unlike the 2D balloon, the 3D geometry of this balloon and the balloon's tendency to oscillate in the beginning requires a longer simulation time in comparison to the square balloon. The mesh settings given below are an attempt to balance a reasonable simulation run time and accurate results.

Table 3.1: 3D Balloon – Mesh settings for all fluid and structural regions

Mesh Settings	
Element Order	Linear
Element Size (m)	0.001
Growth Rate	1.2
Capture Curvature	Yes
Smoothing	Medium

Generally, to capture the behavior of the fluid, the element sizes are smaller and tend to have more elements, in comparison to the solid region. In this case, the fluid and structural region have the same element size. The main reason is to capture the rapid balloon wall expansion better. Generally speaking, more elements and smaller element sizes will numerically capture the behavior of the region better. In the case of this 3D balloon, the walls are growing rapidly, and if the elements are stretched too far then that can cause the simulation to fail. Likewise, if the elements are too small, rapid inflation can cause elements to collapse, which results in a negative volume element. When negative volume happens to an element, the simulation will error.

Table 3.2: 3D Balloon – Mesh properties for the fluid and structural regions

Fluid Region		Structural Region	
Number of Elements	Element Size	Number of Elements	Element Size
101,407	0.001 (m)	33,255	0.001 (m)

Using the settings from Table 3.1 and Table 3.2, the mesh for the 3D balloon are shown in Figure 3.2. and Figure 3.3.

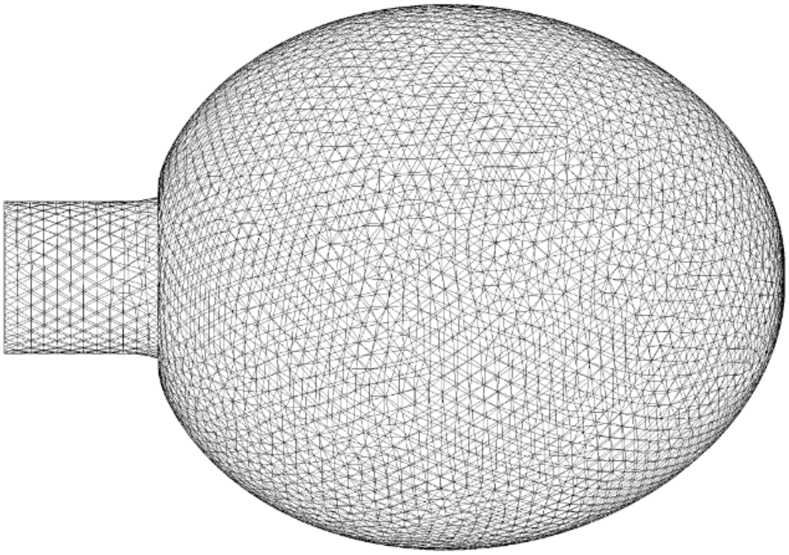

Figure 3.2: 3D Balloon fluid mesh, side view

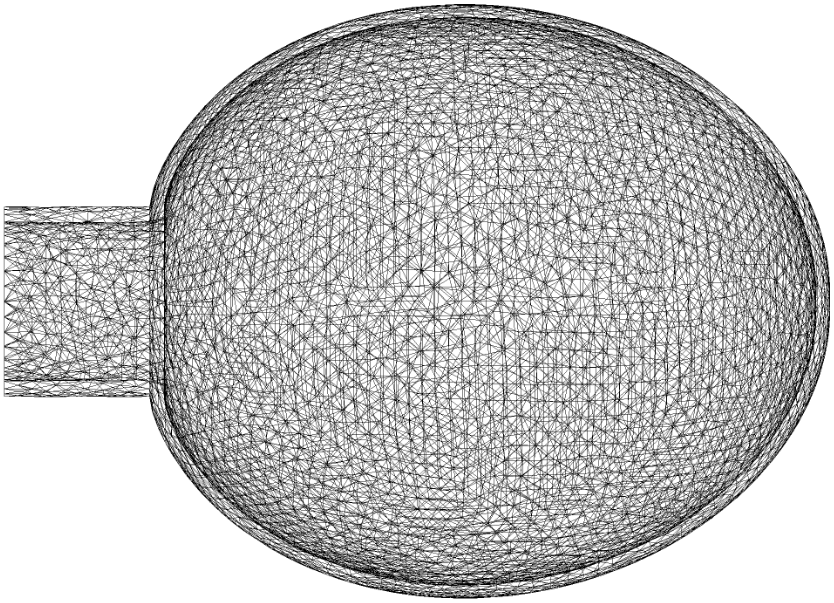

Figure 3.3: 3D Balloon solid mesh, side view

Additional mesh views are shown in Appendix B – Chapter 3: Three-Dimensional Balloon Expansion for this case study.

3.3.2 Boundary Conditions

The BCs in this case study, includes an elastic support. The elastic support BC serves as a stabilizer for the balloon. Without the elastic support the balloon can expand too quickly and will start to physically oscillate, shown in Figure 3.4. In Figure 3.5 are the BCs used in the 3D balloon simulation. The balloon is fixed around the ‘neck’ as indicated with the triangles in the figure. An elastic support (bubbled region) surrounds the whole balloon to provide a stiffness that the balloon must overcome to expand. The elastic support is defined as a pressure that produces a normal force on the surface applied. Which means other forces such as tangential forces will not be affected, only the normal forces on the surface will experience resistance from the BC.

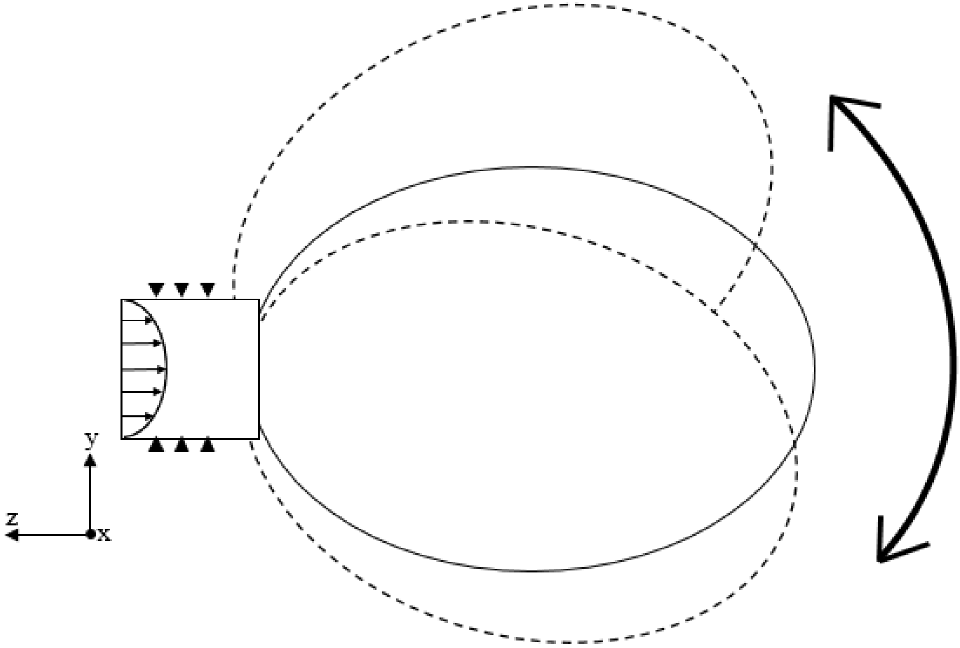

Figure 3.4: 3D Oscillating balloon

When the balloon starts to oscillate, the oscillating motion is near impossible to do in a reasonable amount of time. In order to capture the motion, the step size must be very small, which results in a longer simulation time. The motion is not only complicated and unnecessary but it complicates the results and requires an unfathomable amount of time to simulate. By adding an elastic support solves the oscillation issue that physics presents. Next, an FSI surface BC is on the inside walls of the balloon. This BC couples the fluid and solid components together for the simulation. This surface is where the SC module will perform the computation.

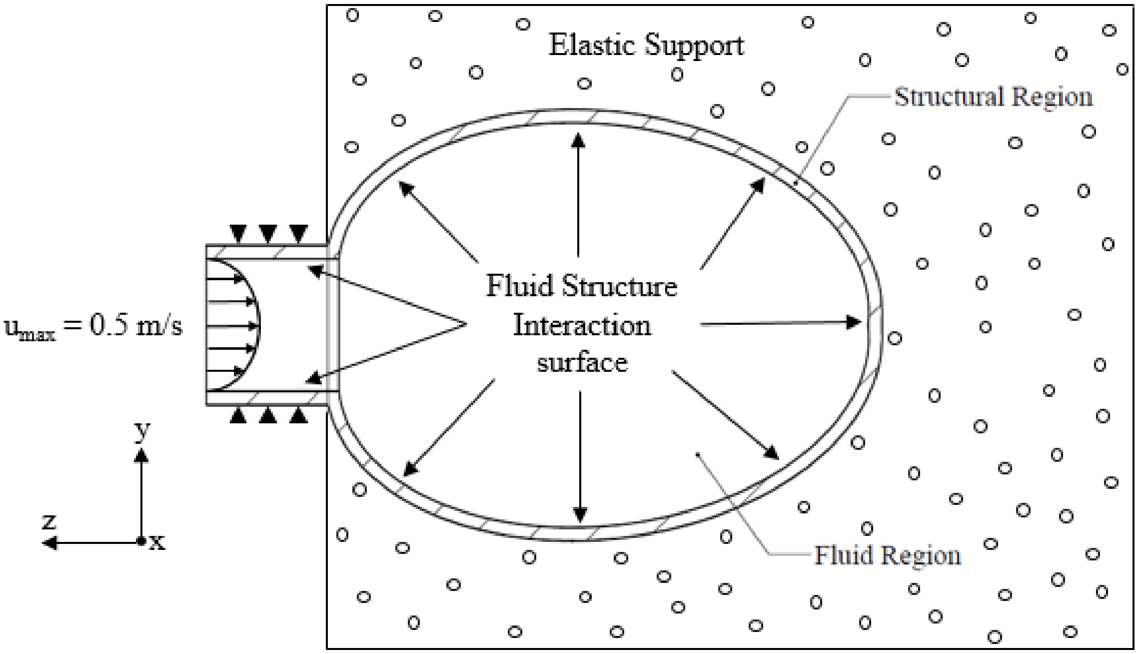

Figure 3.5: Boundary condition of 3D Balloon

The elastic support value used for this simulation is 10,000 (N/m^3). This value is calculated based on a vertical hydrostatic force, F_v, of water. Water is incompressible, and as the height changes the water pressure will change as well. Assuming the volume of the water can be displaced as the balloon expands, the elastic support parameter can be calculated with equation (3.1).

$$F_v = \rho V g \tag{3.1}$$

where ρ is the density, V is the volume, and g is gravity. Since the support is in terms of N/m^3, and knowing ρ = 999 (kg/m^3) and g is 9.806 (m/s^2), F_v/V will come out to be approximately 10,000 (N/m^3).

Lastly, the maximum velocity inlet is 0.5 (m/s). However, the prescribed velocity is not a uniform, constant velocity profile. Similar to the velocity used for the square balloon in Chapter 2, the maximum velocity, u_{max}, from 0 to 1 second is a sinusoidal curve:

$$u_{\max} = \frac{\sin(\pi(t+\frac{3}{2}))+1}{4}\,. \tag{3.2}$$

Subsequently, after the first second the velocity is constant at 0.5 (m/s).

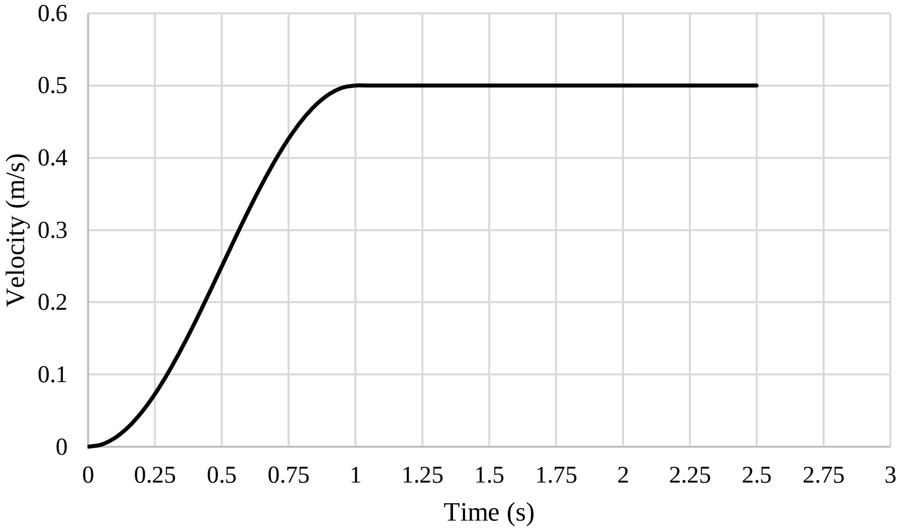

Figure 3.6: Velocity profile for the 3D Balloon

Having a sinusoidal profile in the beginning is to avoid pressure oscillations. In addition, to the sinusoidal profile in the first second, the velocity is constant at 0.5 (m/s) because if the pressure inside the balloon grows too quickly then the elastic support will not be enough to stabilize the balloon. If the balloon is not stable, then it can cause elements in either the solid or fluid regions to change too rapidly, which then can cause negative cell volume or elements that get stretched too thin, in turn causing the simulation to error. Therefore, for this simulation, not only will the velocity have a slow ramping start, but the velocity itself is also fairly slow.

The Re for this 3D balloon case is 3.37 which makes it laminar flow; similar flow to the quasi 2D square balloon. Refer to the Material Properties section for kinematic viscosity value. For the flow to be turbulent, Re must be 4000 or greater.

$$\mathrm{Re} = \frac{\rho u L}{\mu} = \frac{uL}{\upsilon} = 3.37 \tag{3.3}$$

In equation (3.3), ρ is density, u is velocity, L is the characteristic dimension, in this case the diameter, μ is the dynamic viscosity, and υ is the kinematic viscosity.

Similar to Chapter 2, this simulation has a moving boundary that was added to the fluid region. A dynamic mesh moves with the fluid such that the elements re-mesh after every iteration. Simulations with dynamic meshes are used to avoid negative volume, unwanted distortion in the elements, or in most cases a boundary in motion. For this FSI simulation, both smoothing and re-meshing dynamic mesh methods were used. Table 3.3 and Table 3.4 summarizes the settings.

Table 3.3: 3D Balloon – Smooth re-meshing settings

Smoothing	
Diffusion	-
Diffusion Function	Boundary-distance
Diffusion Parameter	1.5

There are several Smooth re-meshing methods, reference 2.3.2 for more details. For this case, the diffusion method was chosen. Next the re-meshing parameters are based upon the mesh scale information, shown in Figure 3.7.

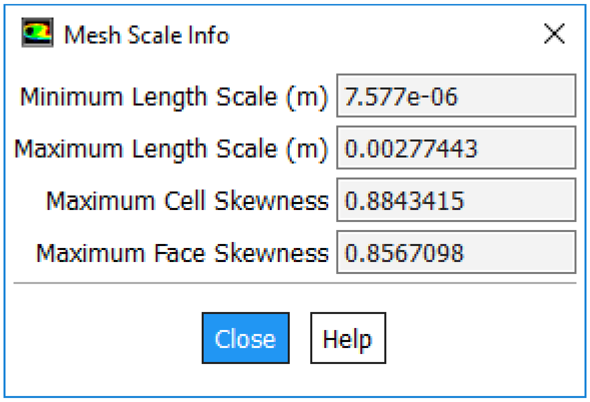

Minimum Length Scale (m) 7.577e-06
Maximum Length Scale (m) 0.00277443
Maximum Cell Skewness 0.8843415
Maximum Face Skewness 0.8567098

Figure 3.7: Mesh scale information of 3D Balloon from ANSYS Fluent

With the given parameters the values in Table 3.4 were used for re-meshing. The mesh must stay between the given thresholds after every iteration. If the elements after every iteration do not meet the criteria in the re-meshing parameter, the mesh will be re-meshed. However, re-meshing can be computational expensive, if possible, refrain from re-meshing every iteration. Re-meshing every iteration can increase the accuracy of the results. However depending the element sizes, number of iterations, and the geometry; it may not be advantageous to re-mesh every iteration.

Table 3.4: 3D Balloon – Re-meshing mesh parameters

Re-meshing Parameter	
Minimum Length Scale (m)	7.6E-06
Maximum Length Scale (m)	0.003
Maximum Cell Skewness	0.7
Maximum Face Skewness	0.7
Size Re-meshing Interval	1

Lastly, with the Smoothing and Re-meshing parameters set, the DMZs will also need to be set. The DMZs are what Fluent uses to map region(s) to the FSI surface(s) on the solid region and allows for the dynamic mesh to actual occur. For this case, there are two zones: the “Interior” and “Wall”.

Table 3.5: 3D Balloon – Dynamic Mesh Zone settings

Dynamic Mesh Zones	
Zone Names	Type
Interior	Deforming
Wall	System Coupling

Referencing Table 3.5, the “Interior” is set to “Deforming”, the elements will deform and move as needed to accommodate the change in the fluid. “Wall” is set to “System Coupling”, this BC is when Fluent will transfer the information to the structural module, where FSI surface will receive the information, and perform its computation.

3.3.3 Material Properties

The materials for the fluid and structural regions are given in Table 3.6 below. To keep the simulation simple, a linear elastic silicone rubber was chosen for the structural region and air is the driving fluid.

Table 3.6: 3D Balloon – Material properties for the fluid and structural regions

Fluid Material Properties	**Parameters**	**Value**
Density, ρ (kg/m^3)	Ideal - gas	-
Specific Heat, Cp (J/kg-K)	Constant	1006.43
Thermal Conductivity, κ (W/m-K)	Constant	0.242
Dynamic Viscosity, μ (kg/m-s)	Constant	1.7894E-05
Molecular Weight, M (kg/kmol)	Constant	28.966
Structural Material Properties	**Parameters**	**Value**
Density, ρ (kg/m^3)	-	1250
Isotropic Elasticity	-	
	Young's Modulus, E (Pa)	7.93E+07
	Poisson's Ratio, υ	0.48
	Bulk Modulus, K (Pa)	6.6083E+08
	Shear Modulus, G (Pa)	2.6791E+07

The silicone rubber material properties were obtained from MatWeb, an online material property database.

3.3.4 Convergence Settings

To ensure the results comply with real world physics, the convergence settings provide the solver guidelines of when the results are satisfactory. Fluid behavior tends to be more complex, therefore most of the convergence settings are for the fluid region. In ANSYS Fluent, the Solution Methods are left at default. The Residual Convergence values are changed to such that the iterative error is minimized and has negligible effect on the results.

Table 3.7: 3D Balloon – Fluid region main convergence settings

Solution Methods	
Scheme	SIMPLE
Gradient	Least Squares Cell Based
Pressure	Second Order
Density	Second Order Upwind
Momentum	Second Order Upwind
Energy	Second Order Upwind
Transient Formulation	First Order Implicit
Residual Convergence	
Continuity	1e-05
x-velocity	1e-05
y-velocity	1e-05
z-velocity	1e-05
Energy	1e-06

Table 3.8 has the convergence settings for the SC. The convergence criteria for data transfers are defaulted to RMS Convergence Target = 0.005. The convergence settings for the SC are independent of the fluid and structural systems. For more details regarding how the SC data transfer works refer to section 2.3.4.

Table 3.8: 3D Balloon – SC Data Transfer settings

Data Transfer 1		**Data Transfer 2**	
Source:	Fluent	Source:	Transient Structural
Region:	Wall-fff_solid 1	Region:	Fluid Solid Interface
Variable:	Force	Variable:	Displacement
Target:	Transient Structural	Target:	Fluent
Region:	Fluid Solid Interface	Region:	Wall-fff_solid 1
Variable:	Force	Variable:	Displacement

Shown in Table 3.9 are the simulation settings for the fluid and structural regions, as well as the SC module. The end time for the simulation from Fluent, Transient Structural, and SC module, must match or the simulation will not run.

Table 3.9: 3D Balloon – Simulation settings for the three modules

	Fluid Region	**Solid Region**	**SC**
Simulation Time (s)	2.5	2.5	2.5
Time Step Size (s)	0.001	0.01	0.01
Number of Time Steps	2500	-	-
Large Deflection	-	On	-
Minimum Iterations	-	-	1
Maximum Iterations	75	-	30

As stated in Chapter 2, when running an FSI simulation in ANSYS, the SC settings override the structural and fluid simulation settings. However, for consistency, the settings for the fluid and structural regions should also be inputted before running the simulation. The step size for each simulation is different.

3.4 Results

As stated previous, only one mesh was used for the simulation. For the BCs given, the simulation can only go up to 2.5 seconds before the simulation fails. This is mainly due to the step size and the element mesh sizes. The chosen material, mesh size, and step size were to optimize the run time. The results section for this chapter will be divided between the solid region and the fluid region. The solid region will focus on the von Mises stresses, equivalent strain, and displacement. While the fluid region will have velocity magnitude in 2D and 3D contours and pressure plots. All contour plots and graphs were created using Tecplot 360 EX 2017 R2.

3.4.1 3D Balloon – Structural Region

Figure 3.8 shows the growth of the balloon and the change in von Mises stresses at six times.

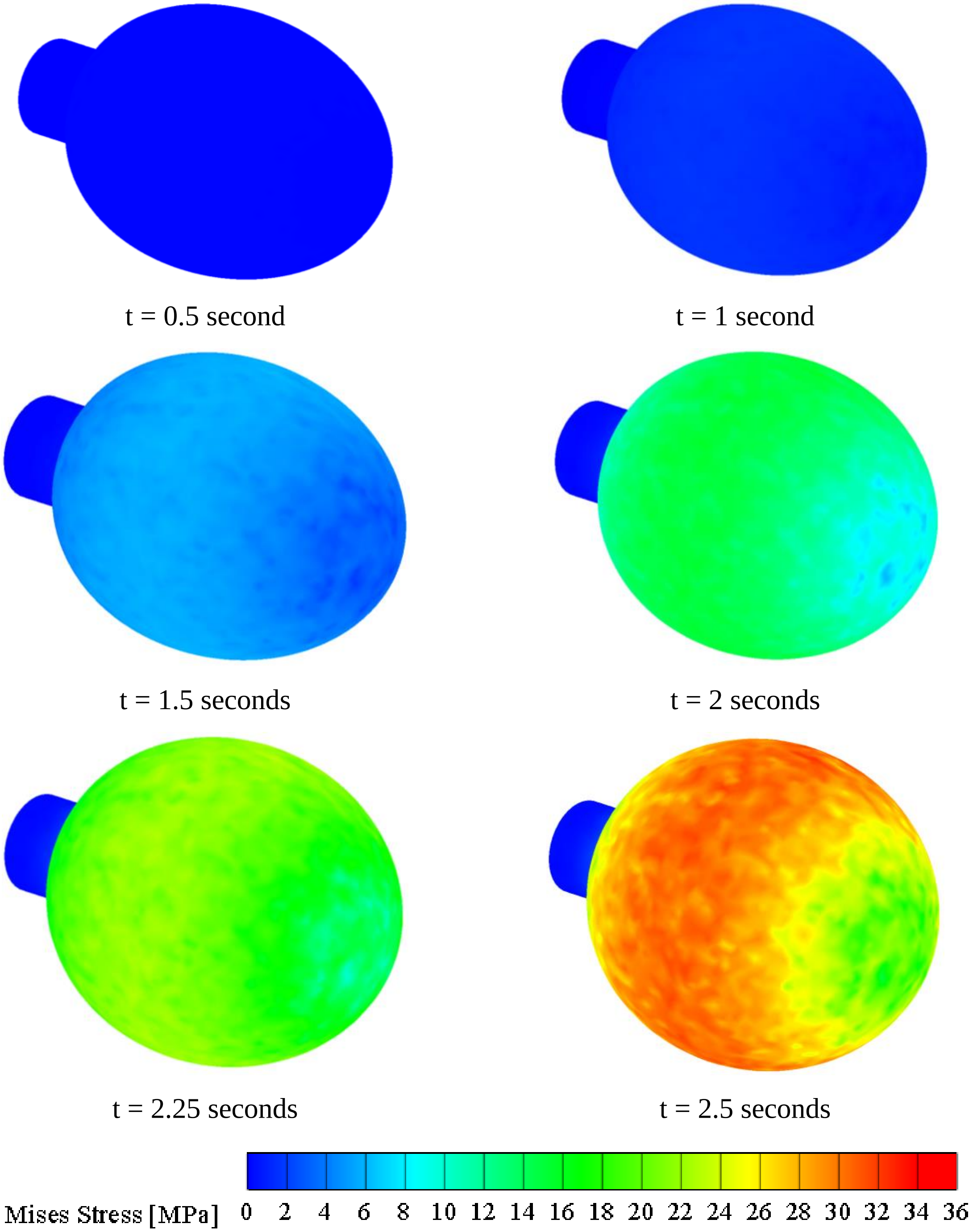

t = 0.5 second

t = 1 second

t = 1.5 seconds

t = 2 seconds

t = 2.25 seconds

t = 2.5 seconds

Figure 3.8: 3D Balloon – von Mises stress at six different times

(Note: The von Mises stress is displayed in MPa for legend simplicity.)

It can be deduced from Figure 3.8, between t = 0.5 second and t = 1 second, that the balloon has minimal growth. Therefore, the stress is not very high. Once the time is greater than one second the stress increases rapidly. Reason being, once the balloon obtains adequate air flow to grow, the pressure from the constant flow of air expands the balloon exponentially.

The fluid pressure increase behavior is shown in Figure 3.24 (b). The maximum von Mises stress value at t = 1 second is ≈ 1 (MPa), then at t = 1.5 seconds the maximum stress is ≈ 7 (MPa), and finally at t = 2.5 seconds the maximum stress is ≈ 34 (MPa). The difference between t = 1 second and t = 1.5 seconds is 6 (MPa), while the difference between t = 1.5 seconds and t = 2.5 seconds is 27 (MPa). Even though the last two compared times are longer by 0.5 second, the growth is not linear. (Please refer to Appendix B – Chapter 3: Three-Dimensional Balloon Expansion for all shown time steps in a larger format).

Shown in the figure below, the maximum stress is not around the transition point between the fixed neck and the body. The maximum stress is around the main body, where the maximum displacement of the body is located.

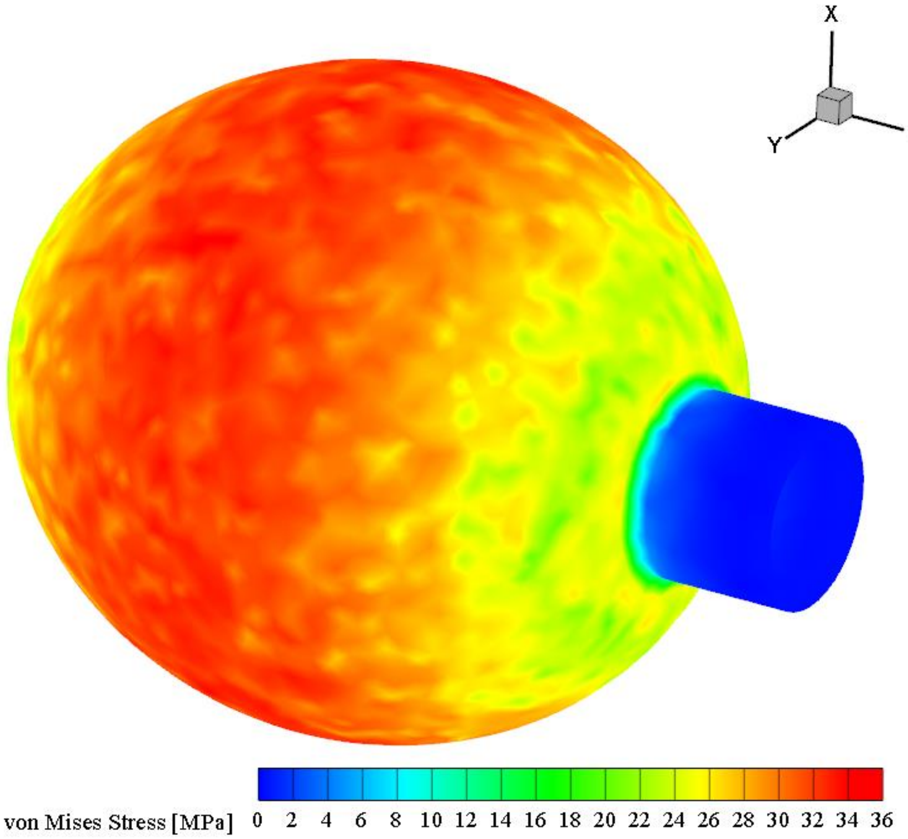

Figure 3.9: 3D Balloon – Rotated isometric view of von Mises stress, t = 2.5 seconds

The explanation for this is that the balloon geometry is similar to a cylindrical pressure vessel. For a cylindrical pressure vessel, the hoop stress (σ_{hoop}) is higher than the longitudinal stress (σ_{long}).

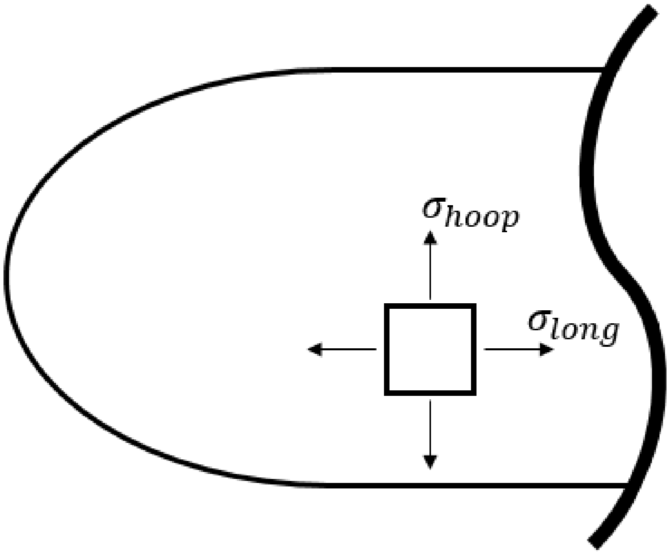

Figure 3.10: 3D Balloon – Cylindrical pressure vessel stress orientation

In Figure 3.10 above are the orientation of the stresses and the equation for the two stresses are shown below.

$$\sigma_{long} = \frac{pd}{4t} \tag{3.4}$$

$$\sigma_{hoop} = \frac{pd}{2t} \tag{3.5}$$

From equations (3.4) and (3.5), it is shown that the hoop stress is twice the longitudinal stress, for certain geometries. For this particular case, the balloon, is more elliptical than cylindrical in geometry. However, analytical equations for elliptical pressure vessels are not readily available. Many researchers have approached this problem through the use of FEA and then analytically solved cylindrical or spherical stresses equations to estimate the stress.

Next are the equivalent strains, similarly in Figure 3.11 the strains are showing exponential growth after 1 second. (Please reference Appendix B – Chapter 3: Three-Dimensional Balloon Expansion for all shown time steps in larger format).

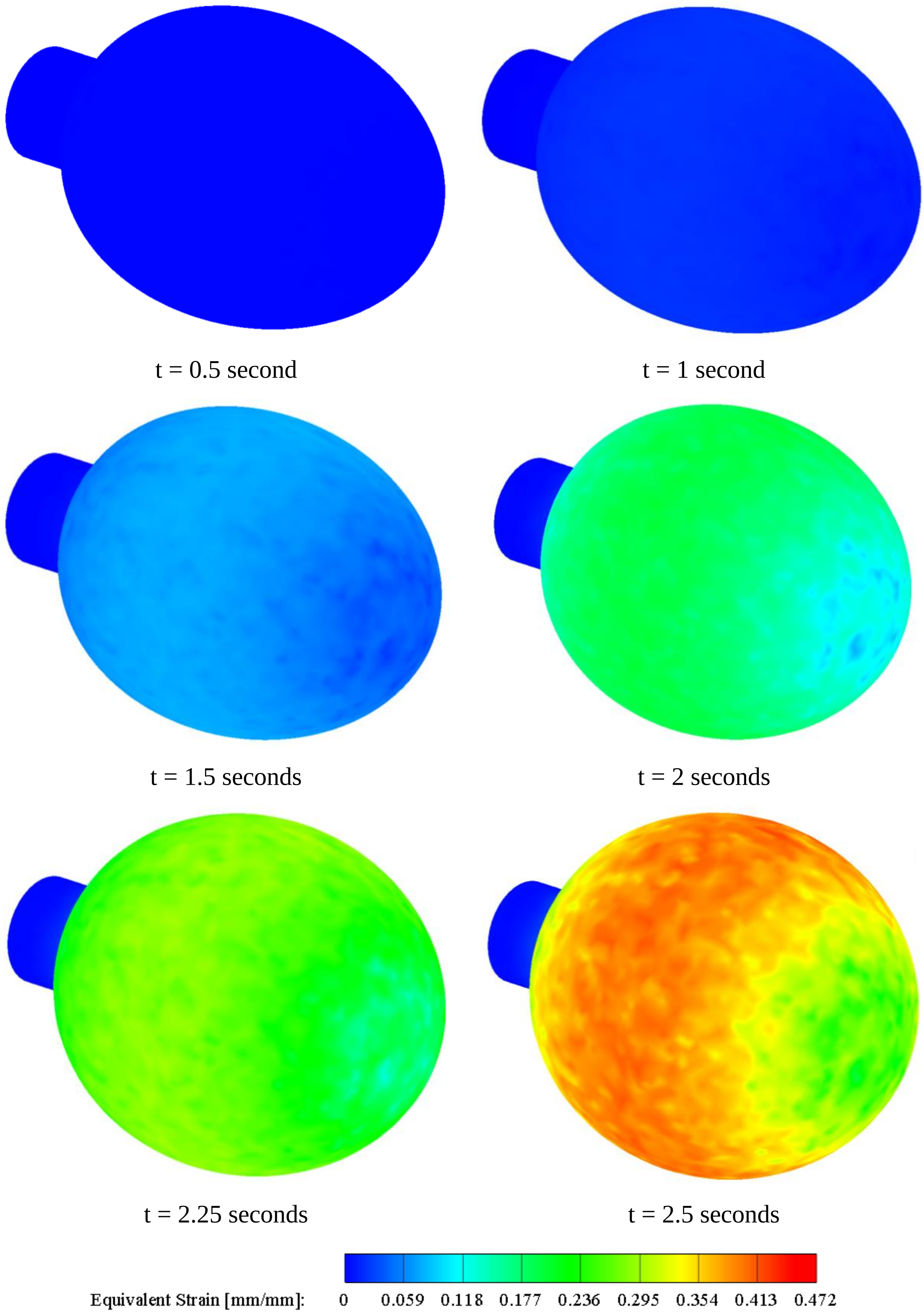

t = 0.5 second

t = 1 second

t = 1.5 seconds

t = 2 seconds

t = 2.25 seconds

t = 2.5 seconds

Figure 3.11: 3D Balloon – Equivalent strain from the same six times as the stresses

Comparing Figure 3.8 and Figure 3.11, it can be observed that the stress and strain have the same contour which is due to the material assignment. The silicone rubber properties are linear isotropic, which results in the stress and strain having proportional behaviors. Having linear properties, according Hooke's Law equation (3.6), will result in a linear relationship for the stress and strain.

$$\sigma = E\varepsilon \tag{3.6}$$

where σ is stress, E is the elastic modulus, and ε is the strain. Shown in Figure 3.12 is the stress-strain curve obtained from the ANSYS simulation of the 3D balloon.

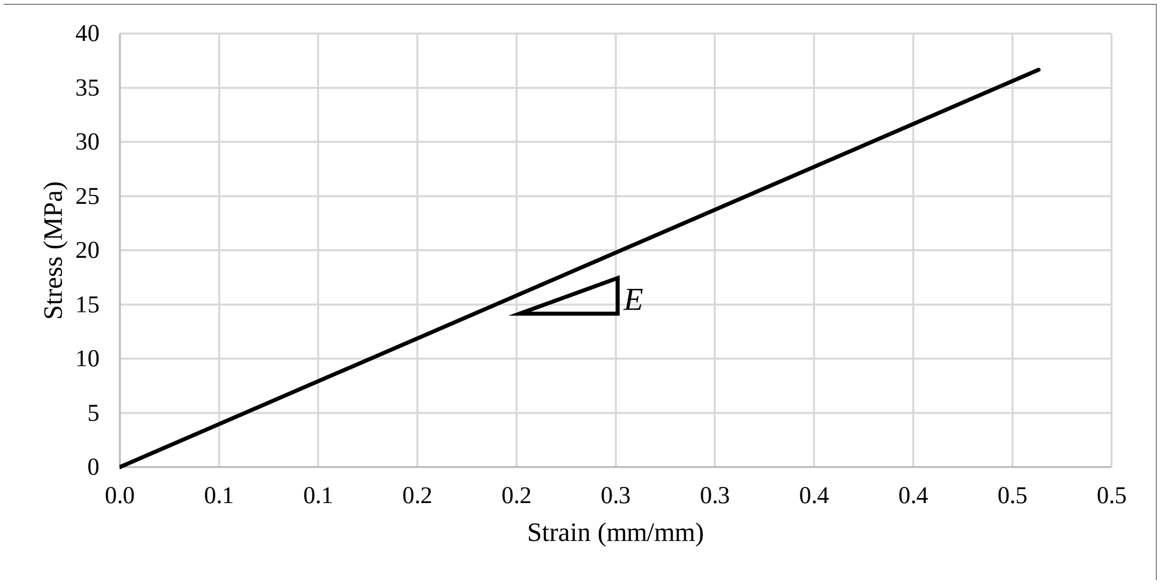

Figure 3.12: 3D Balloon – Stress-strain curve from simulation

As shown in the figure, the stress-strain relationship follows Hooke's Law. Hence, the stress and strain showing similar contours.

Lastly, the displacement of the balloon is shown in Figure 3.13 below. It can be observed from Figure 3.13, at t = 2.5 second, the maximum displacement is in the center of the balloon body. Since the balloon is similar to a cylindrical pressure vessel, the Poisson Effect is in play. *Roylance* [24] showed that the Poisson effect can also be derived from Hooke's Law and shows the relationship between deformation and strain.

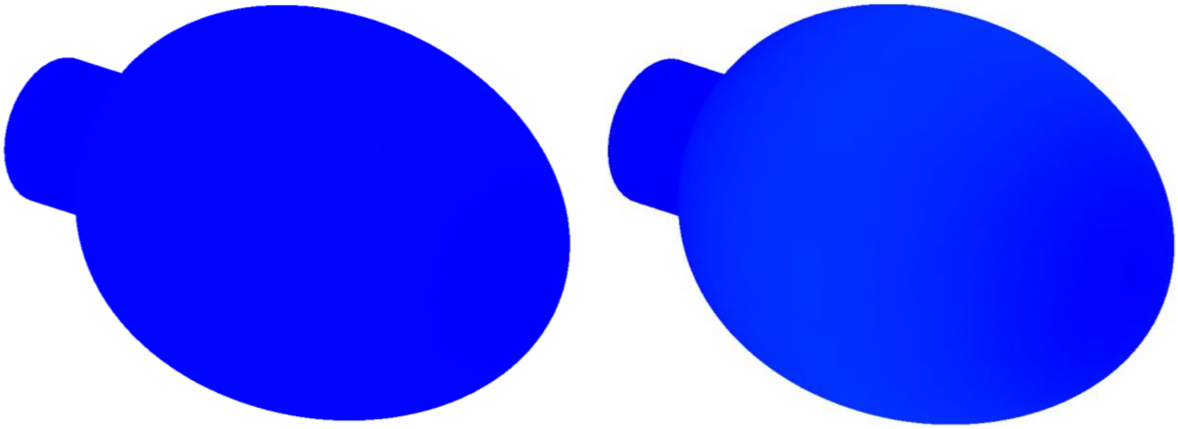

t = 0.5 second

t = 1 second

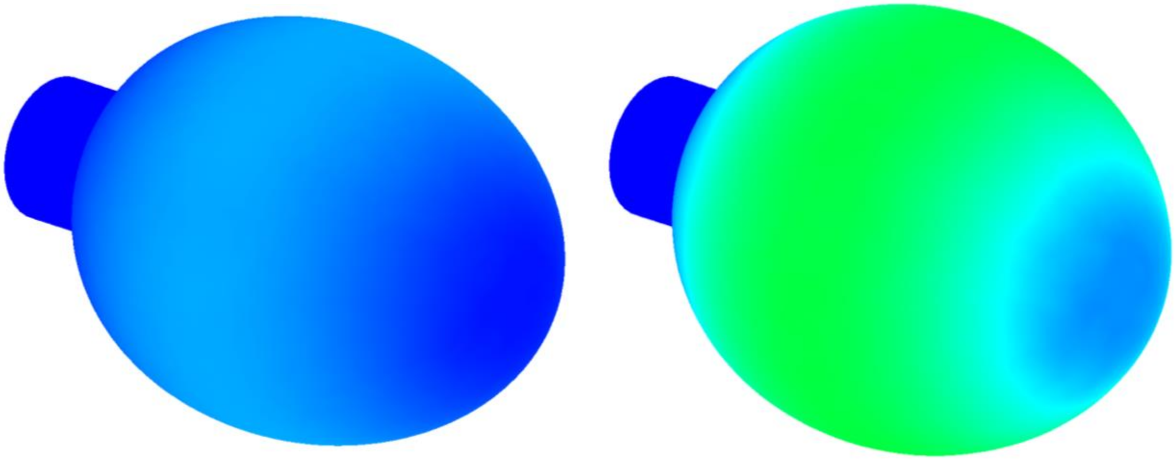

t = 1.5 seconds

t = 2 seconds

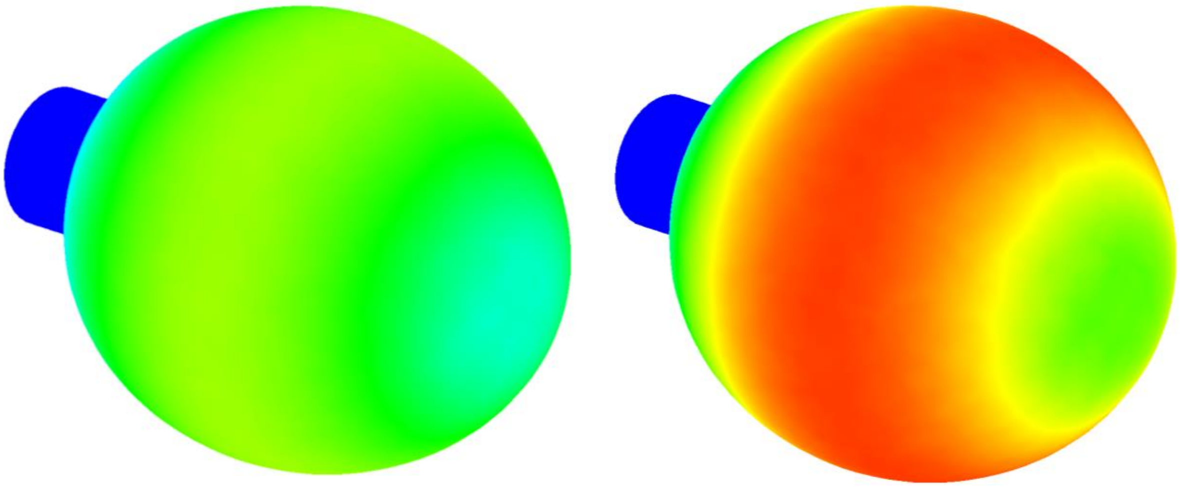

t = 2.25 seconds

t = 2.5 seconds

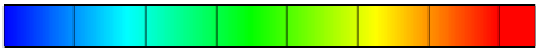

Figure 3.13: 3D Balloon – Displacement from six different times

From Figure 3.13, there is no change in displacement between t = 0.5 second and t = 1 second. Based on the velocity profile graph, Figure 3.6, between t = 0 and t = 1 second, the change in velocity is slowly ramping up and the air has not filled the interior space of the balloon yet, so the change is minimal between these two time steps.

As previously stated, through Hooke's Law the deformation has a Poisson's effect. *Roylance* [24] demonstrated this derivation with the following equations.

$$\varepsilon_\theta = \frac{pr}{2tE} \tag{3.7}$$

$$\delta_C = C\varepsilon_\theta = 2\pi r\left(\frac{pr}{2tE}\right) \tag{3.8}$$

$$\delta_r = \frac{\delta_C}{2\pi} \tag{3.9}$$

$$\delta_r = \frac{pr^2}{2tE} \tag{3.10}$$

Note, θ in equation (3.7) means "hoop" and in equation (3.8), C is for the circumference of the cylinder. Equation (3.10) relates the change in circumference and the corresponding change in radius. Since ANSYS results will be showing the deformation from the reference point, which is the centerline of the balloon, the deformation should be in terms of either diameter or radius. Lastly, equation (3.10) states that the deformation should have a parabolic behavior because of the r^2 value. Shown below is the deformation from the ANSYS simulation.

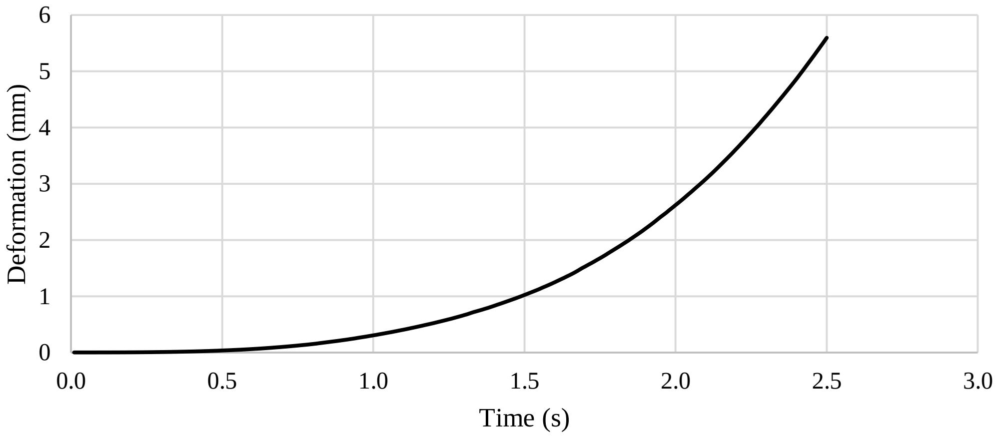

Figure 3.14: 3D Balloon – Deformation with time

As represented in Figure 3.14 the deformation is indeed parabolic as stated in equation (3.10). Additional analysis can be done beyond what this chapter has described to verify the simulation.

A future goal would be to use nonlinear material properties for the rubber and add turbulence to the air flow. Please see the Fluid Region results for further explanation of the behavior of the air inside the balloon.

3.4.2 3D Balloon – Fluid Region

For the Fluid region, the main focus will be the velocity and pressure behavior inside the balloon. Since the velocity of the air going into the balloon is laminar, and the solid region has linear isotropic properties, the flow of air is relatively symmetric. However, the geometry still has sharp corners where the FSI region is. In addition, the “nose” of the balloon provides a “cushion” for the air; also known as a stagnation point, which can cause asymmetric flow in the returning air. If the reverse flow becomes asymmetric, that can cause the incoming flow to become asymmetric as well.

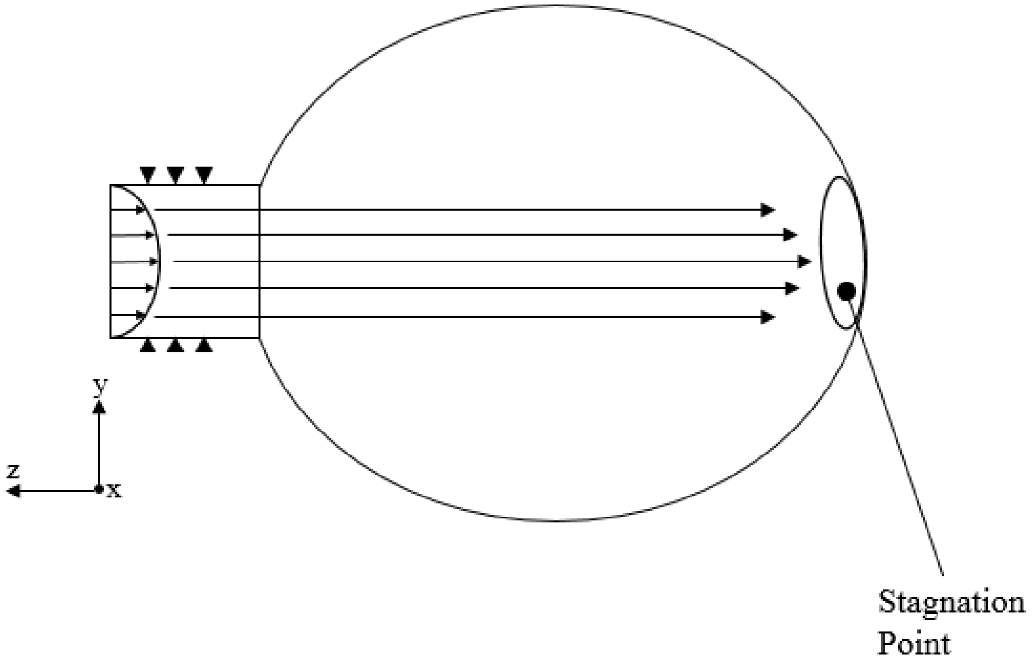

Figure 3.15: 3D Balloon – Behavior of air flow in balloon

The stagnation point can be seen in Figure 3.16 between t = 0.7 second and t = 1.5 seconds; other figures in the chapter also shows this phenomenon.

Starting with the direction of flow for the air, the flow is prescribed in the Z axis direction. Therefore, Figure 3.16 only shows the direction of flow with respect to the Z axis. The figure is from six different times sliced with two planes. The balloon is sliced in the x and y direction to show the flow of the air.

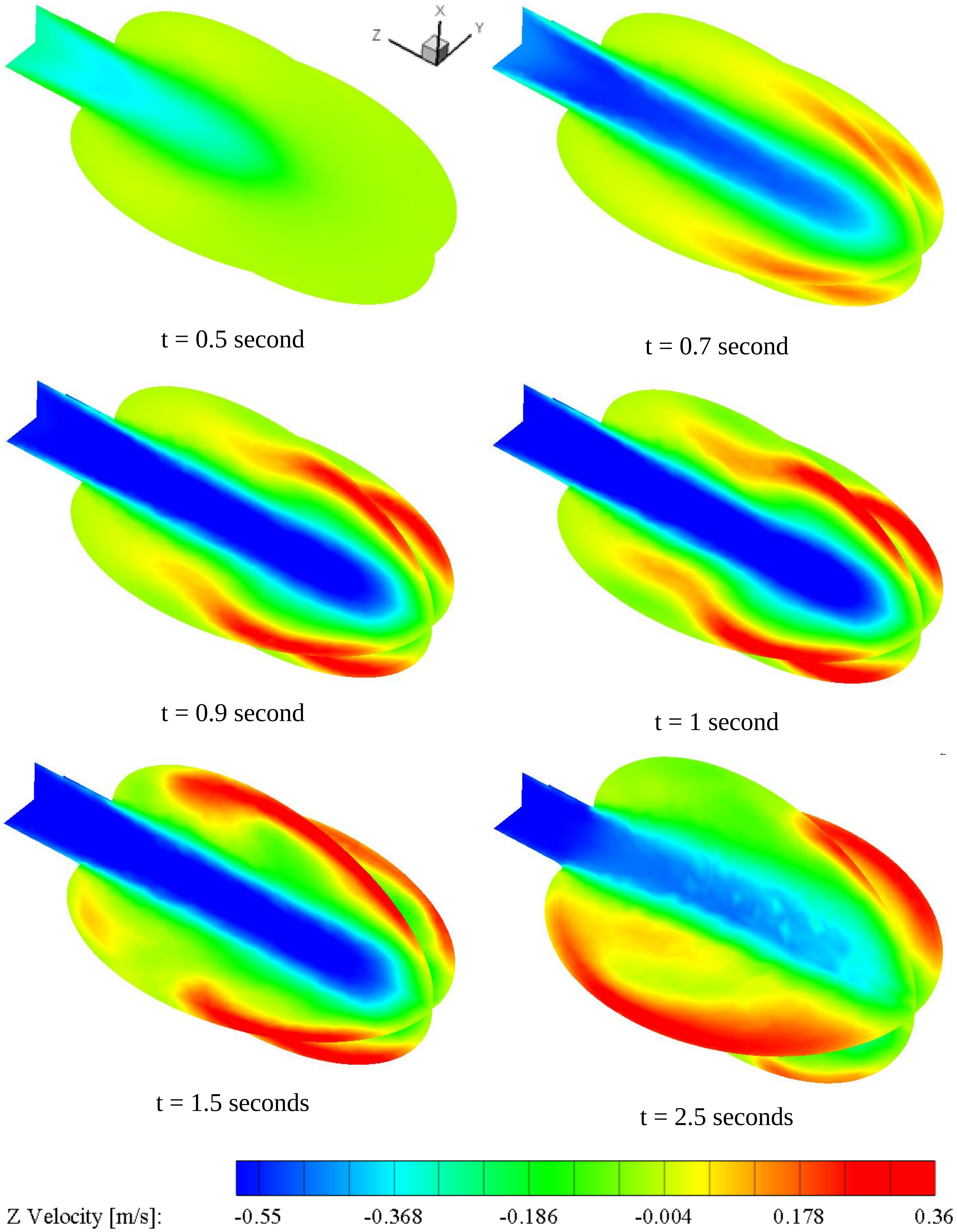

t = 0.5 second

t = 0.7 second

t = 0.9 second

t = 1 second

t = 1.5 seconds

t = 2.5 seconds

Figure 3.16: 3D Balloon – Velocity contour of fluid region at six different times

(Please reference Appendix B – Chapter 3: Three-Dimensional Balloon Expansion for all shown time steps in larger format).The flow of air can be seen flowing backwards along the wall starting at t = 0.7 second. Additionally, at t = 0.9 second and t = 1 second, vortex shedding can be seen around the “bluff” of prescribed air and the reverse flowing air.

Shown in Figures 3.17 – 3.21, are the velocity magnitude from various times. The figures are divided between a 3D isosurface (range between -0.55 and 0.3), two directional slices: horizontal and vertical slice, and the velocity and time of the flow.

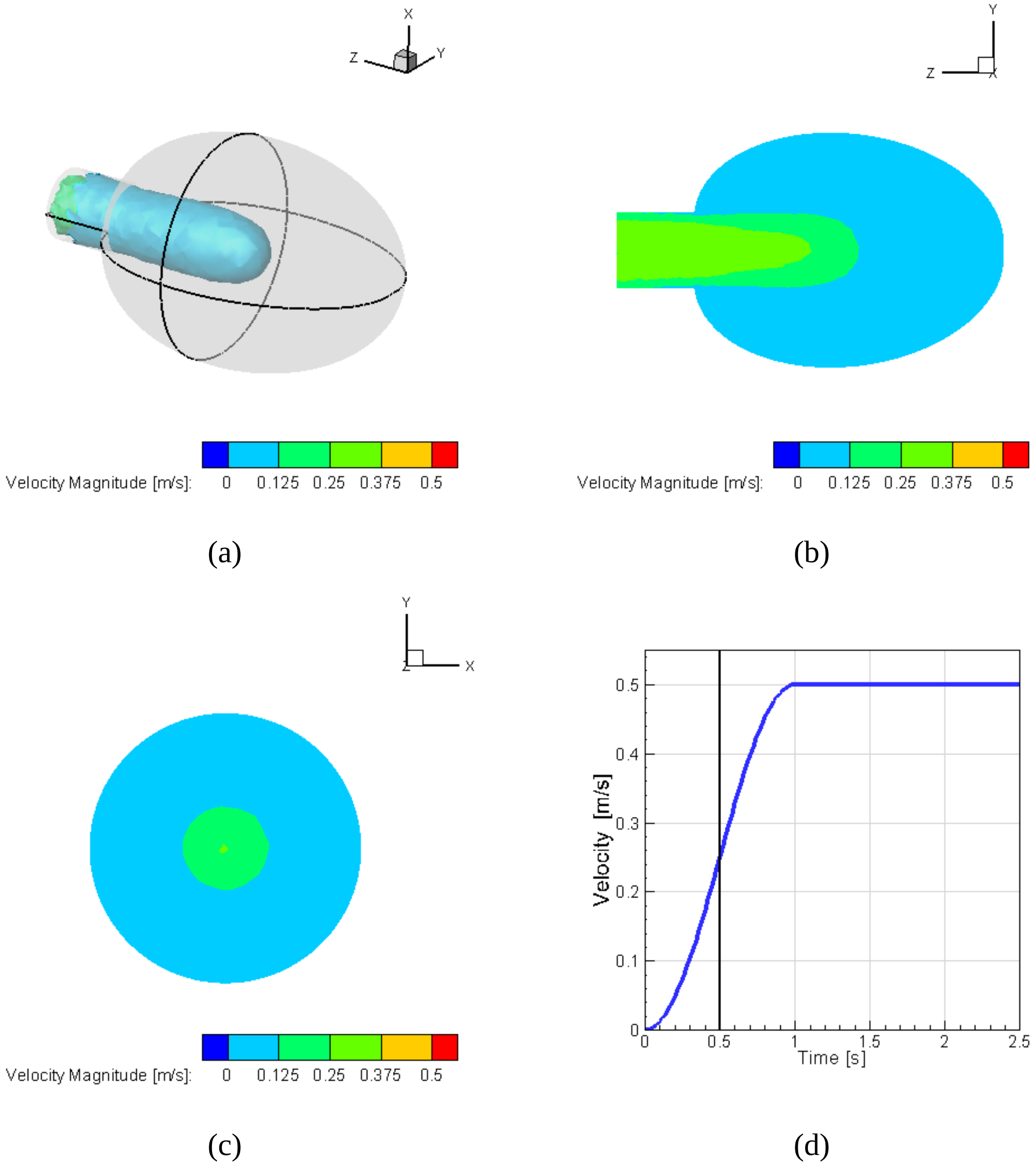

(a) (b) (c) (d)

Figure 3.17: 3D Balloon – Velocity magnitude at t = 0.5 second. (a) 3D isosurface (range between -0.55 and 0.3), (b) horizontal slice, (c) vertical slice, and (d) velocity and time of flow

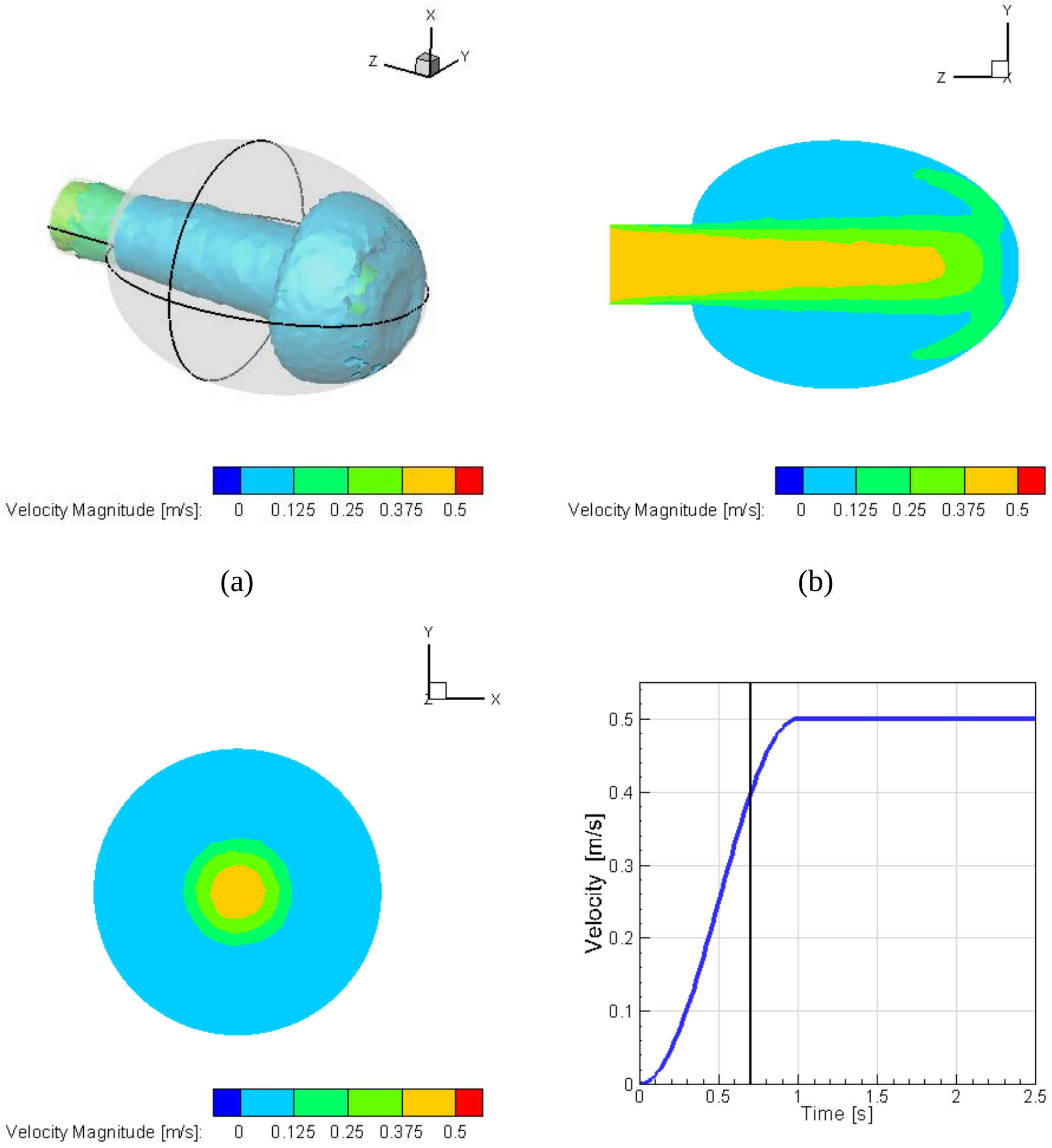

(a) (b)

(c) (d)

Figure 3.18: 3D Balloon – Velocity magnitude at t = 0.7 seconds. (a) 3D isosurface (range between -0.55 and 0.3), (b) horizontal slice, (c) vertical slice, and (d) velocity and time of flow

From Figure 3.18 (a), it can be observed that at t = 0.7 second, the velocity is slowly ramping up to 0.5 (m/s). While figure (b) is showing some reverse flow of the air. Furthermore, the described stagnation point from Figure 3.15, is also visible in Figure 3.18.

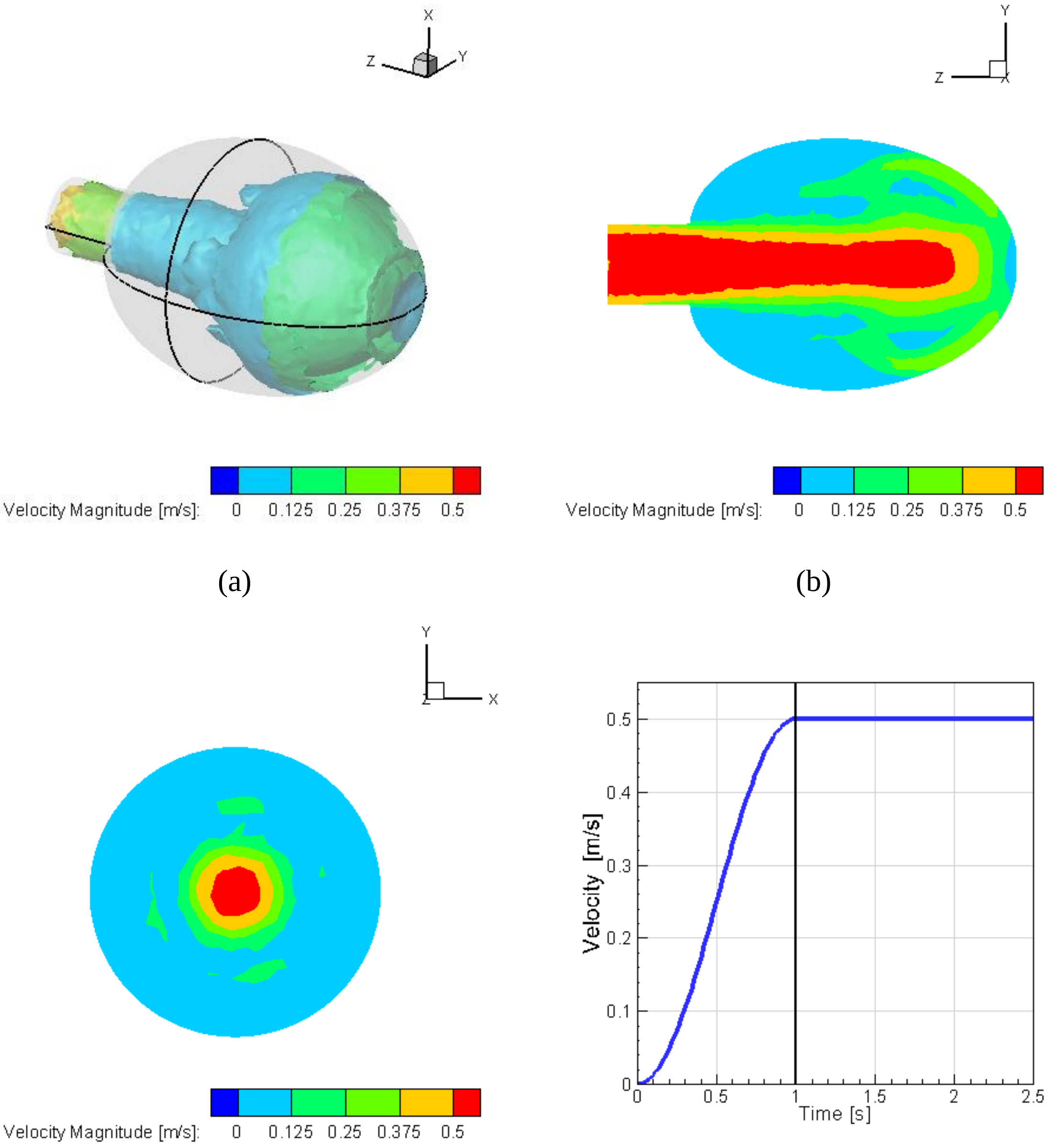

(a) (b)

(c) (d)

Figure 3.19: 3D Balloon – Velocity magnitude at t = 1 second. (a) 3D isosurface (range between -0.55 and 0.3), (b) horizontal slice, (c) vertical slice, and (d) velocity and time of flow

From Figure 3.19, now that t = 1 second, the flow has reached the maximum velocity as seen in (b) and (c). It is also noteworthy, from (a) the isosurface is showing the air has not completely expanded into the balloon yet, so there is not any visual expansion of the balloon that can be observed.

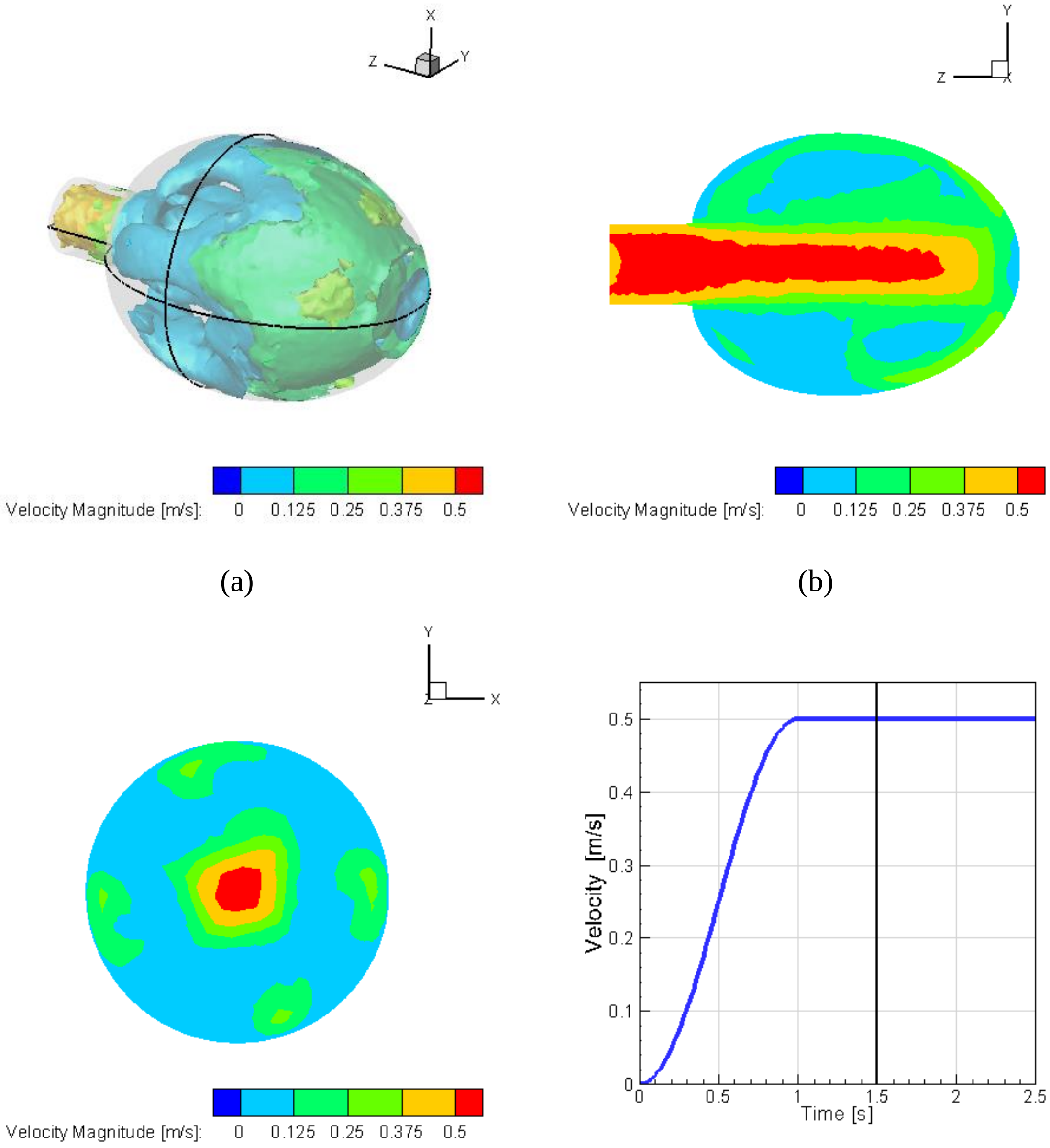

(a) (b)

(c) (d)

Figure 3.20: 3D Balloon – Velocity magnitude at t = 1.5 seconds. (a) 3D isosurface (range between -0.55 and 0.3), (b) horizontal slice, (c) vertical slice, and (d) velocity and time of flow

From Figure 3.20, (b) and (c) are showing slight expansion in the balloon and still maintaining the velocity at 0.5 (m/s). Note from (b) that the air in the entire balloon is moving, pushing against the walls of the balloon, causing the expansion. This can be observed in Figure 3.21 as well.

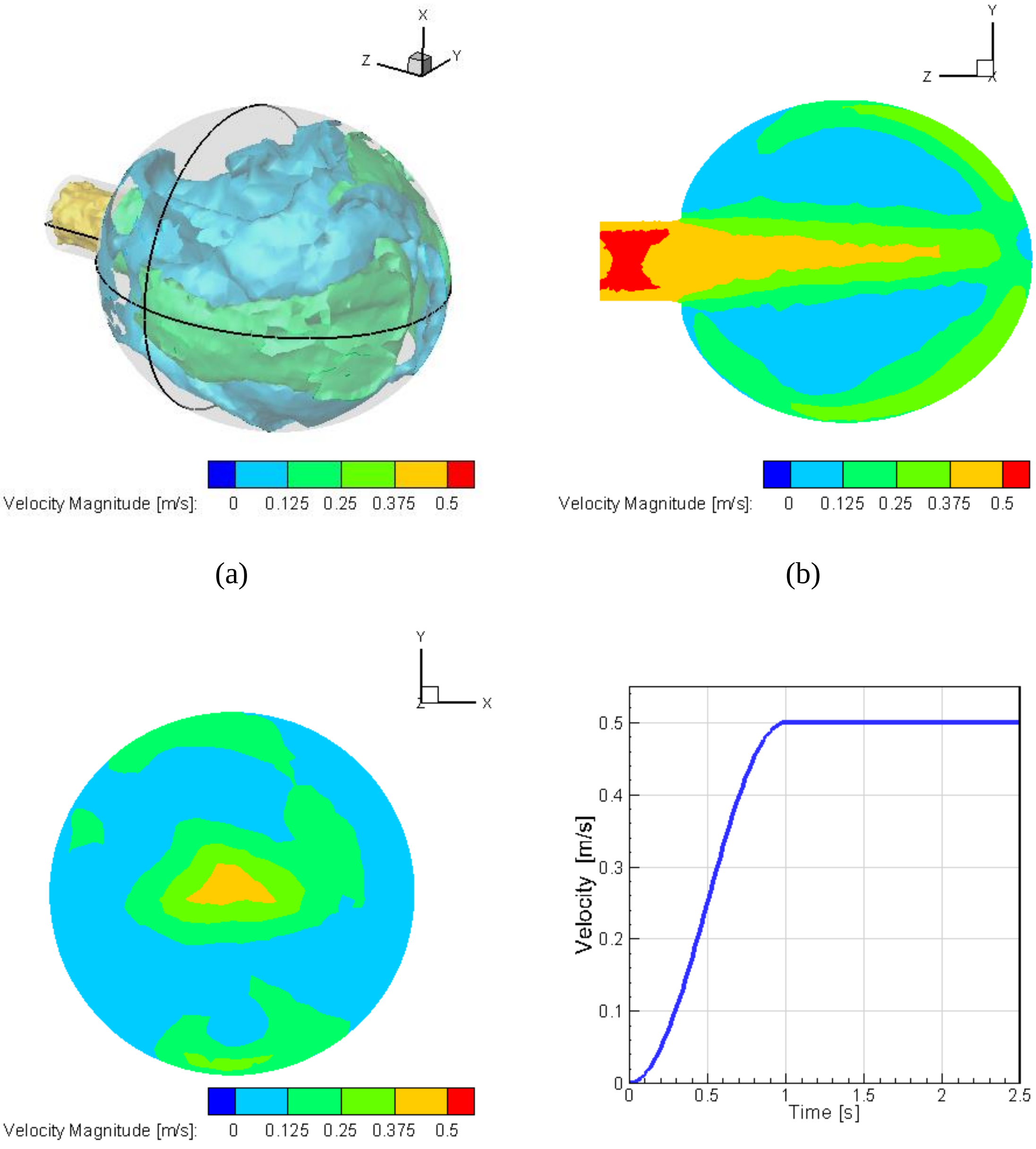

(a)

(b)

(c)

(d)

Figure 3.21: 3D Balloon – Velocity magnitude at t = 2.5 seconds. (a) 3D isosurface (range between -0.55 and 0.3), (b) horizontal slice, (c) vertical slice, and (d) velocity and time of flow

Lastly, from Figure 3.21, this is the last time step for the simulation, however it can be deduced that the balloon will continue to expand if the simulation time were to continue (if the mesh can accommodate as well).

Similarly to the square balloon in Chapter 2, the pressure for the 3D balloon is almost the same everywhere, the difference is minuscule; this can be observed been within Figure

3.22 and Figure 3.23. In addition, the velocity vectors are displayed on top of the pressure to show the flow direction at the chosen times.

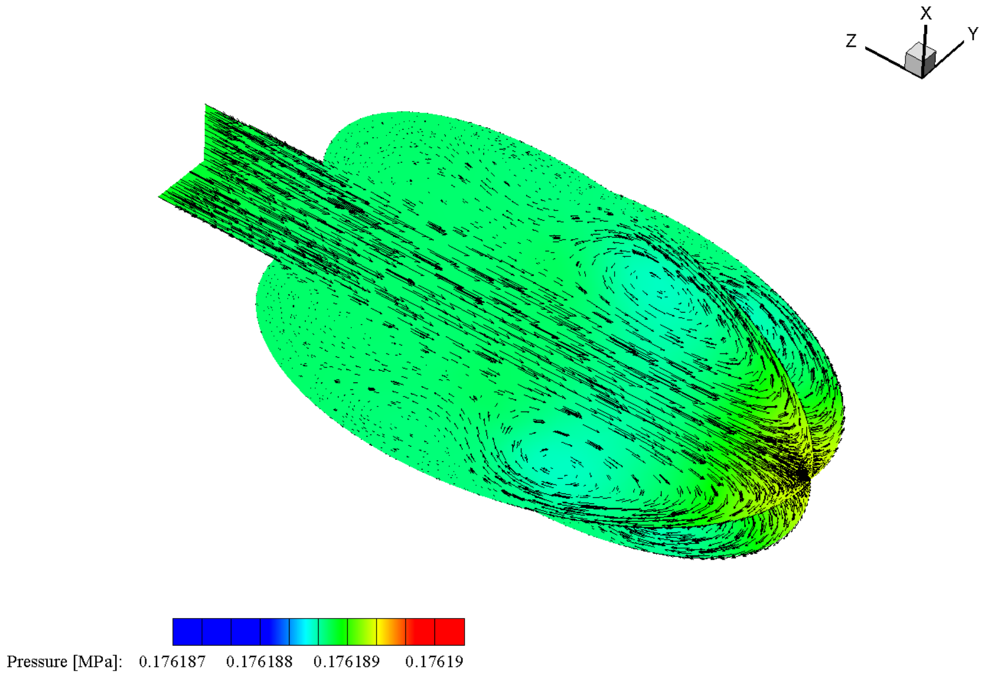

Figure 3.22: 3D Balloon – Pressure contour and velocity vector at t = 1 second

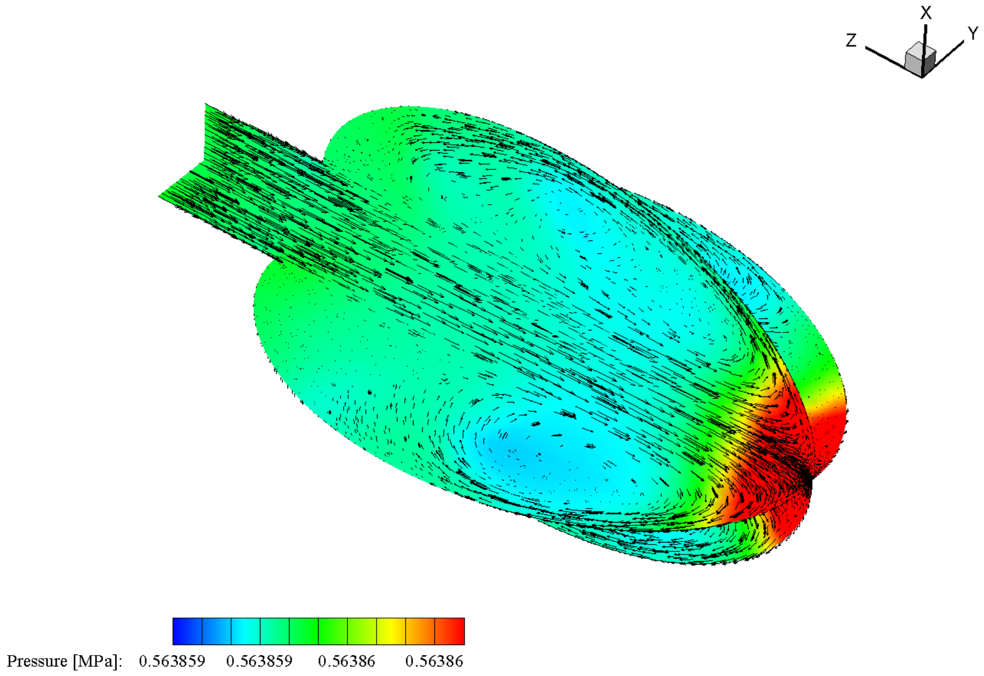

Figure 3.23: 3D Balloon – Pressure contour and velocity vector at t = 1.5 seconds

The two time steps that show the most “drastic change” in pressure were chosen for Figure 3.22 and Figure 3.23. Unfortunately, because the pressure is nearly the same everywhere and is changing rapidly, the scale on the two contours are different. The purpose of the two figures is to show the pressure distribution, with the direction of the velocity. Also note, that the pressure is displayed in MPa, to avoid the use of large numbers. (In Tecplot, if values are too high, the program is unable to show the distribution properly).

Since the pressure changes rapidly, Figure 3.24, the pressure (and velocity) is graphed with time to show the pressure increase.

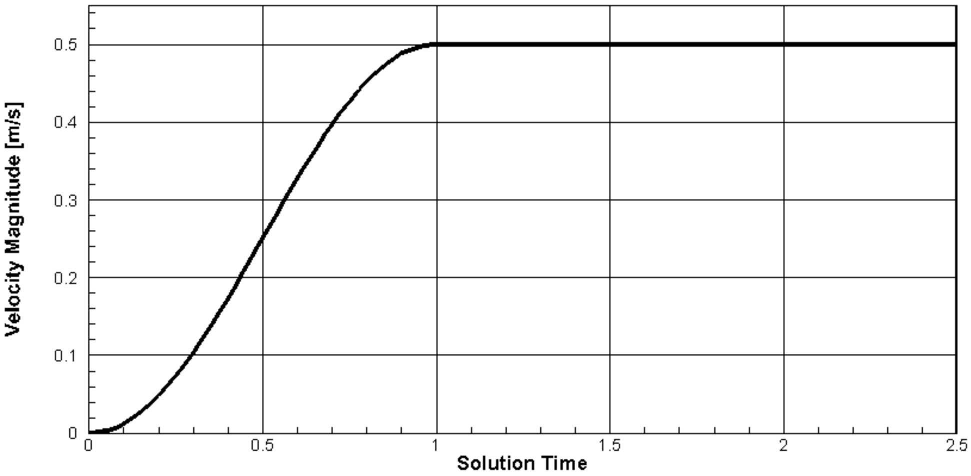

(a) *Solution Time* has units of (s)

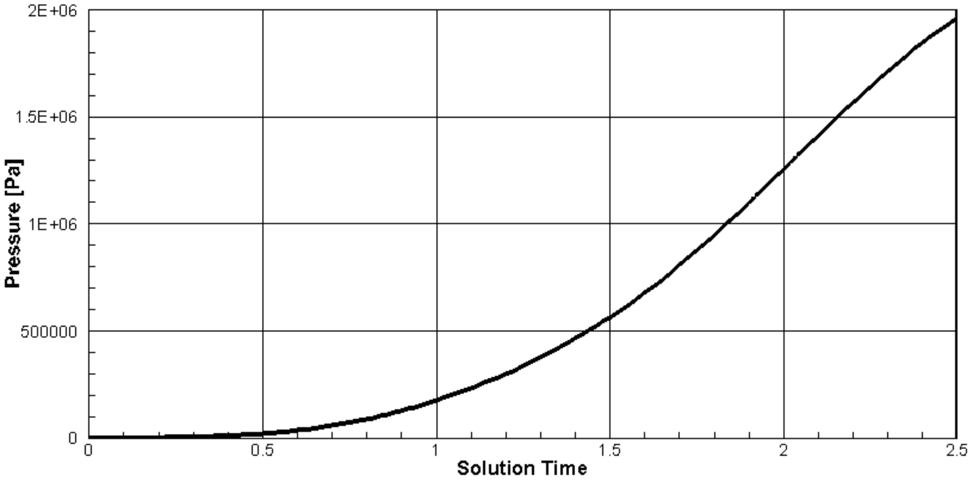

(b) *Solution Time* has units of (s)

Figure 3.24: 3D Balloon – Velocity (a) and Pressure (b) curve from simulation

As shown in Figure 3.24, the pressure change is significant throughout the simulation. The balloon will continue to expand rapidly until infinity if the elements in the mesh can handle the change. It is also noteworthy, from Figure 3.13, the balloon does not start expanding until t = 1 second. The corresponding pressure at the same time is about 1.76E+05 (Pa). This means it takes more than 1.76E+05 (Pa) to overcome the elastic stiffness BC on the structural side to expand the balloon noticeably.

3.5 Conclusion

Although the 3D balloon case study cannot be directly compared to literature balloons, such as stents and pressure vessels; the simulation still provides a good insight into the fluid behavior inside balloon and stress distribution on the exterior balloon wall. The general behavior of the structural portion of the balloon can be modeled as a pressure vessel. The pressure applied is from the fluid region, which can be further calculated through the ideal gas law beyond what this chapter encompasses. For general explanation of the ideal gas law, please reference Chapter 2. A note on the structural region, the material is modeled as a linear isotropic material. Since silicone rubber is nonlinear in nature, this simulation is not very accurate. Future research potential for this simulation would be to apply nonlinear properties to the balloon walls, and then compare the differences. Another improvement would be to add turbulence to the air flow, since there is mostly likely turbulent behavior inside the balloon. This can be seen in Figure 3.21 (b), where the flow becomes asymmetric and turbulent.

This simulation setup can be further developed to model the two lobes in the respiratory system. The purpose of modeling a balloon is to apply the concept to biological studies, like *Chua et al.* [18], *Gervaso et al.* [19], *Zahedmanesh et al.* [20], and *Wang et al.* [21] have attempted. The predominant difference is using an FSI study rather than FEA. Also, similar to Chapter 2 being the stepping stone for this chapter, this simulation will be the stepping stone for Chapter 5 and any future simulations that involves enclosed boundaries.

Chapter 4: PORCINE TRACHEAL MATERIAL PROPERTIES

4.1 Porcine Material Property Characterization

Numerous different attempts have been made to characterized biological tissue, specifically tracheal tissues. *Codd et al.* [25] have characterized ovine tracheal tissue, with linear elastic properties through axial tensile testing. *Holzhäuser et al.* [26] analyzed the mechanics of the trachea cartilage in rabbits through A-Ptm curves. *Codd et al.* [25] and *Holzhäuser et al.* [26] are one of several researchers to look into animal tracheal tissues other than porcine. *Lally et al.* [12], *Shi et al.* [13], *Teng et al.* [14], and *Trabelsi et al.* [11] are among some researchers that characterized porcine tracheal tissue. Lastly, several researchers tested with human tracheal tissue obtained from cadavers. The time from harvest was as short as within 24 hours to tissue being frozen for a short period of time until testing. Different techniques and procedures where use to analyze the human trachea. *Begis et al.* [27] conducted tests within 15 hours of death, and used a hyperelastic model: Mooney-Rivlin for characterization to apply in a FEA of the tracheal cartilage. *Lambert et al.* [28] used segments of the human trachea and based on thin curved beam theory analyzed the predicted deformed shapes. *Rain et al.* [29] tensile stiffness of cartilage rings as well as observing the age effect on the tissue. *Saraf et al.* [30] conducted dynamic loading on human tissues, trachea being one of the tested tissues. *Teng et al.* [31] conducted uniaxial tension test on the axial and circumferential directions of the trachea. *Teng et al.* [31] along with a couple other researchers' described below, will have techniques that this case study drew from. Unfortunately, results from this study cannot be directly compared to the results in the publications due to either the material samples, test method, or the loading pattern being different. However, some general conclusions can be observed between all the studies.

For this study, the focus is to obtain hyperelastic constants for FEA and FSI simulations. Generally, a simulation require material property inputs such as density (ρ), elastic modulus (E), Poisson's Ratio (ν), etc. For a lot of simulations, a linear material constant such as E is enough to describe the material behavior. However, for non-linear materials, E is not powerful enough to describe the behavior of the material, so stress-strain curves or material models are necessary for those cases. In the case of biological materials, the behavior is typically nonlinear. In *Teng et al.* [32], the trachea's collapsibility and compliance was studied using linear and nonlinear material properties. It was shown that although assuming linear does not deviate from the nonlinear properties, there is still some inaccuracies. As many researchers have shown using with both porcine and human tracheal tissue, the elastic properties are nonlinear regardless of the type of loading. To minimize the inaccuracies as much as possible, nonlinearity should be considered. To characterize the nonlinear curve, testing will need to be conducted for validation. *Lally et al.* [12] conducted biaxial testing, *Teng et al.* [14] performed cyclic loading on the cartilage rings themselves, and *Trabelsi et al.* [11] did uniaxial tension testing; all showed the stress-strain/stress-stretch curves to be nonlinear. Moreover, various material curve fitting modelling was also performed by *Lally et al.* [12] and *Trabelsi et al.* [11]; Mooney-Rivlin and Neo-Hookean, respectively. Both hyperelastic models are commonly used, however, another common model, the Ogden model has not been popularly used in the biological curve fitting field. *Teng et al.* [14] used the Ogden model as part of the boundary conditions, however, the ultimate sought-after model in the journal is the Fung-type strain energy density function, which is yet another material characterization. As illustrated in Figure 4.1, to obtain and verify the curve fitting it is a three phase process, which will be described in the sections below.

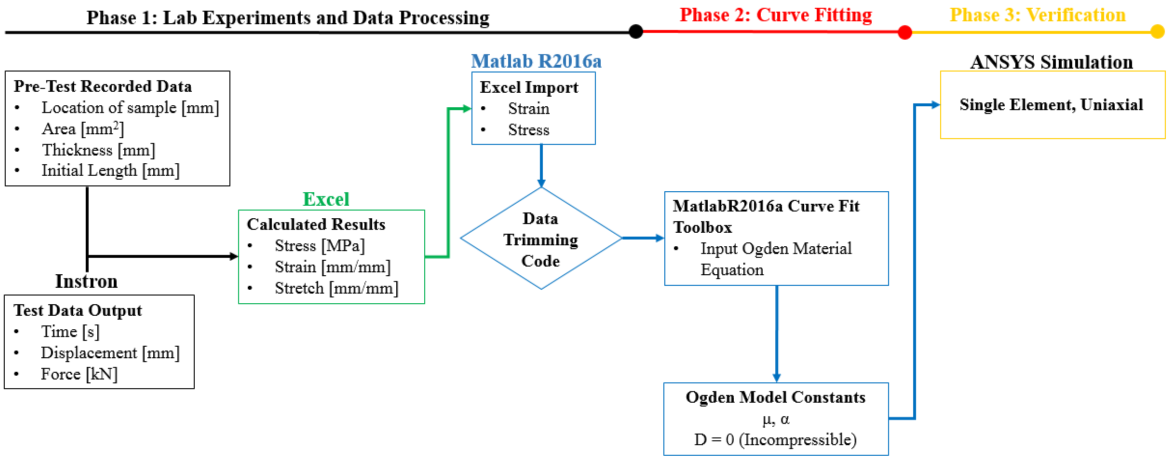

Figure 4.1: Tensile Testing – Material curve fitting and verification approach

The approach for this testing done primarily on the axial direction of the trachea, however some circumferential testing was also conducted as well.

4.2 Phase 1: Lab Experiments – Uniaxial Tensile Testing of Porcine Trachea

As described in section 4.1, various types of experiments have been conducted on biological tissue by many researchers to determine and describe the behavior of the tissue.

However, the input for this case study has not been satisfactorily identified. This study is an attempt to establish a baseline of constants for the Ogden model that can be applied to various types of simulations that may involve tracheal geometry.

4.2.1 Specimen Sample Preparation

To evaluate mechanical properties of porcine trachea, n = 6 adult porcine tracheal specimen were harvested from the University of Idaho Vandal Meats abattoir. The porcine were harvested with the lungs and the trachea still attached. The tracheal tissues were removed, placed in plastic bags to retain moisture and immediately placed in refrigeration 4 (°C) until testing occurred within the next couple of hours to ensure freshness of tissue. The whole tracheal length, measured from the carina to the base of the first sample cut, was recorded.

Table 4.1: Tensile Testing – Length of porcine trachea used in tests

Trachea	Length (cm)
1	143
2	149
3	152
4	160
5	137
6	126
Average	144.5±11.98

The specimen 1, 3, and 5 were then cut using a 3D printed stencil and a scalpel (in the axial direction), approximately 50 (mm) ×10 (mm) were cut along the superior-inferior axis of the trachea (Figure 4.2). Likewise, specimen 2, 4, and 6 were cut (in the circumferential direction). The width and length of the circumferential cuts varied; due to the nature of cartilage rings (Figure 4.3). The soft connective tissue on the dorsal side of the trachea was also cut, to allow the tissue to be flattened for further sample procurement.

Figure 4.2: Axial samples

Figure 4.3: Circumferential samples

The location of each sample, with respect to the carina was also recorded. Each carina is used as a reference point for the samples. Recording the location is to determine whether or not location of the tissue effects the strength of the material.

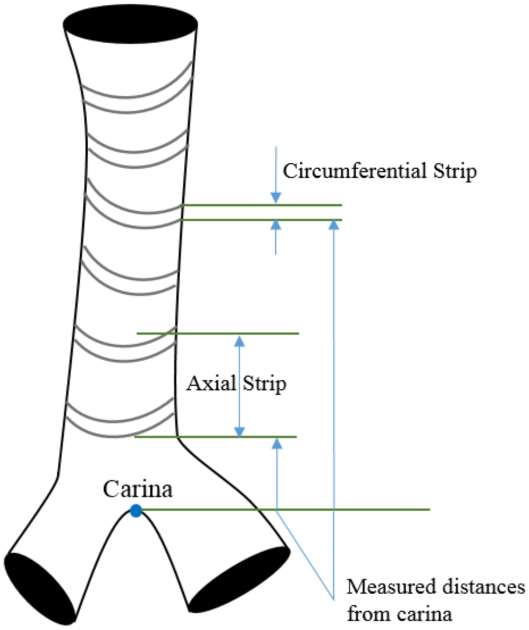

Figure 4.4: Tensile Testing – Example of locational measurements from carina

The width and thickness were measured with a set of digital calipers and recorded. The axial tissue was assumed to have a rectangular cross-section. Each end of the sample was mounted into the top and bottom screw action grip of a mini-Instron load frame. The load frame, software, and load cell used to collect the data are all from made and manufactured by Instron based in Norwood, MA.

Figure 4.5: Mini-Instron load frame

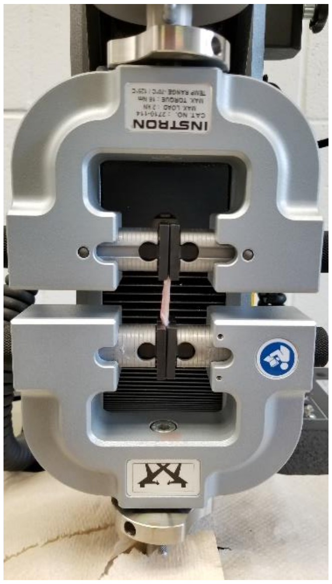

Figure 4.6: Mounted specimen

A 2 kilonewton (kN) capacity load cell was used to measure force data and Bluewood software recorded force and displacement data, and allowed for control of test parameters. The axial tissue samples were preloaded to 1 Newton (N). Front and side view digital images of each trachea sample were obtained. With the calipers, mounted tissue length were then measure and recorded. The length was then used to calculate the velocity, v, based on a set strain rate; $\dot{\varepsilon}$. All axial samples were then pulled to failure and a force-displacement data were record for each sample. Similarly, cartilage rings (circumferential direction) of the trachea were dissected and mounted into the mini-Instron and preloaded to 0.1 (N), then pulled to failure at a rate that ensured the same strain rate as the axial specimen. Lastly, few bronchi samples were also tested using the same procedure as the cartilage rings. All tissue samples were kept hydrated with saline throughout testing. Any samples that maybe an invalid specimen were discarded this included specimens with nicks/notches or aperture with-in the samples.

As stated earlier in the chapter, the purpose of doing the testing is to use the data for material model curve fitting. The curve fitted model could then be used in numerical simulations. Some basic and known properties are used to do the calculation in the section for data processing. Similar testing was done prior to this experiment to obtain values in Table 4.2. Which are used in the calculations for the described tests.

Table 4.2: Tensile Testing – Preliminary material properties of porcine trachea

Fluid Pressure of Human Airway, P (MPa)	0.00294
Diameter of Trachea, d (mm)	20
Thickness of Tracheal Wall, t (mm)	4
Breathing Rate, BR (s)	2
Elastic Modulus, E (MPa)	0.02778
Poisson's Ratio, υ	0.49
Longitudinal Stress, σ_{long} (MPa)	0.00368
Longitudinal Strain, ε_{long} (mm/mm)	0.0437

(Note: Fluid Pressure of Human Airway was converted from 30 cmH_2O). Please see Appendix C – Chapter 4: Porcine Tracheal Material Properties for calculations presented in Table 4.2. Using the values from Table 4.2, the strain rate can be calculated using the following equation.

$$\dot{\varepsilon} = \frac{\varepsilon_{long}}{BR} \tag{4.1}$$

Using equation (4.1) the strain rate is calculated to be $\dot{\varepsilon} = 0.0219(s^{-1})$.

4.2.2 Uniaxial Tensile Testing – Post Processing and Results

From tensile testing the axial specimens on the Instron, force and displacement data was obtained for each curve, example shown in Figure 4.7.

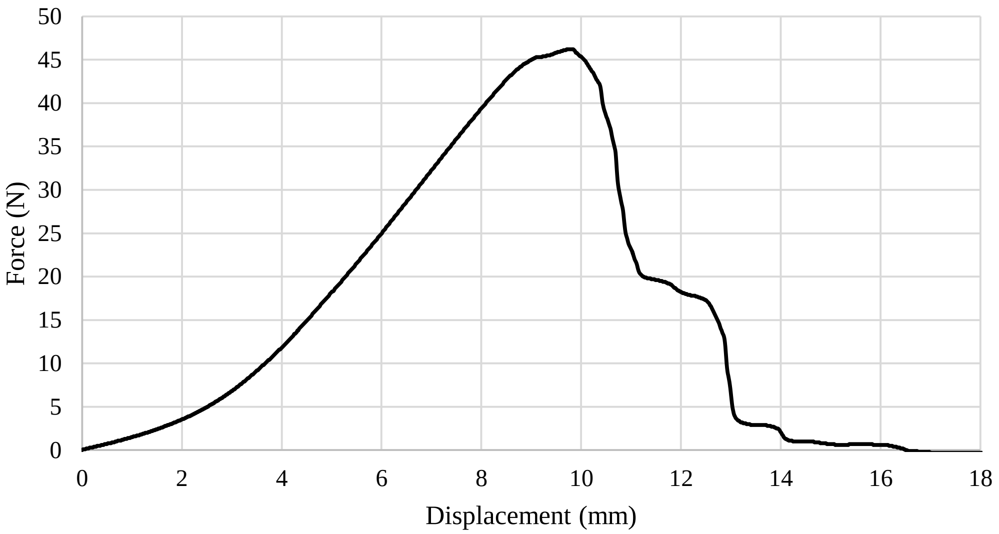

Figure 4.7: Ideal data – Force-Displacement curve of an axial test

From the force displacement data, engineering strain, engineering stress, and stretches were calculated using the following equations.

Engineering Strain, ε (mm/mm)

$$\varepsilon = \frac{\delta}{L} \tag{4.2}$$

Engineering Stress, σ (MPa)

$$\sigma = \frac{F}{A_o} \tag{4.3}$$

Stretch, λ (mm/mm)

$$\lambda = \frac{l}{L} = \varepsilon + 1 \tag{4.4}$$

where, δ is displacement, L is the original length of the specimen, F is the force, A_o is the original area, and l is the current length. The calculated and trimmed results of each individual sample was then plotted, shown in Figure 4.8 and Figure 4.9. The curves have been trimmed up until to the maximum stress, currently failure modeling is not included the study.

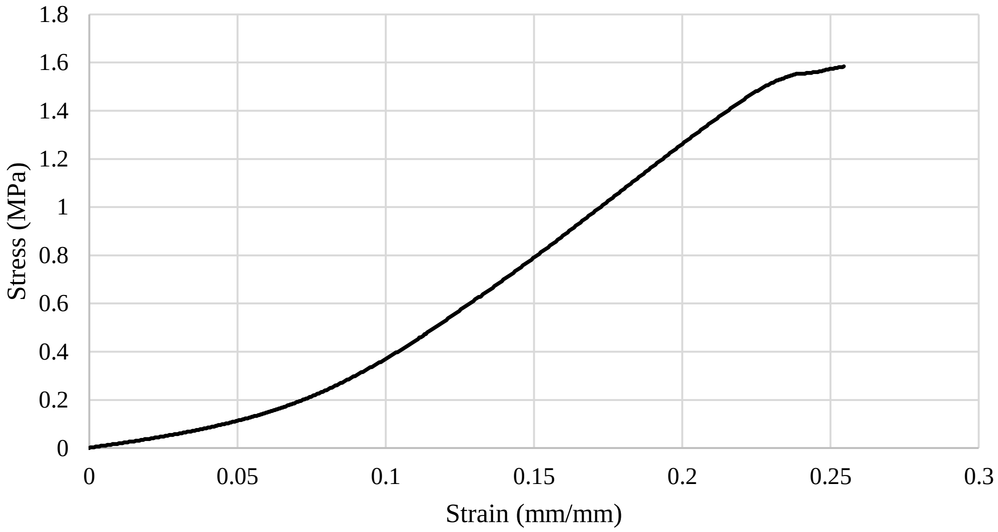

Figure 4.8: Ideal data – Stress-Strain curve of an axial test

In most engineering disciplines stress-strain curves are the primarily the graph to use and obtain information from. However, when graphing biological material or materials that can endure high strains, such as rubbers, it is more common to report and represent the data collected using stress-stretch curves.

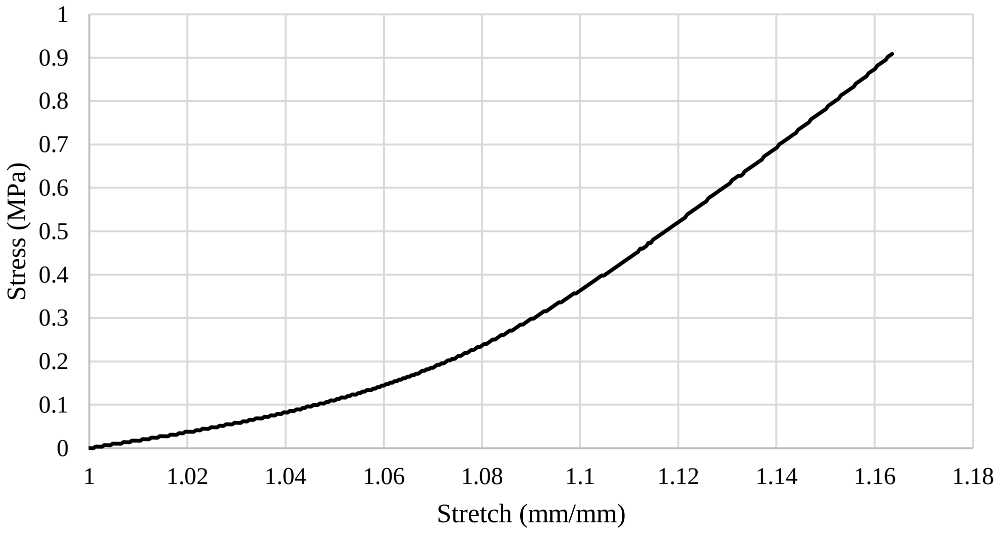

Figure 4.9: Ideal data – Stress-Stretch curve of an axial test

The figures shown above are for each individual sample, in order to combine all the samples into one graph for curve fitting, and to avoid using global maximum stress values another method was used to trim the data. The reason for avoiding the use of maximum stress is because the behavior of each sample under loading is different. Some samples will have a smooth transition to the maximum stress as shown in Figure 4.8. Others may have a behavior shown in Figure 4.10 and Figure 4.11 that requires extra trimming to the data.

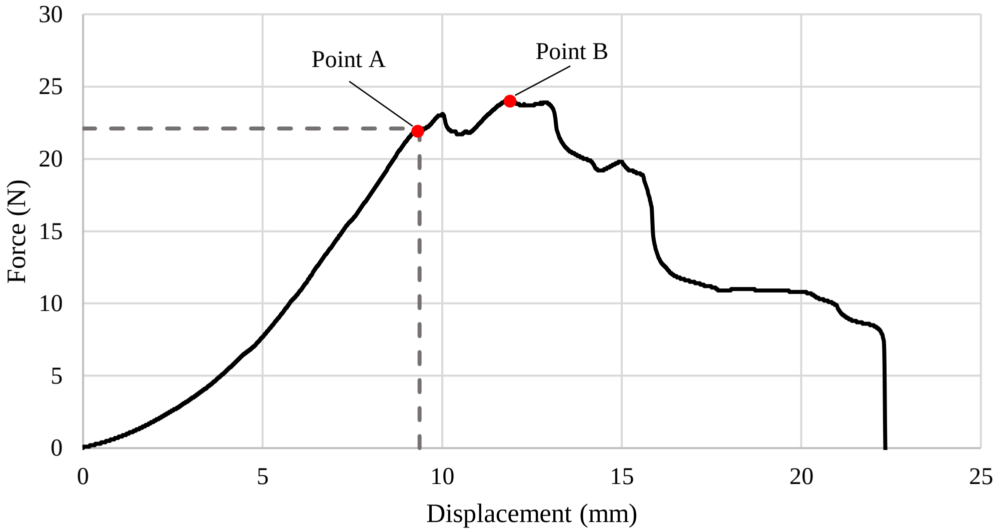

Figure 4.10: Extra trimming required – Force-Displacement curve of an axial test

From the figure above, the stress-strain curve will also show the corresponding local and global maximum. (Note, the stress-stretch curve will look very similar to Figure 4.11, accept the x axis will start from 1, instead of 0).

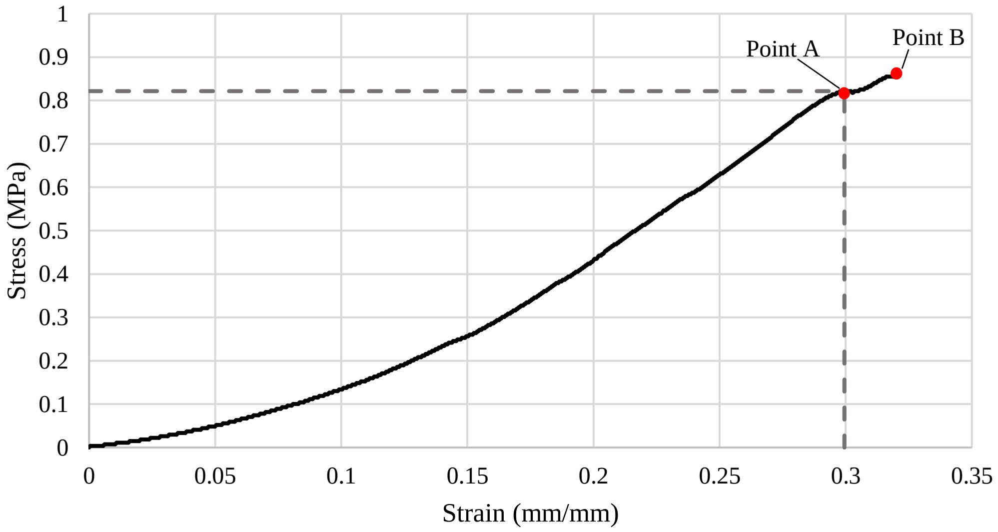

Figure 4.11: Extra trimming required – Stress-Strain curve of an axial testing

If all the axial data were to be trimmed to the maximum stress, the global maximum Point B, will be taken. However knowing that the desired value is actually at Point A; it means the data will need to be trimmed up to Point A. Without having to manually go through the data to do this action, a MATLAB script was written to aid this process. (Please see Appendix C – Chapter 4: Porcine Tracheal Material Properties for the MATLAB code).

The downside of this method is when “good data” can get thrown out. Certain data may have a sharp change in slope towards the beginning of the test. For example, the behavior can be from the sample relaxing or a cartilage ring is breaking. Thus resulting a negative change in slope. The program would automatically set the cut point to the beginning value. To avoid this from happening, the cut point is set to be the first negative slope after half way point. This way possible “good data” can be retained. However, another down side of cutting the data in half and then finding the negative slope, is if there is “bad data” in the beginning that should be thrown out. The “bad data” will not be thrown out, because of the set mid-data cut off point. Even though the cutoff point can be set to any location in the data, the midpoint was chosen because most of the “bad data” in the collect are towards the end of testing. The script used to trim the data is described in Figure 4.12.

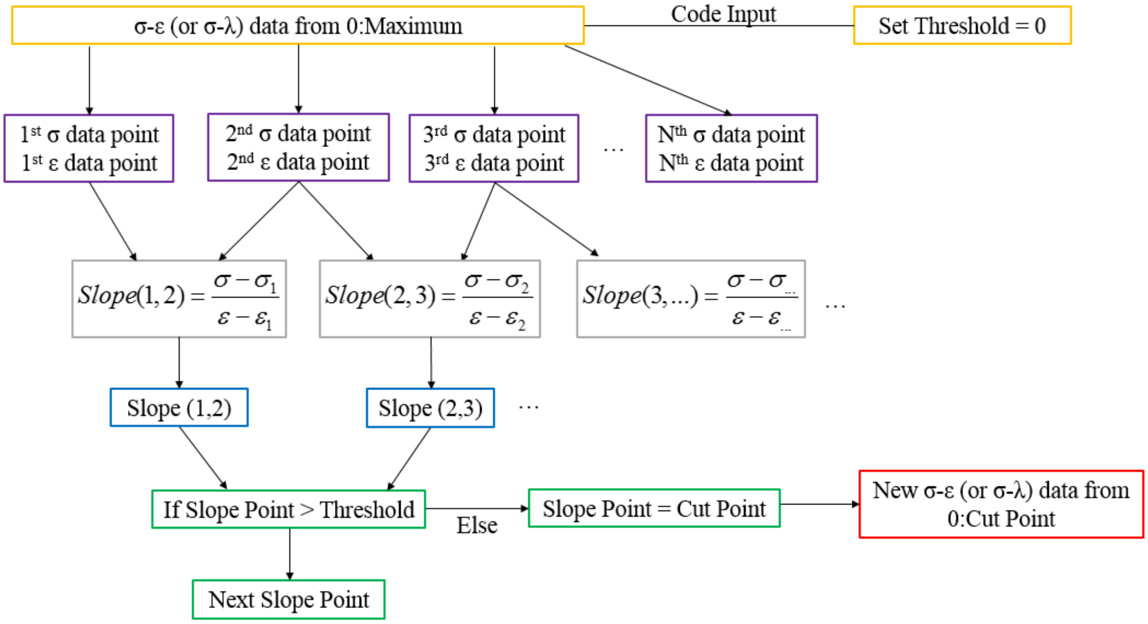

Figure 4.12: Tensile Testing – Flow chart of data trimming for MATLAB code

Based on Figure 4.12, after the slope of the data points are calculated, the value is then fed through a ‘for’ loop to determine the cut point. The cut point is determined when the slope of a nonlinear curve goes negative as shown in Figure 4.13. If the slope changes too quickly, it will result in a sharp, negative change in the slope graph. Using the "slope method", results in a clear definition of where the data is cut off: at the point where there is a rapid negative change in slope.

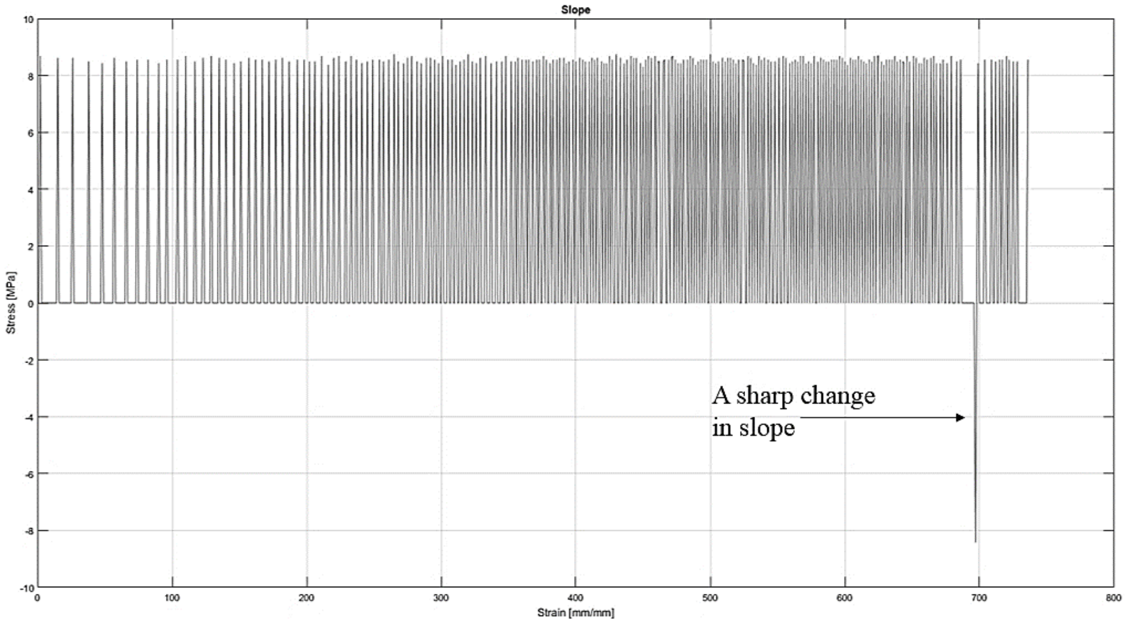

Figure 4.13: Tensile Testing – Graphed slope values, graph created in MATLAB R2016a, x axis is Strain, ε (mm/mm), y axis is Stress, σ (MPa)

After the data is trimmed, the new σ-ε (or σ-λ) curve the data from all the axial testing can be graphed onto one graph to be used for curve fitting.

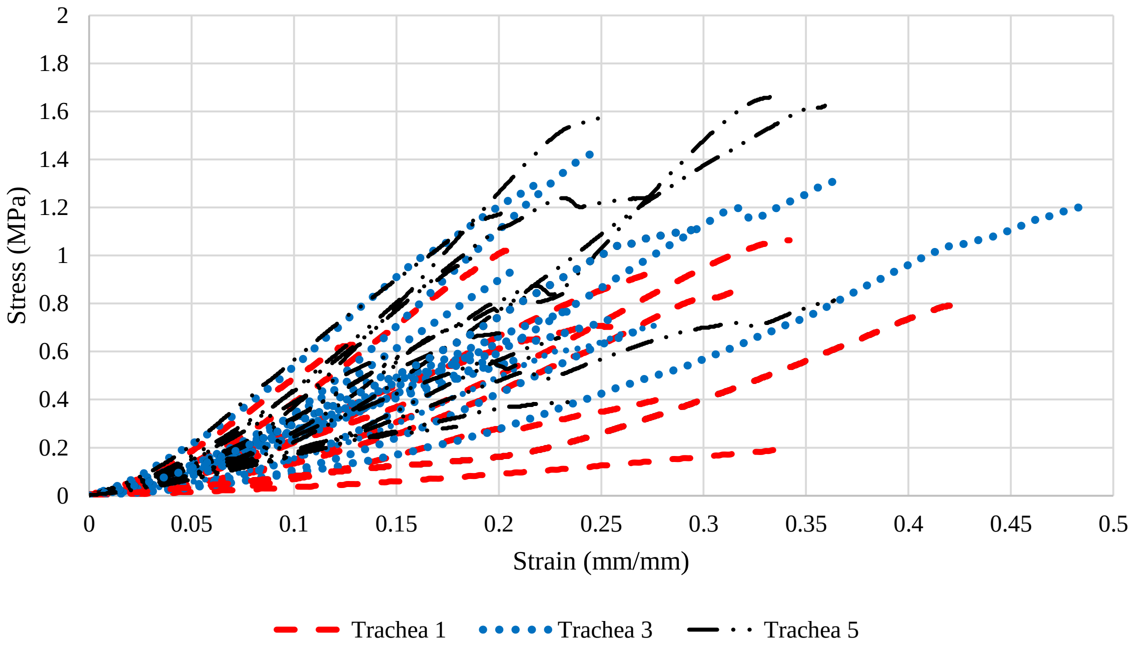

Figure 4.14: All axial data from tensile testing

Some caliper measurements were taken prior to the tensile test to determine whether or not the location of the sample with respect to the trachea mattered. Based on the spreading of Figure 4.14, all the samples regardless of location on the trachea, does not affect the behavior of the material. Since the spread of data is grouped more so by the individual tracheas than the location of the sample. Additional example figures and graphs showing the locations of the samples are in Appendix C – Chapter 4: Porcine Tracheal Material Properties. Comparing the axial data with uniaxial tension test data from *Lally et al.* [12], the stretch values are close to each other, but the stress from this study is lower compared to *Lally et al.* [12].

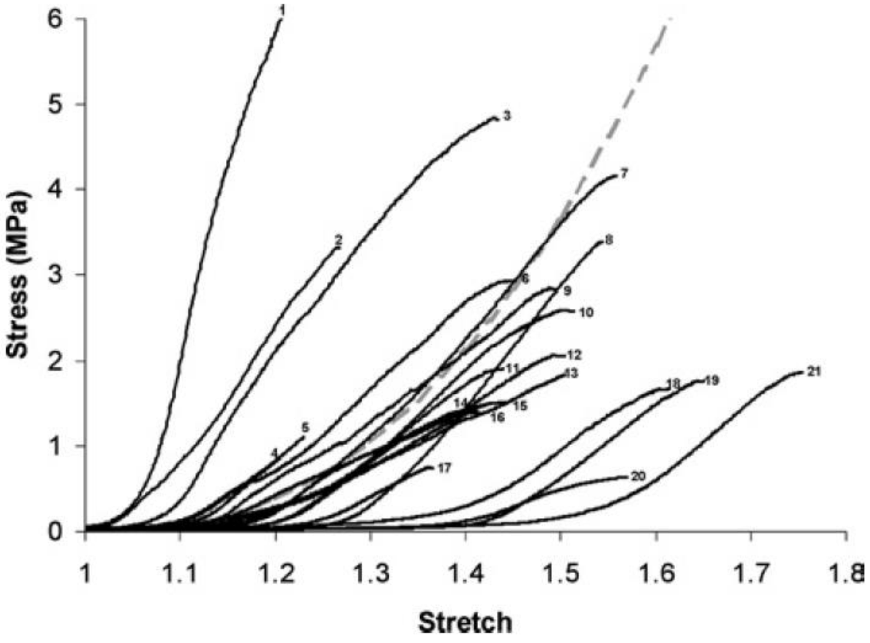

Figure 4.15: Stress-Stretch curve, figure obtained from *Lally et al.* [12]

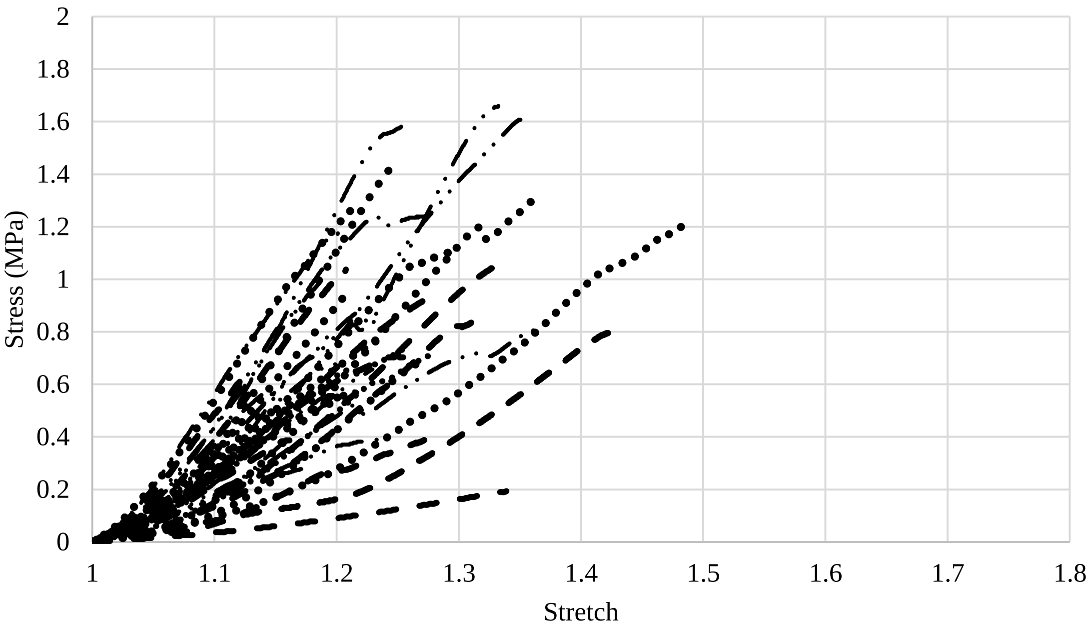

Figure 4.16: Stress-Stretch curve of the axial direction.

The data from *Lally et al.* [12] are seemingly more scattered, in comparison to this study. This is most likely due to preconditioning that *Lally et al.* [12] conducted on their specimen. Another observation between the two studies are the curves are more closely grouped together in this study verses those reported by *Lally et al.* [12]. Again, this is most likely due to the preconditioning.

In addition to testing the trachea axial direction, some circumferential direction were also tested. Using the same procedure as the axial direction the resulting circumferential stress-strain curves are shown in Figure 4.17.

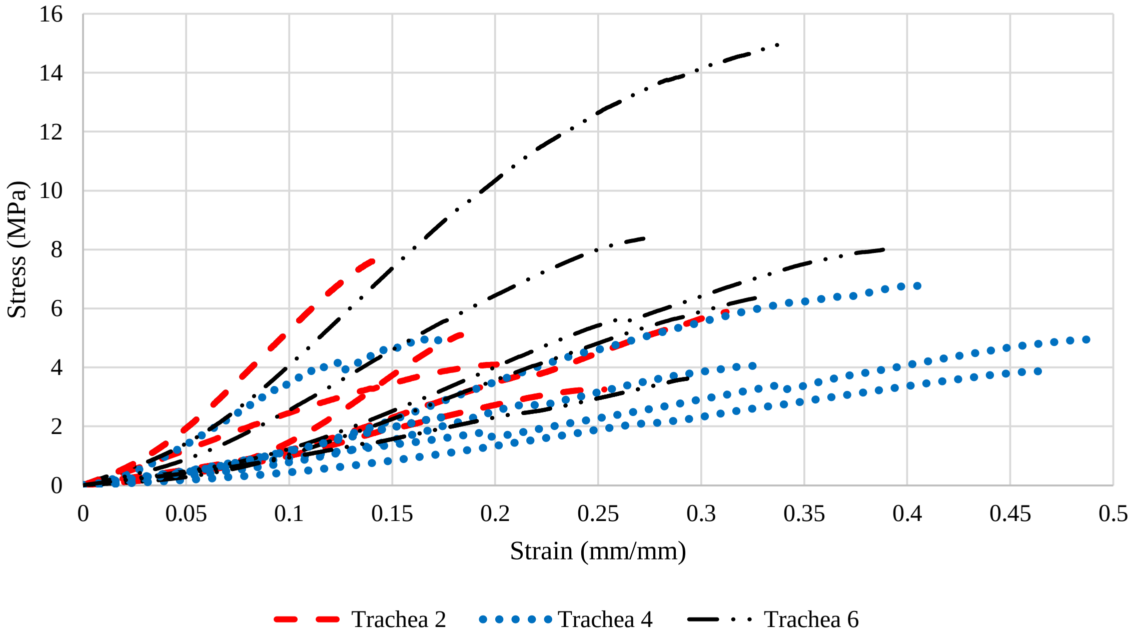

Figure 4.17: All circumferential data from tensile testing

Similar to the axial direction, the location of the sample with respect to the carina does not seem to matter.

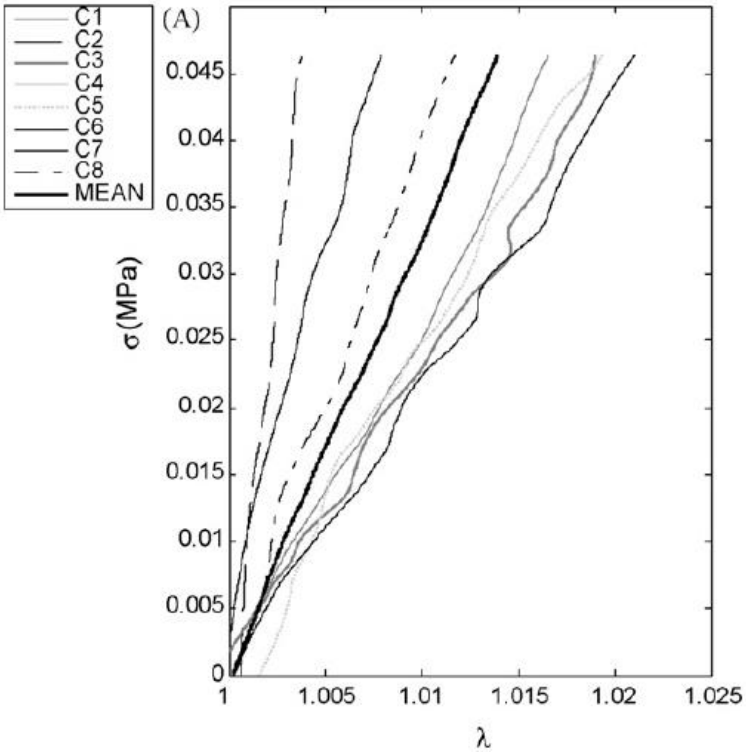

Figure 4.18: Stress-Stretch curve, figure obtained from *Trabelsi et al.* [11]

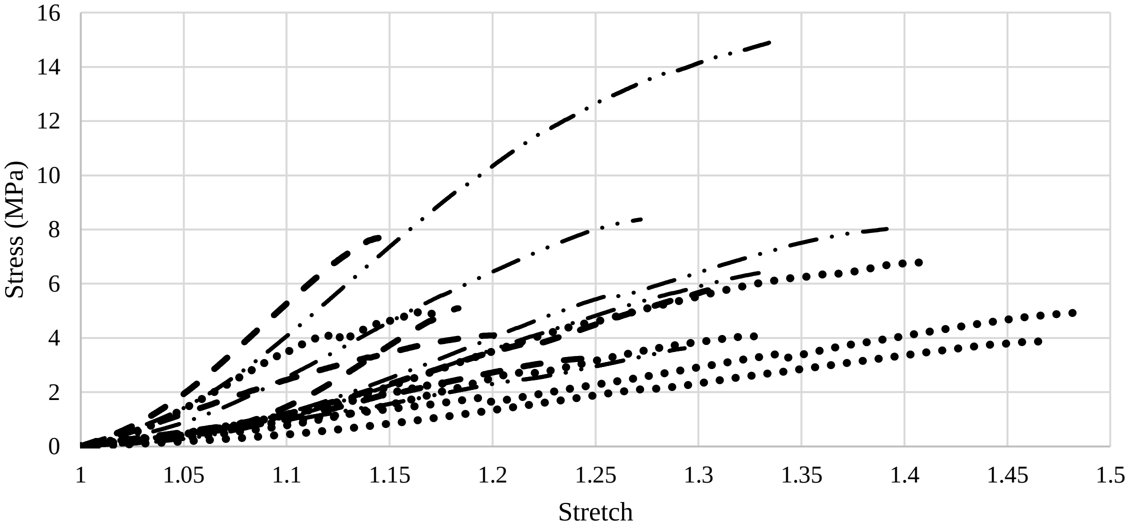

Figure 4.19: Stress-Stretch curve of circumferential data

Similar to *Lally et al.* [12]'s axial direction, *Trabelsi et al* [11] also conducted uniaxial tension tests and curve fitted the data for the circumferential direction. However, there are several differences between the current study and *Trabelsi et al* [11]. First, *Trabelsi et al* [11] conducted tests with human tracheal tissue, while this study used porcine. Second, *Trabelsi et al* [11] obtained tissues after autopsy and the tissues were frozen. The current study harvested the tissue immediately after the animals were harvested, kept moist, and was placed into refrigeration at 4 (°C), with testing occurring on the same day. Lastly, *Trabelsi et al* [11] preconditioned the material, while samples shown in Figure 4.19 were not preconditioned. As stated before, due to differences a direct comparison cannot be performed. It is interesting to note that the difference in behavior is significant given the same material. Each one of the differences, can play a major role in changing the data.

4.3 Phase 2: Curve Fitting – Hyperelastic Material Model

Many material behaviors are modeled with linear elastic stress-strain relationships, up until the yield strength. However, for most materials, linear elastic models do not accurately describe the observed material behavior; especially with hyperelastic materials. Hyperelastic materials in general have a non-linear stress-strain curve. Some regions of the stress-strain curve can be linear, but for the most part the curve is nonlinear. Elastomers and biological materials are classic hyperelastic materials. Most biological material will have a ‘toe region’ on the stress-strain curve followed by a small linear portion, then the curve goes nonlinear, finally peaks at maximum stress, followed by the failure region (Figure 4.20).

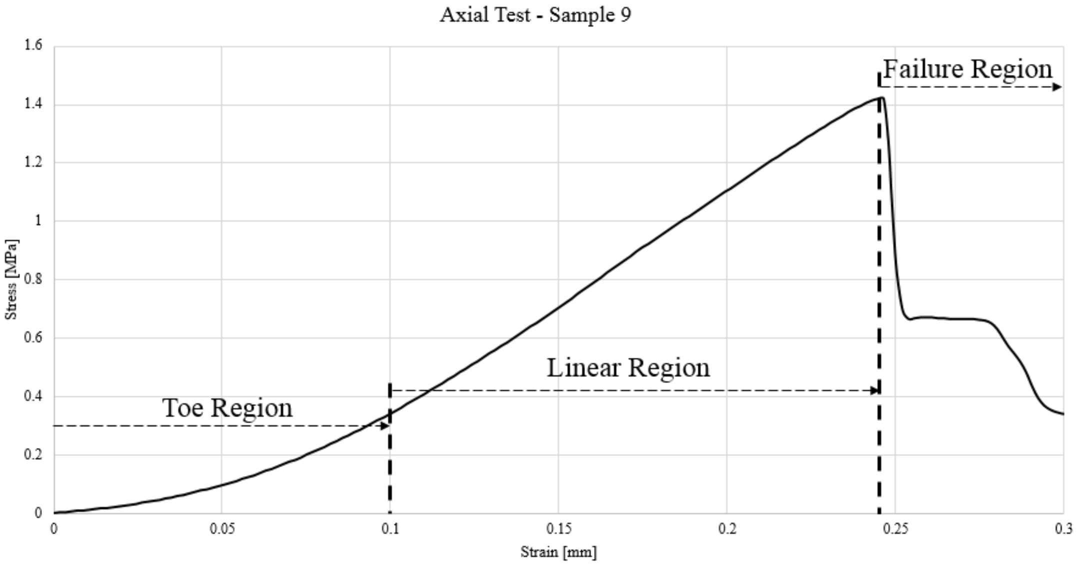

Figure 4.20: Stress-Strain regions

For nonlinear curves, various material models are used to capture the true material behavior. For hyperelastic materials, models such as Neo-Hookean, Moony-Rivlin, Ogden, Arruda-Boyce, and couple of other material models are used commonly. For this study, the Ogden Material Model was chosen because this model is more direct in using experimental data to determine its constants. For this study, the toe region and linear region is the main focus, since modeling failure requires failure models, which is separate from the typical material models such as hyperelastic.

4.3.1 Ogden Material Model

The Ogden material model assumes the material's stress-strain relationship can be described by the strain energy density function. The strain energy density function relates the strain energy (the energy stored) of the material to the deformation gradient. Since, the model assumes a relationship between the energy stored and the deformation, the stress-strain relationship can then be derived as well. The Ogden model uses experimental data in terms of stretches (λ). For the curve fitting described in this chapter, strains (ε) will be used. λ and ε can be converted between each other using equation (4.4). There are several forms of the Ogden material model, the form that ANSYS uses is equation (4.5). *Ogden et al.* [33] and *Teng et al.* [32] used this form of the Ogden strain energy density equation for their experimental study and derivation, respectively. Note, that the full strain energy density equation has a second half that takes into account compressibility/volumetric change. For this study, the trachea samples are assumed to be incompressible; thus neglecting the second half resulting in equation (4.5).

$$W\left(\lambda_1, \lambda_2, \lambda_3\right) = \sum_{p=1}^{N} \frac{\mu}{\alpha_p}\left(\lambda_1^{\alpha_p} + \lambda_2^{\alpha_p} + \lambda_3^{\alpha_p} - 3\right) \tag{4.5}$$

For hyperelastic materials the strain energy density function (W) can be derived and expressed in terms of stress (σ). Equations (4.6) and (4.7) shows this relationship.

$$\sigma_i = \lambda_i \frac{\partial W}{\partial \lambda_i} \tag{4.6}$$

$$\sigma_i = \frac{\partial W}{\partial \lambda_i} \tag{4.7}$$

According to *Ogden et al.* [33], the difference between equation (4.6) and (4.7) is dependent on whether the area of each sample was measured or not. If area is assumed the same, uniform across all samples, one would use equation (4.6). If the area of each sample was measured, then one would use equation (4.7). Incompressible is an assumption made when deriving the model therefore, equation (4.8) was used to calculate λ.

$$\lambda_1\lambda_2\lambda_3 = 1 \tag{4.8}$$

$$\lambda_1 = \lambda = 1+\varepsilon \tag{4.9}$$

$$\lambda_2 = \lambda_3 = \frac{1}{\sqrt{\lambda}} \tag{4.10}$$

For this, study the Ogden model was taken to the second order for better accuracy in the curve fit. Notice, that equations (4.9) and (4.10) are derived from equation (4.8) by assuming incompressibility; as stated previously. By using equations (4.4), (4.5), (4.7), (4.9), and (4.10), and taking the Ogden model to the 2nd order, equation (4.11) is obtained.

$$\sigma = \mu_1\left(1+\varepsilon\right)^{\alpha_1-1} - \mu_1\left(1+\varepsilon\right)^{-\frac{\alpha_1}{2}-1} + \mu_2\left(1+\varepsilon\right)^{\alpha_2-1} - \mu_2\left(1+\varepsilon\right)^{-\frac{\alpha_2}{2}-1} \tag{4.11}$$

Please see Appendix C – Chapter 4: Porcine Tracheal Material Properties for derivation.

4.3.2 MATLAB Curve Fitting Toolbox

Using equation (4.11) and MATLAB R2016a curve fitting toolbox, and the custom equation setting; the constants for the axial direction is described in Table 4.3.

Table 4.3: 2nd Order Ogden material constants for the axial direction.

Constants	Values
μ_1 (MPa)	5.334
μ_2 (MPa)	-5.136
α_1	11.53
α_2	11.63
D_1 (MPa^{-1})	0
D_2 (MPa^{-1})	0

D_1 and D_2 are constants that are in the volumetric change portion of the Ogden equation. As stated before, the samples are considered to be incompressible. Even though, the material considered incompressible ANSYS still requires an input for constants D_1 and D_2. It is stated in the ANSYS theory manual that, if the material is assumed to be incompressible, D_1 and D_2

need to be set to zero. Using the constants in Table 4.3, the following curve is generated and overlaid on top of the data.

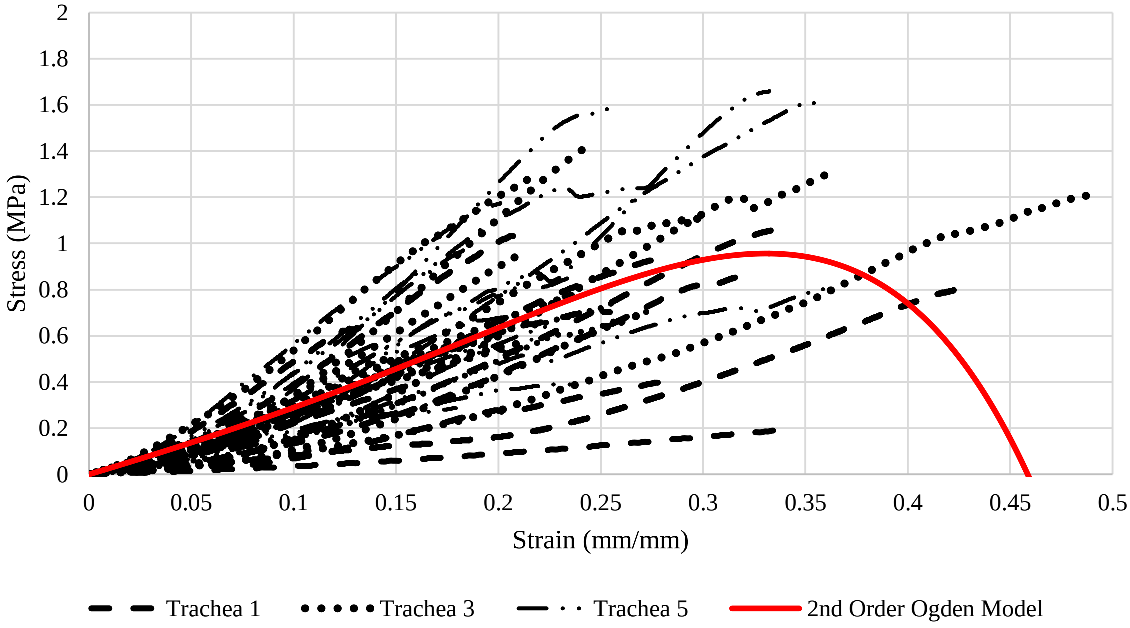

Figure 4.21: Ogden Model curve fit on axial data

Since failure modeling was not incorporated in the curve fitting; values past ε = 0.3 should not be used.

In the MATLAB curve fitting toolbox, the fit options are show in Table 4.4. The Levenberg-Marquardt algorithm is chosen as the algorithm for curve fitting this data. In addition, *Wu et al.* [34] used the same algorithm for their study into using Ogden model for curve fitting as well. According to the MATLAB R2016a curve fitting toolbox, the R^2 values is 0.9962 for this curve fit, which is a desirable number.

Table 4.4: Fit Option settings for axial curve fit in MATLAB

Fit Options for MATLAB Curve Fitting Toolbox	
Robust	LAR
Algorithm	Levenberg-Marquardt
DiffMinChange	1E-08
DiffMaxChange	1E-05
MaxFunEvals	10000
MaxIter	1000

Continuation of Table 4.4			
TolFun		1E-06	
TolX		1E-06	
Coefficients	StartPoint	Lower	Upper
α_1	11	-Inf	Inf
α_2	12	-Inf	Inf
μ_1	2	-Inf	Inf
μ_2	-2	-Inf	Inf

Similarly, the constants for the circumferential direction was computed with similar settings in the curve fitting toolbox. The constants for the circumferential direction are summarized in Table 4.5. Again, D_1 and D_2 are 0, assuming incompressibility of the material.

Table 4.5: 2nd Order Ogden material constants for the circumferential direction

Constants	Values
μ_1 (MPa)	18.53
μ_2 (MPa)	18.887
α_1	0.313
α_2	0.2881
D_1 (MPa^{-1})	0
D_2 (MPa^{-1})	0

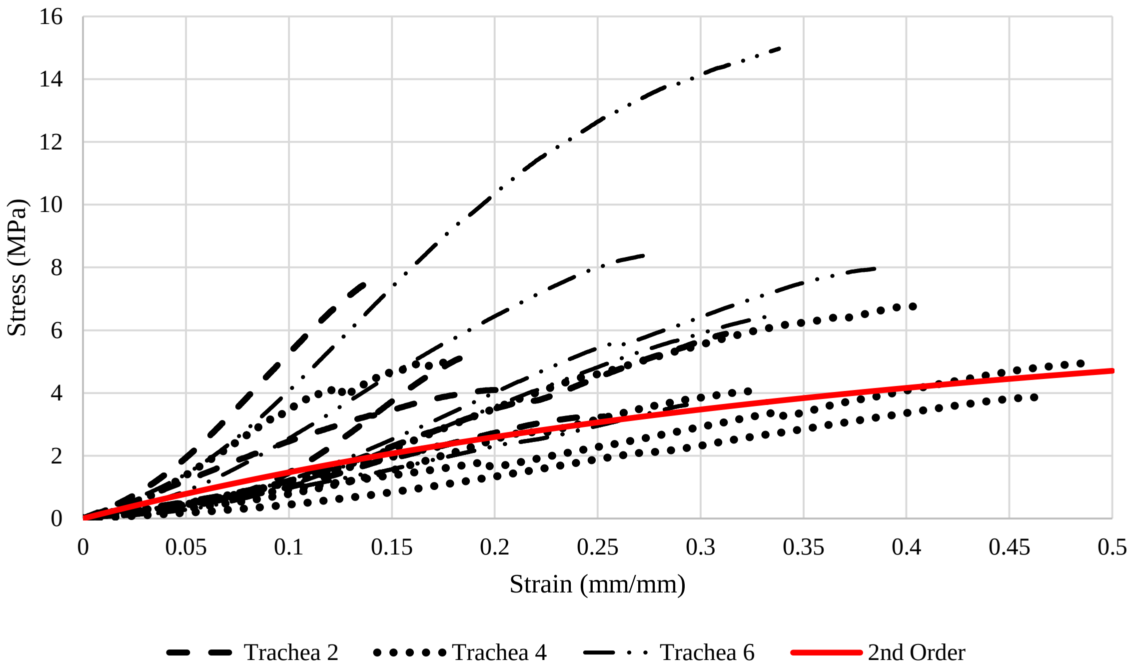

Figure 4.22: Ogden model curve fit for circumferential data

The procedure and settings for the circumferential fit option are the same as the axial direction (Table 4.4). The only differences are the starting points for the coefficients, which are summarized in Table 4.6. Likewise, according to MATLAB, the R^2 values is 0.9831 for this curve fit, which is a desirable number.

Table 4.6: Starting values of the constants for the circumferential direction

Coefficients	StartPoint
α_1	0.1419
α_2	0.4218
μ_1	0.9157
μ_2	0.7922

Similar to the axial curve fitting, values past $\varepsilon = 0.3$ should not be used since failure modeling was not incorporated in the curve fitting.

With known constants, the next step is to verify the numbers in a simple simulation before using the values in a complex simulation. After the values are verified, knowing the elements are going to behave the way the curve fit says it will, the values can then be applied in Chapter 5 – FSI Human Trachea Simulation. Note that, since both the axial and circumferential material properties are nonlinear, putting in a different guess, if the algorithm, or the robust setting gets changed, the constants will be different than the ones obtained in this study.

4.4 Phase 3: Single Element Model

Simple single element models (SEMs) in FEA are often used to evaluate the accuracy of a material model before applying the material model to complex simulations. This concept was first introduced by *Robinson* [35]. The purpose of the SEM is to test the material model's accuracy in terms of the behavior of the elements and other defined material properties such as incompressibility. SEM models can be 2D or 3D, for this case, a 3D model was selected. There is not a major different between running a 2D element simulation versus a 3D. *Robinson* [35] used a 2D simulation example, however for this case, the material model is going to be used in a 3D geometry therefore a 3D selection was chosen.

4.4.1 Geometry, Mesh, Boundary Conditions, and Material

The geometry for this simulation is a 1 (mm^3) cube. The mesh size is one element. The BCs for the element are shown in Figure 4.23 and summarized in Table 4.7.

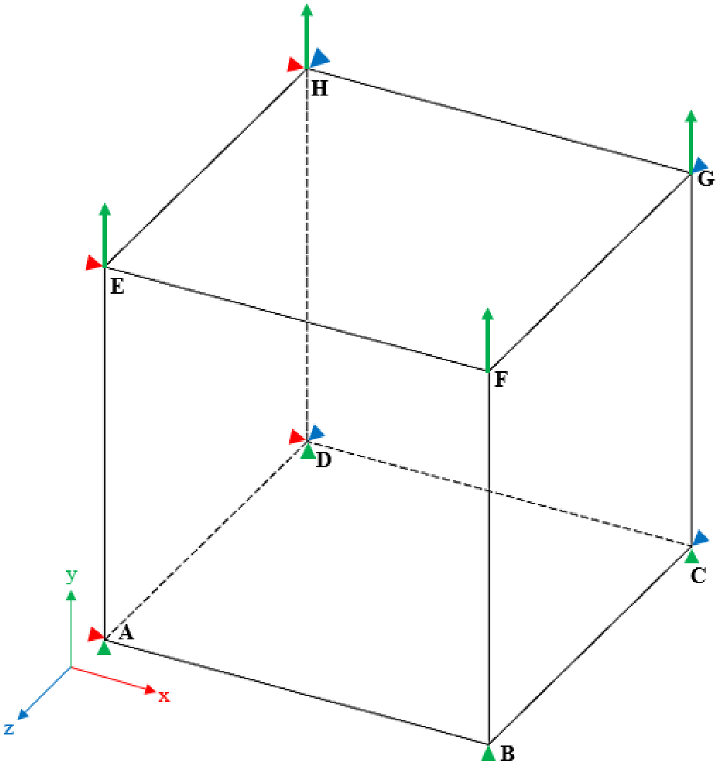

Figure 4.23: Boundary conditions for SEM simulation

The following table below describes the BCs as shown in the figure above. The constraints prescribed on the element are done on the eight corners of the cube. It is worthy to note, that this “corner” method is not the only way of prescribing the BCs. Another method would be to prescribe proper conditions on the surfaces in the respective axis directions as shown in Figure 4.23. However for possible debugging purposes the “corner” method was used.

Table 4.7: BCs for SEM

	A	**B**	**C**	**D**	**E**	**F**	**G**	**H**
X Axis	0	Free	Free	0	0	Free	Free	0
Y Axis	0	0	0	0	Input	Input	Input	Input
Z Axis	Free	Free	0	0	Free	Free	0	0

Described in Table 4.7, nodes E, F, G, and H are prescribed with various displacements or forces in the Y direction. (For this case, displacement was used.) Nodes A, D, E, and H are all fixed in the X direction, creating a plane of symmetry on the element. Similarly for Nodes C, D, G, and H are fixed in the Z direction creating a symmetry BC there.

The material used in the single element simulation (SES) are the constant from the 2nd order Ogden material model curve fitted in the axial and circumferential directions. Two different SES were simulated using the respective constants from the two testing directions. The constants can be found in Table 4.3 and Table 4.5. In addition to the Ogden constants, a density, ρ, must be supplied even though the value is not used. For the two simulations, a ρ = 1.05 E-06 (kg/mm^3) was used. The density value can be an arbitrary value, however for the two SEM simulations, the density was estimated by approximating cartilage to be composed of 80% water. *Fox et al.* [36] described the abundance of water in the articular cartilage. Therefore, a fair approximation for density of porcine trachea, which is composed of mostly cartilage and some connective tissue, both of which are hydrophilic, is close to that of water.

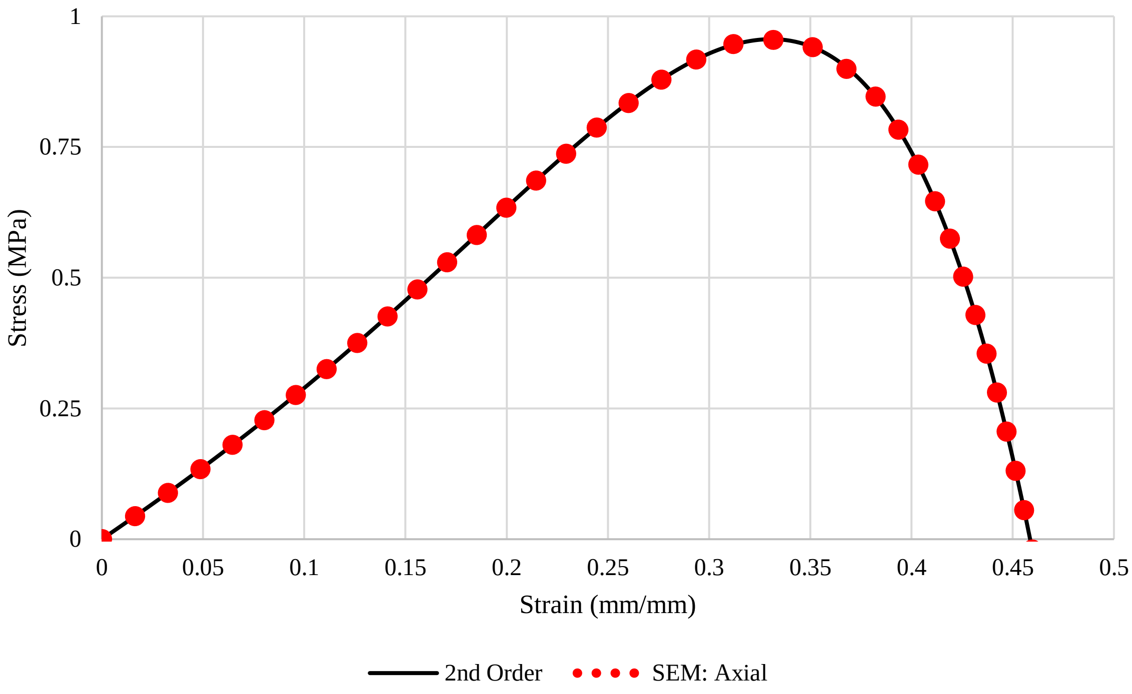

Figure 4.24: Axial – single element simulation results

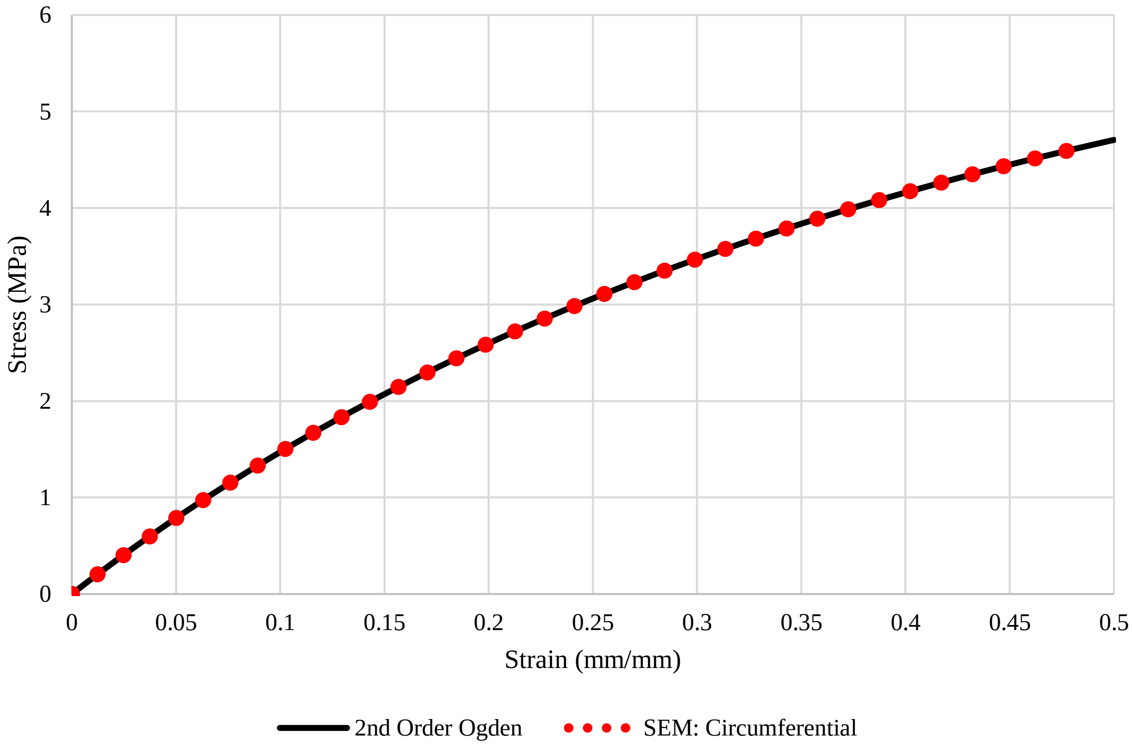

Figure 4.25: Circumferential – single element simulation results

It can be seen in Figure 4.24 and Figure 4.25 that the SEM results matches perfectly with the material constants. Which means when the material models are applied, the elements will behave properly.

4.5 Conclusion

Many attempts have been made to characterize tracheal tissue, though only a few studies have been conducted for curve fitting the data. Curve fitting data will allow others to use the constants in FEA and FSI simulations; therefore it is desirable to curve fit the data. *Lally et al*. [12], *Teng et al.* [14], and *Trabelsi et al* [11] are researchers who have conducted experiments and curve fit the data. For this study, the Ogden model was the desired model to use for future simulations therefore, new testing was conducted and the data was curve fitted. There are several differences between this case study and usual biological testing. First, only a small preload was applied and no preconditioning was done. Secondly, the samples were pulled to failure, without doing cyclic loading. Lastly, the curve fit for this study was verified through a FEA simulation. It is important to verify the behavior of the elements, to ensure accuracy of simulation models. From this study which involves testing, curve fitting and simulation, the individual processes provided a verification process. With the verified constants, they can be applied to a real lung geometry.

Chapter 5: FSI HUMAN UPPER AIRWAY SIMULATION

5.1 Human Airways

The human lung and conducting airway is comprised of a series of complex tubular structures that eventually terminate in the alveoli where the majority of respiratory gas exchange occurs. From a purely mechanical standpoint; the complexity of the structural geometry itself offers many challenges. To include other studies such as mucus clearance, inflammation of alveolar tissue, or a diseased lung/loss of physiological compliance would increase the complexity even more. Researchers such as *Button et al*. [37] have conducted studies specifically on mucus clearance. Mucus clearance is essential to enhance efficiency and ease of respiratory gas exchange. However, as *Button et al*. [37] concluded, further studies still need to be conducted to fully grasp how the viscoelastic material behaves. Similarly, *Aghasafari et al.* [38] have conducted a study on strain-induced inflammation of alveoli tissue due to mechanical ventilation. Both researchers utilized a reductionist approach and targeted a specific area of the lung. However, for this FSI study the main focus is on the upper airway.

As stated earlier, researchers have conducted FSI or FEA simulations on the human lung in various locations in the airway tree. *Malvè et al.*[6] used a CT scan geometry for an FSI simulation and reported the differences between normal breathing and PCV ventilation; specifically on the trachea. Later *Malvè et al.* [39] conducted an FSI simulation on a healthy and stenotic (abnormal narrowing) human trachea under impedance-based boundary conditions. Similar to the first study, the focus was on the trachea alone. *Yoshihara et al.* [40] conducted an FSI study for local deformation imposed from a volumetric constraint standpoint onto the bifurcated airway and in the overall lung itself (left and right lobes). Other researchers such as *Xia et al*. [5] and *Liu et al.* [41] have also conducted FSI simulations in the airway, but at specific chosen locations. *Xia et al*. [5] chose the 3rd and 4th bifurcation for laminar flow conditions. The reason being, is that the initial generation (the trachea) has turbulent flow which once again adds complexity to the flow in the airway. While *Liu et al.* [41] chose the 5th-11th branch to simulate for a similar reason. In addition, *Calay et al*. [4] conducted CFD simulations of the first and second bifurcation in the human lung. Since CFD simulations only look at fluid flow, the structural portion of the lung wall was not taken into account. Lastly, *Teng et al*. [32] and *Sera et al.* [42] each have conducted simulations on the material properties and diseased lungs, respectively. Similar to *Button et al*. [37] and *Aghasafari et al.* [38] these simulations focused on a specific aspect of the lung.

For this study, material properties, velocity ventilator flow profile, and geometry up to the 4th generation (G4) of the lung airway are taken into account. The simulation applies material properties from the tensile testing study and BCs used for the 3D balloon are also incorporated in addition to the ventilation flow conditions. The main goal of this study is to conduct a feasibility study on the stresses and air flow for PCV flow condition.

5.2 Lung Geometry

The lung geometry is derived from a CT scan of a human lung. CT images are DICOM files, which are encrypted medical files. In order to use the geometry for simulations, the DICOM file must be converted to a STL file. This process was done using an open source software, 3D Slicer [43, 44].

Figure 5.1: 3D Slicer [43, 44] generated human lung geometry

Figure 5.1 shows the anterior (front) view of the lung. A way to determine the orientation is by looking in the lateral (side to side) direction of Figure 5.1, the right bronchus is slightly elongated while the left bronchus veers laterally. The lateral component is for the heart that is also located on the anatomical left side of the human.

For this study, the focus is to simulate the first three generations of the model, therefore the model was further trimmed and processed such that thin sections/branches were also removed. This is because thin sections and branches are hard to mesh and causes complications during simulations. Future studies can correct these complications for a more realistic approach.

Figure 5.2: Fluid geometry for human lung model

Similar to Figure 5.1, the view shown in Figure 5.2 is an anterior view of the upper airway. Shown in Figure 5.2 is the fluid region. The fluid geometry was then imported into Pointwise, a meshing generating software, to create the structural region. A “shell” was created over the fluid region with a uniform thickness of 1 (mm). Creating multi-thickness shell will add more complexity to the model. Since the current research is just a feasibility study, the thickness was kept uniform for simplicity.

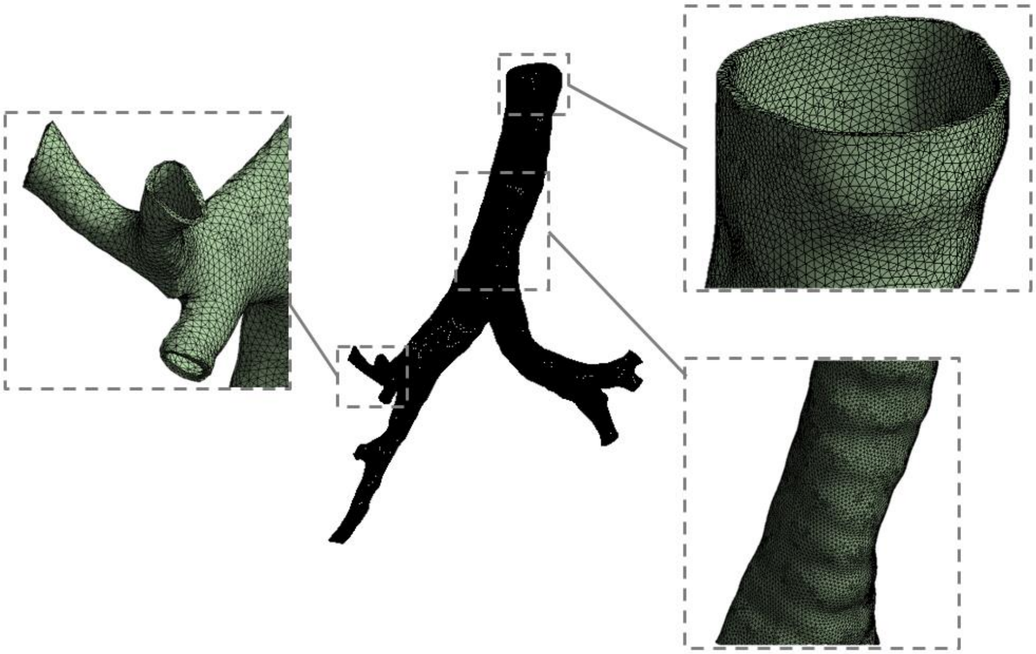

Figure 5.3: Structural geometry for human lung model

Note that Figure 5.3 is showing the STL geometry and not the mesh. An STL file only describes the surface geometry, hence the unstructured triangular surface. Lastly, both the fluid and structural geometries are imported into ANSYS for meshing.

5.3 Lung FSI Methods

Similar to pervious chapter Method sections, it is divided into several sections: Mesh, Boundary Conditions, Material Properties, and Convergence Settings. Like the 3D balloon, this simulation only has one mesh size. ANSYS uses existing analytical systems along with the SC module to perform FSI analyses. For this simulation, ANSYS Fluent and Transient Structural are the main analytical systems, which are coupled using the SC module (shown in Chapter 2, Figure 2.2).

5.3.1 Mesh

Unstructured elements were used for both the fluid and solid regions. Similar to the 3D balloon, the mesh settings given below are an attempt to balance a reasonable simulation run time and accurate results. Table 5.1 are the general settings for both the fluid and structural regions.

Table 5.1: Mesh settings for lung geometry

Mesh Settings	
Element Order	Linear
Element Size (m)	0.0005
Growth Rate	1.2
Capture Curvature	Yes
Smoothing	Medium

Same logic as the 3D balloon, in this simulation the fluid and structural region have the same element size. The main goal is to capture the behavior of the structural region, hence, the structural region having more elements.

Table 5.2: Human Lung – Mesh properties for the fluid and structural regions

Fluid Region		**Structural Region**	
Number of Elements	Element Size	Number of Elements	Element Size
215,772	0.5 - 1 (mm)	422,235	0.5 (mm)

Table 5.2 shows that the element size for the fluid region is in between 0.5 and 1 (mm). This is because on certain regions a “Meshing sizing” was added to refine the mesh in the specified regions, the FSI surface is set at 0.5 (mm); everything else is set to 1 (mm). Since the geometry of the lung is not a regular uniform geometric shape like the balloons, it will be difficult to display the entire mesh in detail. Therefore, only certain regions where magnified to show the detail of the meshes. One last thing to note in regard to the mesh, is the use of unstructured elements. Using unstructured elements, can play into numerical difficulties. However, given the geometry the use of an unstructured mesh is more convenient. For future studies, a better mesh should be created.

Using the settings from Table 5.1 and Table 5.2, the mesh for the lung geometry are shown in Figure 5.4. and Figure 5.5.

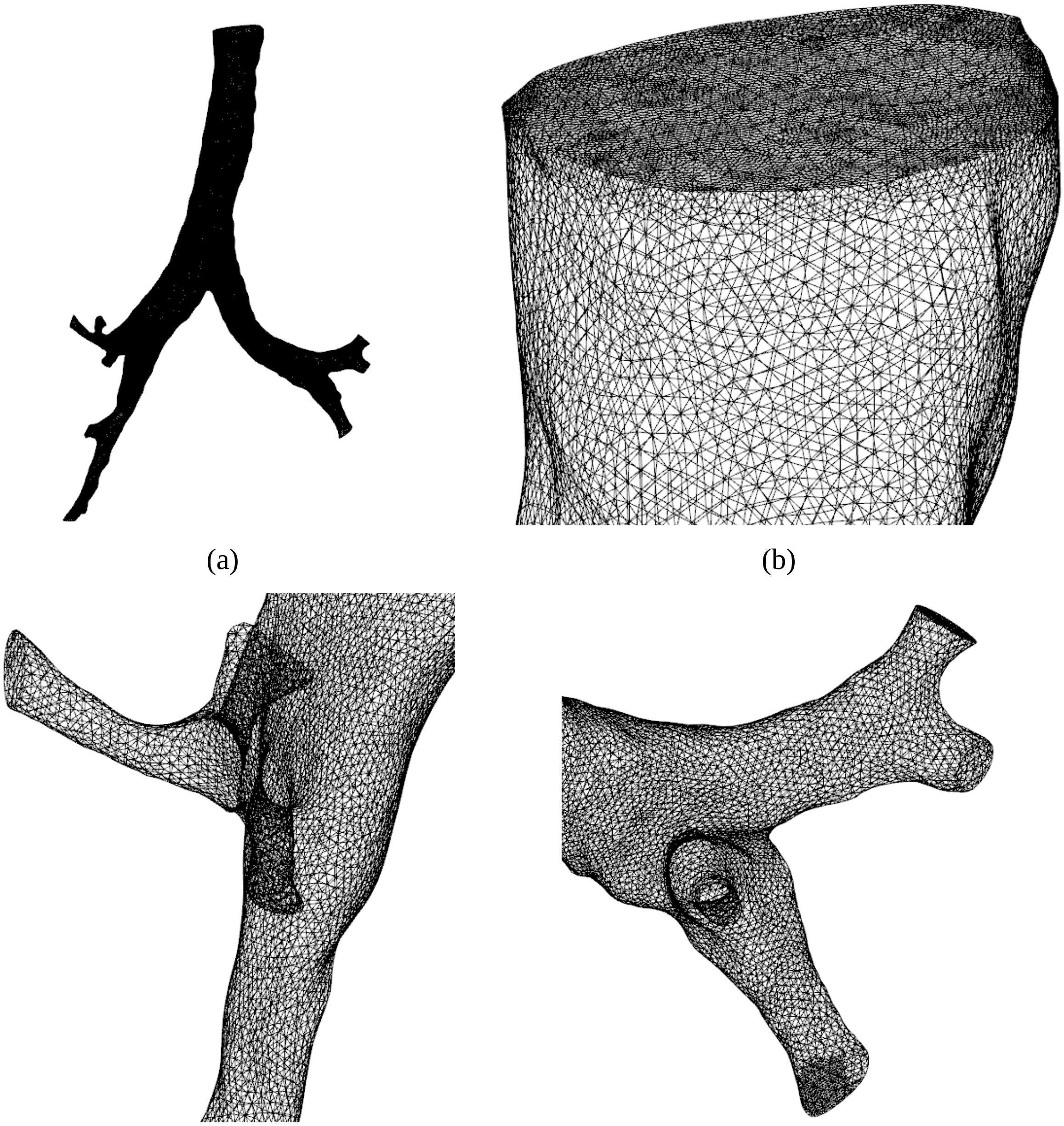

(a) (b)

(c) (d)

Figure 5.4: Human Lung – Fluid region mesh: (a) Isometric view of mesh, (b) upper trachea, (c) lower left bronchi, and (d) lower right bronchi.

Similar to the fluid mesh, shown in Figure 5.5 are zoomed in regions of the structural mesh. Areas similar to the fluid region where chosen for consistency.

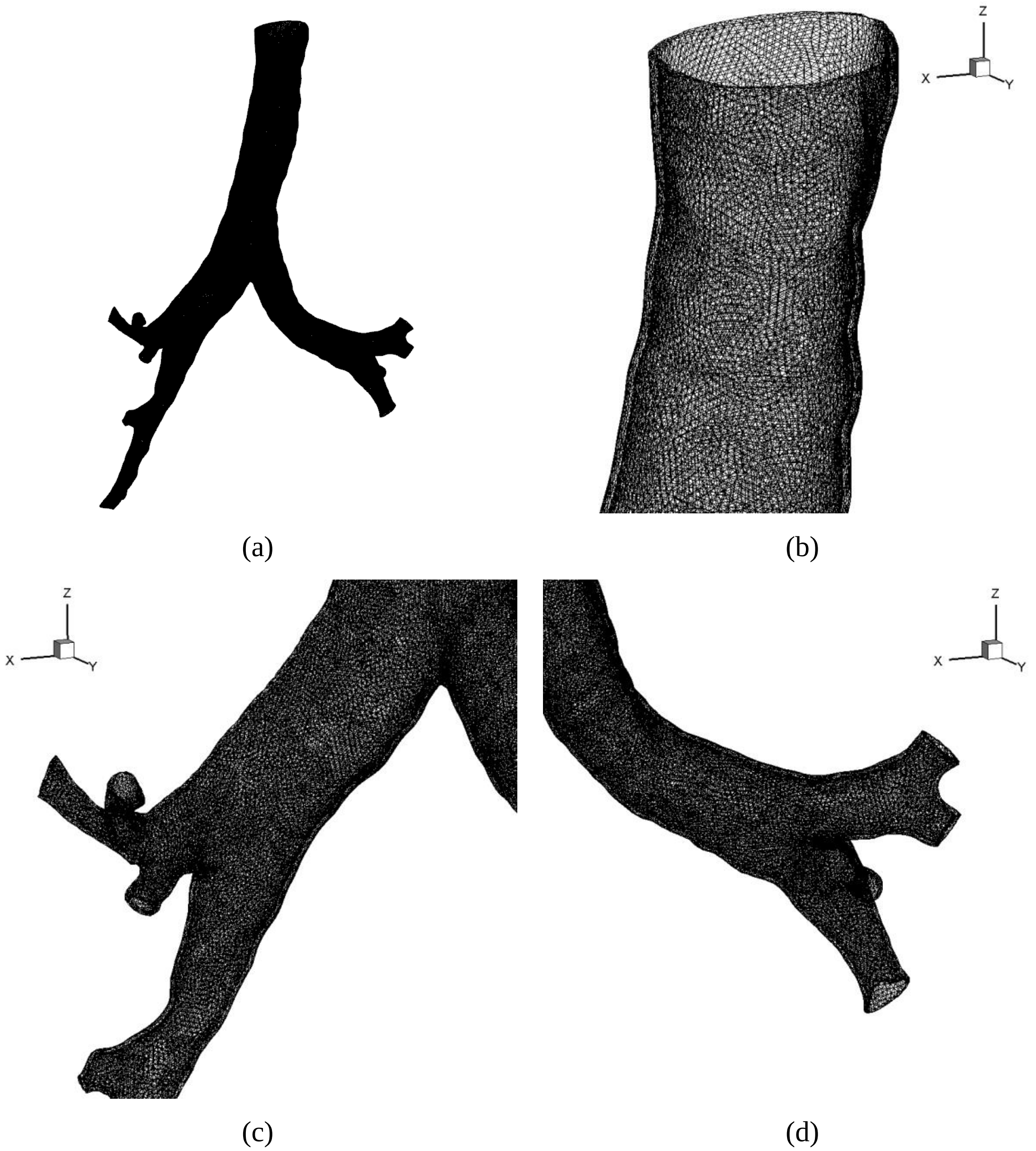

Figure 5.5: Human Lung – Structural region mesh: (a) Isometric view of mesh, (b) upper trachea, (c) lower left bronchi, and (d) lower right bronchi.

5.3.2 Boundary Conditions

The BCs shown in Figure 5.6 are the conditions used in the lung simulation. The lung is fixed on the top surface of the trachea as indicated with the triangles in the figure. An elastic support (bubbled region) surrounds the whole lung to act as the support from the pleural cavity fluid. More details in regards to the elastic support are presented in Chapter 3. Next, an FSI surface BC is on the inside walls of the lung. This BC couples the fluid and solid components together for the simulation. This surface is where the SC module will perform the computation.

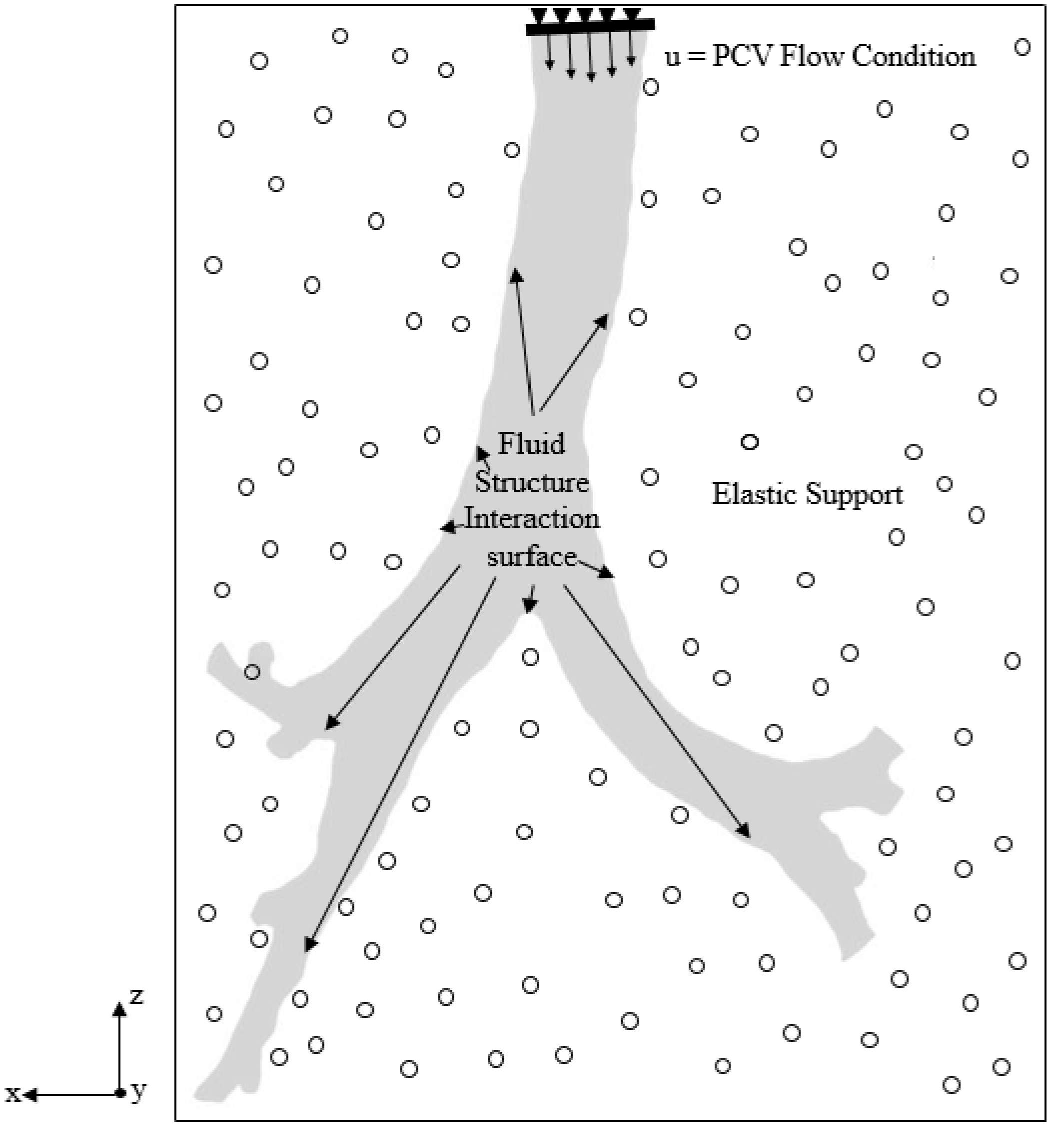

Figure 5.6: Human Lung Model – Boundary condition

The same elastic support value from the 3D balloon simulation was used: 10,000 (N/m^3). Since the value is that of water for the 3D balloon, similar values can be used for the pleural cavity fluid, since it closely resembles water.

Lastly, the velocity profile prescribed is a PCV ventilator flow condition. Only one breathing cycle was simulated. Shown Figure 5.7 is the velocity profile used in the simulation.

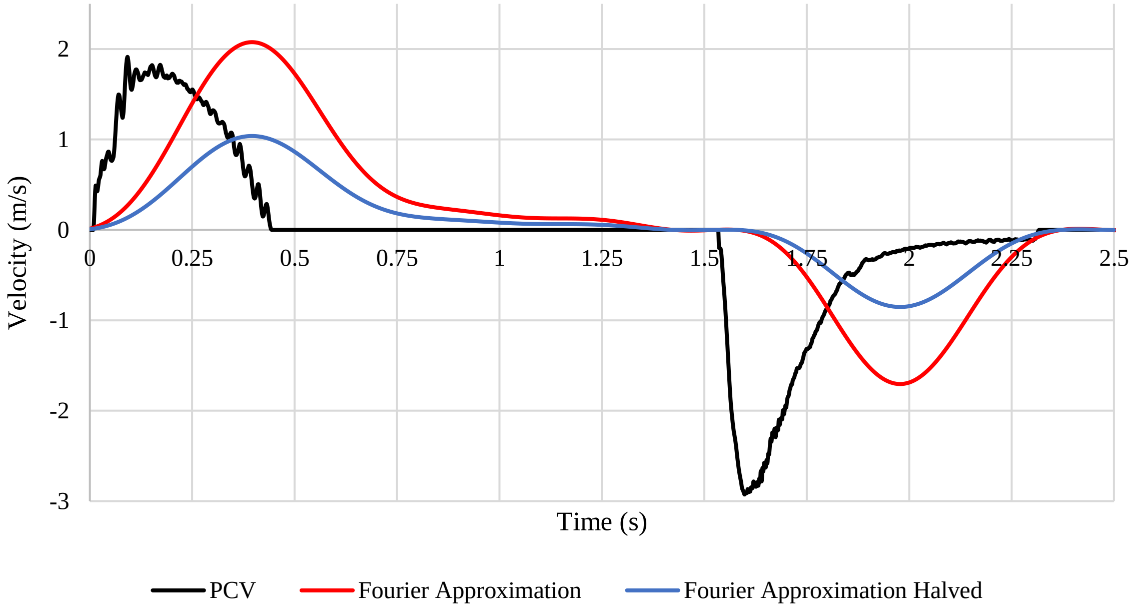

Figure 5.7: Human Lung Model – Prescribed PCV velocity

Shown in the graph above are three profiles: flowmeter measured PCV, a Fourier Approximation, and Fourier Approximation Halved. The velocity profile used for the simulation is the Fourier Approximation Halved (Code for Fourier velocity profile can be found in Appendix D – Chapter 5: FSI Human Upper Airway Simulation). The flowmeter measured PCV velocity has a lot of noise and the step size is not flexible. The noise causes fluctuations and additional computation time; both are unnecessary aspects to add to the simulation. Secondly, having a flexible step size will allow the simulation to be simulated to user’s desired accuracy. Generally smaller time step means higher accuracy. The flowmeter velocity is set at 0.002 (s), the step size, resulting in a fixed step size. The Fourier approximation has the step size flexibility but lacks the “true” behavior of the PCV flow condition, as seen in the figure. A better approach would be using a piecewise function, which allows for more flexibility in the shape of the profile; this would be a future study. Lastly, as stated previously, the flow that is actually used is the “Fourier Approximation Halved”. Due to the sensitive mesh, used in this case study, a peak velocity of 2 (m/s) will crash the simulation. Therefore, it was decided that the shape of the profile will be halved to simulate the general behavior. However, an eventual study should incorporate a piecewise function and a better mesh should be used to simulate the PCV flow condition.

5.3.3 Material Properties

The materials for the fluid and structural regions are given in Table 5.3 below. The fluid region is left at default for the air properties. In the structural region, a 2nd Order Ogden Material was used.

Table 5.3: Human Lung Model – Material properties for the fluid and structural regions

Fluid Material Properties	**Parameters**	**Value**
Density, ρ (kg/m^3)	Ideal - gas	-
Specific Heat, Cp (J/kg-K)	Constant	1006.43
Thermal Conductivity, κ (W/m-K)	Constant	0.242
Dynamic Viscosity, μ (kg/m-s)	Constant	1.7894E-05
Molecular Weight, M (kg/kmol)	Constant	28.966
Structural Material Properties	**Parameters**	**Value**
Density, ρ (kg/mm^3)	-	1.05E-06
2nd Order Ogden Material Model	-	
	μ_1 (MPa)	5.334
	μ_2 (MPa)	11.53
	α_1 (MPa)	-5.136
	α_2 (MPa))	11.63
	D_1 (MPa^{-1})	0
	D_2 (MPa^{-1})	0

The material properties for the 2nd order Ogden model is for axial tracheal tissue. The constants are obtained through testing. The density is an estimation based on cartilage being composed of mostly water. For the structural properties used, refer to Chapter 4 for further explanation.

5.3.4 Convergence Settings

To ensure the results comply with real world physics, the convergence settings provide the solver guidelines of when the results are satisfactory. Fluid behavior tends to be more complex, therefore most of the convergence settings are for the fluid region. In ANSYS

Fluent, the Solution Methods are left at default. The Residual Convergence values are changed to such that the numeric error is reduced and solution is achieved.

Table 5.4: Human Lung Model – Fluid region main convergence settings

Solution Methods	
Scheme	SIMPLE
Gradient	Least Squares Cell Based
Pressure	Second Order
Density	Second Order Upwind
Momentum	Second Order Upwind
Energy	Second Order Upwind
Transient Formulation	First Order Implicit
Residual Convergence	
Continuity	1e-05
x-velocity	1e-05
y-velocity	1e-05
z-velocity	1e-05
Energy	1e-06

Figure 5.5 has the convergence settings for the SC. The convergence criteria for data transfers are defaulted to RMS Convergence Target = 0.005. The convergence settings for the SC are independent of the fluid and structural systems. For more details regarding how the SC data transfer works refer to section 2.3.4.

Table 5.5: Human Lung Model – SC Data Transfer settings

Data Transfer 1		**Data Transfer 2**	
Source:	Transient Structural	Source:	Fluent
Region:	Fluid Solid Interface	Region:	Wall
Variable:	Displacement	Variable:	Force
Target:	Fluent	Target:	Transient Structural
Region:	Wall	Region:	Fluid Solid Interface
Variable:	Displacement	Variable:	Force

Shown in Table 5.5 are the simulation settings for the fluid and structural regions, as well as the SC module. The end time for the simulation from Fluent, Transient Structural, and SC module, must match or the simulation will not run.

Table 5.6: Human Lung – Simulation settings for the three modules

	Fluid Region	**Solid Region**	**SC**
Simulation Time (s)	2.5	2.5	2.5
Time Step Size (s)	0.005	0.01	0.01
Number of Time Steps	500	-	-
Large Deflection	-	On	-
Minimum Iterations	-	-	1
Maximum Iterations	50	-	2

As stated in Chapter 2, when running an FSI simulation in ANSYS, the SC settings override the structural and fluid simulation settings. However, for consistency, the settings for the fluid and structural regions should also be inputted before running the simulation. The step size for each simulation is different.

5.4 Results

Only one mesh was used for this simulation. With the given BCs, the simulation run for 2.5 seconds, since that is the duration of one inhale and exhale for PCV ventilation. The results section for this chapter will be divided between the solid region and the fluid region. The solid region will focus on the von Mises stresses, equivalent strain, and displacement. While the fluid region will have velocity magnitude and pressure shown in 3D contour plots with slices to show the fluid behavior inside the lung. All contour plots and graphs were created using Tecplot 360 EX 2017 R2.

5.4.1 Human Lung Model – Structural Region

Figure 5.8 shows the selected time the stress, strain, and displacement graphs are obtained. There are 10 different time steps to show the respected results of the lung model. The locations are chosen to observe the maximum change in stress, strain, and displacement.

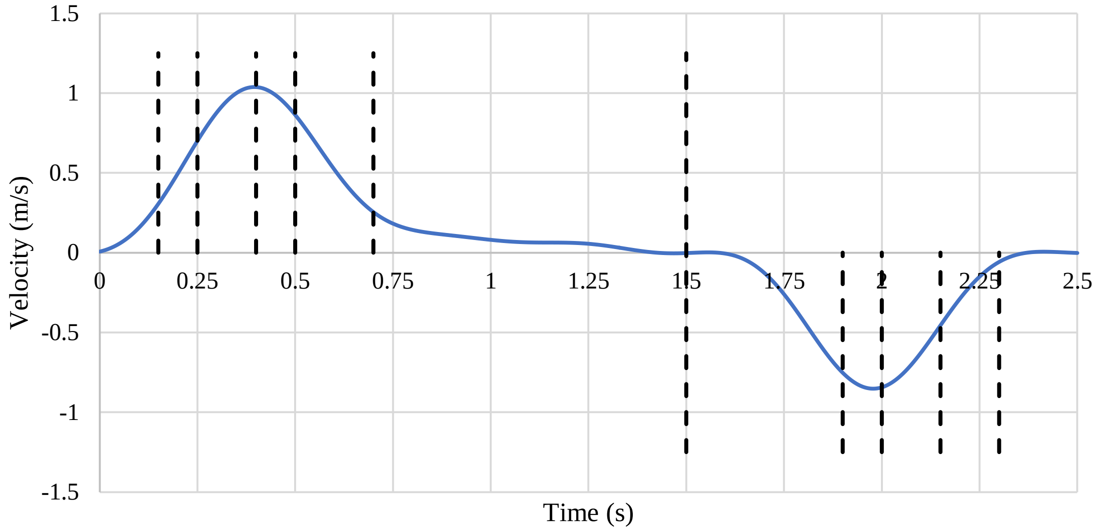

Figure 5.8: Human Lung – Reference for the selected time steps.

Shown in Figure 5.9 are the von Mises stresses in the structural region if the upper airway. The legend is fixed, to show the overall change in stress throughout the simulation time.

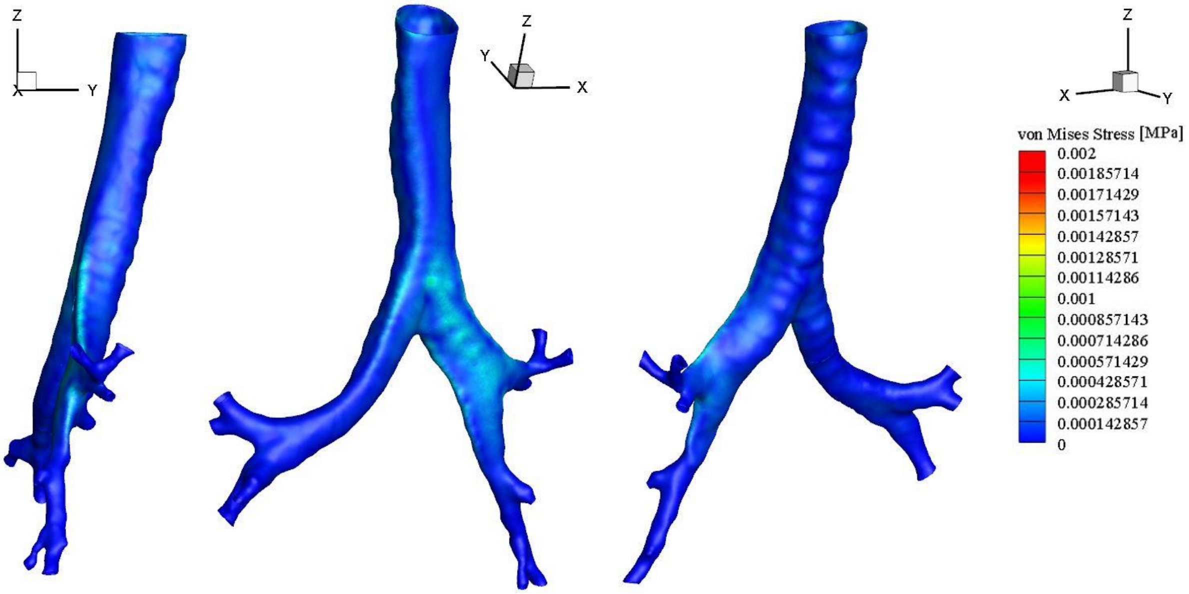

(a) t = 0.15 second

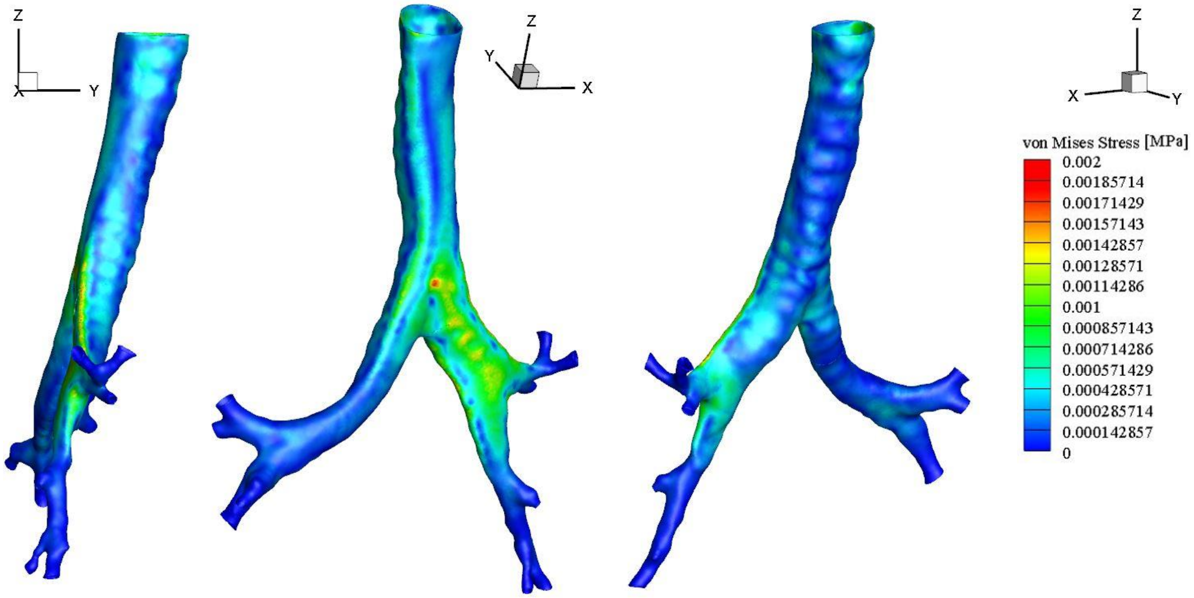

(b) t = 0.25 second

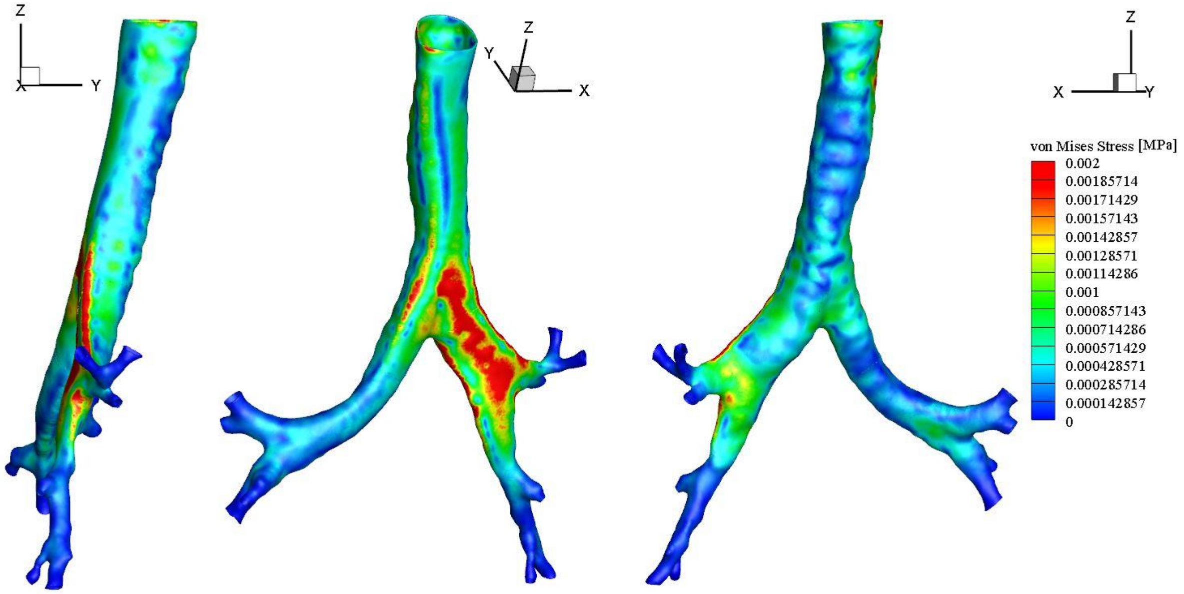

(c) t = 0.4 second

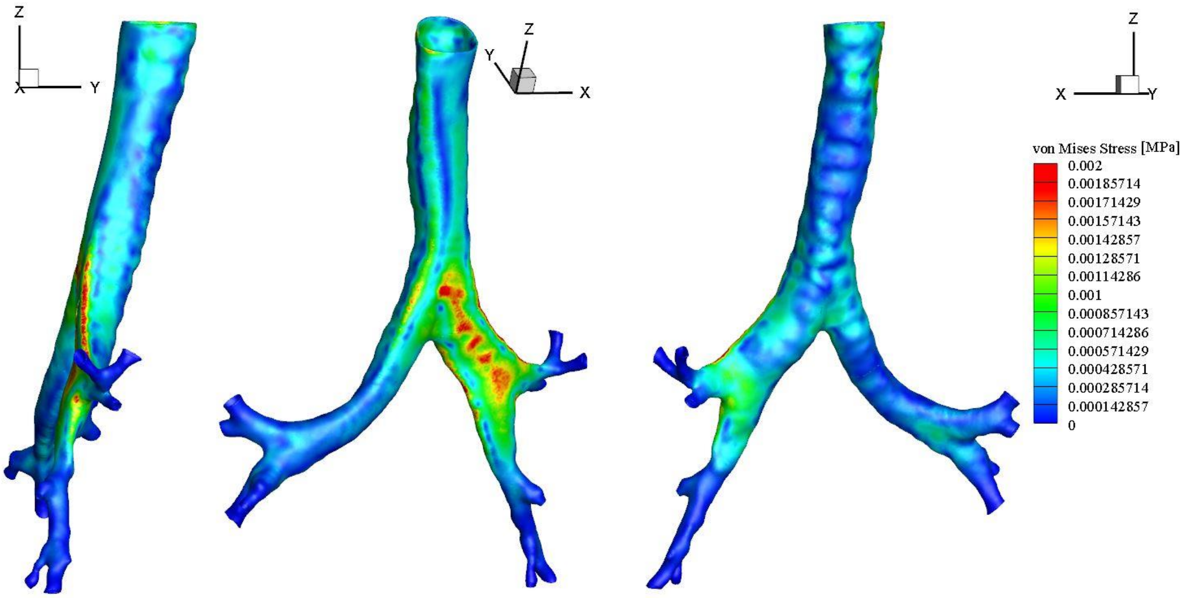

(d) t = 0.5 second

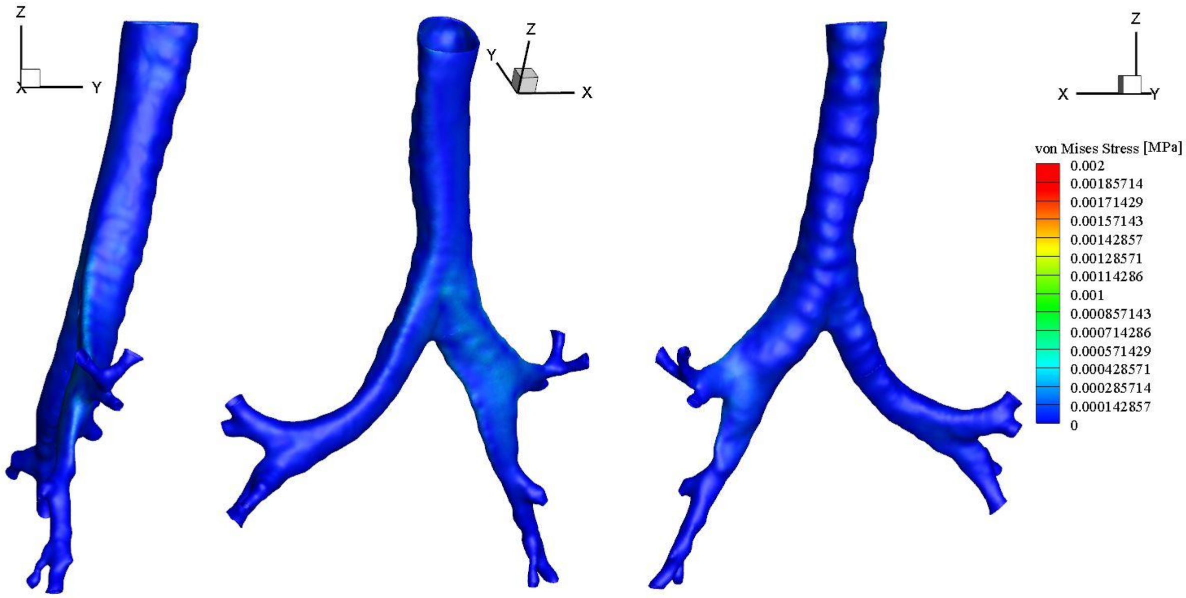

(e) t = 0.7 second

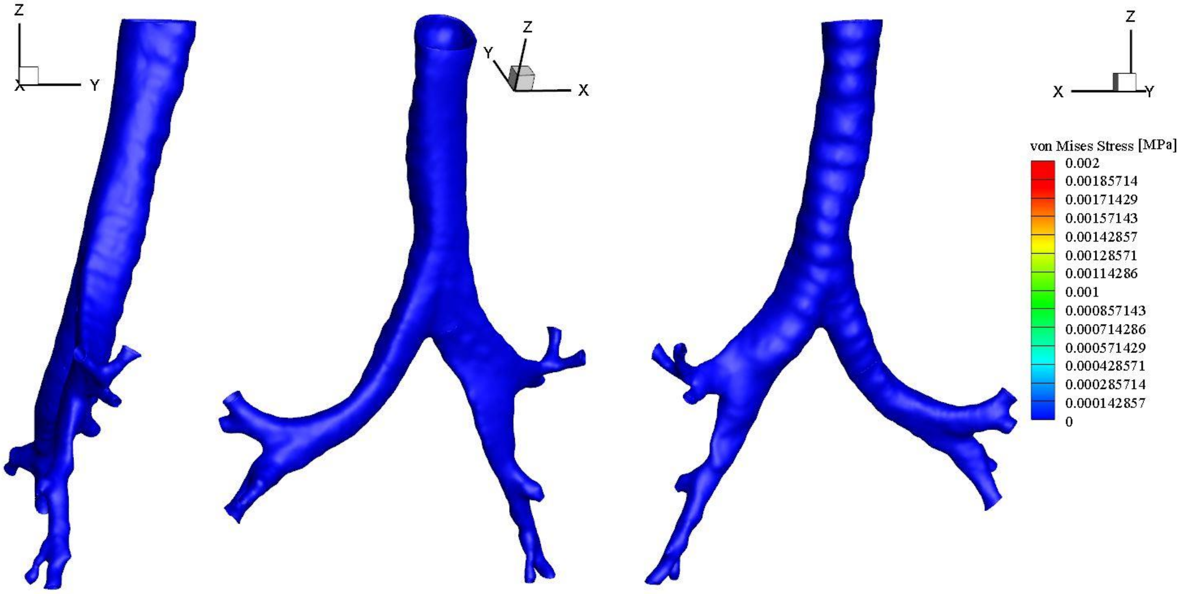

(f) t = 1.5 seconds

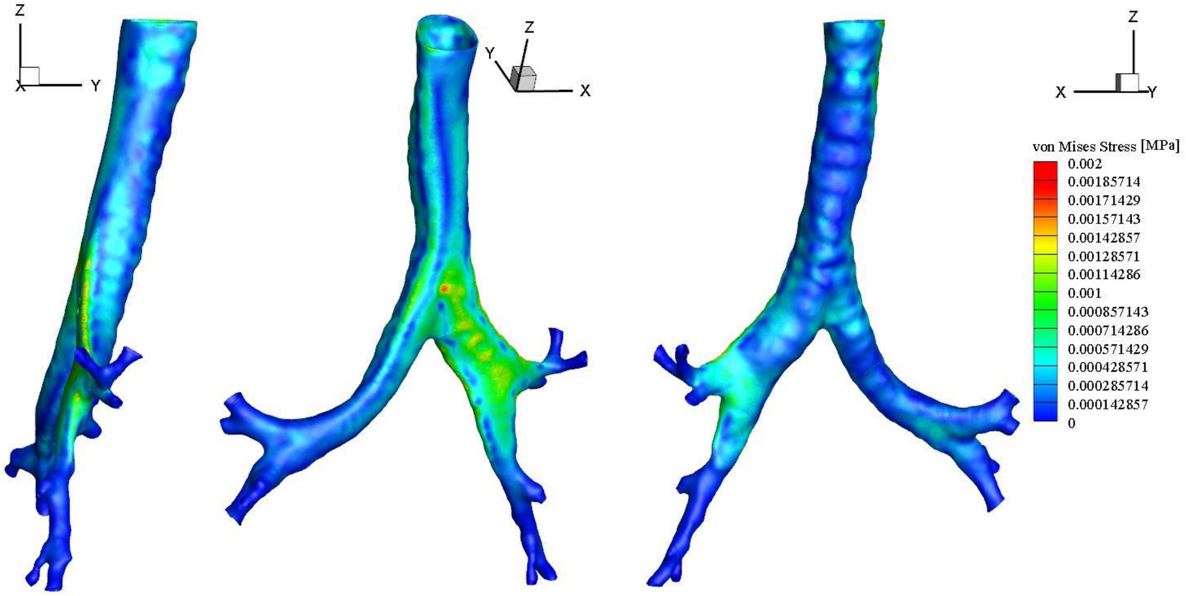

(g) t = 1.9 seconds

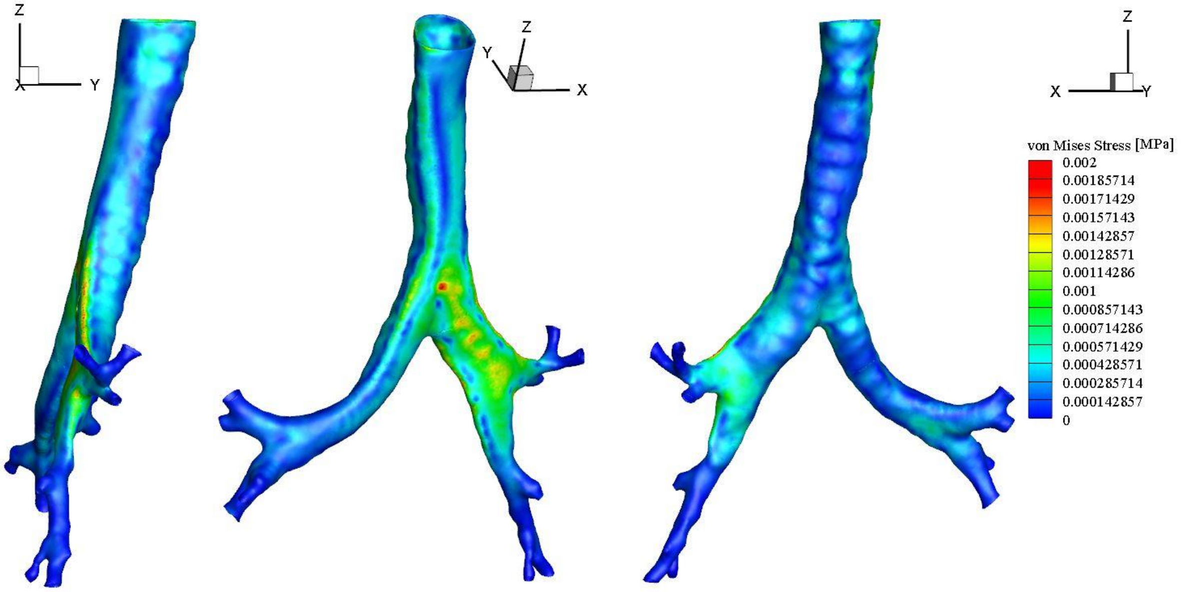

(h) t = 2 seconds

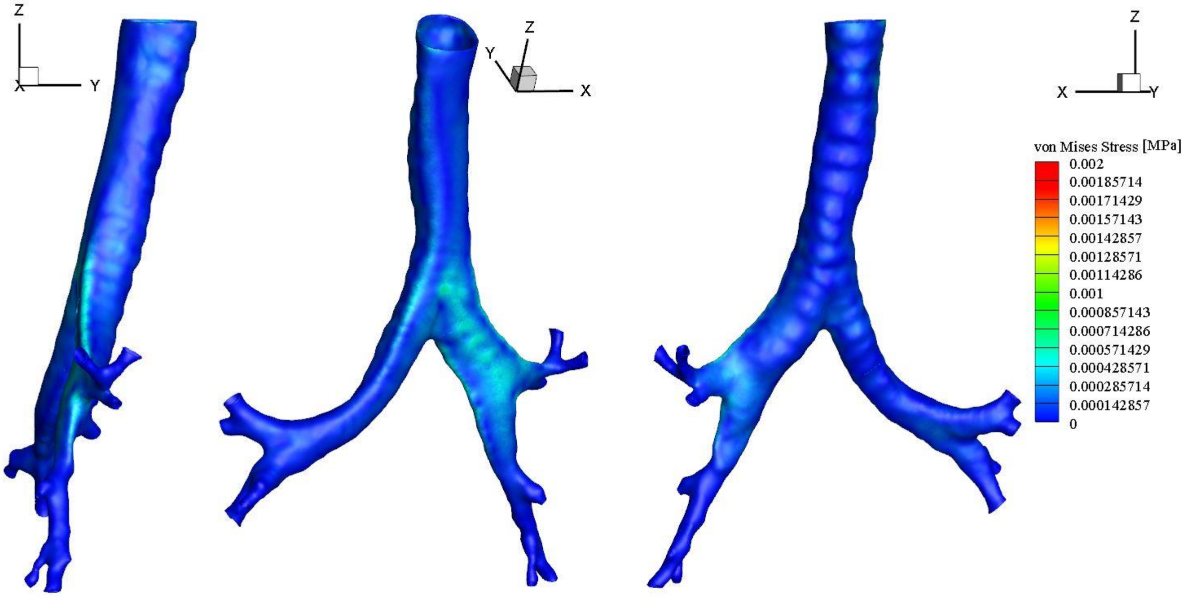

(i) t = 2.15 seconds

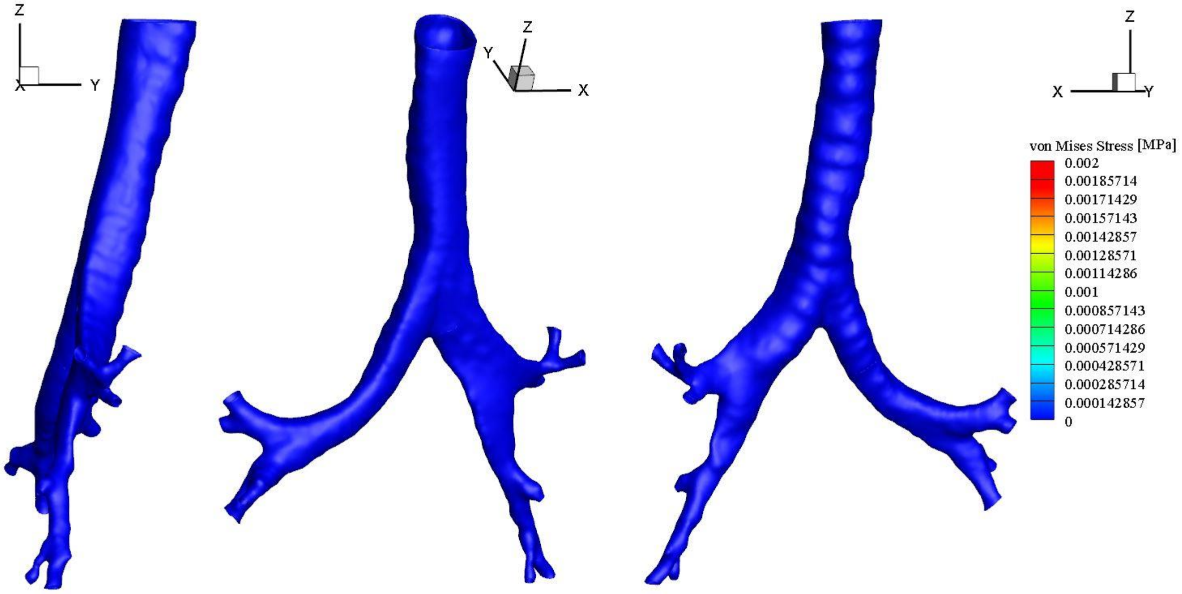

(j) t = 2.3 seconds

Figure 5.9: von Mises Stress of the Human Lung model

Looking at the von Mises stresses, the maximum stress is occurring at t = 0.4 second, which is at the peak of the curve. Hence having the higher stress at that point is reasonable. Correspondingly, the stress at t = 2 second is not as high, but that is also because the peak time is a little before t = 2 second. Additionally, the highest stress is occurring on a flat region of the outer wall. This observation is reasonable, since the lung is mostly cylindrical in shape, with the exception of the small flat portion on the back side of the upper airway.

Lastly, the location of the maximum stress (flat region on the back side of the upper airway) was probed to create a time series plot of the stress at the specified location. A time series plot will show the change in stress over time. An advantage of looking at a time series plot instead of the just contours is the unbiased number that a contour plot sometimes cannot provide.

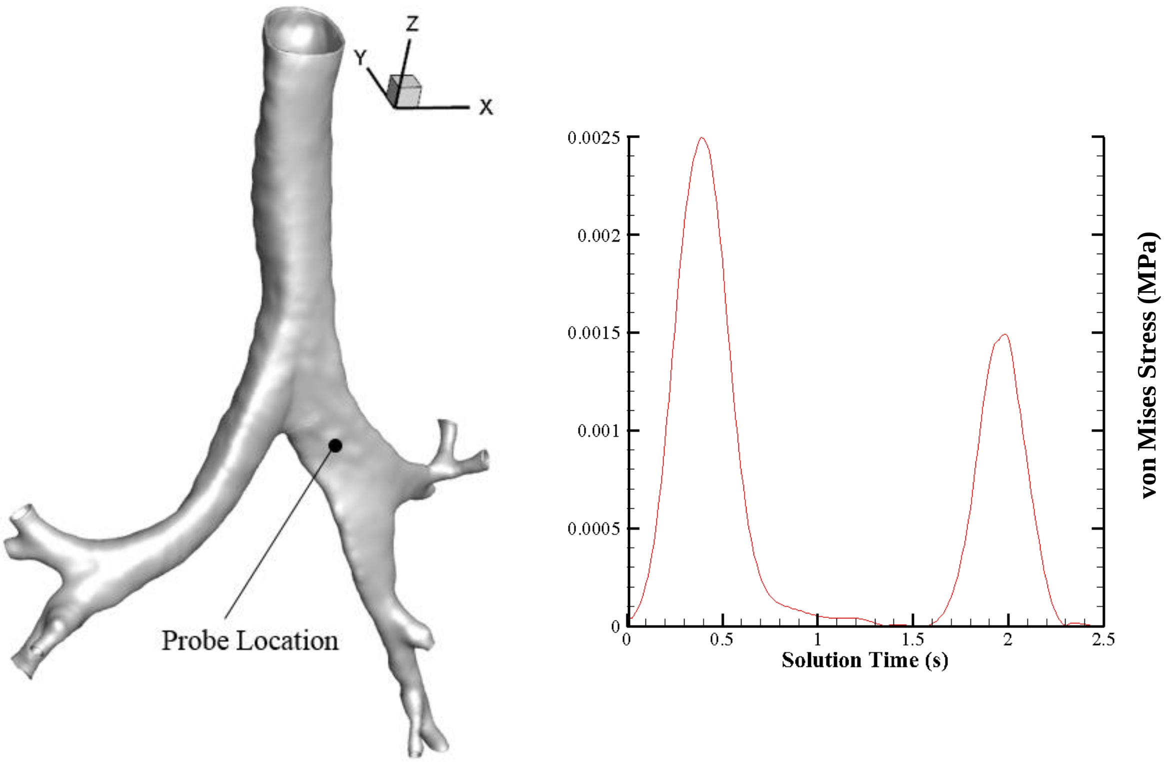

Figure 5.10: Time series plot of maximum stress for human lung model

As shown in Figure 5.10, the maximum stress peaked out at t = 0.4 second, which corresponds to the maximum inhalation velocity. While the lower peak occurring around t = 2 seconds is the maximum exhalation velocity. In theory, the stress should be closer to one another in terms of magnitude. There are several reasonable explanations, first the plot was created on the surface of the lung. Which may not be an accurate location to probe, a more appropriate location would the same area, but on inside of the lung. Another explanation, could be the geometry and material of the lung. The nonlinear material properties and uneven surfaces are causing the lung to easily expand, but hard to collapse. Last reason could be that the stress is in compression at t = 2 seconds, however again because of the material and geometry it can only collapse to a certain amount, resulting in a lower stress at t = 2 seconds compared to t = 0.4 second.

Shown in Figure 5.11 are the equivalent strains for the structural region of the lung model. The same time locations were chosen for the figure (reference Figure 5.8). Notice the maximum strain value on the legend is set to be the same value as the maximum stress: 0.002. This is to show that the material is behaving nonlinearly. If the material were to be linear, then the stress and strain will have the same contour in the same regions.

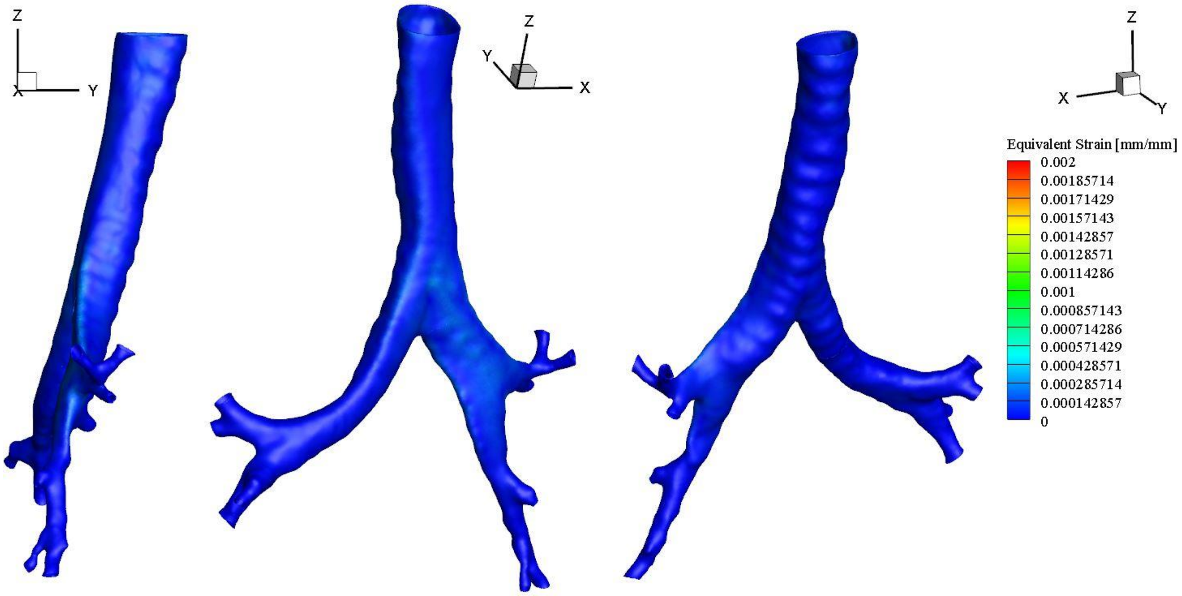

(a) t = 0.15 second

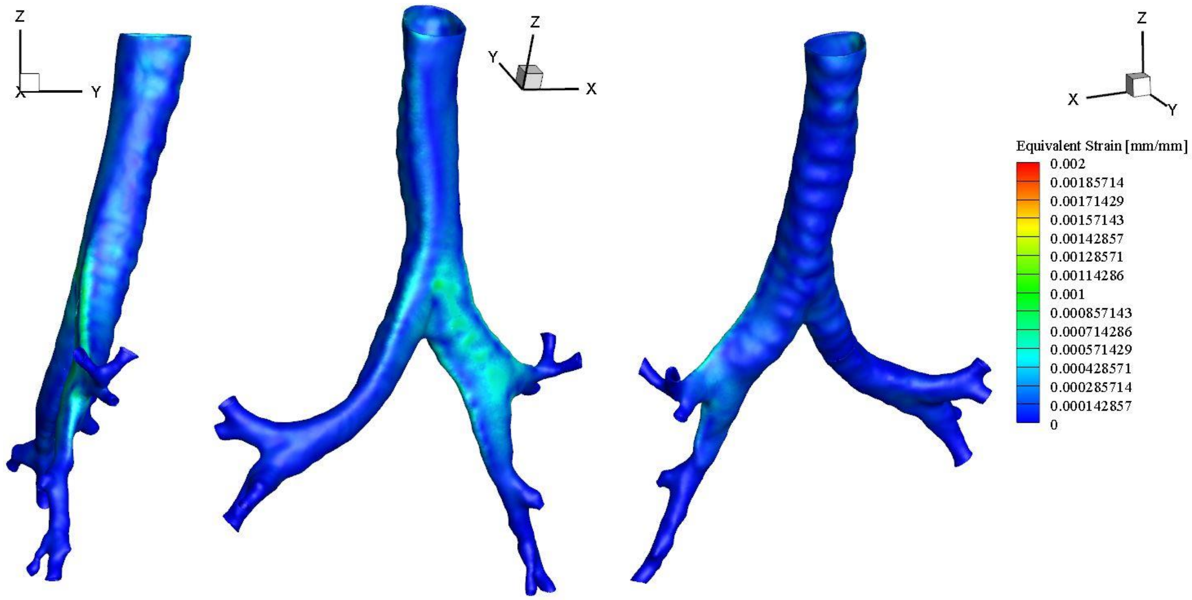

(b) t = 0.25 second

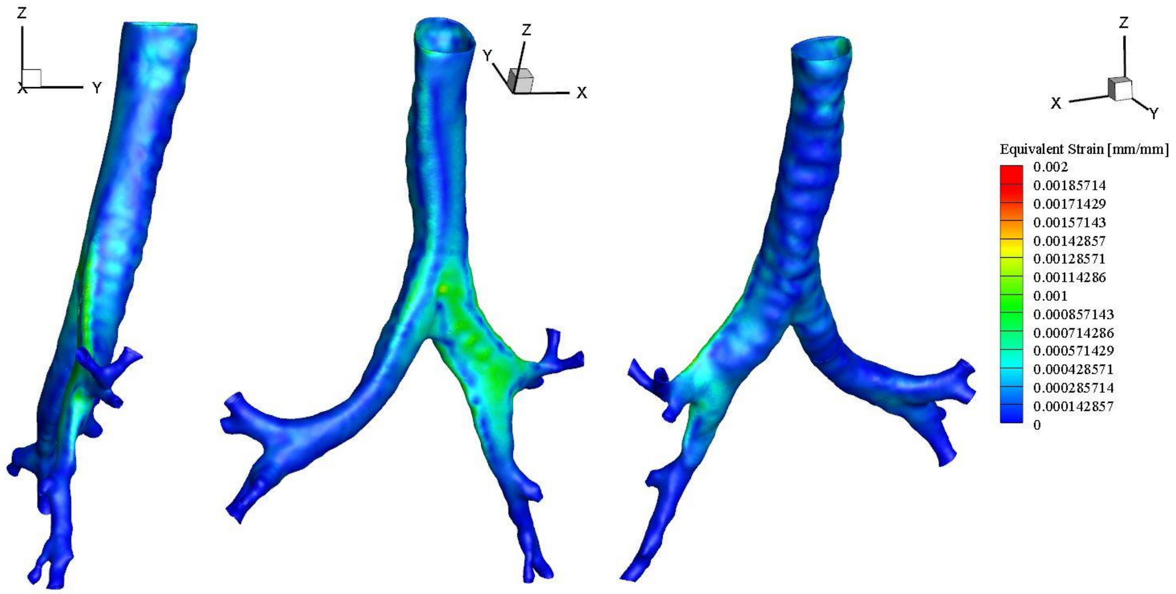

(c) t = 0.4 second

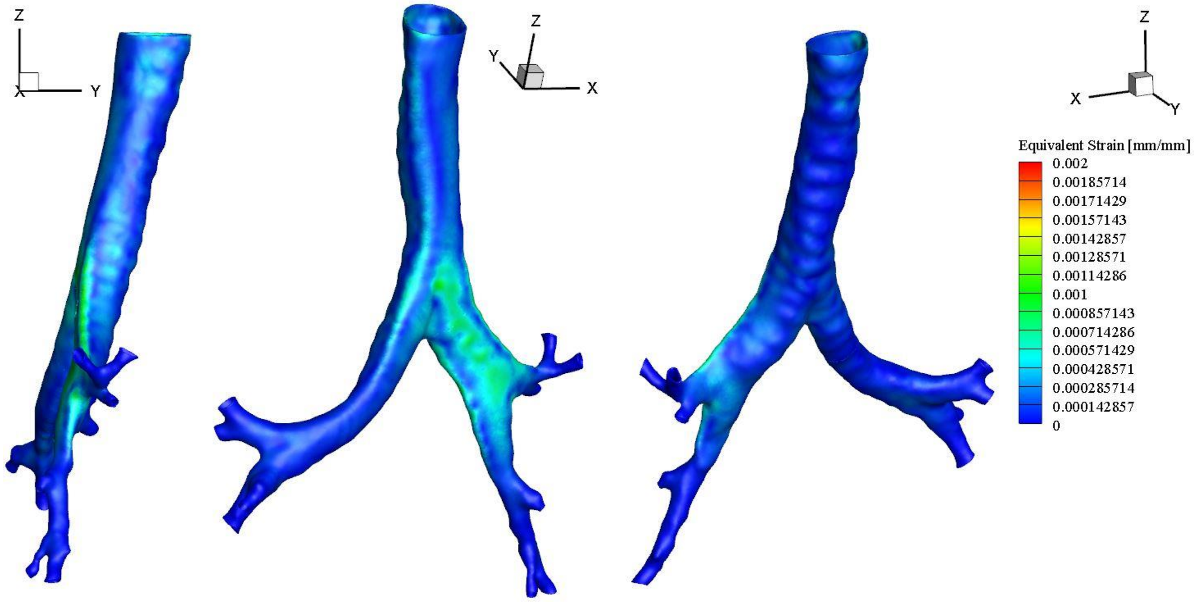

(d) t = 0.5 second

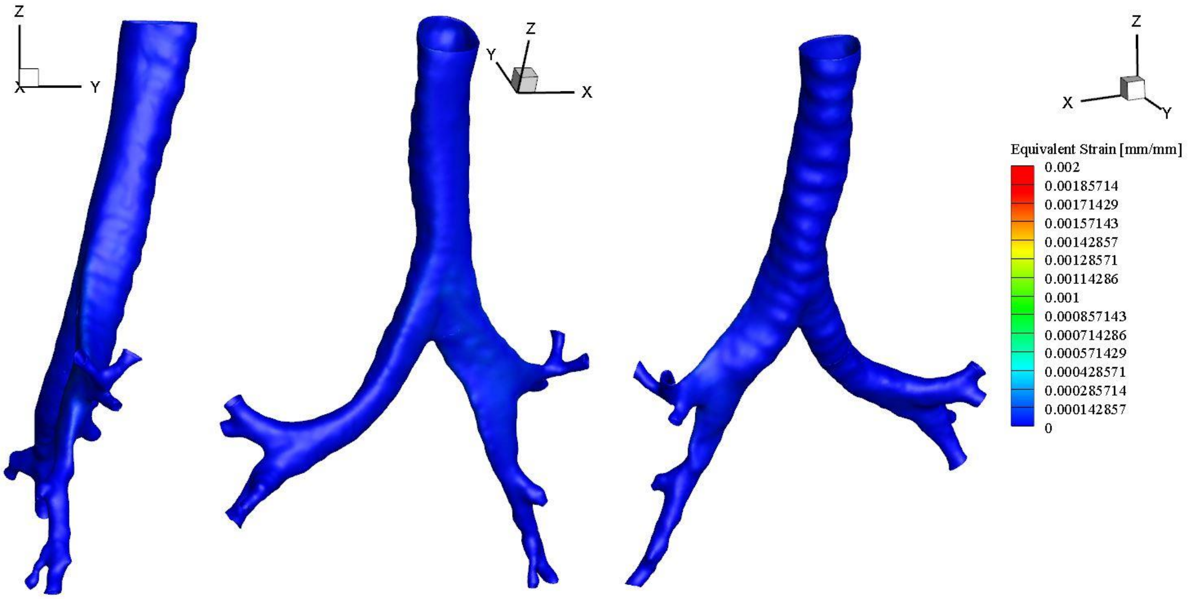

(e) t = 0.7 second

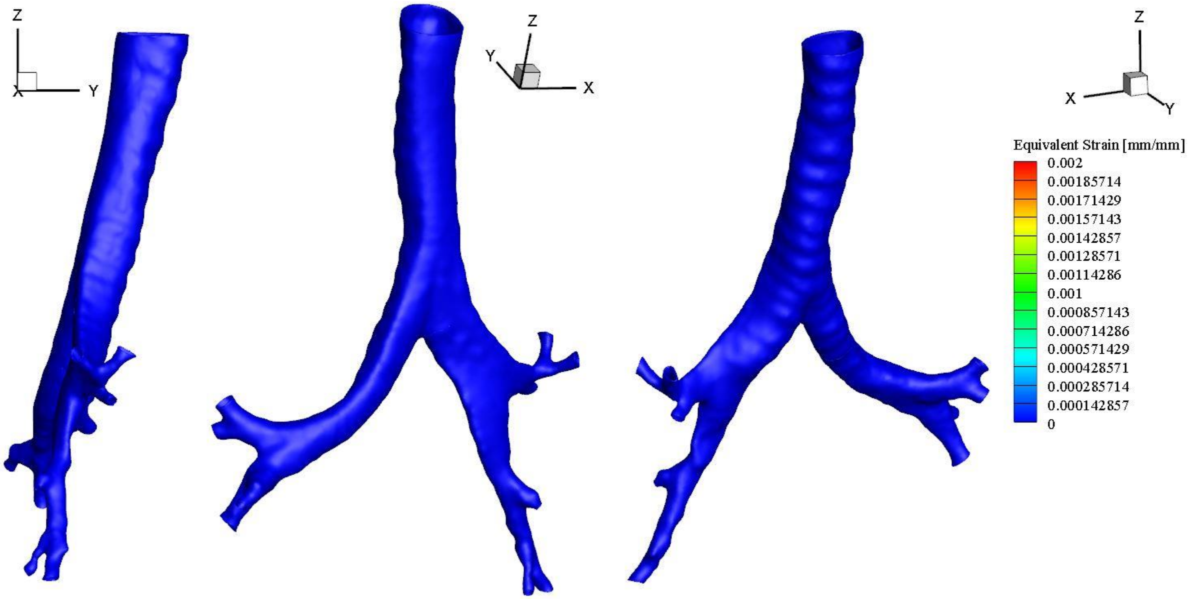

(f) t = 1.5 seconds

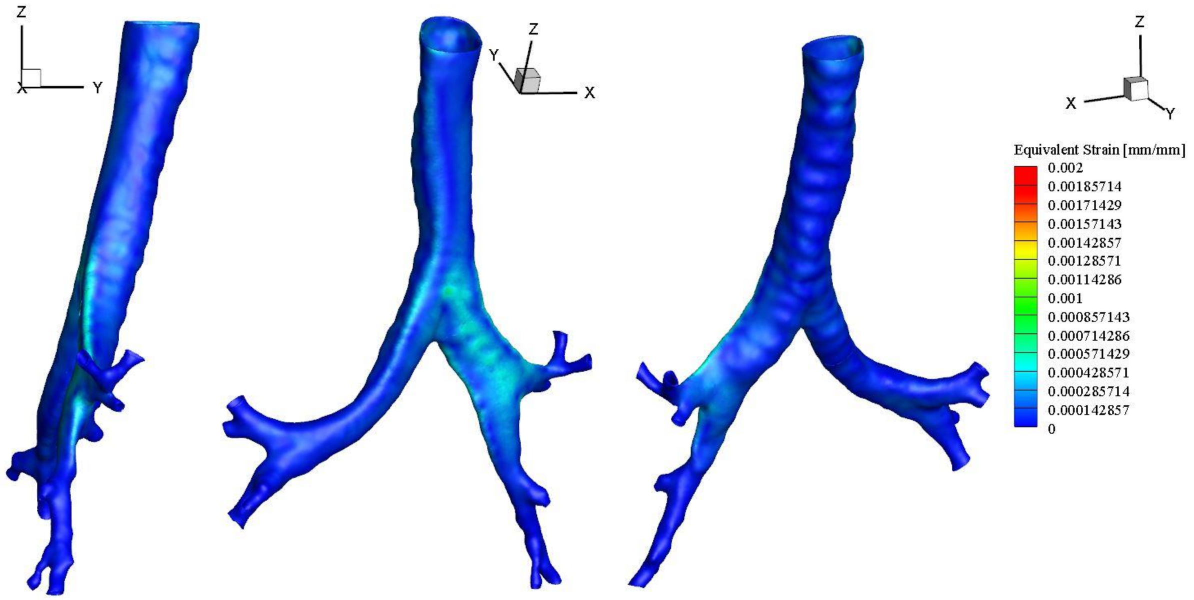

(g) t = 1.9 seconds

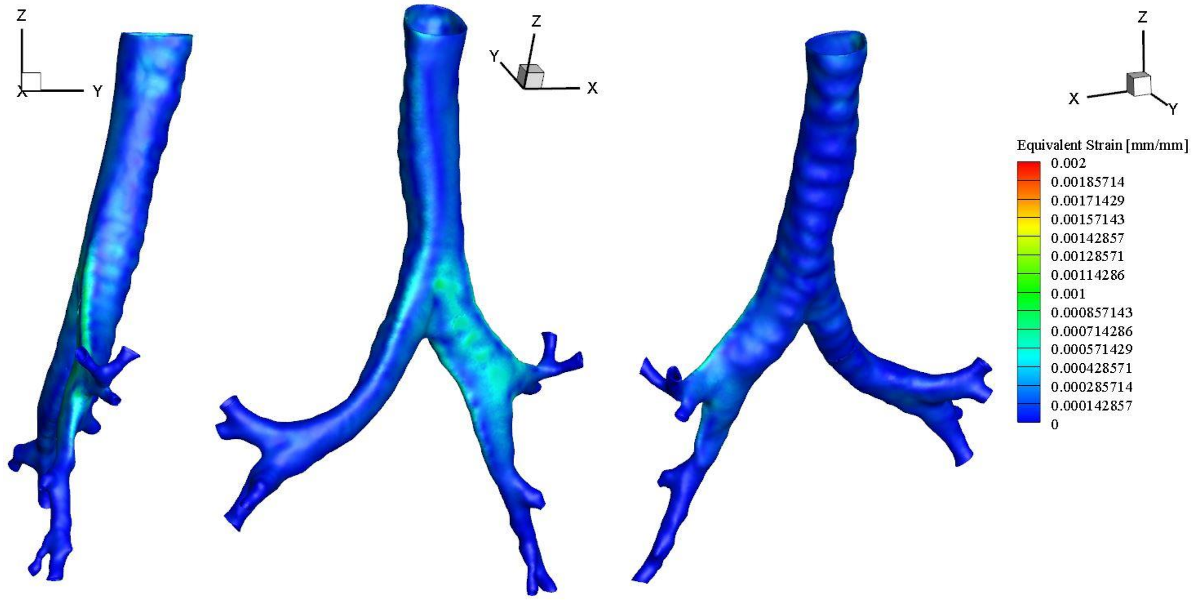

(h) t = 2 seconds

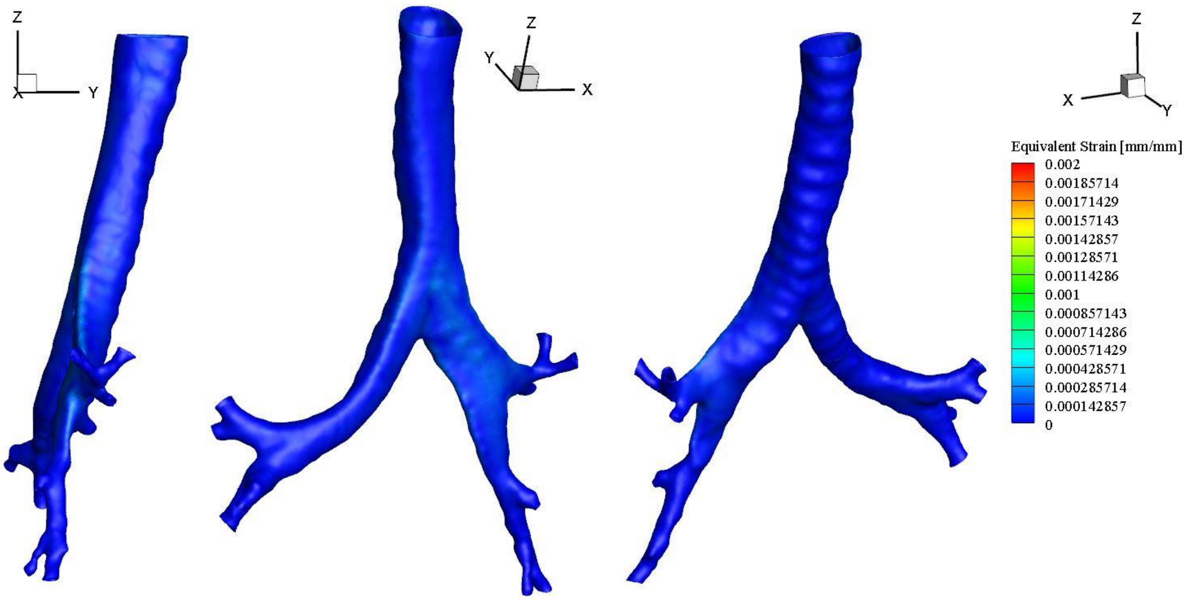

(i) t = 2.15 seconds

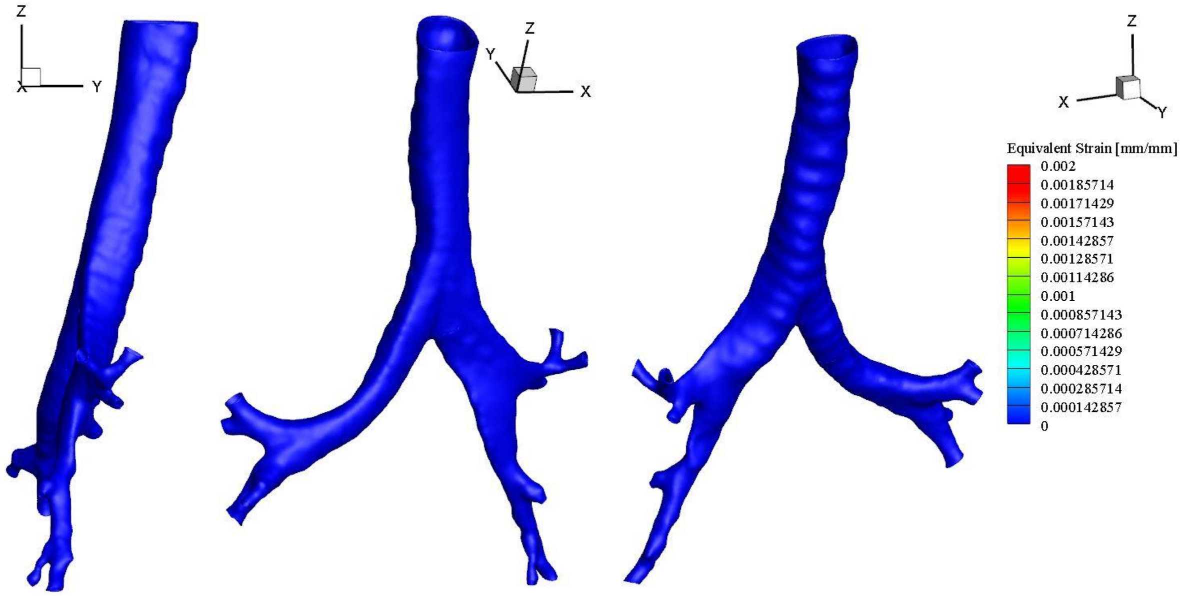

(j) t = 2.3 seconds

Figure 5.11: Equivalent Strains of the human lung model

As stated previously, the maximum strain value on the legend is set to be the same value as the maximum stress: 0.002. If the material were to be linear, then the stress and strain fields will have the same contour in the same regions. However, looking at the corresponding stress and strain contour plots, at t = 0.4 second, the contours are different. The strain is significantly lower than the stress in the same regions. Similar to the stress, the strain is fairly low, which indicates that the lung material can stretch even more than what is shown prior to failure. In the context of this case study for ventilator flow, this is a good thing. This means, at the velocity provided the flow is unlikely to cause significant damage to the lung.

In Figure 5.12 are the displacements for the structural region. Main item to note for the displacement is the location of the maximum displacement. The maximum displacement is side the lung that has a straighter bronchi branch than the other side.

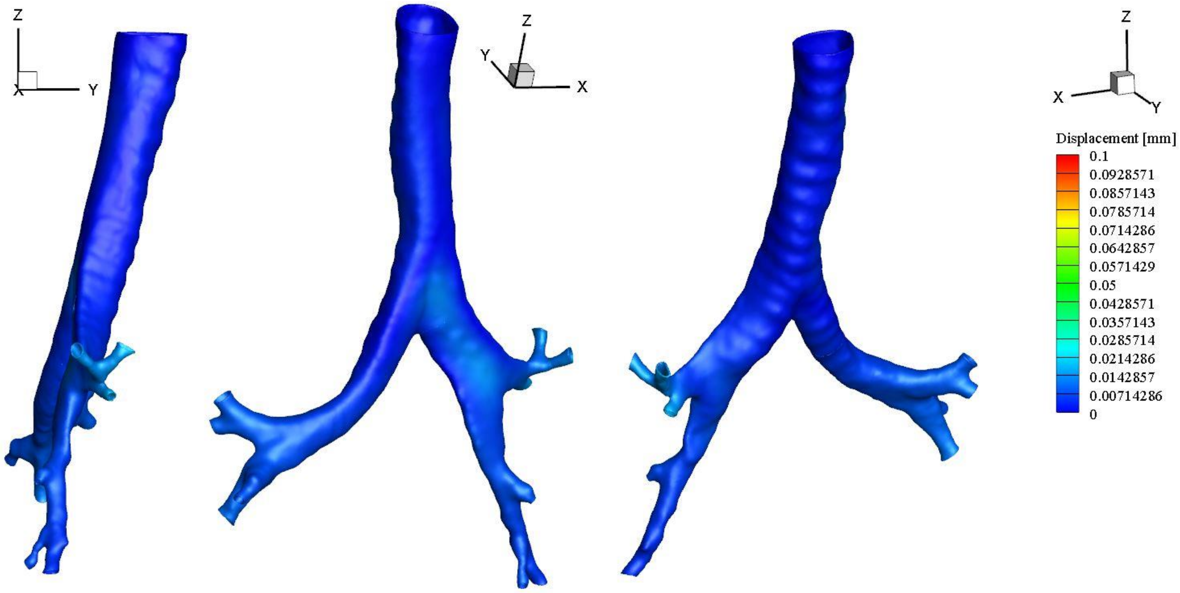

(a) t = 0.15 second

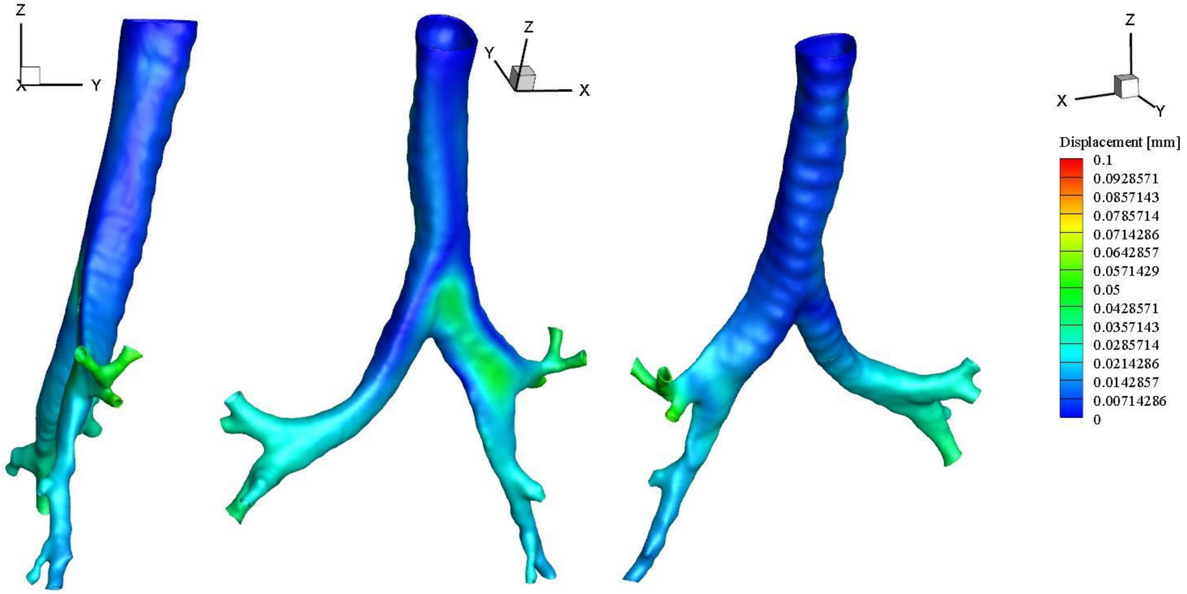

(b) t = 0.25 second

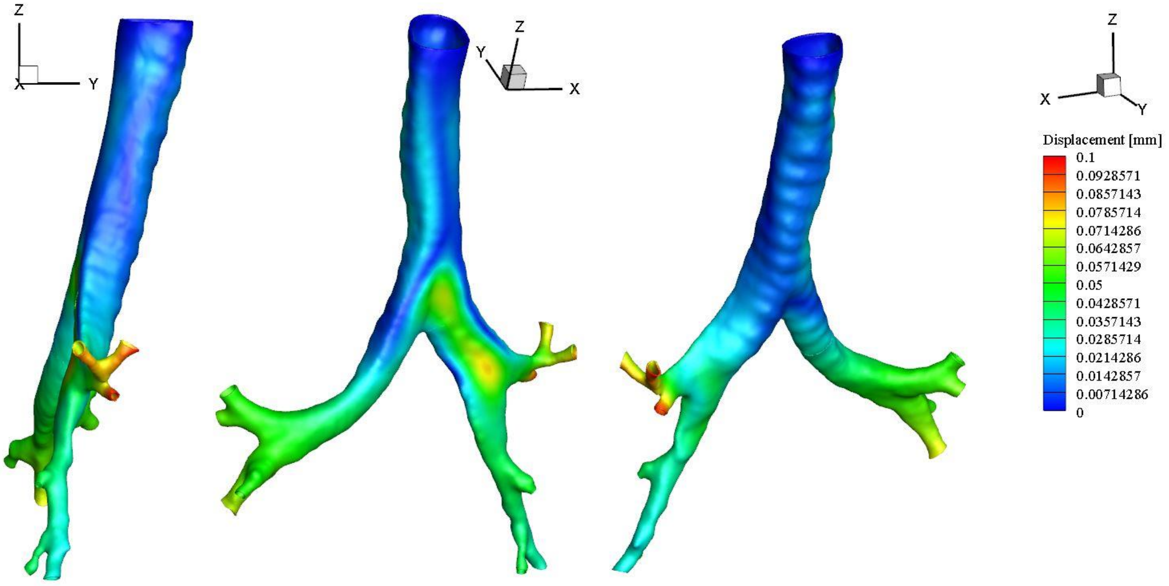

(c) t = 0.4 second

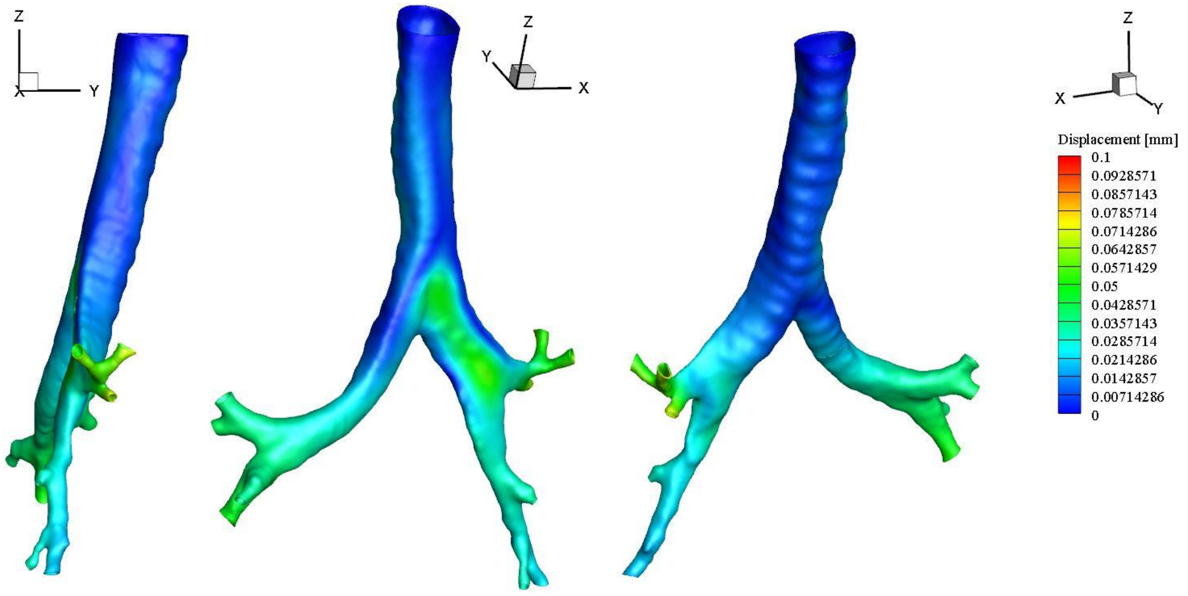

(d) t = 0.5 second

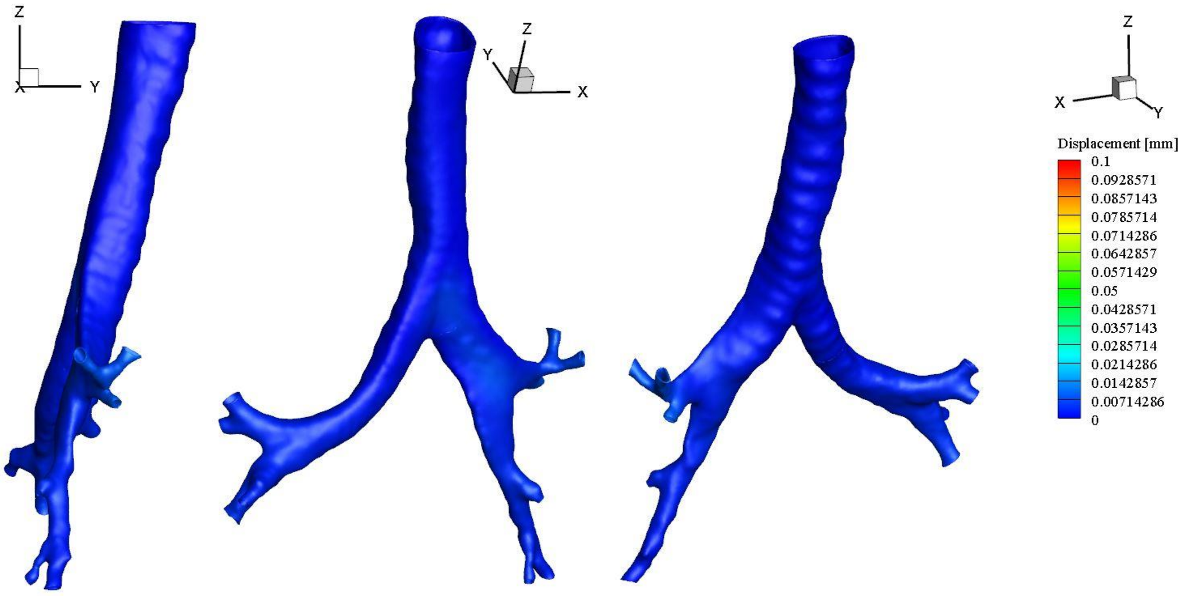

(e) t = 0.7 second

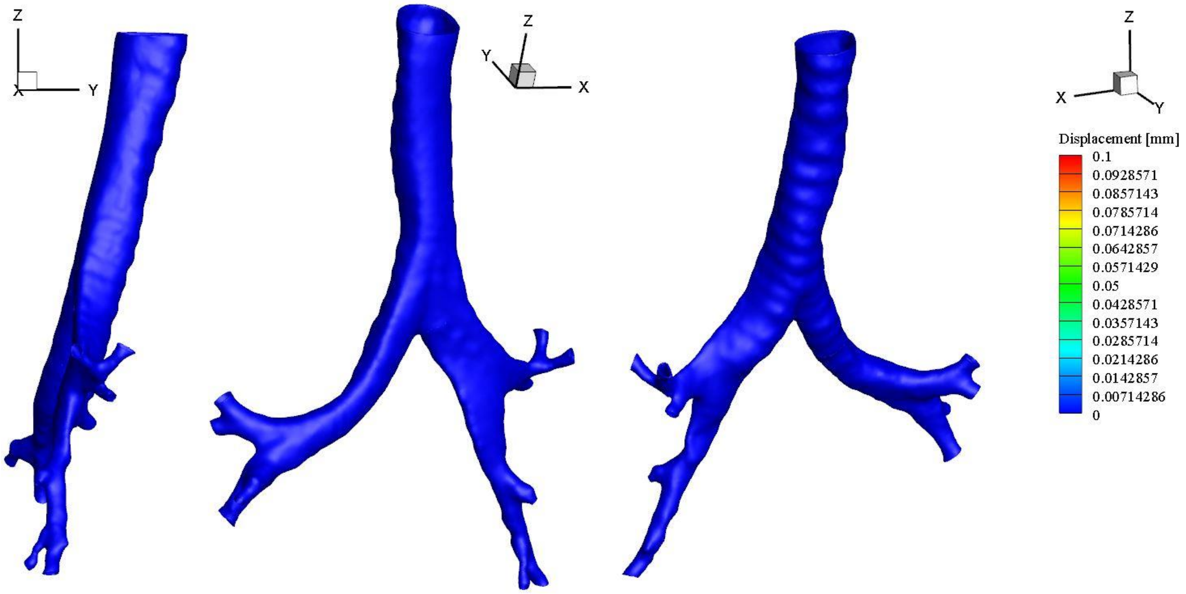

(f) t = 1.5 seconds

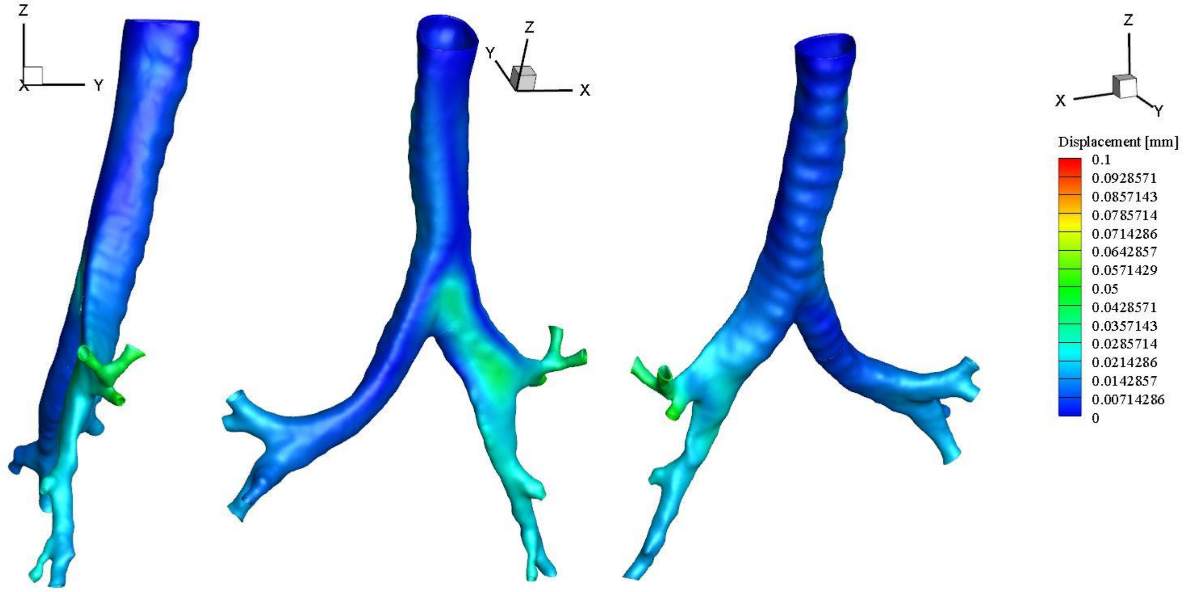

(g) t = 1.9 seconds

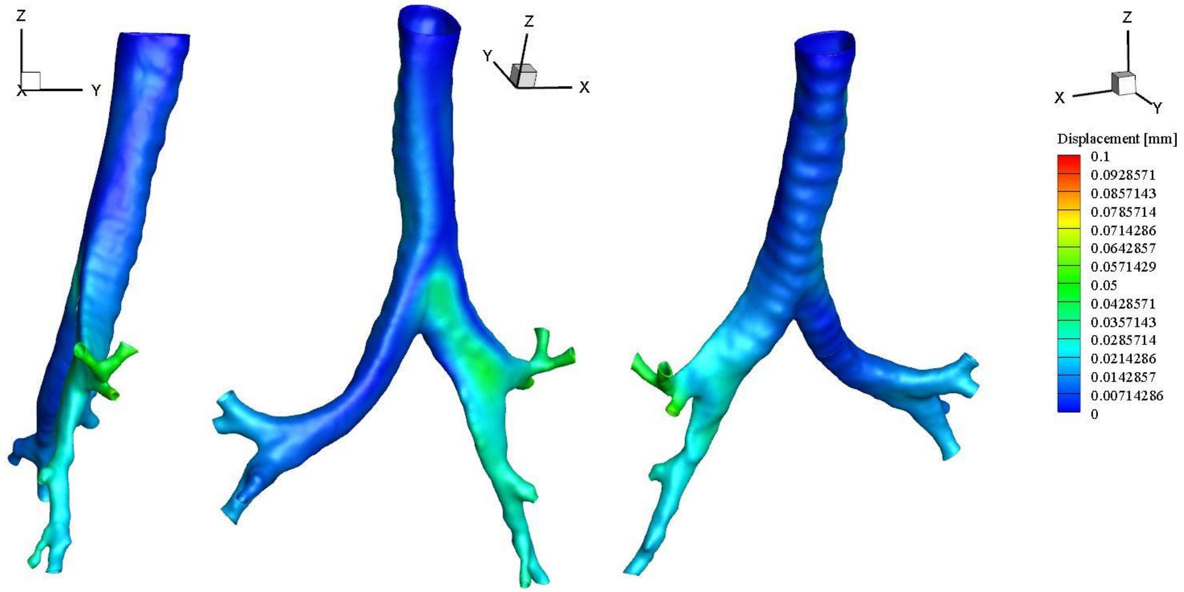

(h) t = 2 seconds

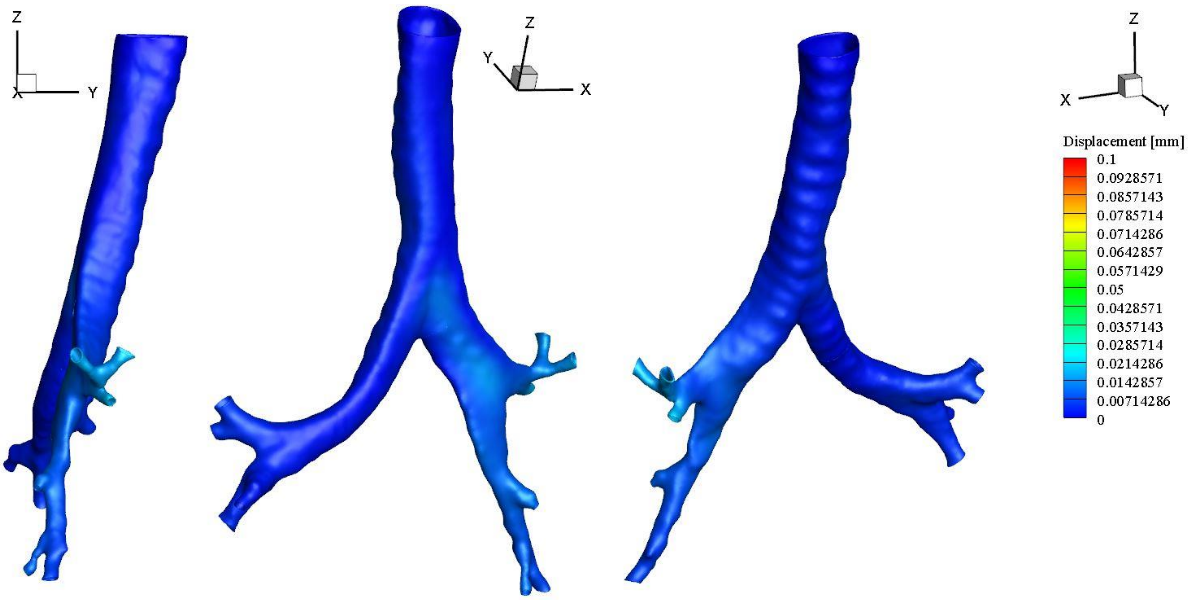

(i) t = 2.15 seconds

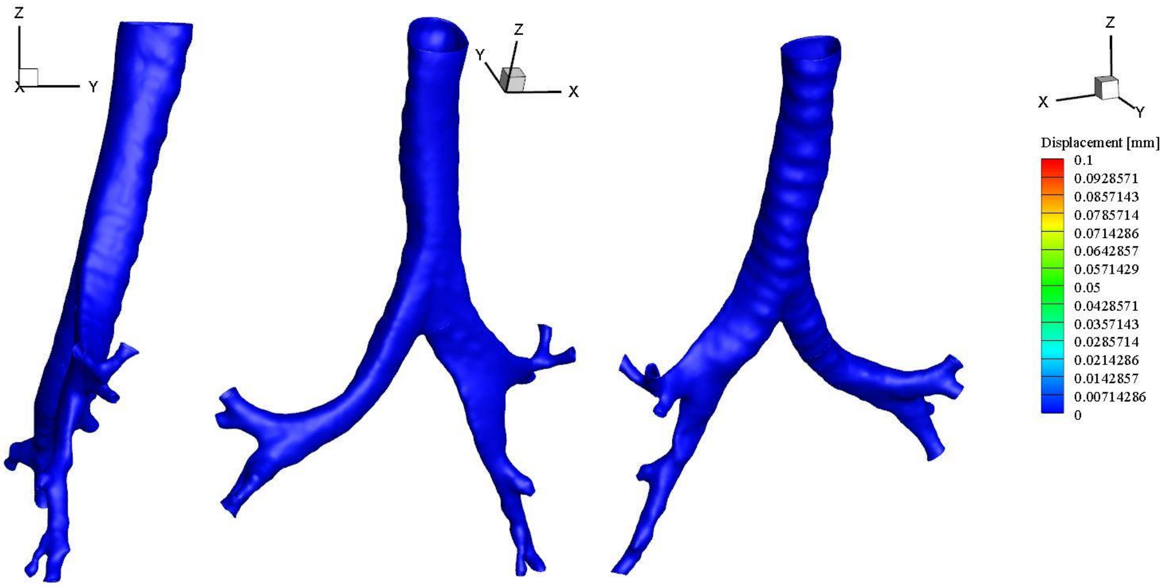

(j) t = 2.3 seconds

Figure 5.12: Displacements of the human lung model

The maximum displacement is occurring on the right side with the straighter bronchi. This observation is potentially a representation that the airflow is following the path of least resistance, again as would be physically expected with conventional ventilation.

5.4.2 Human Lung Model – Fluid Region

For the Fluid region, the main focus will be the velocity and pressure behavior inside the human lung. Slices were added to the contour plots to show the behavior inside the fluid region. Same time locations as the structural region were selected for consistency. In addition, the referenced fluid point for the graph shown in the figure, is obtained from the origin of the geometry, which is at the center of the velocity inlet.

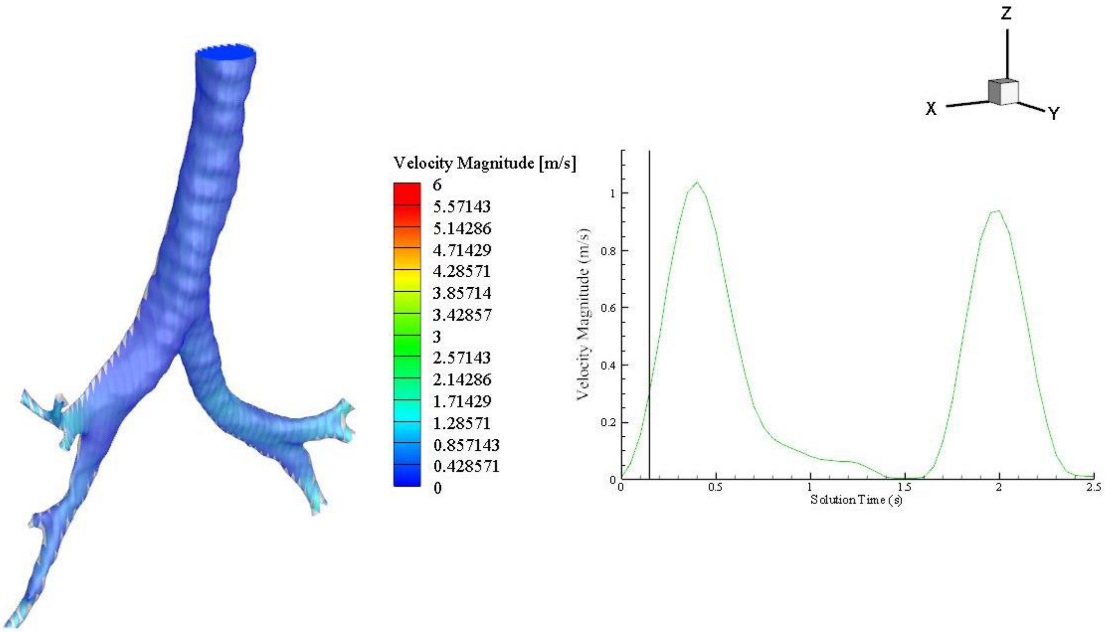

(a) t = 0.15 second

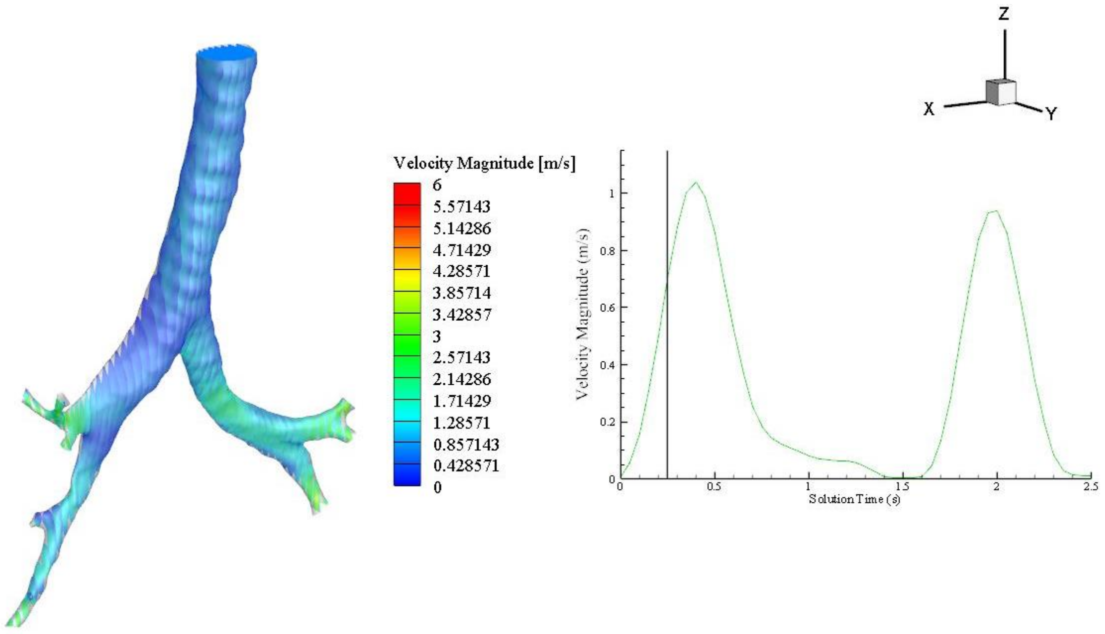

(b) t = 0.25 second

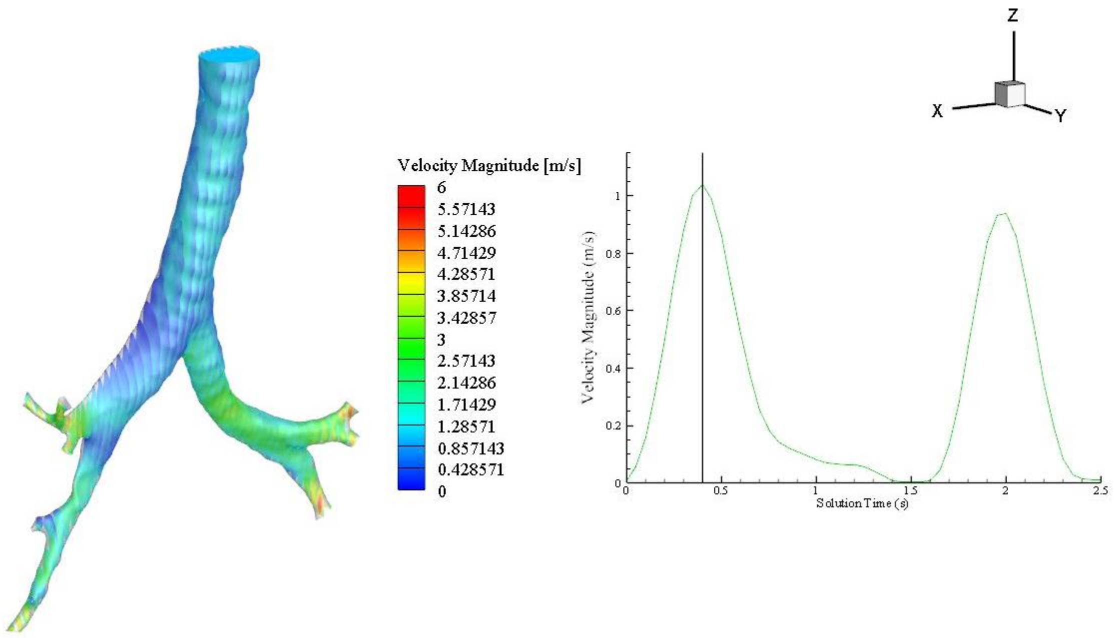

(c) t = 0.4 second

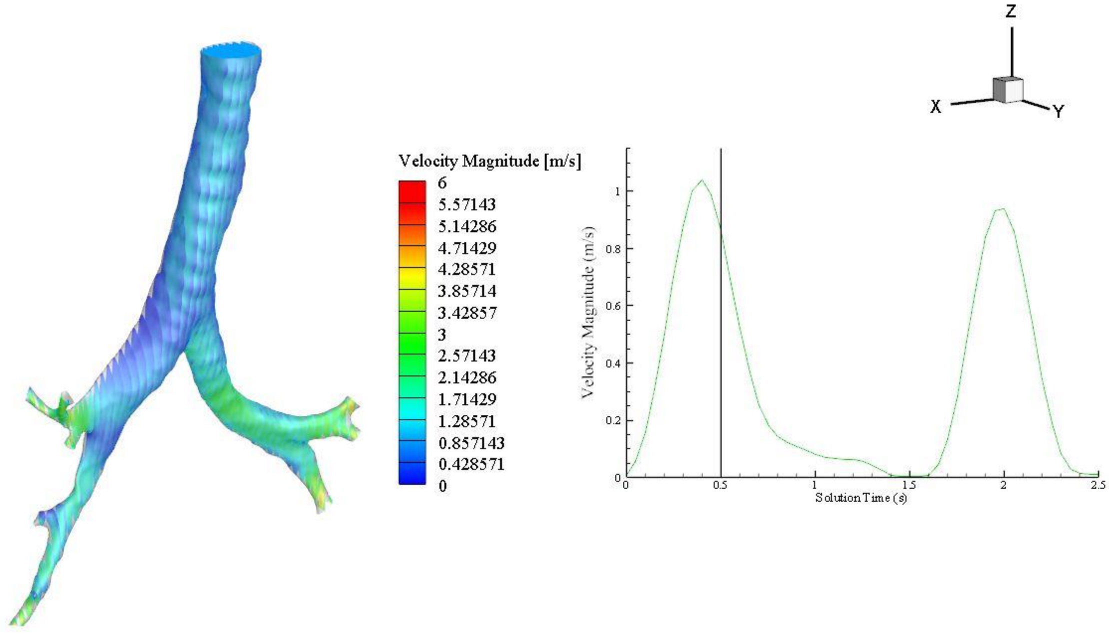

(d) t = 0.5 second

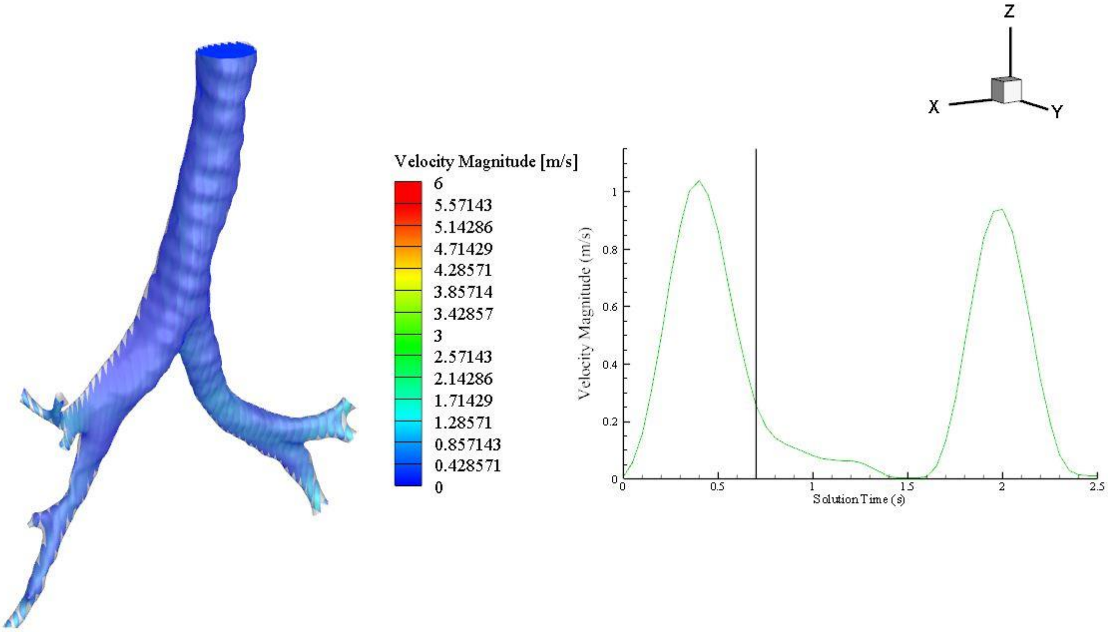

(e) t = 0.7 second

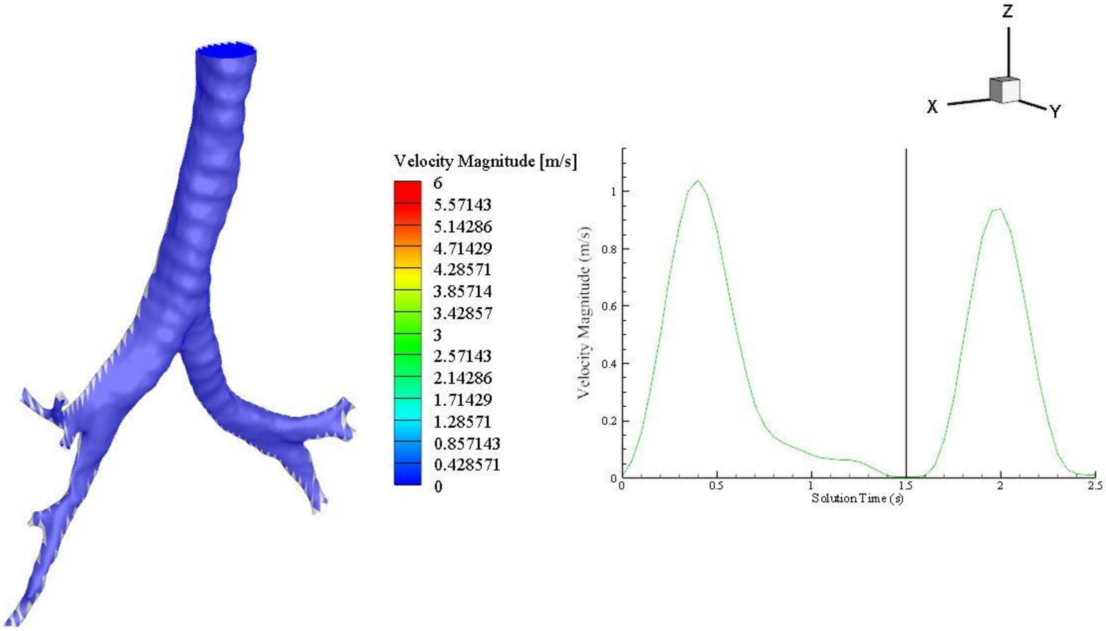

(f) t = 1.5 seconds

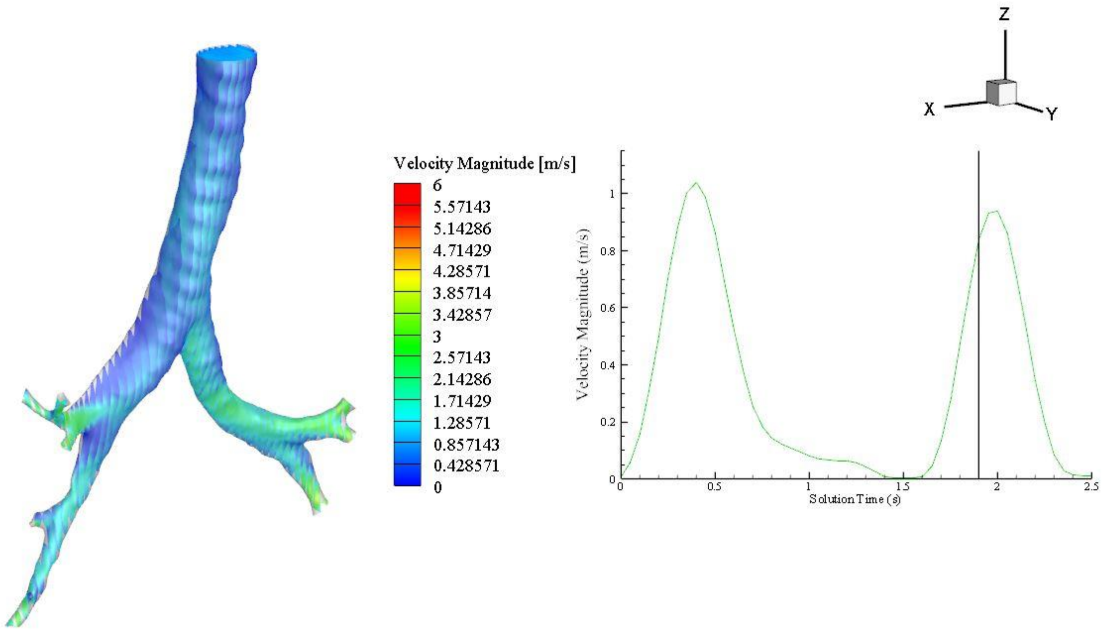

(g) t = 1.9 seconds

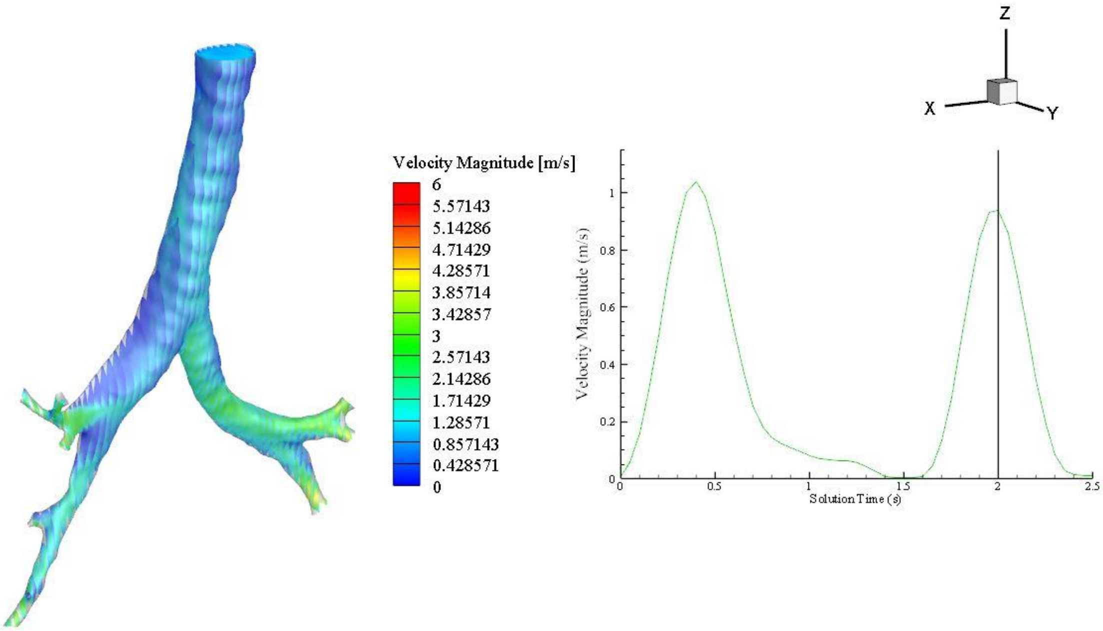

(h) t = 2 seconds

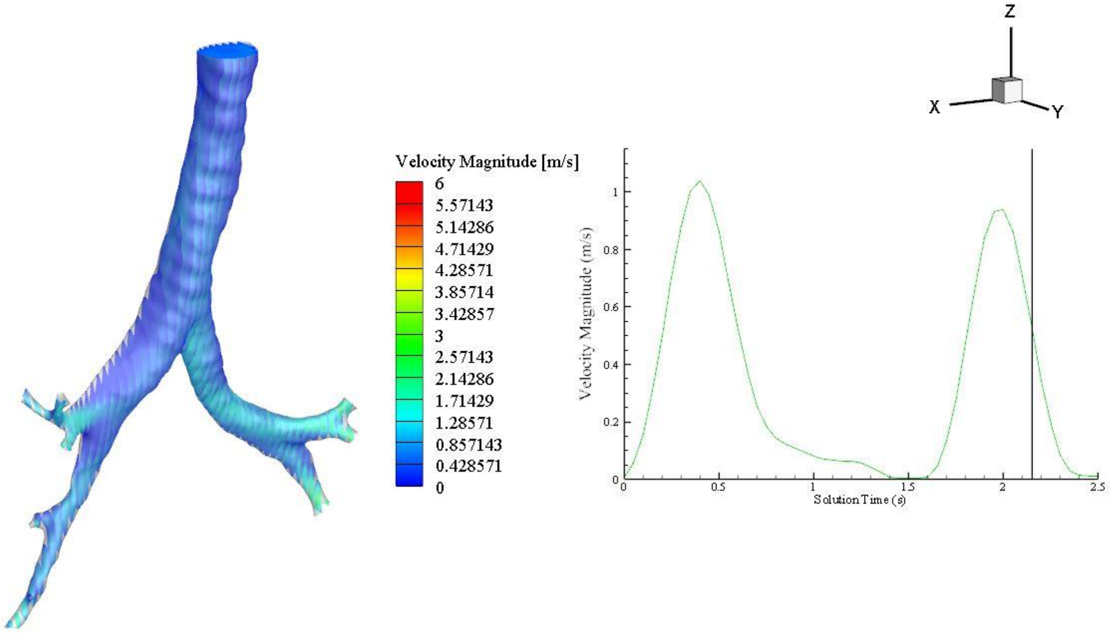

(i) t = 2.15 seconds

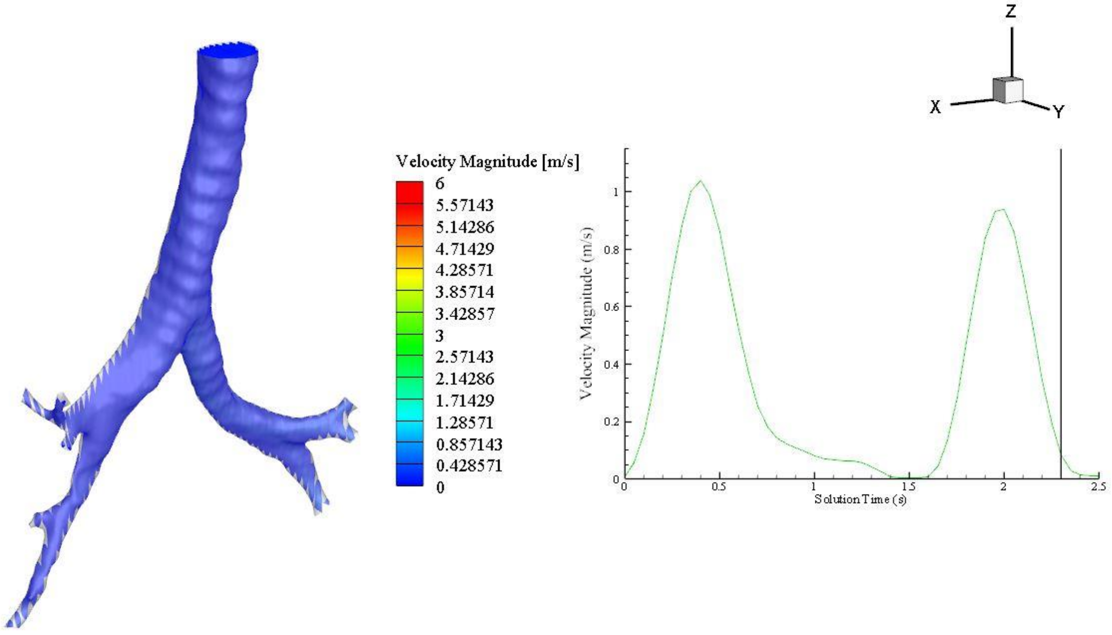

(j) t = 2.3 seconds

Figure 5.13: Velocity Magnitude contour plots for human lung model

The maximum prescribed velocity is around 1 (m/s). However, as shown in Figure 5.13, the maximum velocity is beyond 1 (m/s). The peak value is around 6 (m/s) around the tips of the bronchi. The velocity at the tip is higher because the diameter is small, which in turn forces the air to go through a narrower channel, creating a higher velocity.

Pressure contours are provided below. Similar to the other contour plots thus far, the time locations are the same. The figures shown below all have the same contour legend, thus making the pressure look uniform on several of the plots. Additional pressure contour plots are provided in Appendix D – Chapter 5: FSI Human Upper Airway Simulation to show the difference in pressure for every time location.

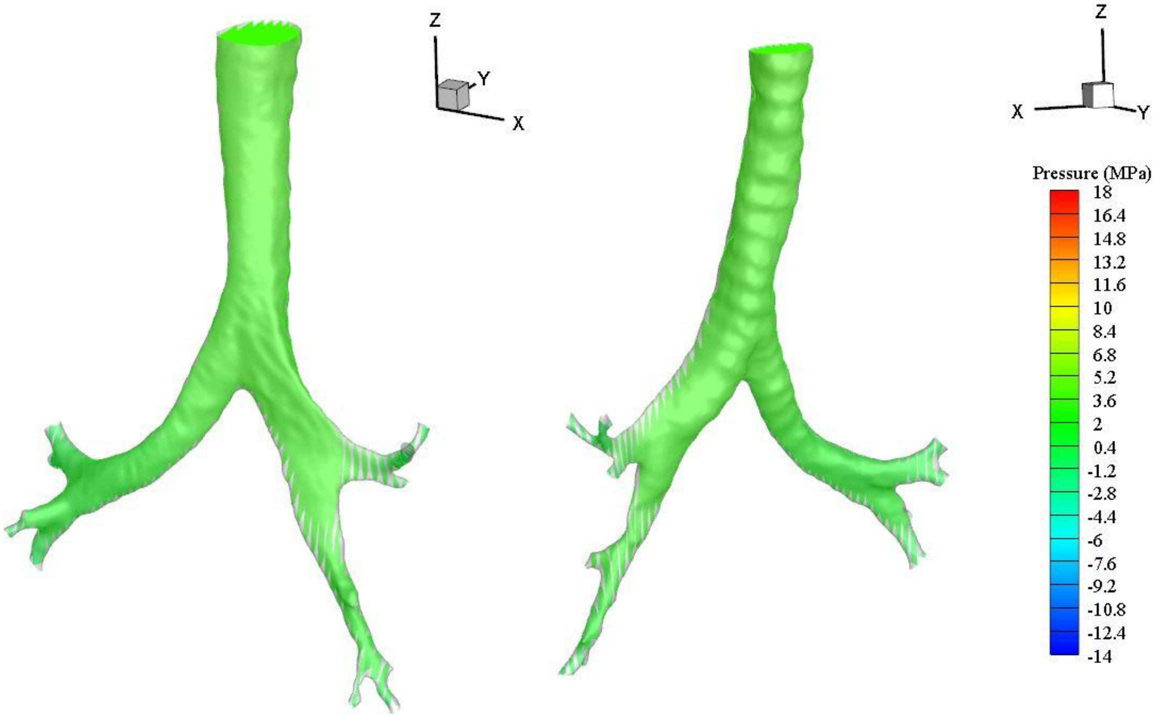

(a) t = 0.15 second

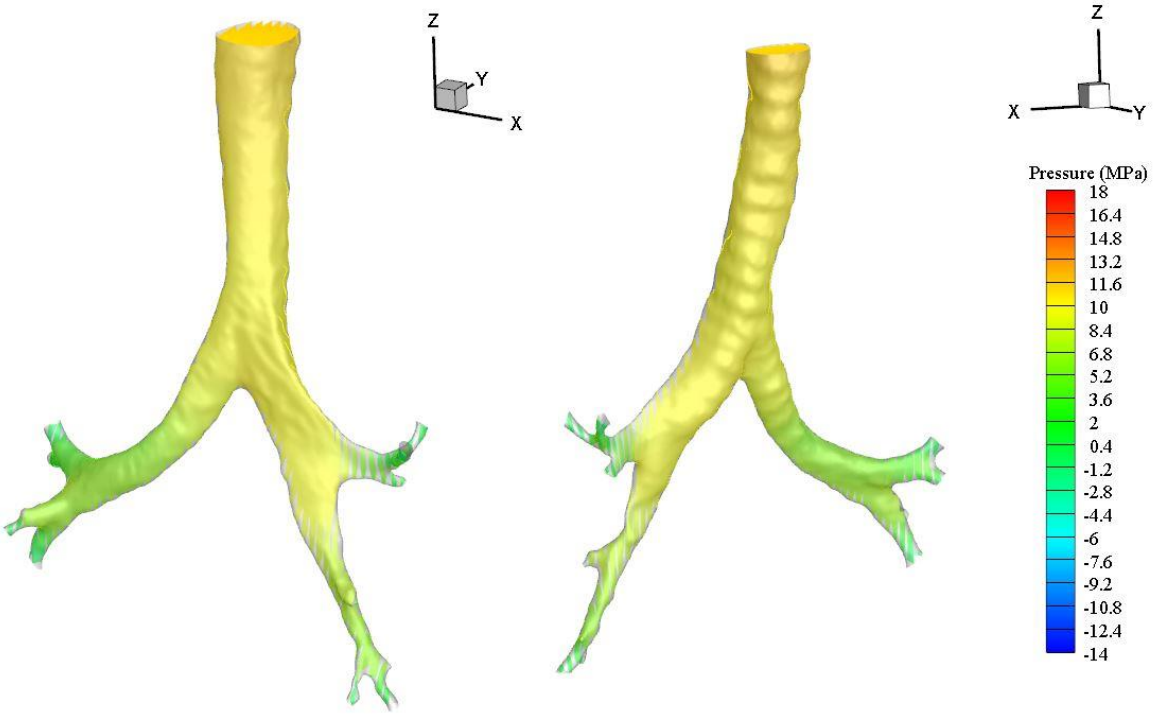

(b) t = 0.25 second

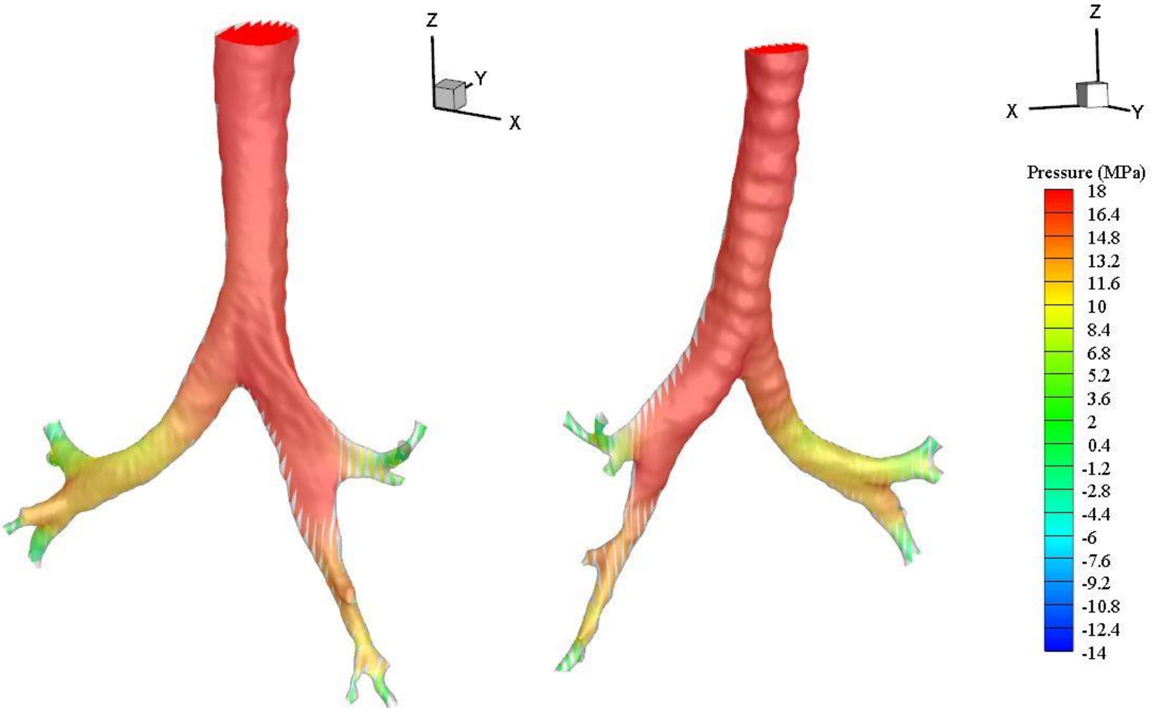

(c) t = 0.4 second

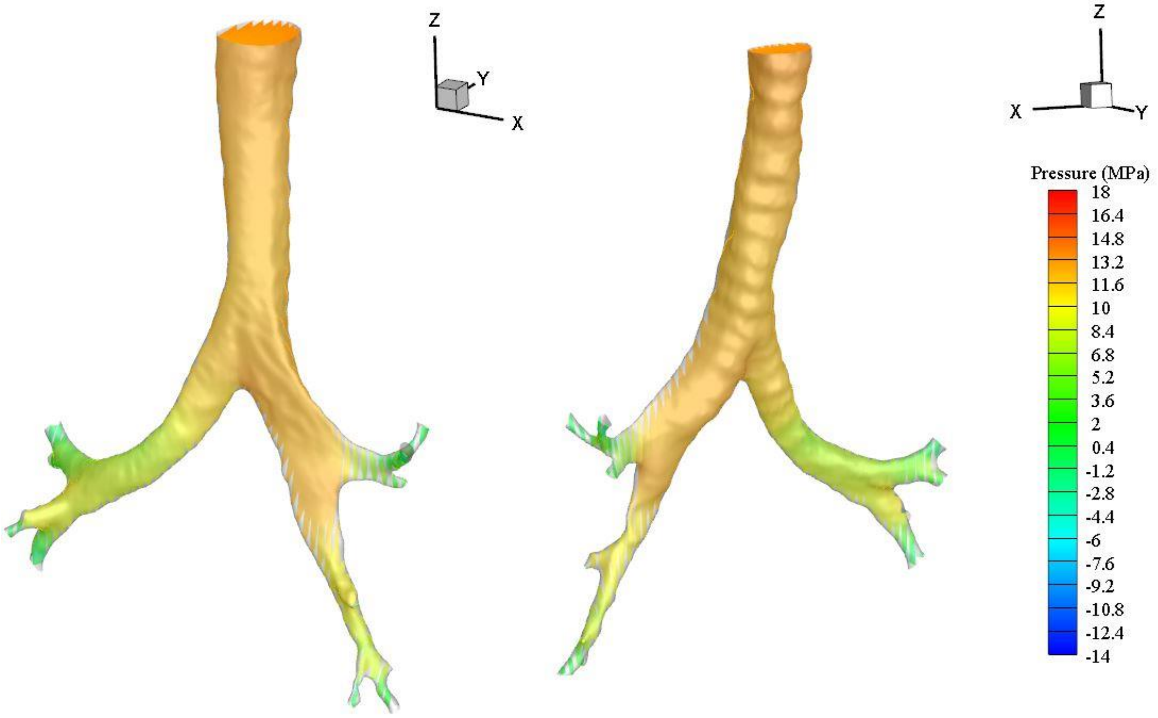

(d) t = 0.5 second

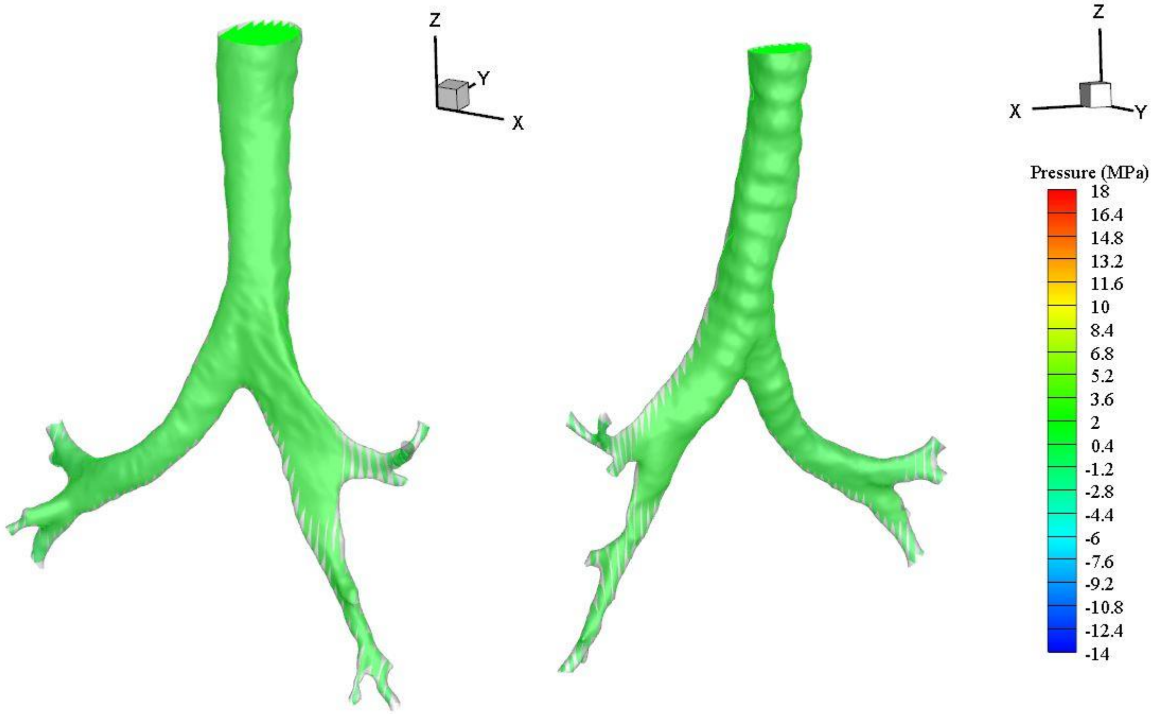

(e) t = 0.7 second

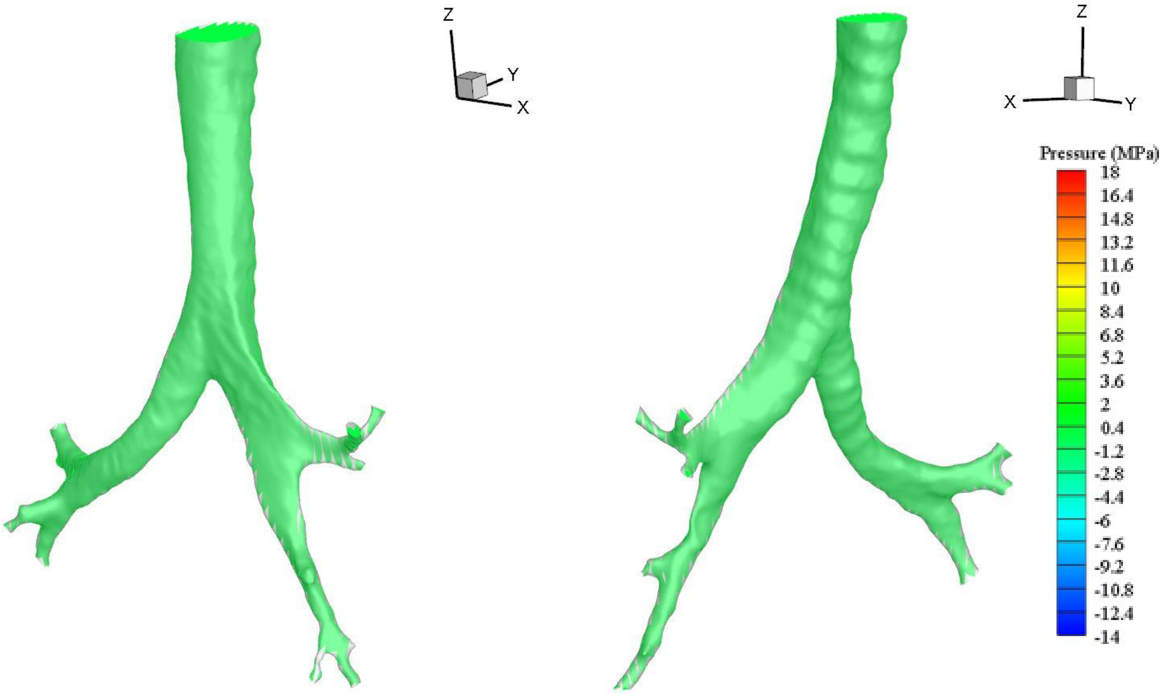

(f) t = 1.5 seconds

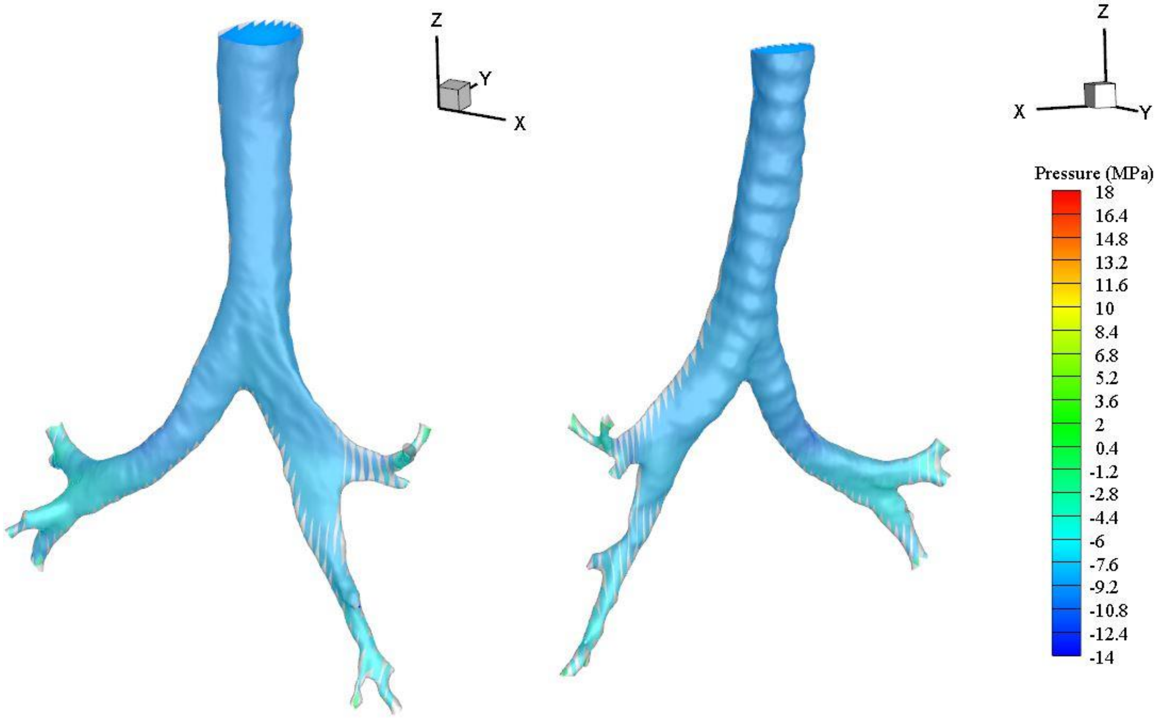

(g) t = 1.9 seconds

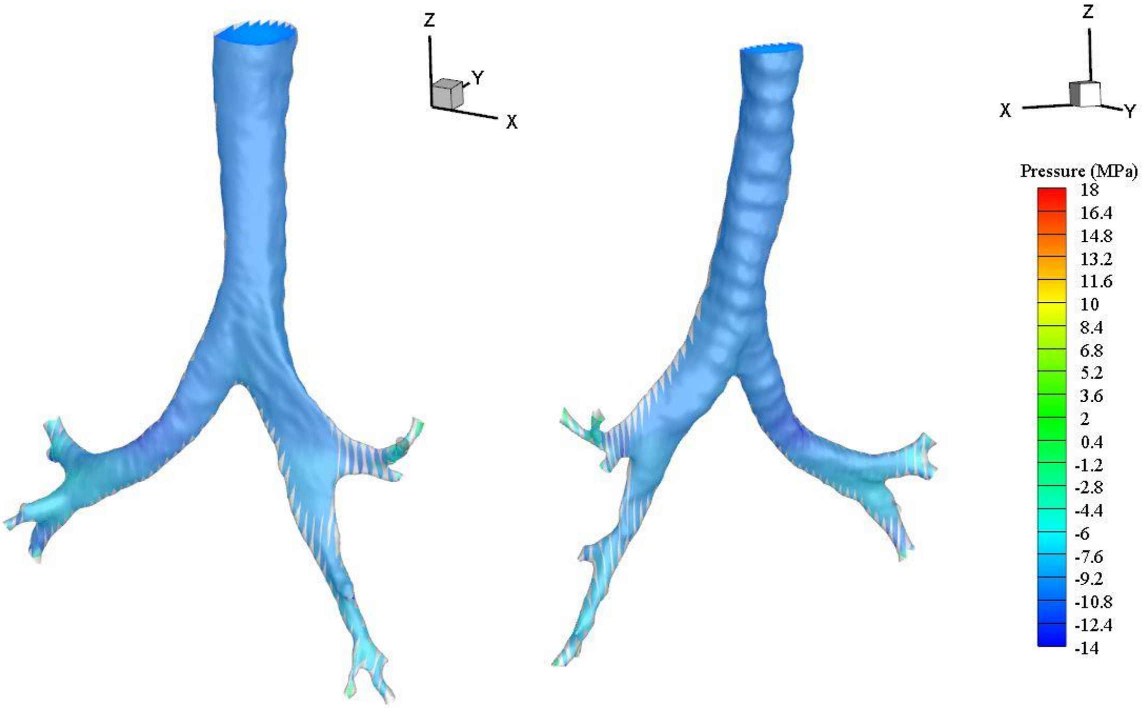

(h) t = 2 seconds

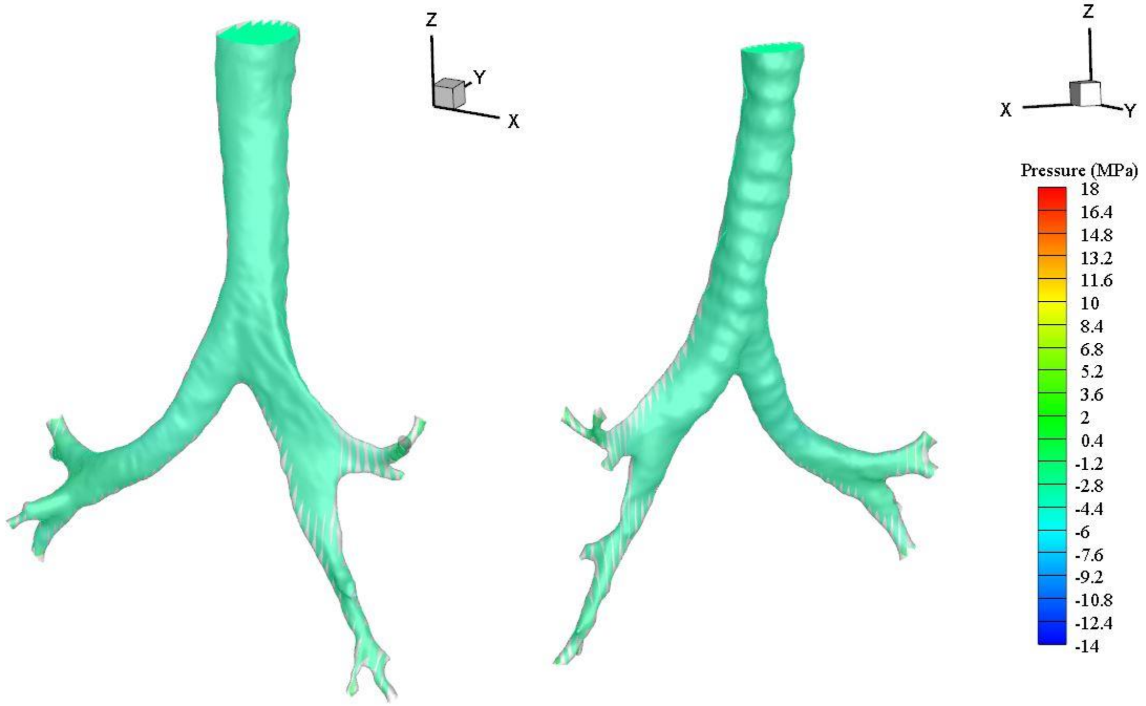

(i) t = 2.15 seconds

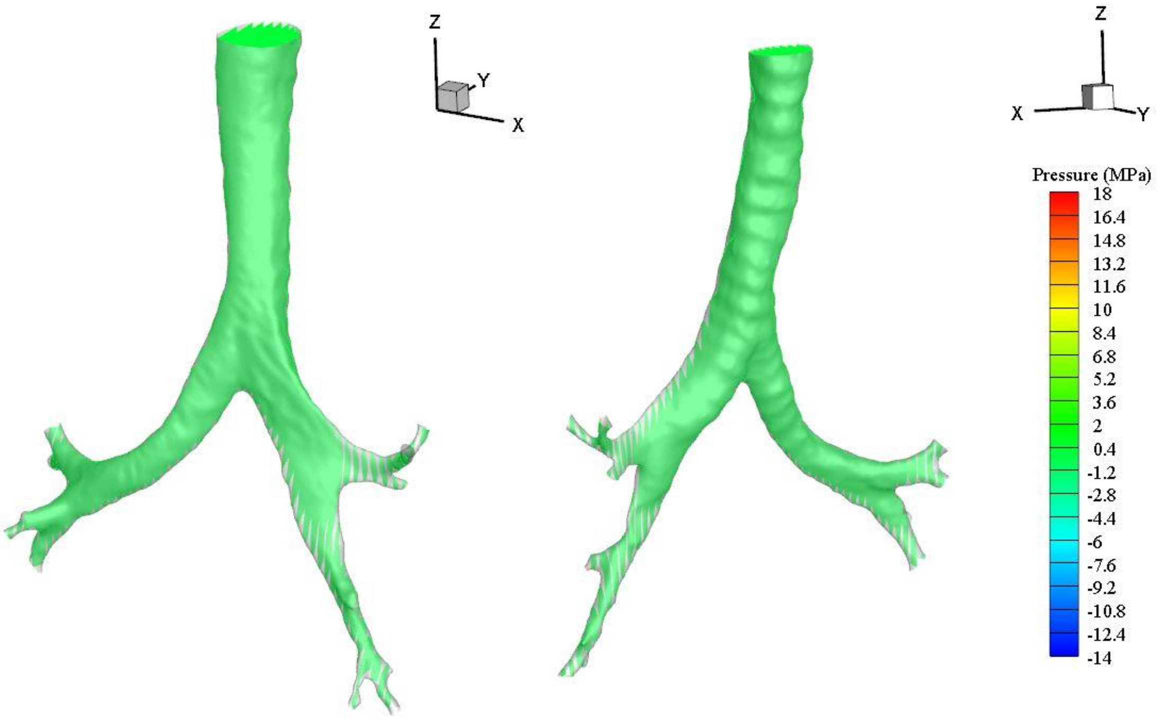

(j) t = 2.3 seconds

Figure 5.14: Fluid pressure contour plots for human lung model

Shown in Figure 5.14, the pressure again peaked at t = 0.4 second while the peak negative pressure is at t = 2 seconds. The pressure is mostly uniform, with the exception of the pressure outlets (tip of the bronchi). The difference in pressure can be clearly observed in Figure 5.14 (d) at t = 5 seconds. This difference in pressure is most likely the BCs prescribed to the outlets. The BCs for the outlets are defined pressure outlets (static gauge pressure). The gauge pressure is a reference to the atmospheric pressure, and the pressure will remain constant throughout the simulation time. If the pressure inside of the lung is not the same as the reference pressure then there will be pressure differences.

5.5 Conclusion

Direct comparisons to literature was not performed due to the differences in BCs and geometry. However, our results indicate that the values obtained are reasonable given the BCs. It was observed that the stress and strains were relatively low given the ventilator velocity conditions. This shows that the prescribed velocity is unlikely to damage the lungs especially if they are healthy, given the velocity magnitude. As previously stated, the velocity magnitude was decreased by half due to the sensitive mesh. For a more accurate prediction of the stress and strain, the velocity should be simulated at proper magnitude.

Next, looking at the fluid velocity and pressure of the air inside the lung, differences can be can be observed. The velocity contours are showing maximum velocity at the outlets. This is expected since the diameter of the outlets are significantly smaller than the diameter of the trachea. Lastly, looking at the fluid pressure and structural stresses, the maximum pressure is at t = 0.4 second; correspondingly the maximum stress is at the same time and same general location as the fluid pressure. Similarly the maximum displacement is occurring at the time and location as the peak velocity, also at t = 0.4 second. Thus far, all observations are indicating that the simulation is showing the correct behavior in terms of stress/pressure and displacement/velocity at the various selected locations. The simulation will need to be further refined prior to yielding a perfectly accurate model that can be used for validation against *in situ* or *in vivo* experiments.

Chapter 6: CONCLUSIONS AND FUTURE RESEARCH

This chapter focuses on future studies as well as some general thesis project conclusions that can be reported following these experiments. The conclusion section will provide a summary of the overall conclusions of both the individual studies and overall project. It is also of interest how the individual case studies can be built upon for better accuracy and have even more realistic characteristics to further improve the models.

6.1 Summary and Conclusions

Each case study was unique, but yet necessary to perform the real lung geometry simulation. The square balloon provided the basic methodology for the 3D balloon. Since the square balloon was able to achieve monotonic convergence that ensured the values and approach for the FSI simulation was accurate enough to use the methodology elsewhere. Therefore, when simulating the 3D balloon the same methodology was used. The only drawback was the time it took to run the 3D simulation. The square balloon took around three hours to run the finest mesh, while the 3D balloon with the coarsest possible mesh without divergence took a week to simulate.

The tensile testing and curve fitting provided the necessary confidence to use the material properties from testing. The tensile testing method can be improved upon as well as the curve fitting. However, given the knowledge, the tensile testing was adequate and the curve fitting resulted in a good approximation of the experimental behavior. Then, using a one-element simulation to verify the model gave confidence in applying calculated material constants to the lung geometry.

Lastly, when simulating the lung with different ventilation flows one can achieve great insight into the behavior of the lung, distribution of structural stresses, and the air flow. Further improvements can be made, however since this is the first FSI simulation using ANSYS, the results are satisfactory.

In conclusion, square balloon simulation, 3D balloon simulation, the tensile testing and the real lung simulation would be considered a very successful first step for ANSYS FSI simulations and testing. Many more variations in any of the cases studies can be done to improve upon what has already been shown in this thesis. The project started with a simple quasi 2D simulation, and through various forms of verification and validation, was built upon to the complex lung geometry simulation. This shows, that simplicity is always a good starting point for any project, it is also important to thoroughly understand some of the theory and physics behind the simulations and models before fully applying the knowledge without a solid foundation.

This study aimed to further bridge the knowledge gap through FSI simulations and mechanical tissue testing. The current studies drew upon and expanded on methods from the limited number of studies reported by other researchers. Using case studies such as the qusi-2D balloon and curve fitting are among some examples of how the current study is built on some of the previous research. Relatively new methods such as using ANSYS for FSI simulation and conducting a 3D balloon simulation would be considered unique to this study. Though direct comparison cannot be made, the methods, results, and conclusions can generally be compared to other studies as well. Even though more detailed simulations and testing can be conducted, due to some limitations stated above, the overall conclusion of this study is that the goal has been achieved, with some traditional techniques as well as with some relatively new ones. Ultimately, this thesis provides tissue properties and modeling methods that are essential towards the ability to model gas exchange in a complex structure such as the human respiratory tract.

6.2 Potential Future Research

This section is split between the individual case studies; as each case study is unique but they are all vital for the final simulation presented in Chapter 5 – FSI Human Trachea Simulation.

6.2.1 3D Balloon

The 3D balloon uses linear elastic properties as the material for the balloon walls. Silicone rubber in reality is a hyperelastic material and cannot be effectively quantified by an elastic modulus alone. Through simple testing, such as uniaxial tension testing, nonlinear material properties can be applied to the model. Or alternatively we can apply chosen material properties that already exists in literature to the model. Nonlinear materials can stretch beyond what the elastic modulus would allow. Uniaxial tension testing is the simplest test that solid mechanics researchers can perform, there are more accurate experimental testing such as biaxial testing and cyclic loading that may ultimately improve our model accuracy. Although cyclic loading is not generally done on hyperelastic material. It would be useful because even hyperelastic materials will have a cyclic failure rate and it can be determined with fatigue testing.

The 3D balloon simulation was run using only one mesh size, for both the fluid and structural regions. Additional mesh refinement and, if possible, a solution verification study similar to that of the square balloon can be conducted for estimating the grid/time-step errors and uncertainties. In addition, the mesh used for this study for both regions was extremely coarse. This was done to allow the simulation to run in a shorter amount of time, to facilitate replication time. Solution verification study on systematically refined grids and time-step sizes will be needed to estimate the numerical errors and uncertainties. The model should be validated using experimental data as available. These will allow assessing the true accuracy of the simulation results. A figure in Appendix B – Chapter 3: Three-Dimensional Balloon Expansion (Figure B.1.c) shows a “pole” on the fluid mesh. A pole is generally undesirable in meshes, however, due to the elliptical geometry, a pole may be unavoidable; but it can be improved upon. For example by using either (or a combination of both) linear and quadratic elements or using mesh facing features in ANSYS the region can be further improved.

Also, this simulation was only run with one velocity profile. Additional profiles can also be used for comparing results. Profiles such as the PCV and HFPV are good candidates. Since a balloon has the capability to expand in size in a relatively short time, the balloon simulations with the ventilator profiles are good visualization tools to use before applying the profiles to the lung geometry.

6.2.2 Tensile Testing and Curve Fitting

The testing done on the axial samples were preloaded to 1 Newton (N) and the circumference were preloaded to 0.1 (N). Though not shown, but was mentioned, in Chapter 4, some unrecorded axial testing was done prior to the actual testing. Those samples were preloaded to 0.1 (N) then pulled to failure. Comparing the data, it would appear that the axial specimens should be preloaded to somewhere between 0.1 (N) and 1 (N). If another round of testing were to occur, a preload value in between 0.1-1 (N) should be the starting point. As stated previously, uniaxial tensile testing is the simplest but yet a powerful mechanical test. However, to obtain more accurate data for materials, other tests such as biaxial testing and cyclic testing should also be done for the tracheal material. Further, since there is natural variability in tissue across individuals evaluation of this in a greater number of samples would improve the general utility of the data. Since this research has the potential to be expanded into lung damage, or even diseased lungs, having the proper mechanical properties for comparison will be beneficial.

The axial and circumferential samples were curve fitted using the Ogden material model. Various other models such as the Mooney-Rivlin model or the Neo-Hookean model could also be used. The Ogden model was chosen, because the author thought it fits the data better. However, without comparing the curve fit directly with other models, it remains an unknown if the Ogden model provides the best fit or not. In addition, a more detailed statistical analysis of the Ogden curve fit can also be done to verify the model, further than the single element model.

6.2.3 FSI Human Lung

For the human lung FSI simulation chapter, having a more refined mesh for the structural region and ensuring the fluid region mesh is also optimal would help with the simulation. In the chapter, only one breathing cycle of the PCV was simulated. Better results of the air flow behavior would require longer simulated time. For the PCV velocity profile, a Fourier approximation was used to estimate the PCV velocity profile. A better way estimating the velocity profile would be to create a piecewise function, instead of using Fourier approximation. A piecewise function is easier to control and prescribe than a Fourier approximation. Also, since the study is only done with a conventional ventilation flow, another ventilation flow should be done for comparison, such as a HFPV flow. In addition, other flow profiles can be applied for verification purposes. Also, to simulate certain lung conditions, a good starting point would be to “plug” or cap one or more of the outlets to simulate mucus blockage. Other improvements to ensure a more accurate model would be to incorporate multiple materials and more generations (branches). An improvement on the structural side would be to have multiple thicknesses, currently the lung has a uniform shell of 1 (mm), when in reality the thickness actually varies. One last thing that can be incorporated, is a proper value or boundary condition for the trachea. Instead of using a “water elastic support” a proper value or proper tracheal support can be added to increase the accuracy of the model.

To summarize, some limitations of the current study would include the 3D balloon simulation that has not been validated with experimental results. A solution verification study should be conducted for the 3D balloon as well. For material testing, the experiments were only conducted with uniaxial tension testing, when other testing such as biaxial maybe more accurate. In addition, the material model curve fitting is only fitted with the Ogden material model, when other models such as Moony-Rivlin may provide more accurate results. Lastly, a convergence study for the lung simulation should be performed and the detail lung geometry can be more accurate (more generations). Other researchers have conducted similar studies, specifically on tensile testing porcine tissue or different regions of FSI simulations of the upper airway. However, most are not directly comparable to this study, which in turn makes it a limitation as well.

REFERENCES

[1] R. Dutta, T. Xing, C. Swanson, J. Heltborg, and G. K. Murdoch, "Comparison of flow and gas washout characteristics between pressure control and high-frequency percussive ventilation using a test lung," *Physiological measurement,* vol. 39, no. 3, p. 035001, 2018.

[2] U. Lucangelo *et al.*, "Effects of mechanical load on flow, volume and pressure delivered by high-frequency percussive ventilation," *Respiratory physiology & neurobiology,* vol. 142, no. 1, pp. 81-91, 2004.

[3] A. R. Lambert, P. T. O'shaughnessy, M. H. Tawhai, E. A. Hoffman, and C.-L. Lin, "Regional deposition of particles in an image-based airway model: large-eddy simulation and left-right lung ventilation asymmetry," *Aerosol Science and Technology,* vol. 45, no. 1, pp. 11-25, 2011.

[4] R. Calay, J. Kurujareon, and A. E. Holdø, "Numerical simulation of respiratory flow patterns within human lung," *Respiratory physiology & neurobiology,* vol. 130, no. 2, pp. 201-221, 2002.

[5] G. Xia, M. H. Tawhai, E. A. Hoffman, and C. L. Lin, "Airway wall stiffening increases peak wall shear stress: a fluid-structure interaction study in rigid and compliant airways," *Ann Biomed Eng,* vol. 38, no. 5, pp. 1836-53, May 2010.

[6] M. Malvè, A. P. del Palomar, O. Trabelsi, J. López-Villalobos, A. Ginel, and M. Doblaré, "Modeling of the fluid structure interaction of a human trachea under different ventilation conditions," *International Communications in Heat and Mass Transfer,* vol. 38, no. 1, pp. 10-15, 2011.

[7] J. Ladyof Hats, "Respiratory system complete," 13 December 2007 ed. Wikipedia, 2016, pp. The respiratory system consists of the airways, the lungs, and the respiratory muscles that mediate the movement of air into and out of the body.

[8] H. Kitaoka, R. Takaki, and B. Suki, "A three-dimensional model of the human airway tree," *Journal of Applied Physiology,* vol. 87, no. 6, pp. 2207-2217, 1999.

[9] U. Küttler, C. Förster, and W. A. Wall, "A solution for the incompressibility dilemma in partitioned fluid–structure interaction with pure Dirichlet fluid domains," *Computational Mechanics,* vol. 38, no. 4-5, pp. 417-429, 2006.

[10] A. E. Bogaers, S. Kok, B. D. Reddy, and T. Franz, "Extending the robustness and efficiency of artificial compressibility for partitioned fluid–structure interactions," *Computer Methods in Applied Mechanics and Engineering,* vol. 283, pp. 1278-1295, 2015.

[11] O. Trabelsi, A. P. Del Palomar, J. López-Villalobos, A. Ginel, and M. Doblaré, "Experimental characterization and constitutive modeling of the mechanical behavior of the human trachea," *Medical engineering & physics,* vol. 32, no. 1, pp. 76-82, 2010.

[12] C. Lally, A. Reid, and P. J. Prendergast, "Elastic behavior of porcine coronary artery tissue under uniaxial and equibiaxial tension," *Annals of biomedical engineering,* vol. 32, no. 10, pp. 1355-1364, 2004.

[13] H. C. Shi *et al.*, "Biomechanical properties of adult-excised porcine trachea for tracheal xenotransplantation," *Xenotransplantation,* vol. 16, no. 3, pp. 181-186, 2009.

[14] Z. Teng *et al.*, "Nonlinear mechanical property of tracheal cartilage: A theoretical and experimental study," *Journal of biomechanics,* vol. 41, no. 9, pp. 1995-2002, 2008.

[15] A. Rohatgi. (2018, September 10). *WebPlotDigitizer*. Available: https://automeris.io/WebPlotDigitizer

[16] T. Xing and F. Stern, "Factors of safety for Richardson extrapolation," *Journal of Fluids Engineering,* vol. 132, no. 6, p. 061403, 2010.

[17] T. Xing and F. Stern, "Closure to "Discussion of 'Factors of Safety for Richardson Extrapolation'"(2011, ASME J. Fluids Eng., 133, p. 115501)," *Journal of Fluids Engineering,* vol. 133, no. 11, p. 115502, 2011.

[18] S. D. Chua, B. MacDonald, and M. Hashmi, "Finite element simulation of slotted tube (stent) with the presence of plaque and artery by balloon expansion," *Journal of Materials Processing Technology,* vol. 155, pp. 1772-1779, 2004.

[19] F. Gervaso, C. Capelli, L. Petrini, S. Lattanzio, L. Di Virgilio, and F. Migliavacca, "On the effects of different strategies in modelling balloon-expandable stenting by means of finite element method," *Journal of biomechanics,* vol. 41, no. 6, pp. 1206-1212, 2008.

[20] H. Zahedmanesh, D. J. Kelly, and C. Lally, "Simulation of a balloon expandable stent in a realistic coronary artery—Determination of the optimum modelling strategy," *Journal of Biomechanics,* vol. 43, no. 11, pp. 2126-2132, 2010.

[21] Q. Wang, S. Kodali, C. Primiano, and W. Sun, "Simulations of transcatheter aortic valve implantation: implications for aortic root rupture," *Biomechanics and modeling in mechanobiology,* vol. 14, no. 1, pp. 29-38, 2015.

[22] G. A. Holzapfel, M. Stadler, and C. A. Schulze-Bauer, "A layer-specific three-dimensional model for the simulation of balloon angioplasty using magnetic resonance imaging and mechanical testing," *Annals of biomedical engineering,* vol. 30, no. 6, pp. 753-767, 2002.

[23] Q. Liu, Z. Wu, M. Zhu, and W. Xu, "A comprehensive numerical model investigating the thermal-dynamic performance of scientific balloon," *Advances in Space Research,* vol. 53, no. 2, pp. 325-338, 2014.

[24] D. Roylance, "Pressure vessels," *Department of Material Science and Engineering, Massachusetts Institute of Technology, Cambridge, MA,* vol. 2139, 2001.

[25] S. Codd, R. Lambert, M. Alley, and R. Pack, "Tensile stiffness of ovine tracheal wall," *Journal of Applied Physiology,* vol. 76, no. 6, pp. 2627-2635, 1994.

[26] U. Holzhäuser and R. K. Lambert, "Analysis of tracheal mechanics and applications," *Journal of applied physiology,* vol. 91, no. 1, pp. 290-297, 2001.

[27] D. Begis, C. Delpuech, P. Le Tallec, L. Loth, M. Thiriet, and M. Vidrascu, "A finite-element model of tracheal collapse," *Journal of applied physiology,* vol. 64, no. 4, pp. 1359-1368, 1988.

[28] R. Lambert, E. Baile, R. Moreno, J. Bert, and P. Pare, "A method for estimating the Young's modulus of complete tracheal cartilage rings," *Journal of Applied Physiology,* vol. 70, no. 3, pp. 1152-1159, 1991.

[29] J. Rains, J. Bert, C. Roberts, and P. Pare, "Mechanical properties of human tracheal cartilage," *Journal of Applied Physiology,* vol. 72, no. 1, pp. 219-225, 1992.

[30] H. Saraf, K. Ramesh, A. Lennon, A. Merkle, and J. Roberts, "Mechanical properties of soft human tissues under dynamic loading," *Journal of biomechanics,* vol. 40, no. 9, pp. 1960-1967, 2007.

[31] Z. Teng, O. Trabelsi, I. Ochoa, J. He, J. H. Gillard, and M. Doblare, "Anisotropic material behaviours of soft tissues in human trachea: an experimental study," *Journal of biomechanics,* vol. 45, no. 9, pp. 1717-1723, 2012.

[32] Z. Teng, I. Ochoa, Z. Li, Z. Liao, Y. Lin, and M. Doblare, "Study on tracheal collapsibility, compliance, and stress by considering nonlinear mechanical property of cartilage," *Annals of biomedical engineering,* vol. 37, no. 11, pp. 2380-2389, 2009.

[33] R. Ogden, G. Saccomandi, and I. Sgura, "Fitting hyperelastic models to experimental data," *Computational Mechanics,* vol. 34, no. 6, pp. 484-502, 2004.

[34] Y. Wu, H. Wang, and A. Li, "Parameter identification methods for hyperelastic and hyper-viscoelastic models," *Applied Sciences,* vol. 6, no. 12, p. 386, 2016.

[35] J. Robinson, "A single element test," *Computer Methods in Applied Mechanics and Engineering,* vol. 7, no. 2, pp. 191-200, 1976.

[36] A. J. Sophia Fox, A. Bedi, and S. A. Rodeo, "The basic science of articular cartilage: structure, composition, and function," *Sports health,* vol. 1, no. 6, pp. 461-468, 2009.

[37] B. Button, R. C. Boucher, and U. o. N. C. V. L. Group, "Role of mechanical stress in regulating airway surface hydration and mucus clearance rates," *Respiratory physiology & neurobiology,* vol. 163, no. 1-3, pp. 189-201, 2008.

[38] P. Aghasafari, I. B. M. Ibrahim, and R. Pidaparti, "Strain-induced inflammation in pulmonary alveolar tissue due to mechanical ventilation," *Biomechanics and modeling in mechanobiology,* vol. 16, no. 4, pp. 1103-1118, 2017.

[39] M. Malvè *et al.*, "FSI analysis of a healthy and a stenotic human trachea under impedance-based boundary conditions," *Journal of biomechanical engineering,* vol. 133, no. 2, p. 021001, 2011.

[40] L. Yoshihara, C. J. Roth, and W. A. Wall, "Fluid-structure interaction including volumetric coupling with homogenised subdomains for modeling respiratory mechanics," *International journal for numerical methods in biomedical engineering,* vol. 33, no. 4, p. e2812, 2017.

[41] Y. Liu, R. M. C. So, and C. H. Zhang, "Modeling the bifurcating flow in an asymmetric human lung airway," *Journal of Biomechanics,* vol. 36, no. 7, pp. 951-959, 2003.

[42] T. Sera, S. Satoh, H. Horinouchi, K. Kobayashi, and K. Tanishita, "Respiratory flow in a realistic tracheostenosis model," *Journal of biomechanical engineering,* vol. 125, no. 4, pp. 461-471, 2003.

[43] A. Fedorov *et al.*, "3D Slicer as an image computing platform for the Quantitative Imaging Network," *Magnetic resonance imaging,* vol. 30, no. 9, pp. 1323-1341, 2012.

[44] (2018, 11/13/2018). *3D Slicer* [Downloadable program]. Available: https://www.slicer.org/

APPENDIX A – Chapter 2: The Quandary of Compressibility

The following are supplemental materials for Chapter 2: The Quandary of Compressibility.

Summary of Figures	**Page**
Square Balloon Meshes	143
Simulation 3 - Fluid pressure and structural stress contour plot	144
Simulation 3 - Fluid velocity magnitude and structural strain contour plot	146
Simulation 3 - Fluid velocity vector and structural deformation contour plot	148
Simulation 2 - Fluid pressure and structural stress contour plot	150
Simulation 2 - Fluid velocity magnitude and structural strain contour plot	152
Simulation 2 - Fluid velocity vector and structural deformation contour plot	154
Square Balloon Velocity Inlet Profile Code	156

Square Balloon Meshes

Fluid Region **Solid Region**

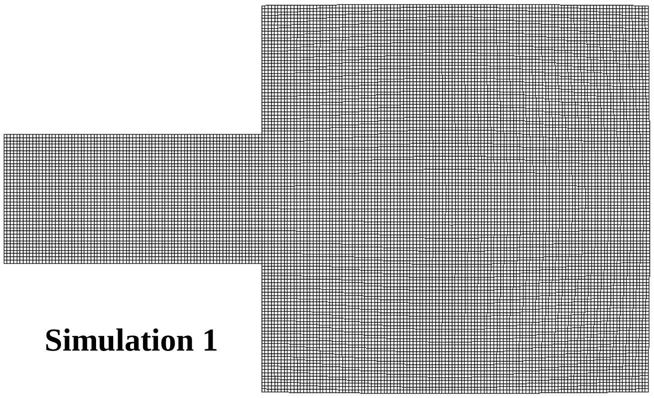

Simulation 1

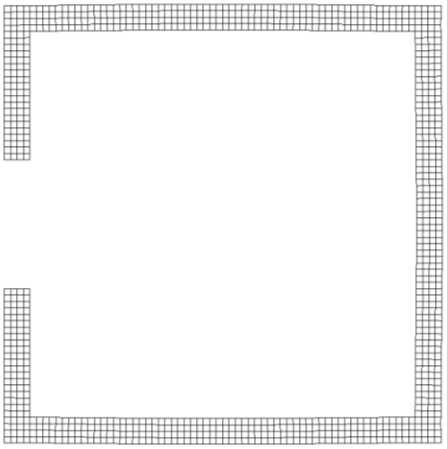

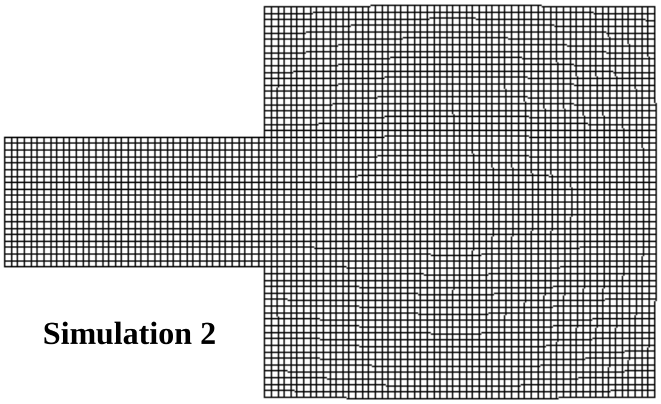

Simulation 2

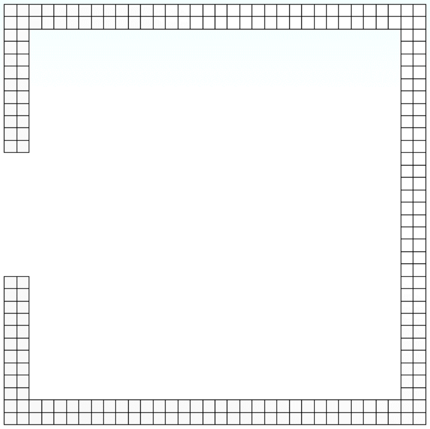

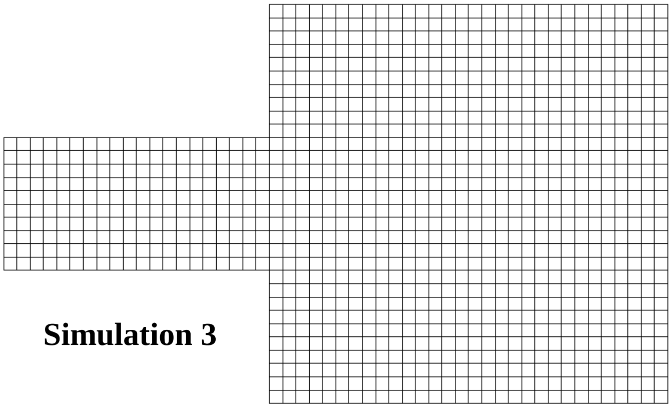

Simulation 3

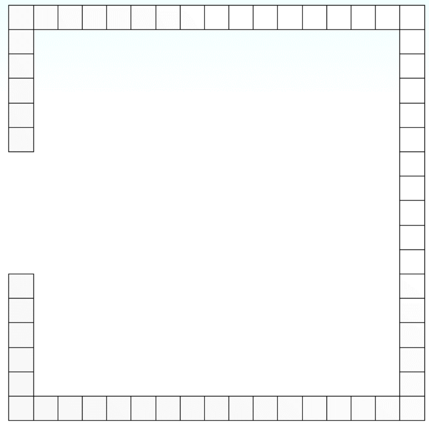

Simulation 3 - Fluid pressure and structural stress contour plot

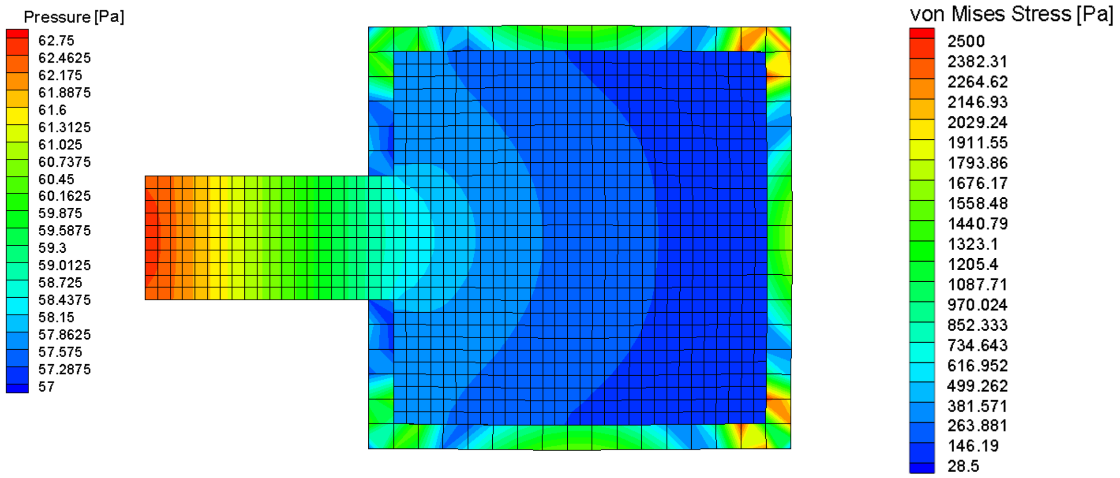

Figure A.2: Simulation 3 – Fluid pressure and structural stress contour plot at t = 0.5 second

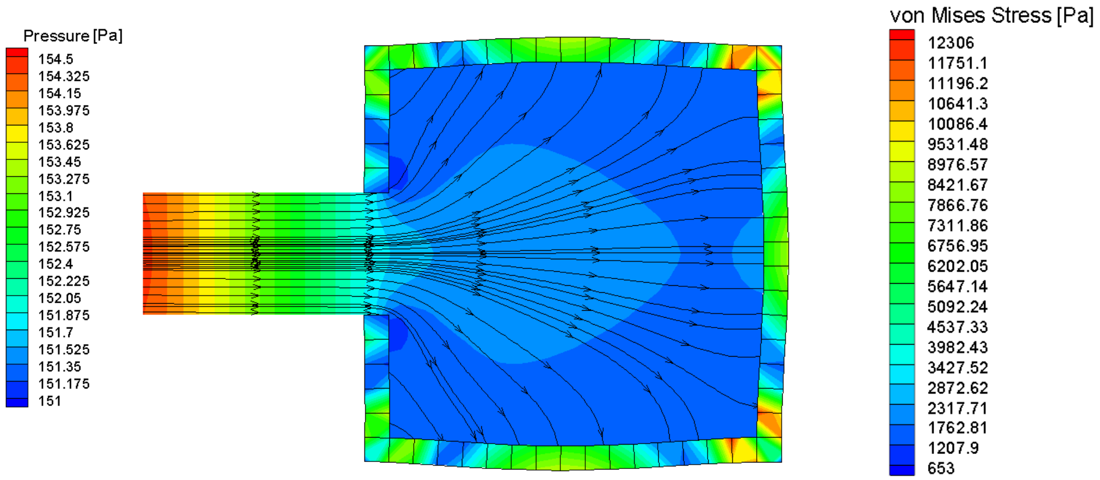

Figure A.3: Simulation 3 – Fluid pressure and structural stress contour plot at t = 1 second

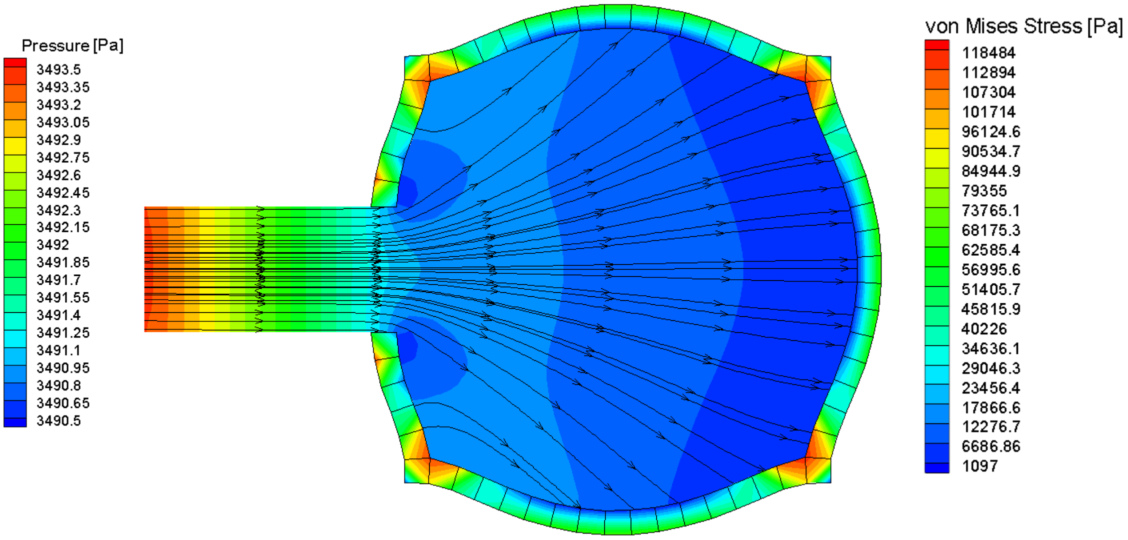

Figure A.4: Simulation 3 – Fluid pressure and structural stress contour plot at t = 5 seconds

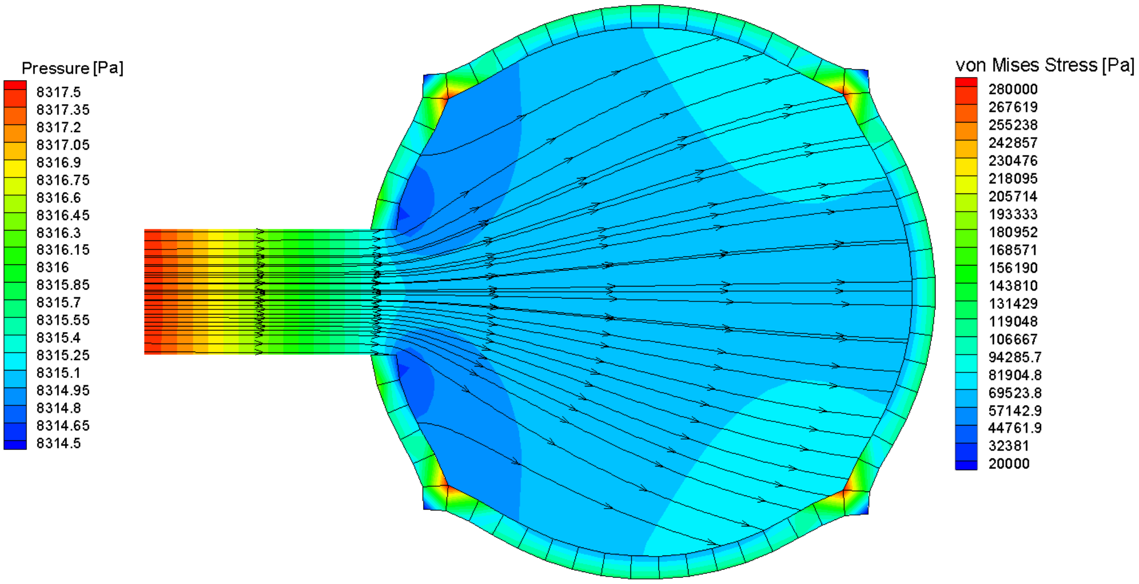

Figure A.5: Simulation 3 – Fluid pressure and structural stress contour plot at t = 9 seconds

Simulation 3 - Fluid velocity magnitude and structural strain contour plot

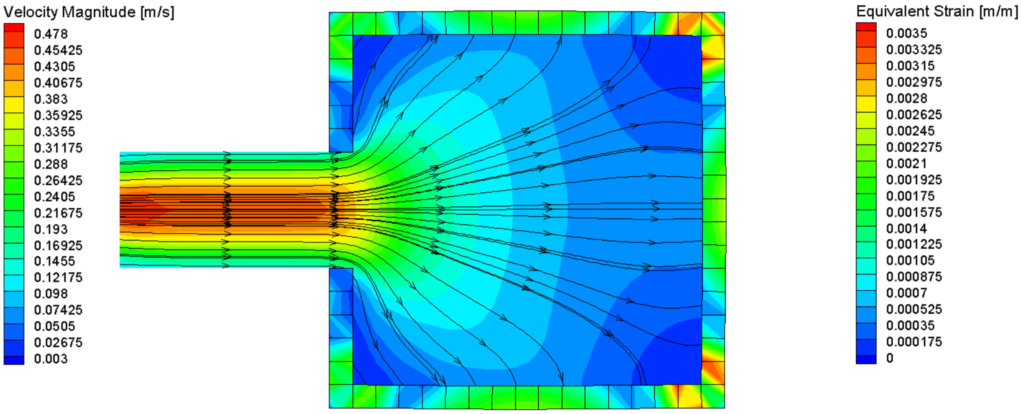

Figure A.6: Simulation 3 – Fluid velocity magnitude and structural strain contour plot for t = 0.5 second

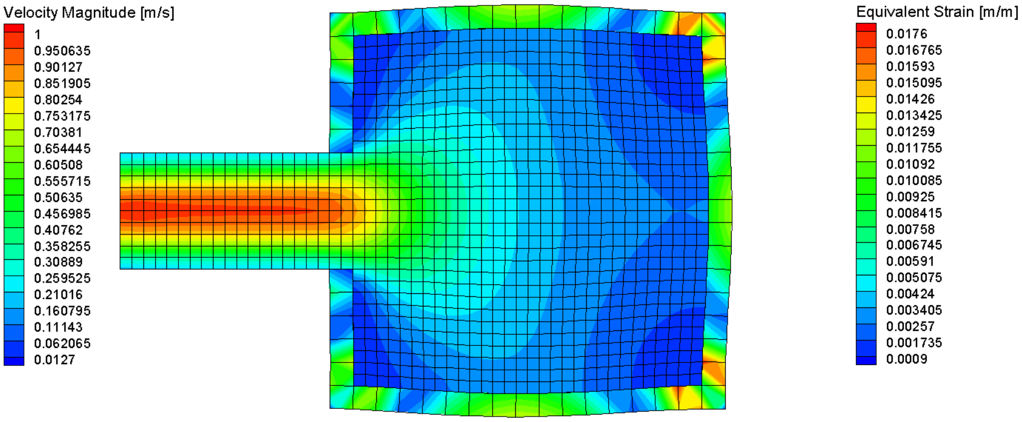

Figure A.7: Simulation 3 – Fluid velocity magnitude and structural strain contour plot for t = 1 second

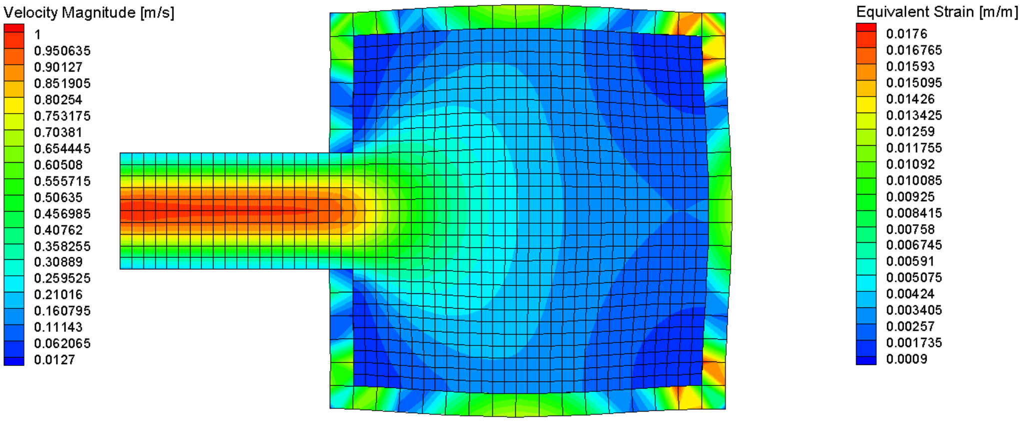

Figure A.8: Simulation 3 – Fluid velocity magnitude and structural strain contour plot for t = 5 seconds

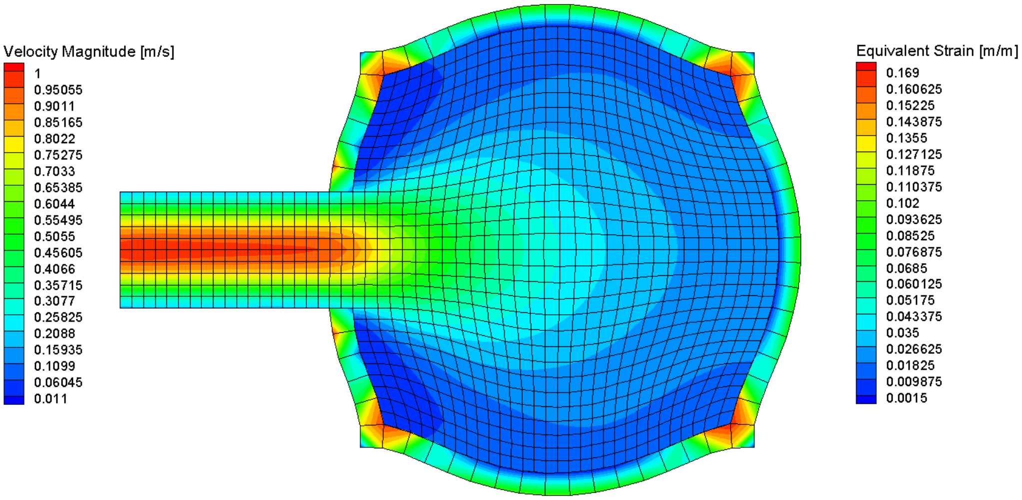

Figure A.9: Simulation 3 – Fluid velocity magnitude and structural strain contour plot for t = 9 seconds

Simulation 3 - Fluid velocity vector and structural deformation contour plot

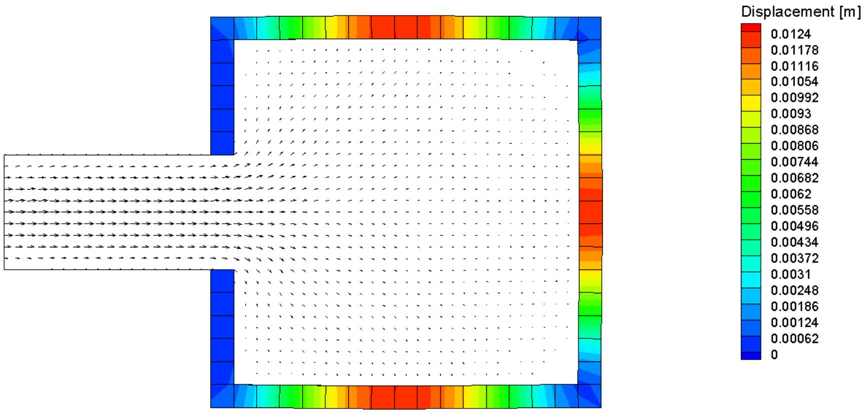

Figure A.10: Simulation 3 – Fluid velocity vector and structural deformation contour plot for t = 0.5 second

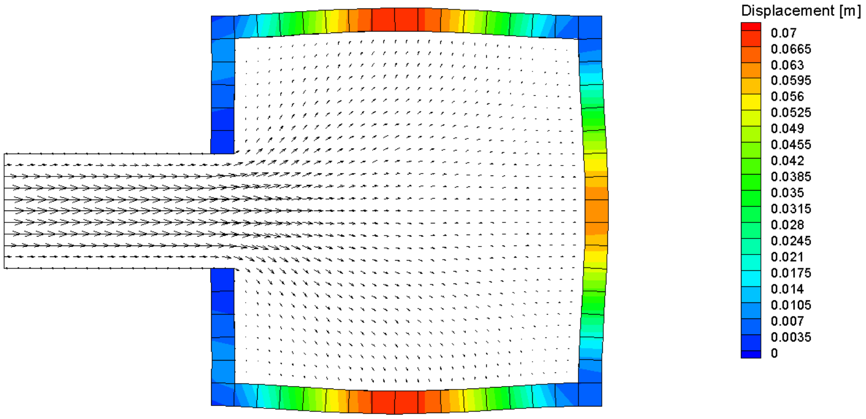

Figure A.11: Simulation 3 – Fluid velocity vector and structural deformation contour plot for t = 1 second

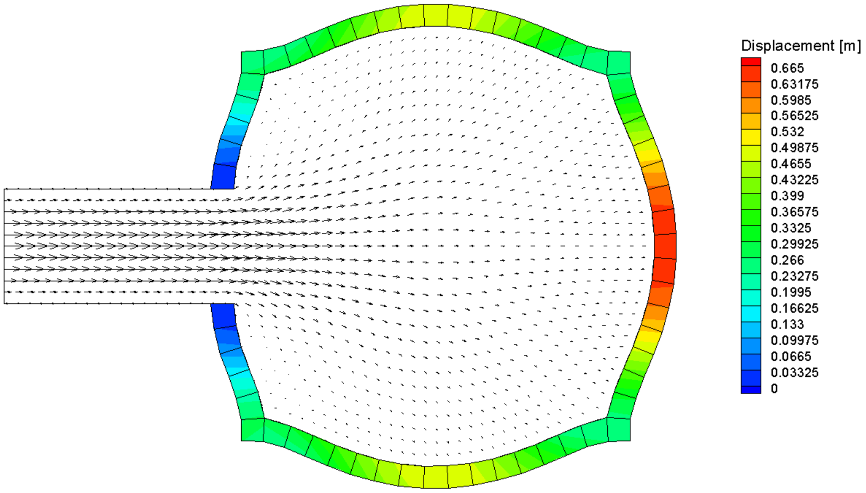

Figure A.12: Simulation 3 – Fluid velocity vector and structural deformation contour plot for t = 5 seconds

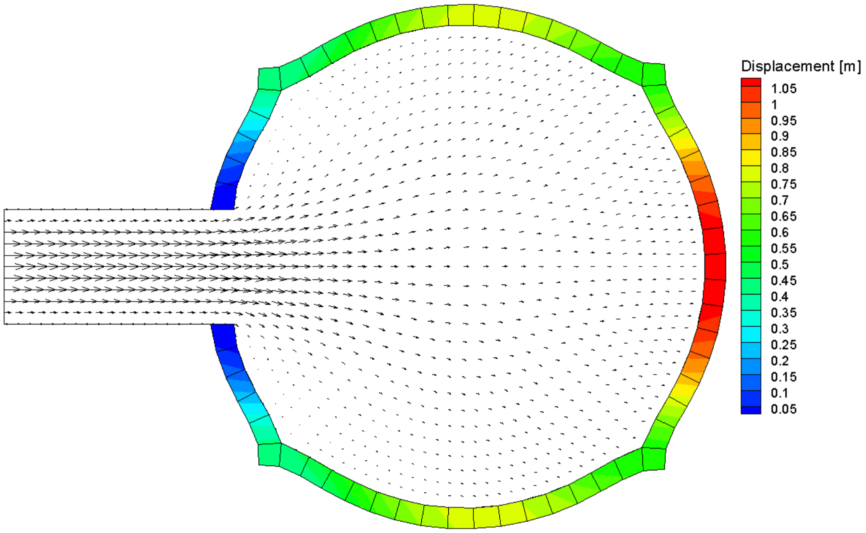

Figure A.13: Simulation 3 – Fluid velocity vector and structural deformation contour plot for t = 9 seconds

Simulation 2 - Fluid pressure and structural stress contour plot

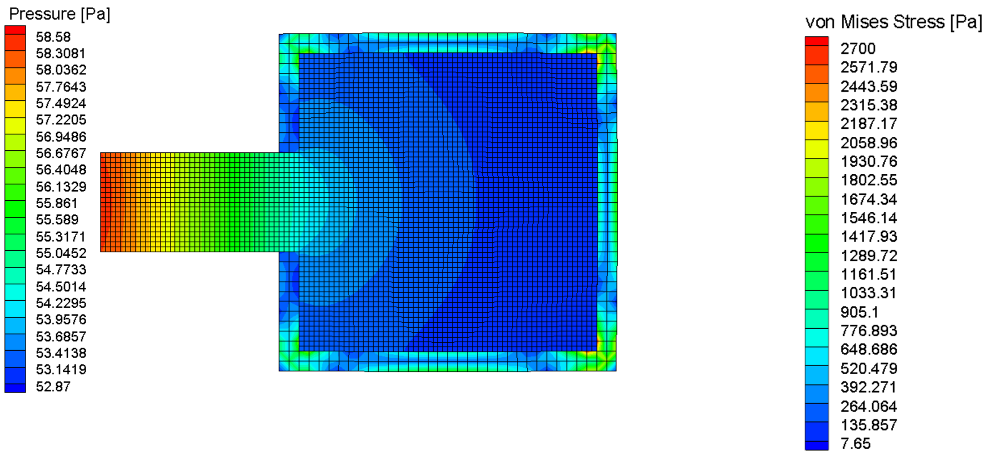

Figure A.14: Simulation 2 – Fluid pressure and structural stress contour plot at t = 0.5 second

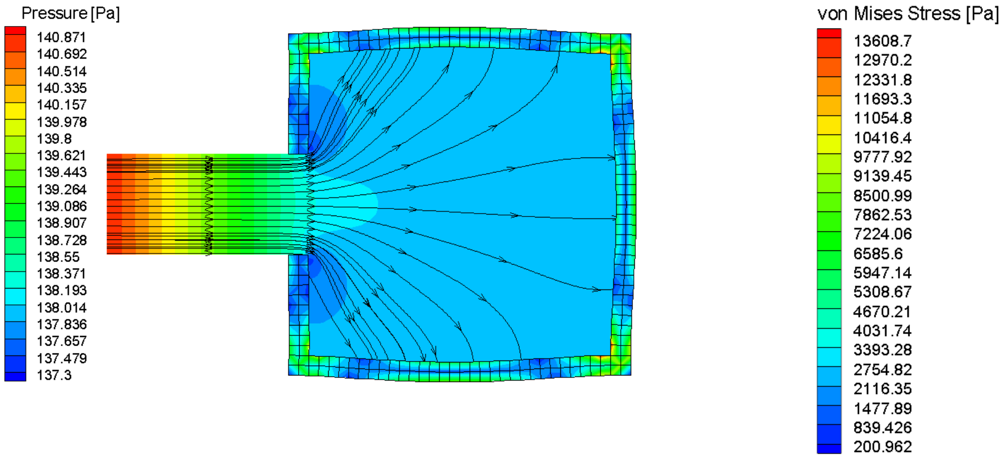

Figure A.15: Simulation 2 – Fluid pressure and structural stress contour plot at t = 1 second

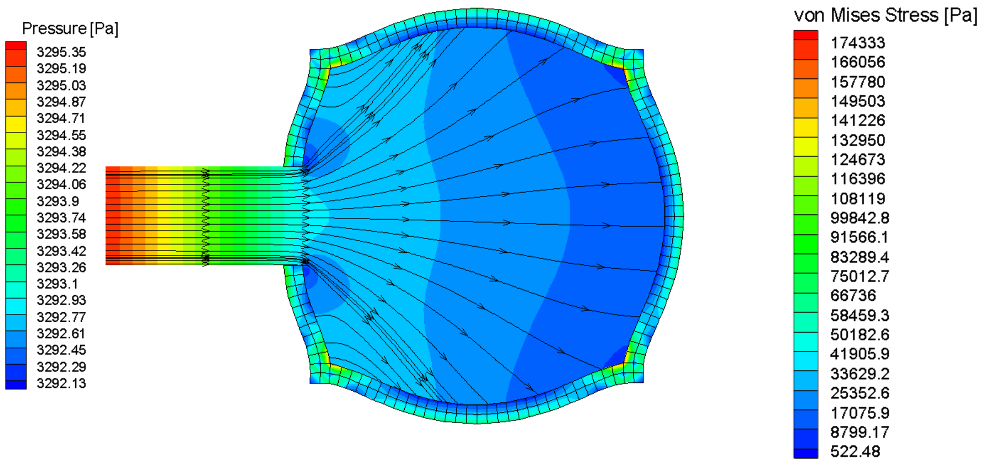

Figure A.16: Simulation 2 – Fluid pressure and structural stress contour plot at t = 5 seconds

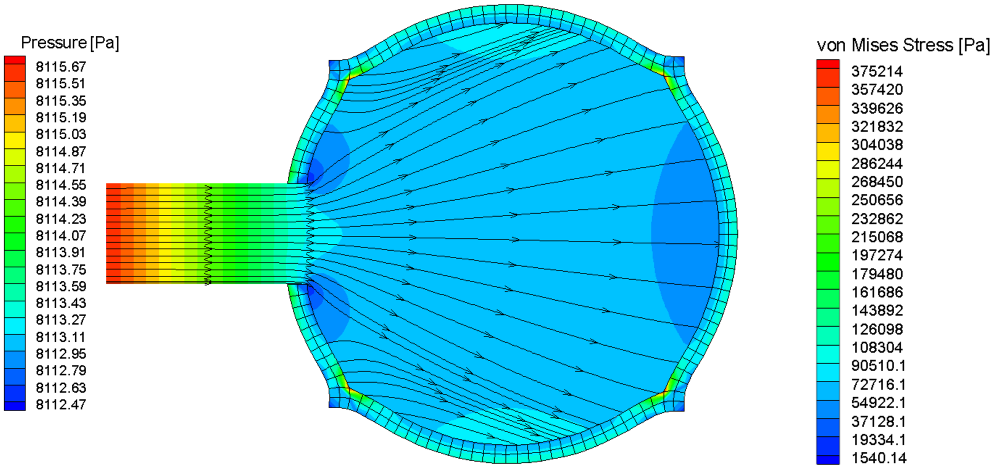

Figure A.17: Simulation 2 – Fluid pressure and structural stress contour plot at t = 9 seconds

Simulation 2 - Fluid velocity magnitude and structural strain contour plot

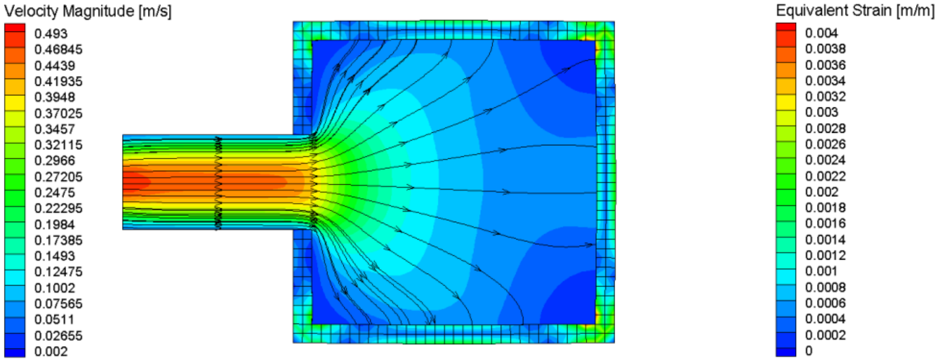

Figure A.18: Simulation 2 – Fluid velocity magnitude and structural strain contour plot for t = 0.5 second

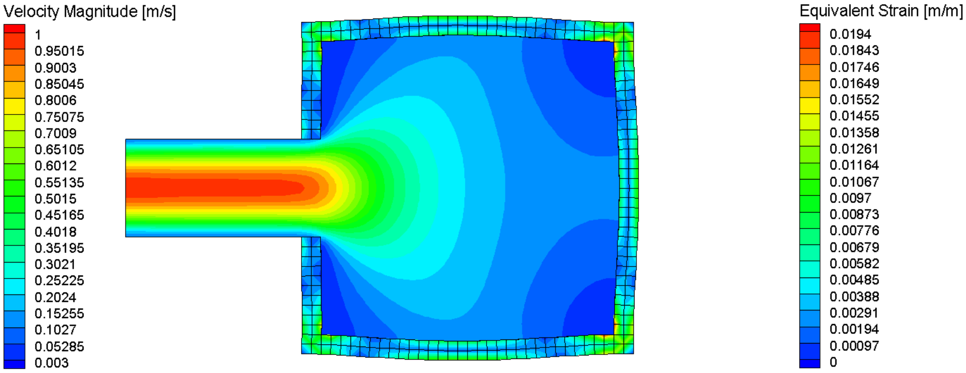

Figure A.19: Simulation 2 – Fluid velocity magnitude and structural strain contour plot for t = 1 second

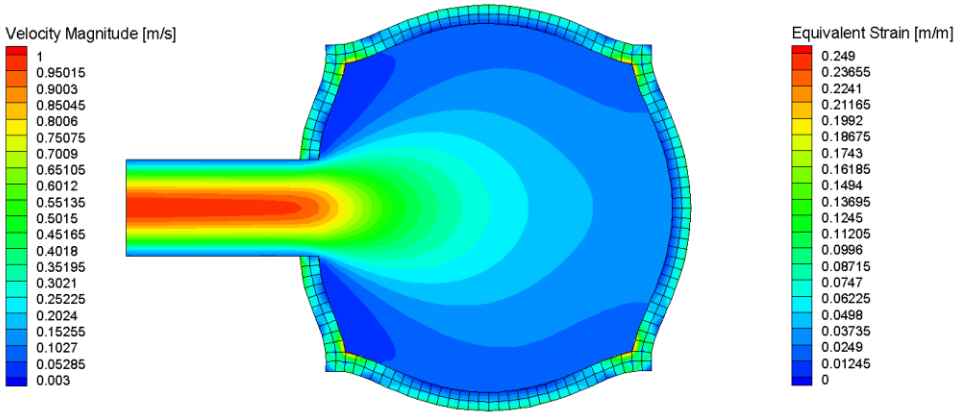

Figure A.20: Simulation 2 – Fluid velocity magnitude and structural strain contour plot for t = 5 seconds

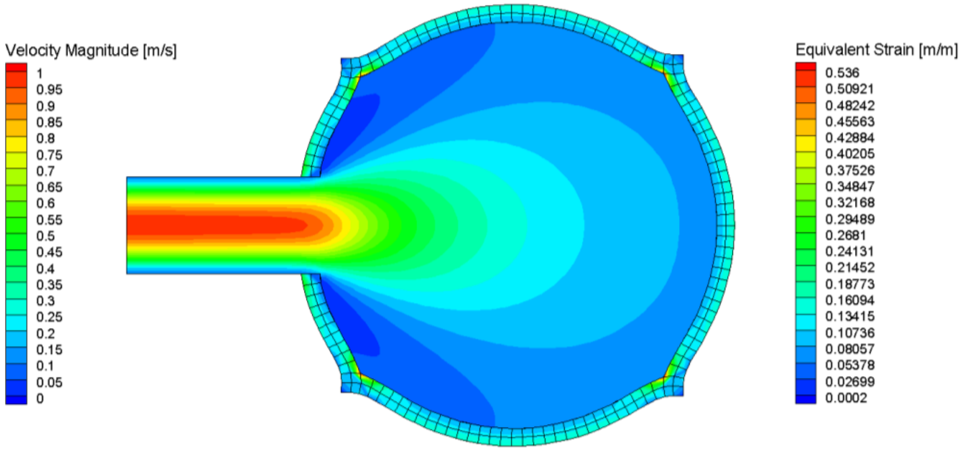

Figure A.21: Simulation 2 – Fluid velocity magnitude and structural strain contour plot for t = 9 seconds

Simulation 2 - Fluid velocity vector and structural deformation contour plot

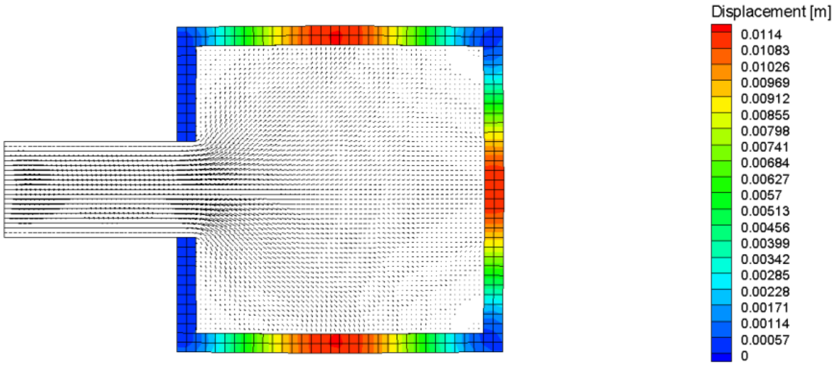

Figure A.22: Simulation 2 – Fluid velocity vector and structural deformation contour plot for t = 0.5 second

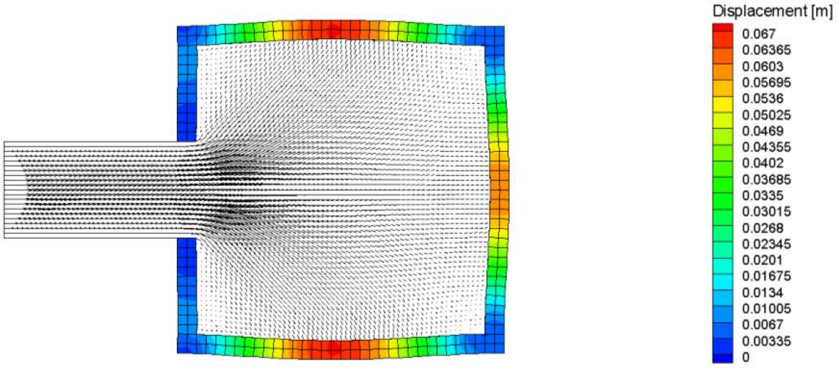

Figure A.23: Simulation 2 – Fluid velocity vector and structural deformation contour plot for t = 1 second

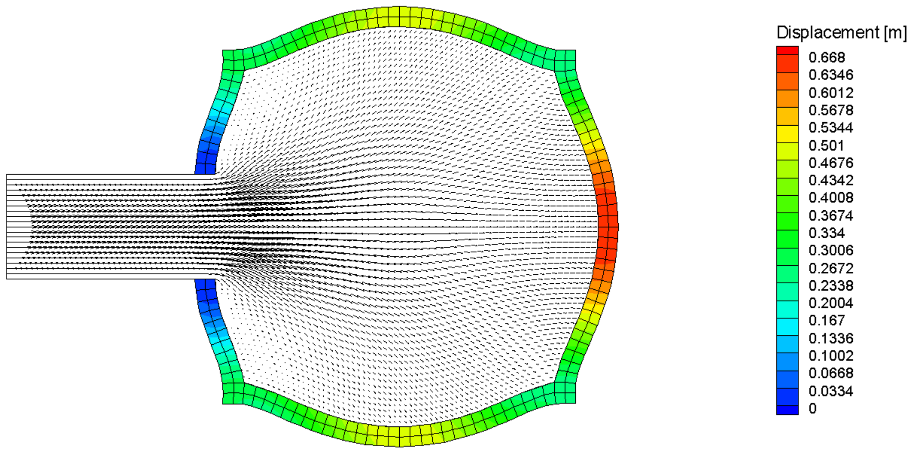

Figure A.24: Simulation 2 – Fluid velocity vector and structural deformation contour plot for t = 5 seconds

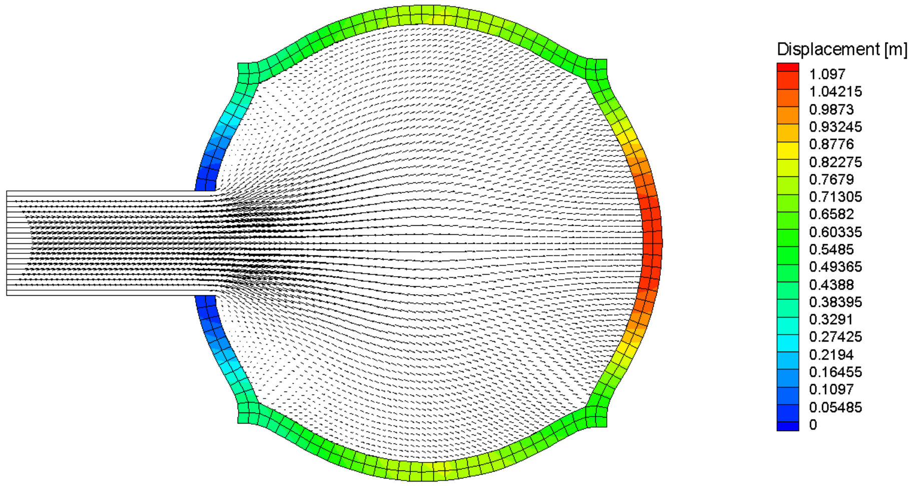

Figure A.25: Simulation 2 – Fluid velocity vector and structural deformation contour plot for t = 9 seconds

Square Balloon Velocity Inlet Profile Code

```
/**********************************************************************
UDF for specifying parabolic sinusoidal velocity profile boundary condition
***********************************************************************/
#include "udf.h"
DEFINE_PROFILE(Square_Balloon_velocity, thread, position)
{
        real x[ND_ND];
        real y;
        real umax;
        face_t f;
        real t = CURRENT_TIME;
        begin_f_loop(f, thread)
        {
                F_CENTROID(x, f, thread);
                y = x[1];
                if (t < 1.)
                {
                        umax = (sin(3.1412*(t + 1.5)) + 1) / 2;
                }
                else
                {
                        umax = 1.0;
                }
                F_PROFILE(f, thread, position) = umax - y*y / (0.5*0.5)*umax;
        }
        end_f_loop(f, thread)
}
```

APPENDIX B – Chapter 3: Three-Dimensional Balloon Expansion

The following are supplemental materials for Chapter 3: Three-Dimensional Balloon Expansion.

Summary of Figures	Page
3D Balloon Meshes	158
3D Balloon Structural Region: von Mises Stress	159
3D Balloon Structural Region: Equivalent Strain	162
3D Balloon Structural Region: Deformation	165
3D Balloon Fluid Region: Z Velocity Contour	168
3D Balloon Fluid Region: Velocity Magnitude Contour	172
3D Balloon Fluid Region: Velocity Vector	176
3D Balloon Velocity Inlet Profile Code	180

3D Balloon Meshes

Fluid Region **Solid Region**

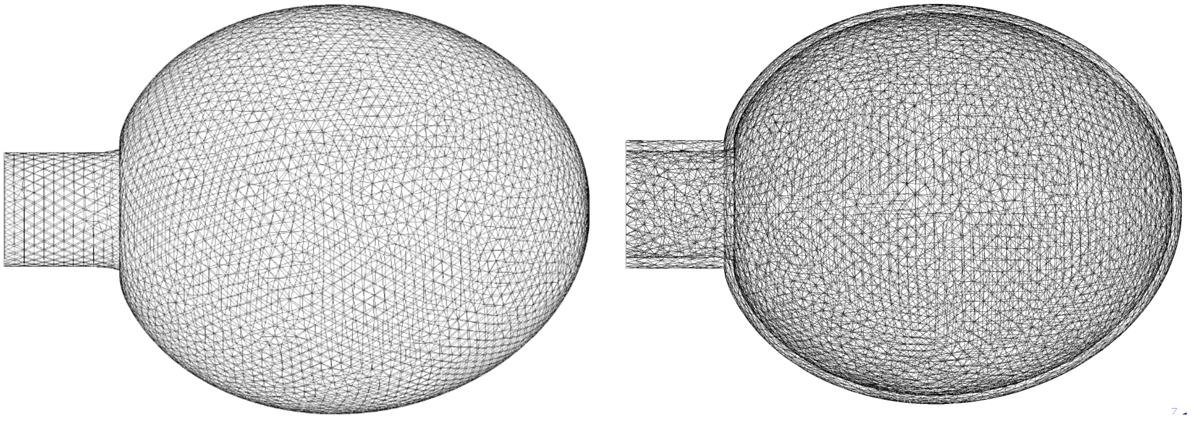

(a) Fluid Mesh Side View (b) Solid Mesh Side View

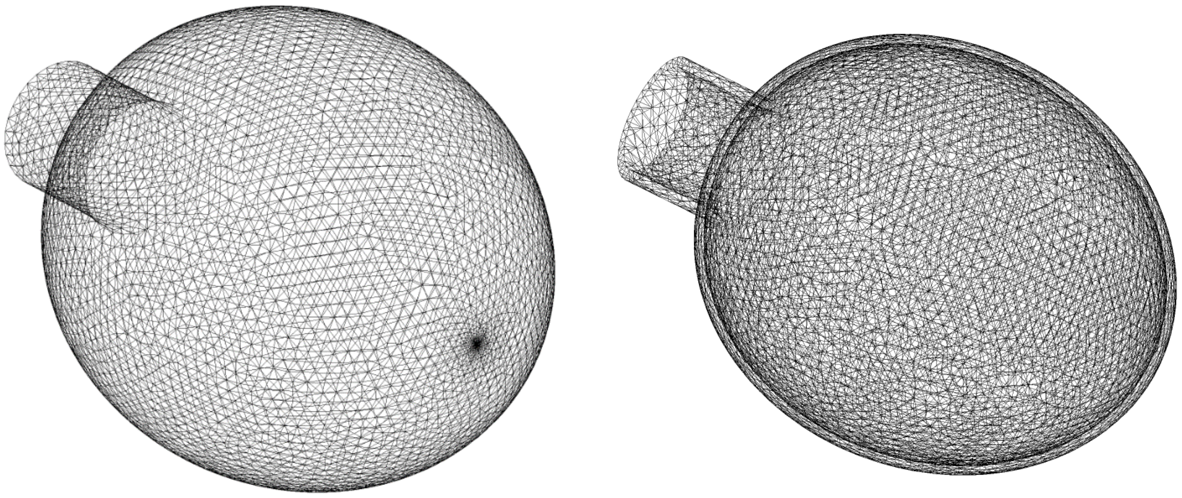

(c) Fluid Mesh Angled View (d) Solid Mesh Angled View

Figure B.1: Additional 3D balloon meshes

3D Balloon Structural Region: von Mises Stress

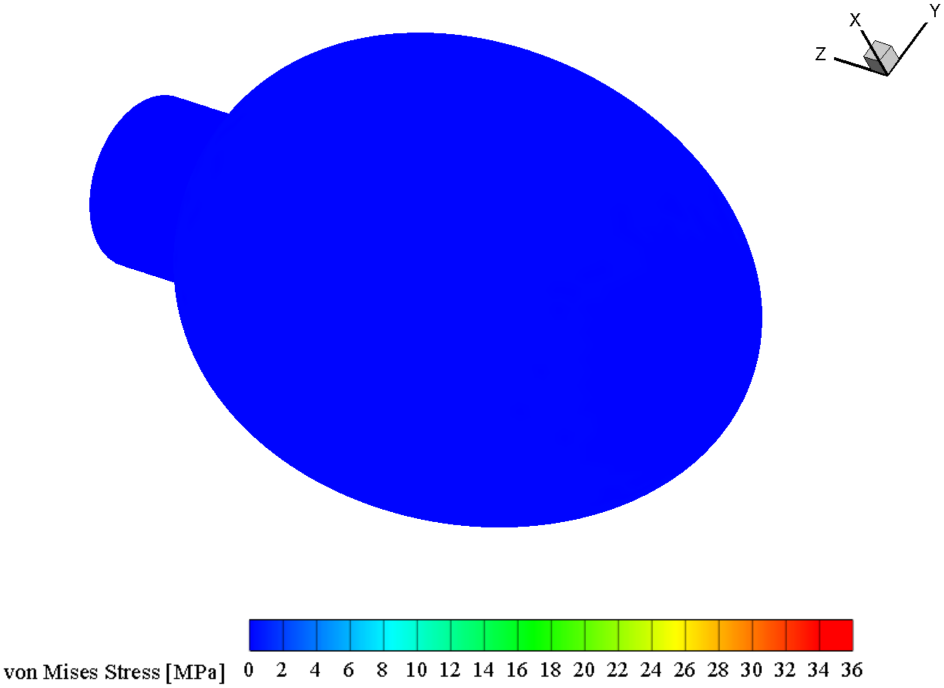

Figure B.2: von Mises stresses at t = 0.5 second

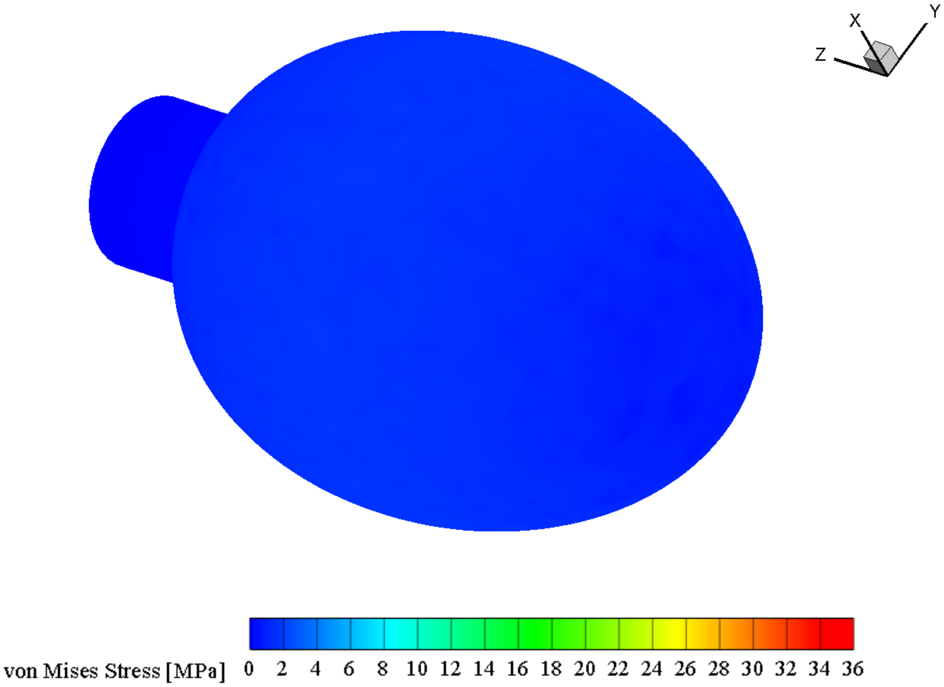

Figure B.3: von Mises stresses at t = 1 second

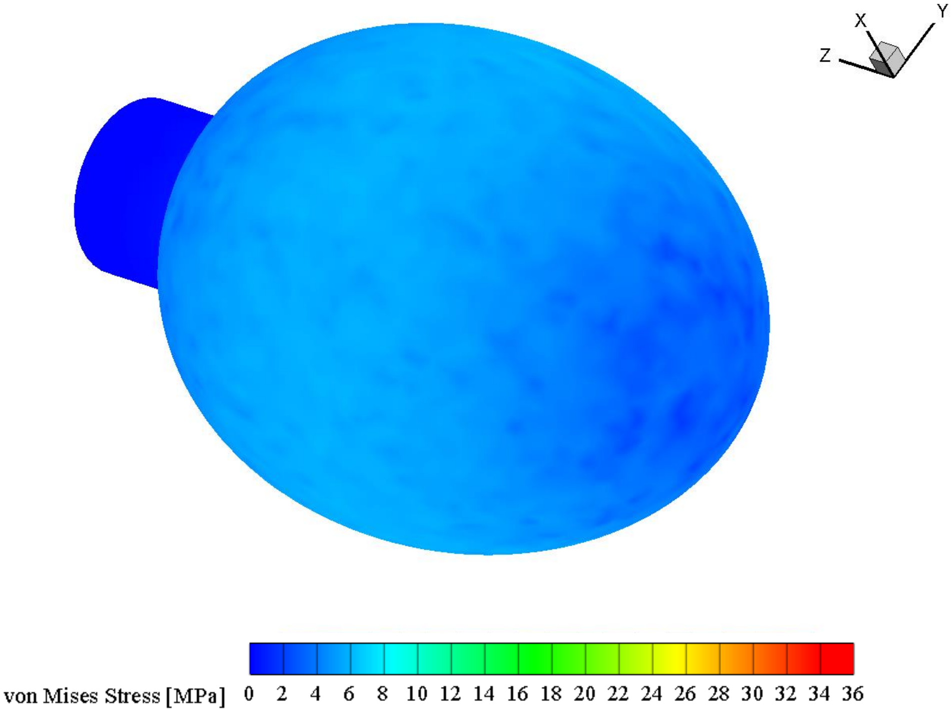

Figure B.4: von Mises stresses at t = 1.5 seconds

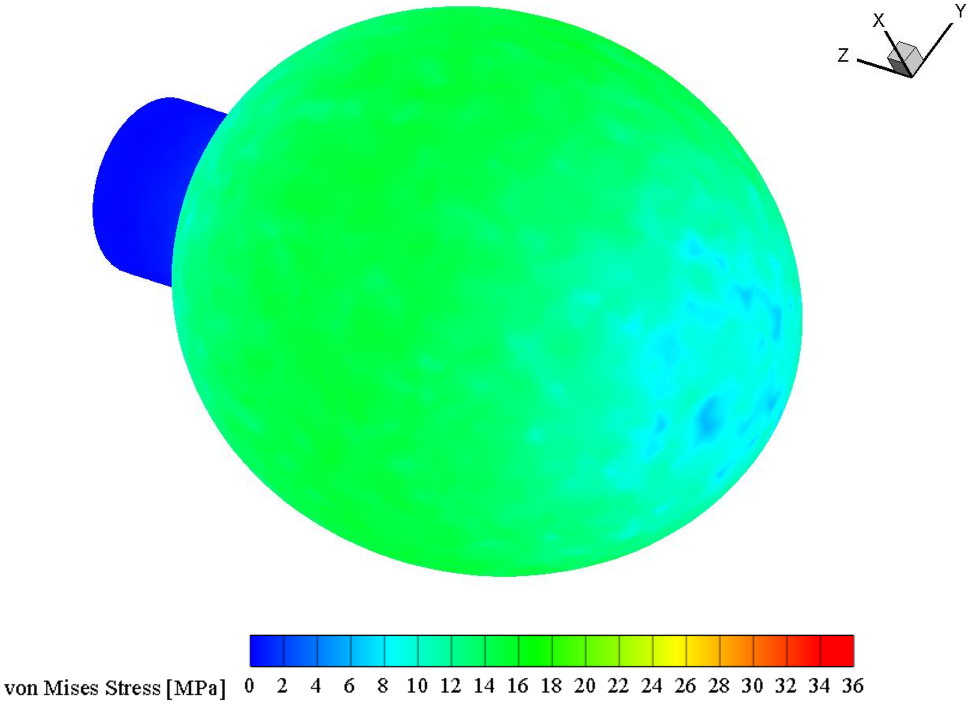

Figure B.5: von Mises stresses at t = 2 seconds

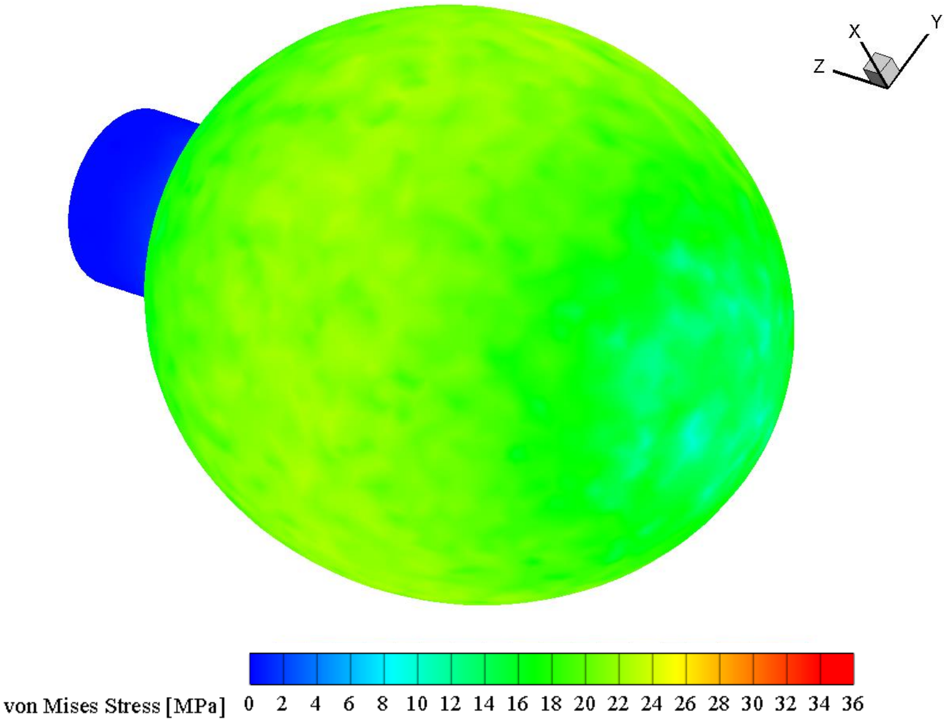

Figure B.6: von Mises stresses at t = 2.25 seconds

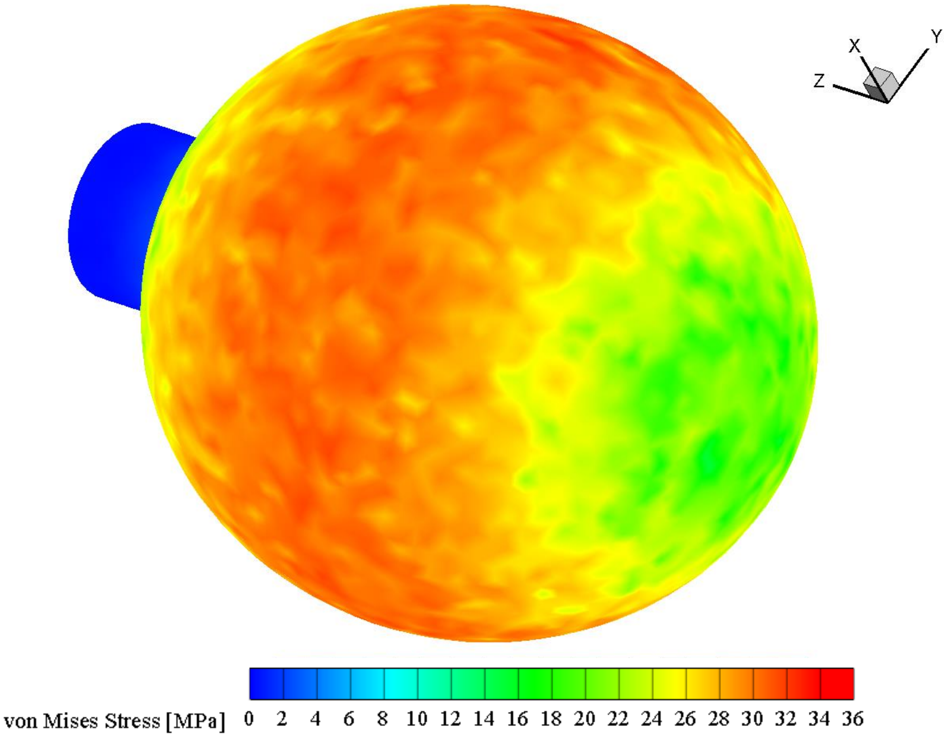

Figure B.7: von Mises stresses at t = 2.5 seconds

3D Balloon Structural Region: Equivalent Strain

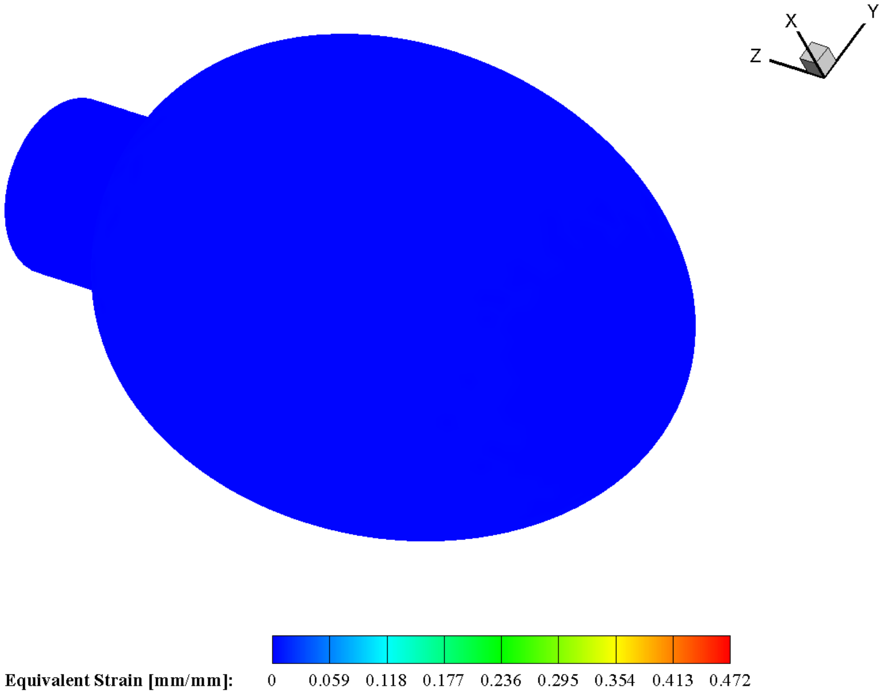

Figure B.8: Equivalent strain at t = 0.5 second

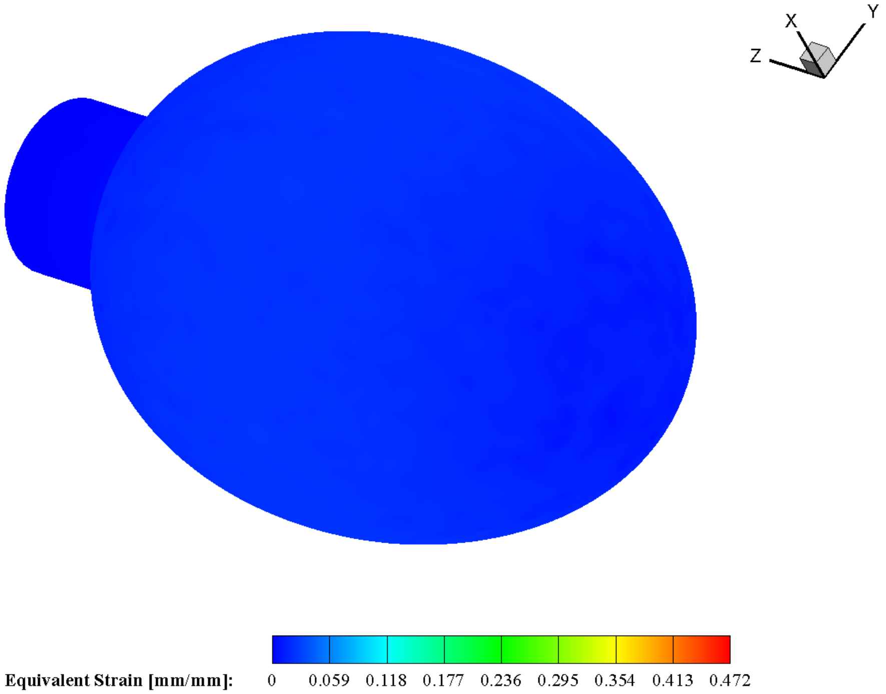

Figure B.9: Equivalent strain at t = 1 second

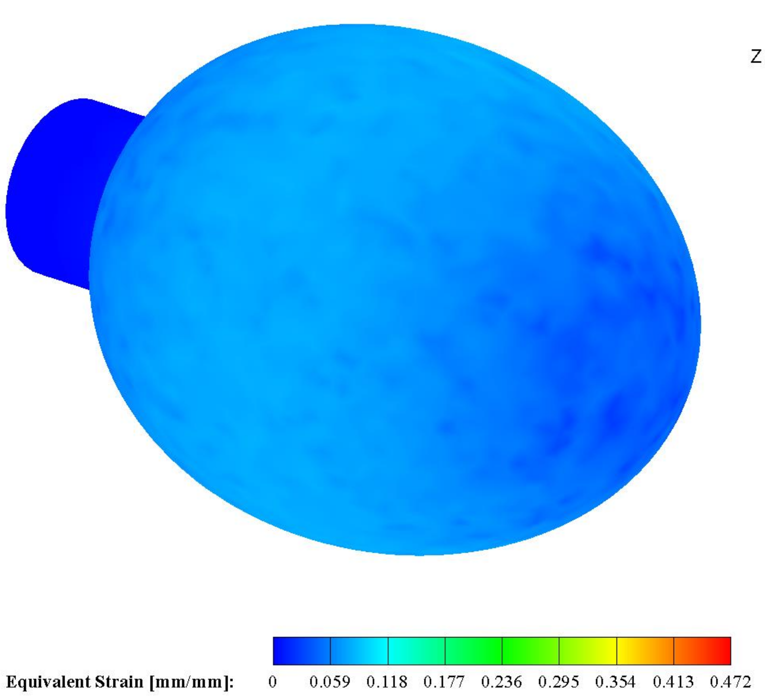

Figure B.10: Equivalent strain at t = 1.5 seconds

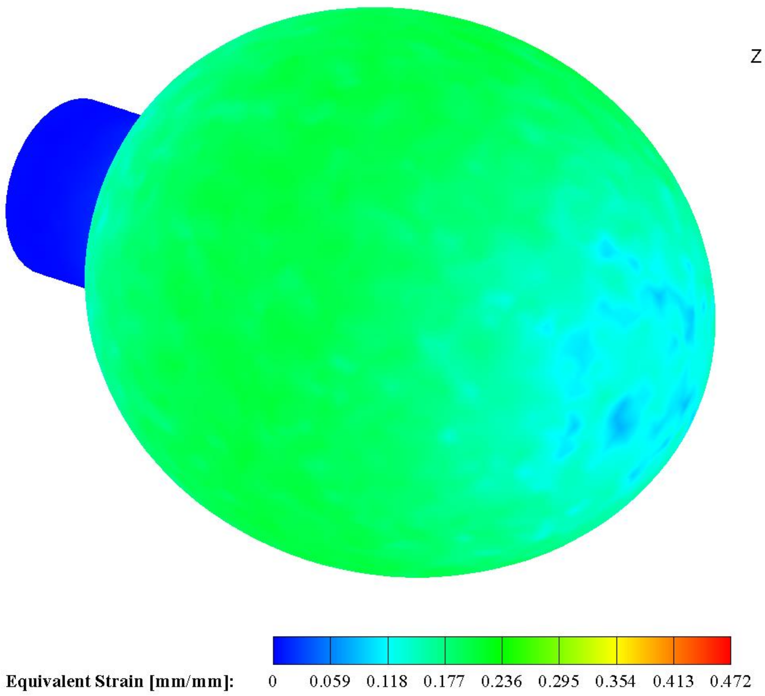

Figure B.11: Equivalent strain at t = 2 seconds

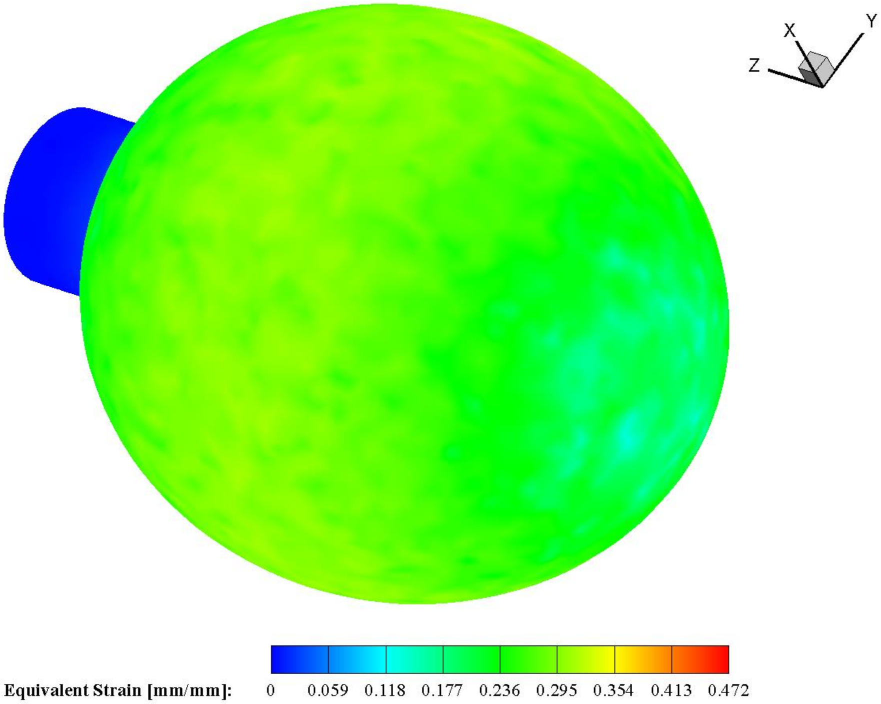

Figure B.12: Equivalent strain at t = 2.25 seconds

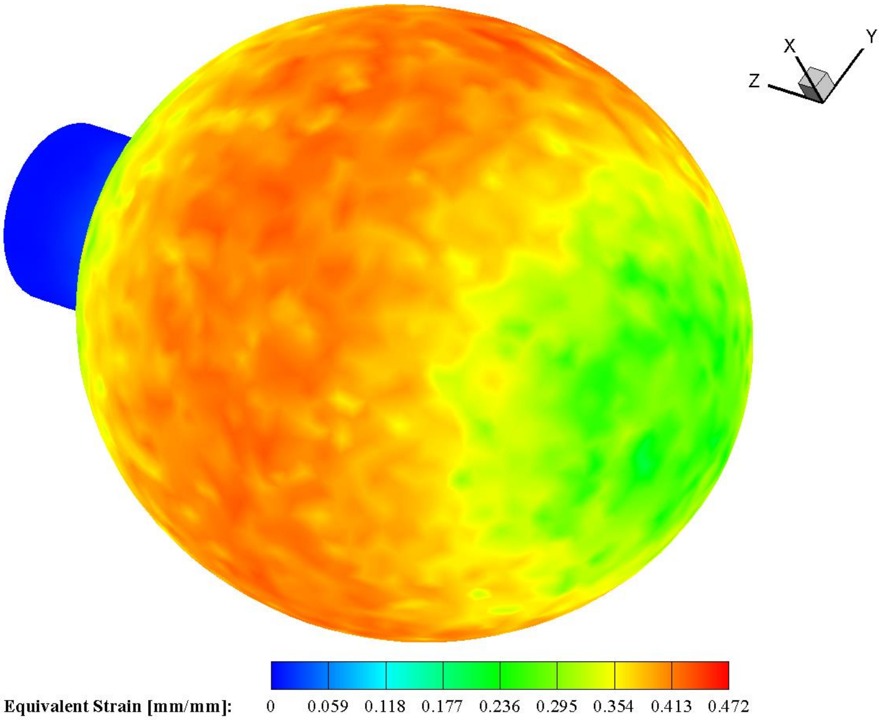

Figure B.13: Equivalent strain at t = 2.5 seconds

3D Balloon Structural Region: Deformation

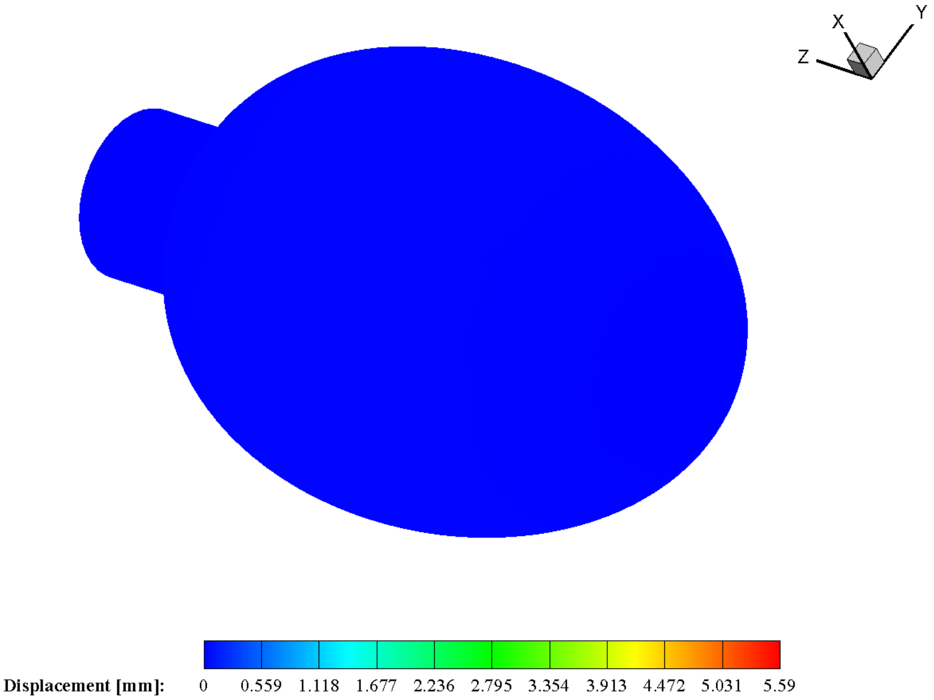

Figure B.14: Displacement at t = 0.5 second

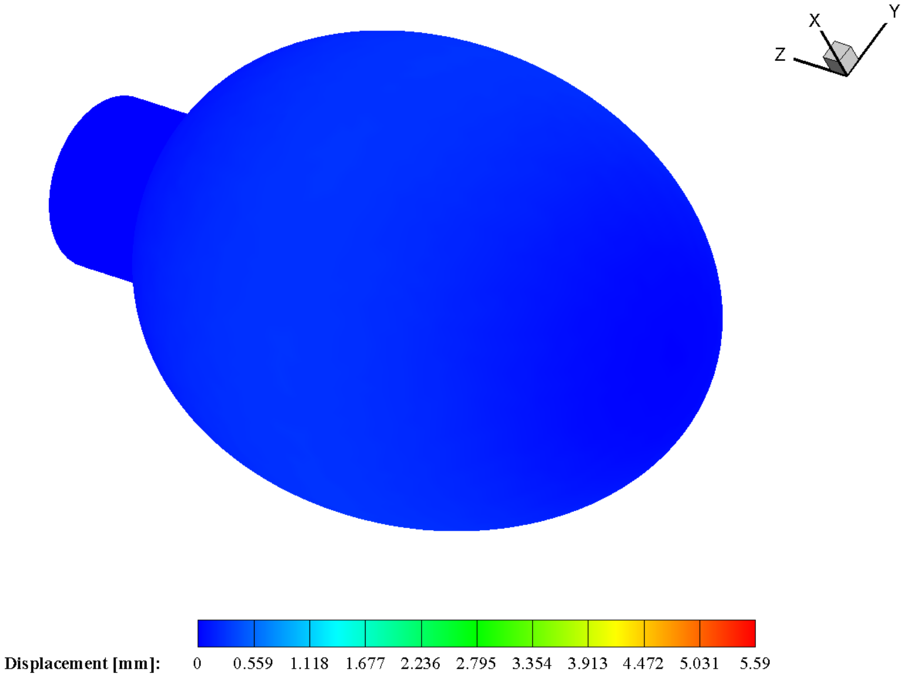

Figure B.15: Displacement at t = 1 second

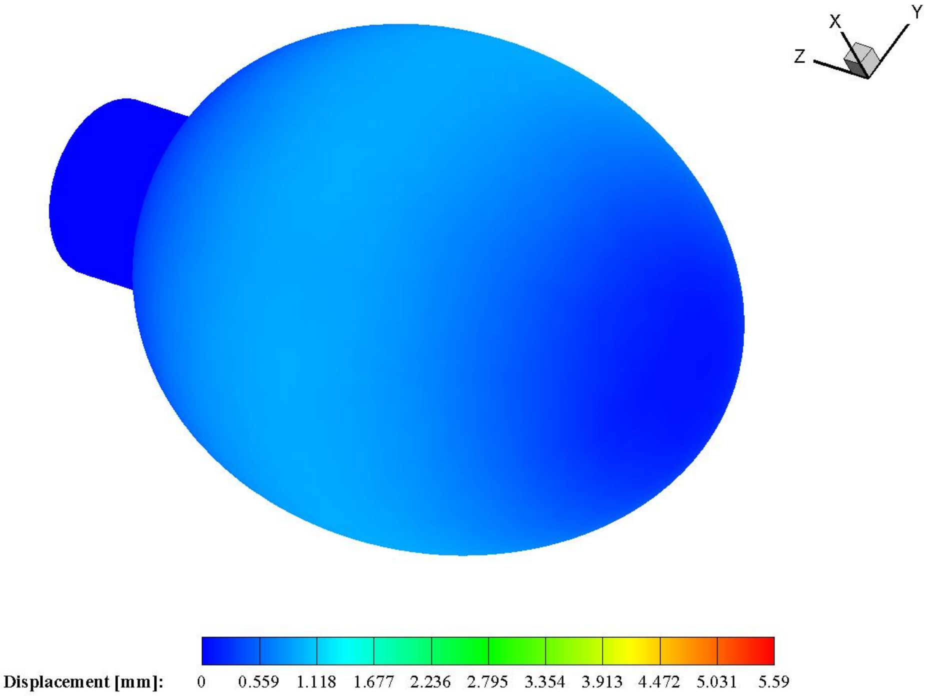

Figure B.16: Displacement at t = 1.5 seconds

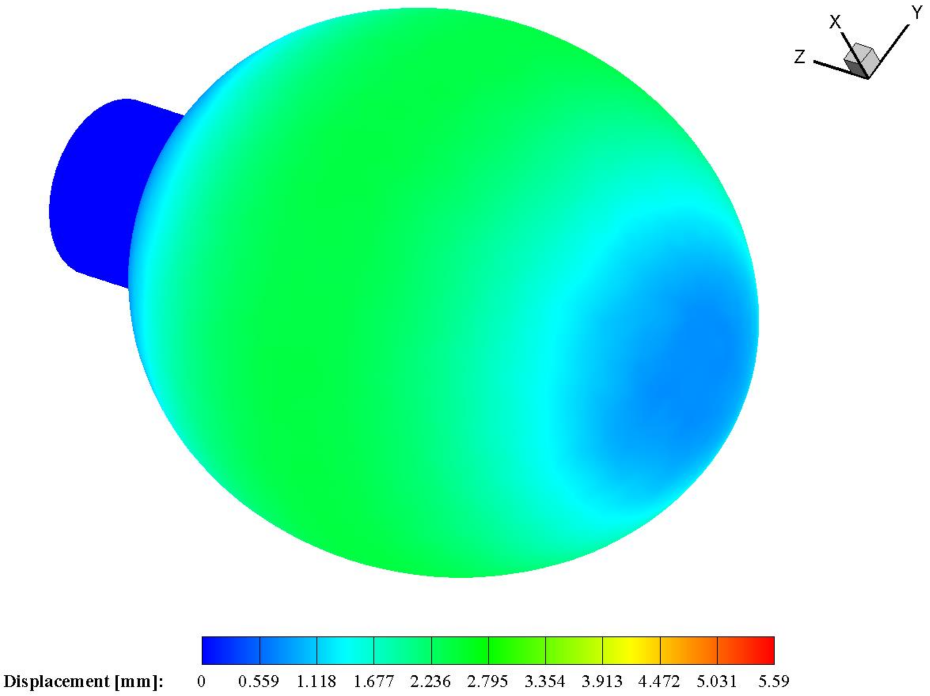

Figure B.17: Displacement at t = 2 seconds

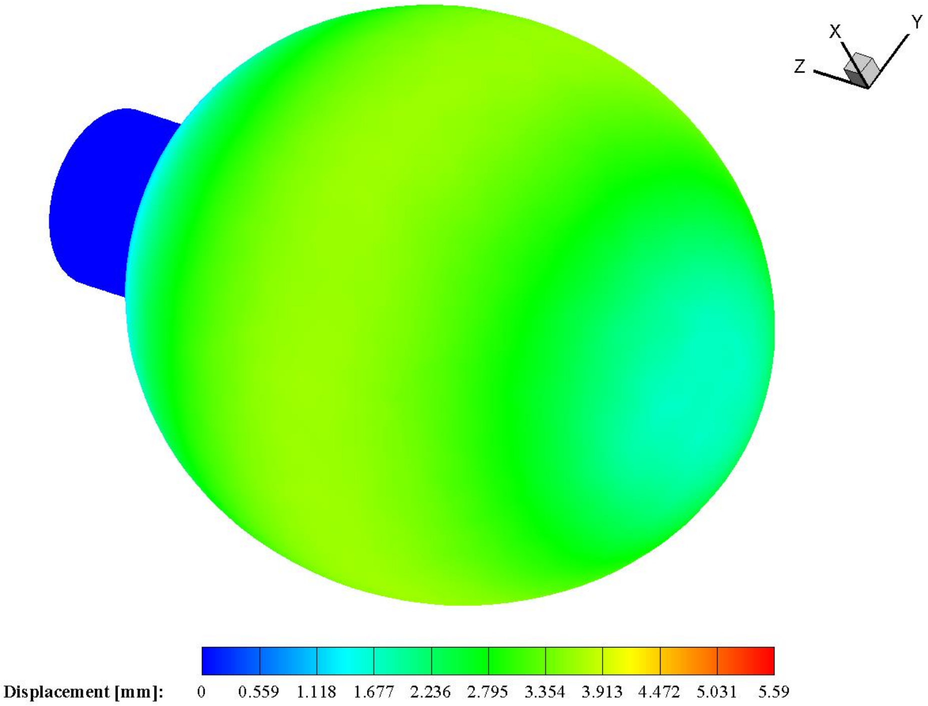

Figure B.18: Displacement at t = 2.25 seconds

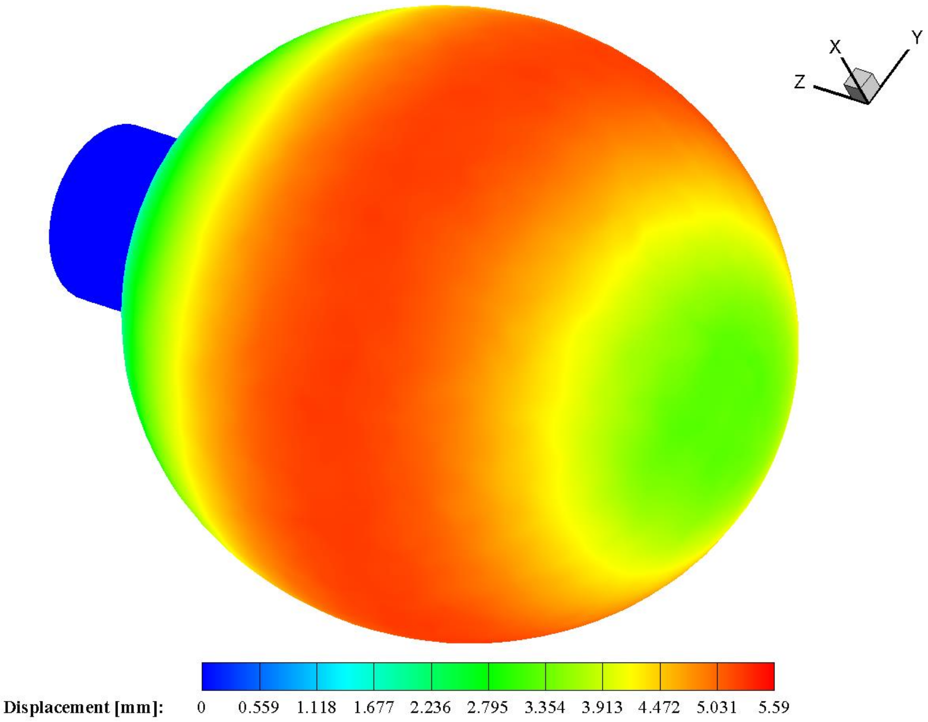

Figure B.19: Displacement at t = 2.5 seconds

3D Balloon Fluid Region: Z Velocity Contour

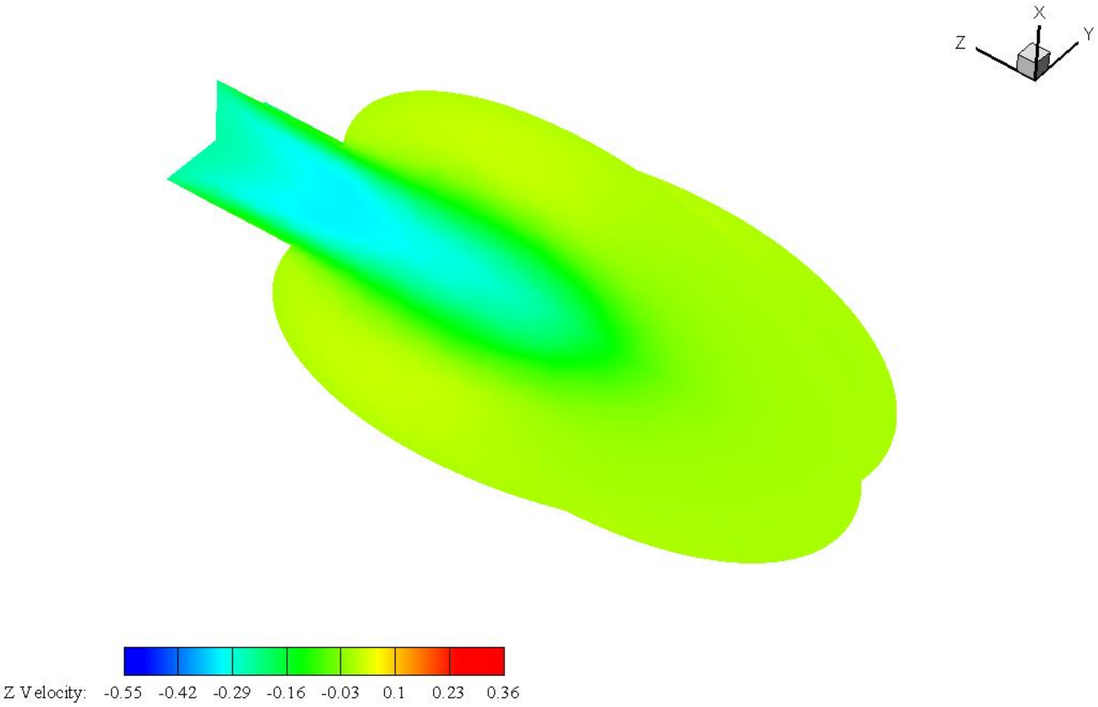

Figure B.20: Z velocity contour (m/s) at t = 0.5 second

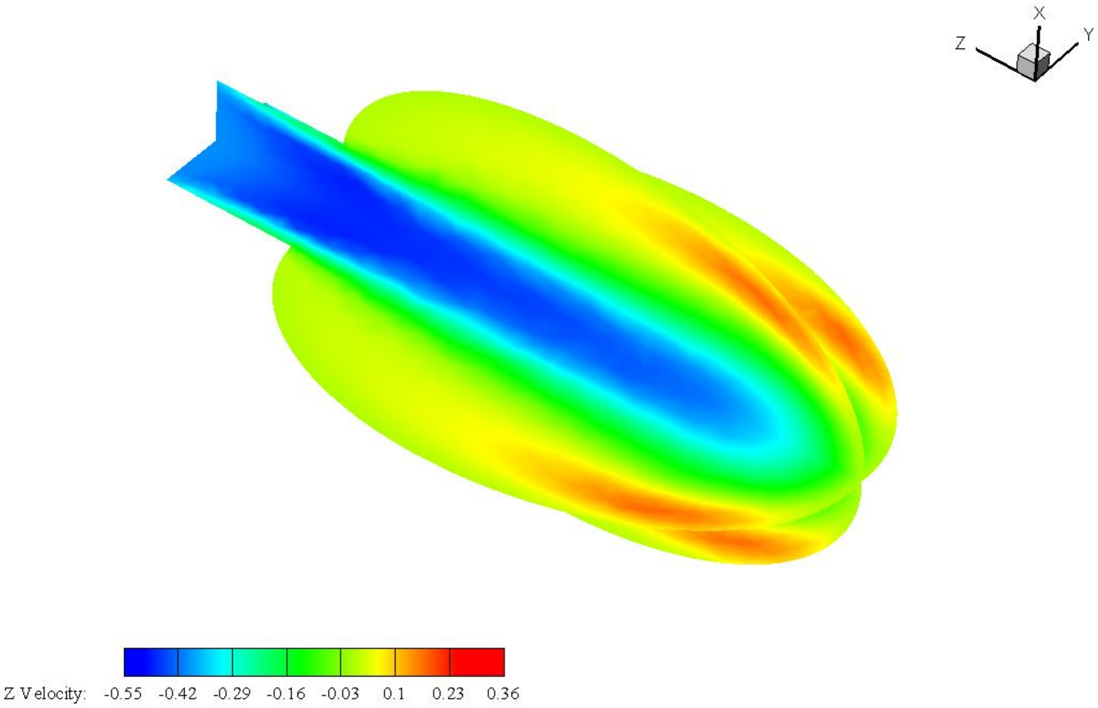

Figure B.21: Z velocity contour (m/s) at t = 0.7 second

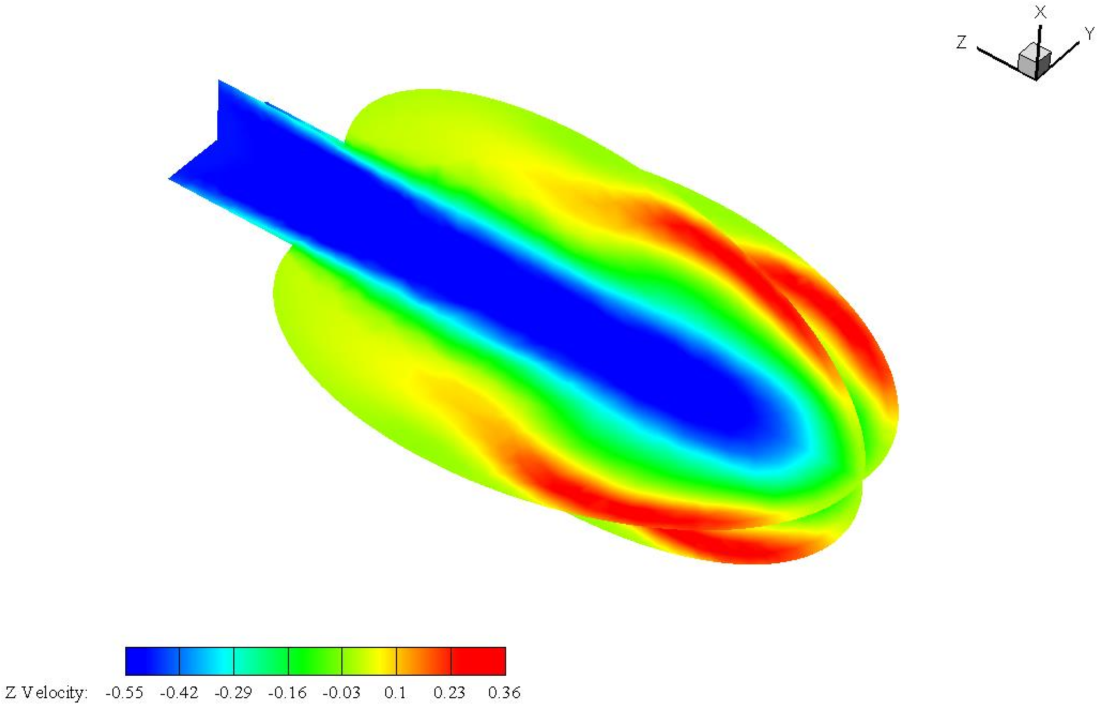

Figure B.22: Z velocity contour (m/s) at t = 0.9 second

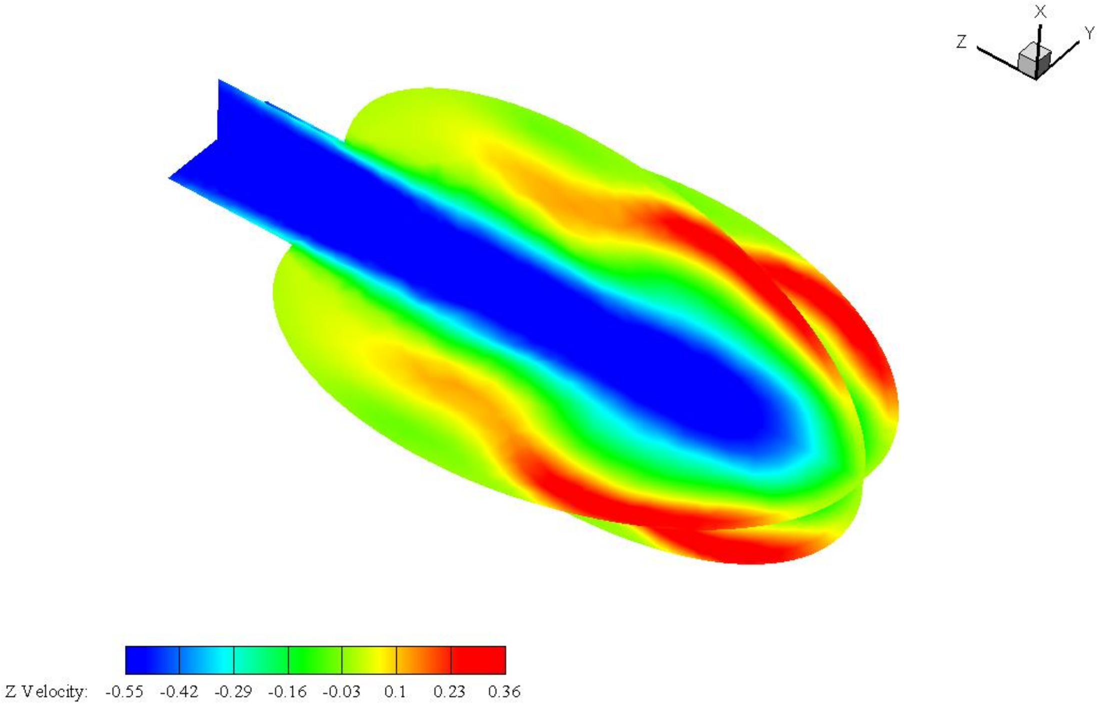

Figure B.23: Z velocity contour (m/s) at t = 1 second

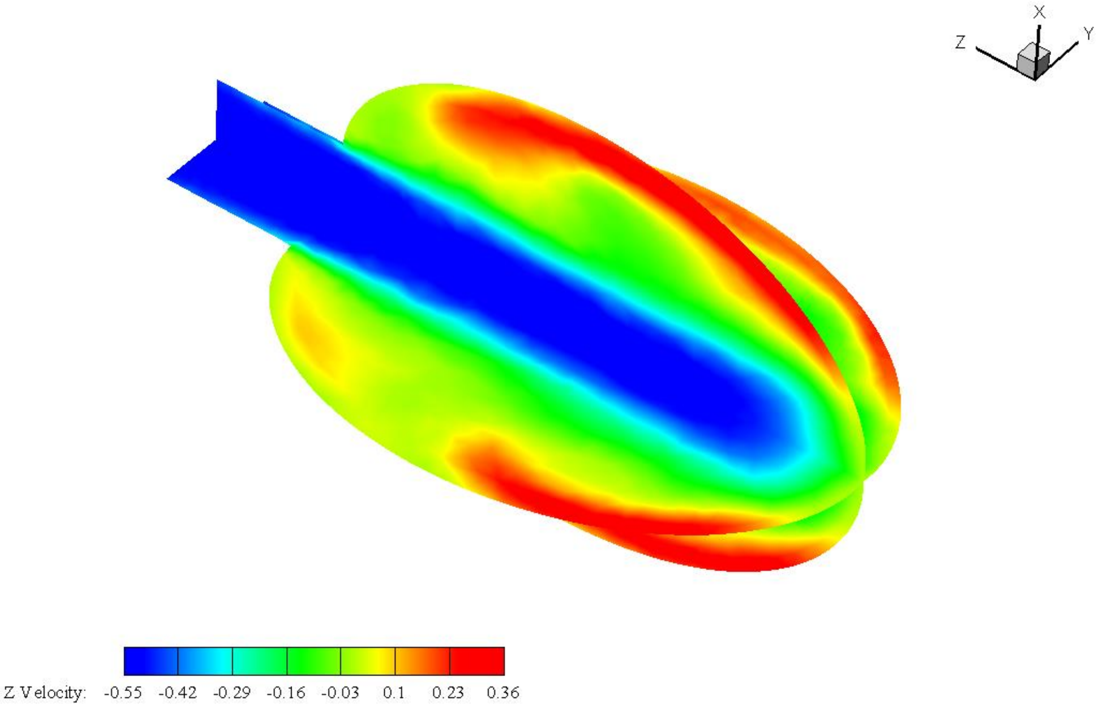

Figure B.24: Z velocity contour (m/s) at t = 1.5 seconds

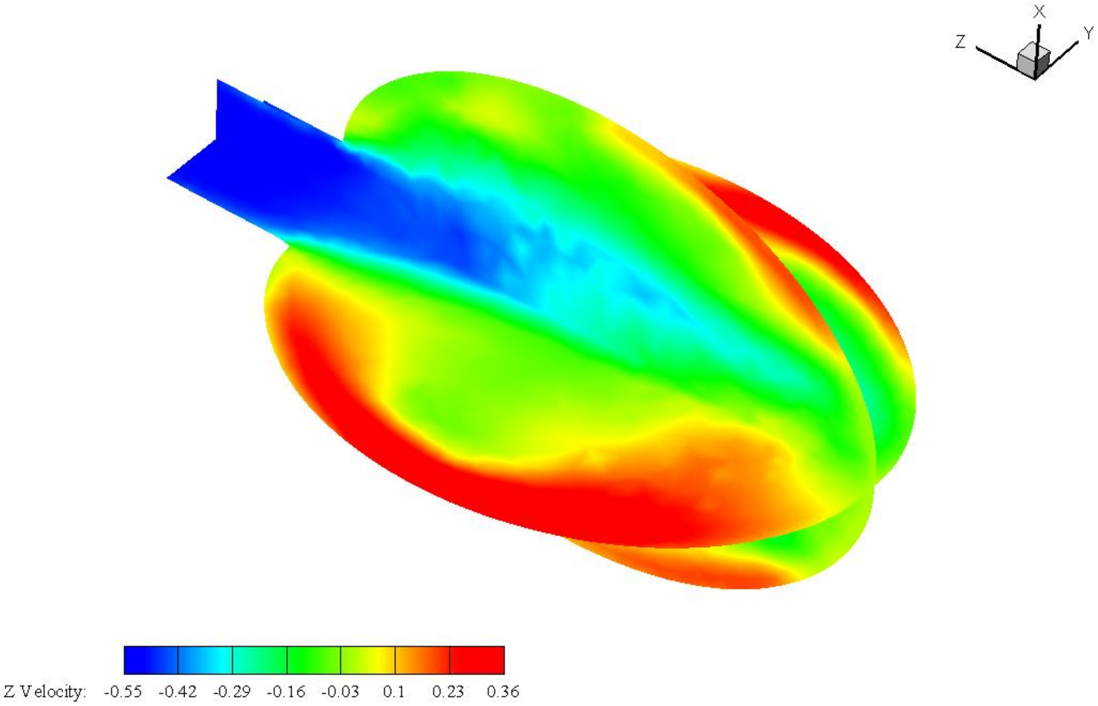

Figure B.25: Z velocity contour (m/s) at t = 2 seconds

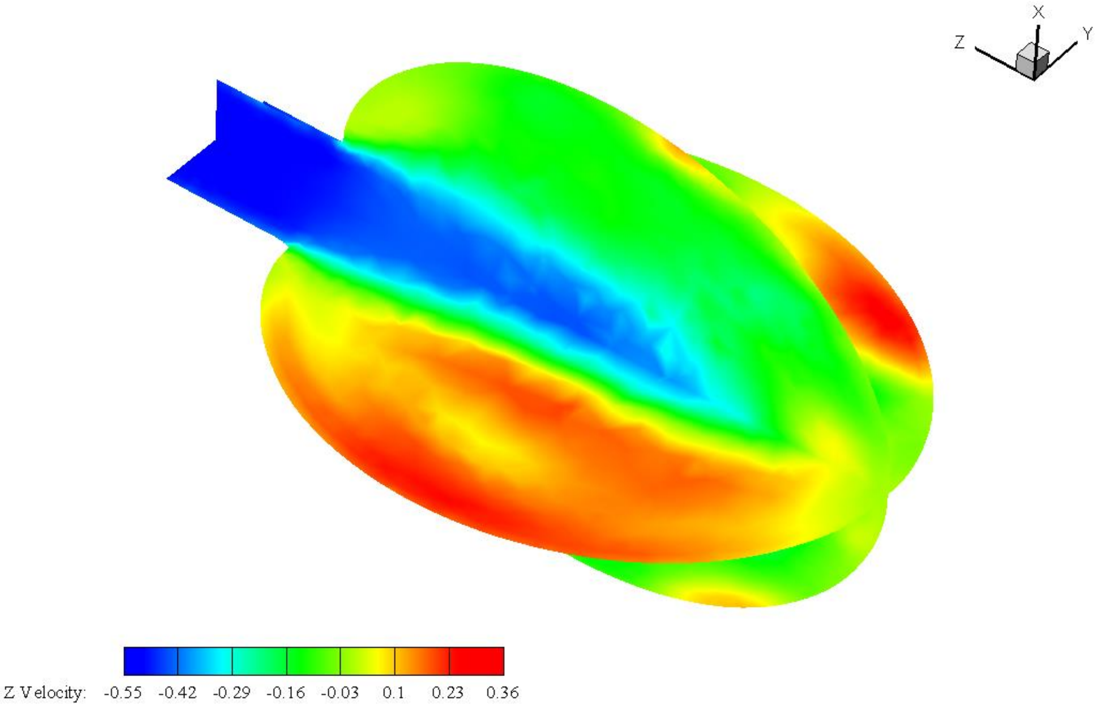

Figure B.26: Z velocity contour (m/s) at t = 2.25 seconds

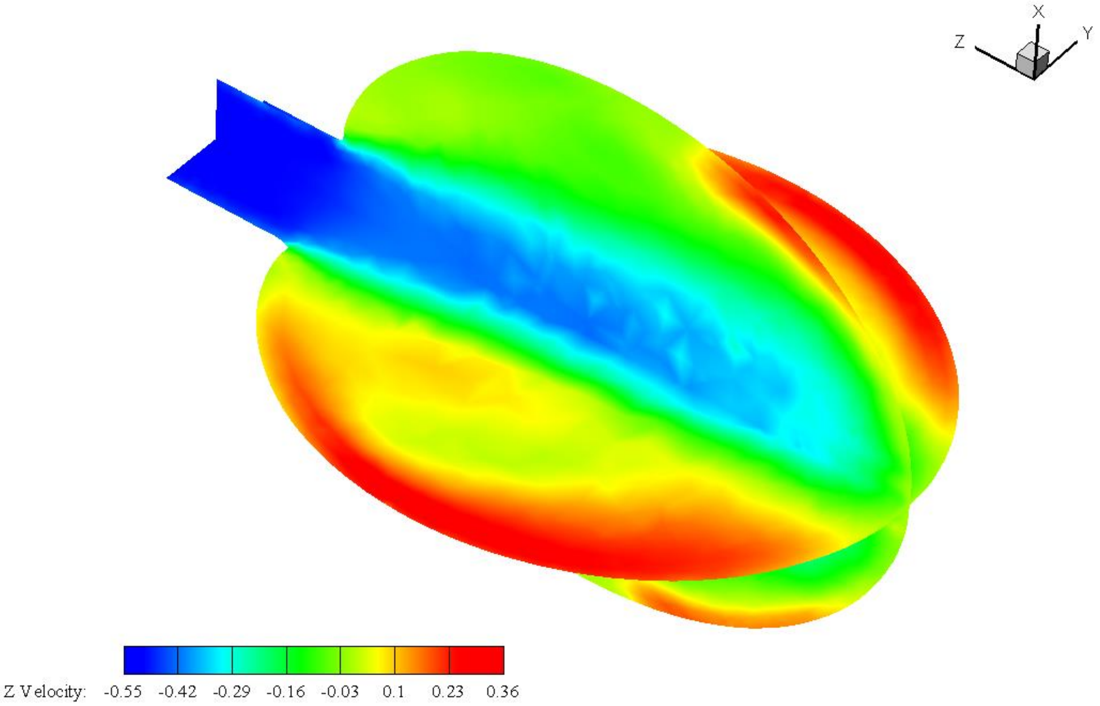

Figure B.27: Z velocity contour (m/s) at t = 2.5 seconds

3D Balloon Fluid Region: Velocity Magnitude Contour

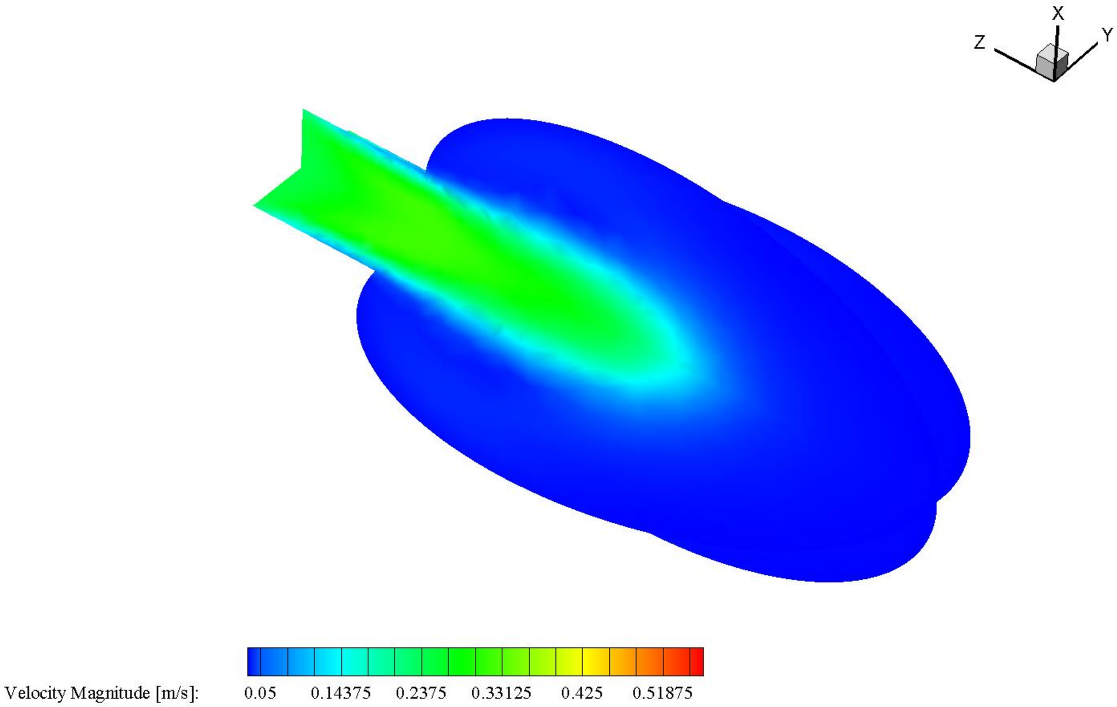

Figure B.28: Velocity magnitude contour at t = 0.5 second

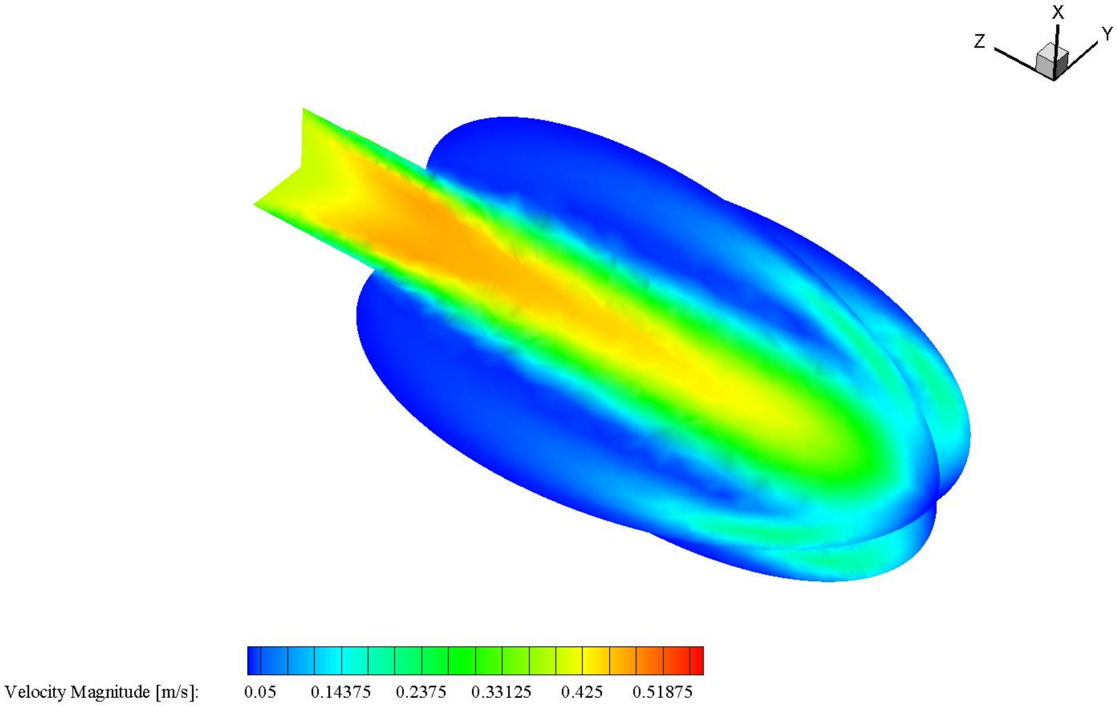

Figure B.29: Velocity magnitude contour at t = 0.7 second

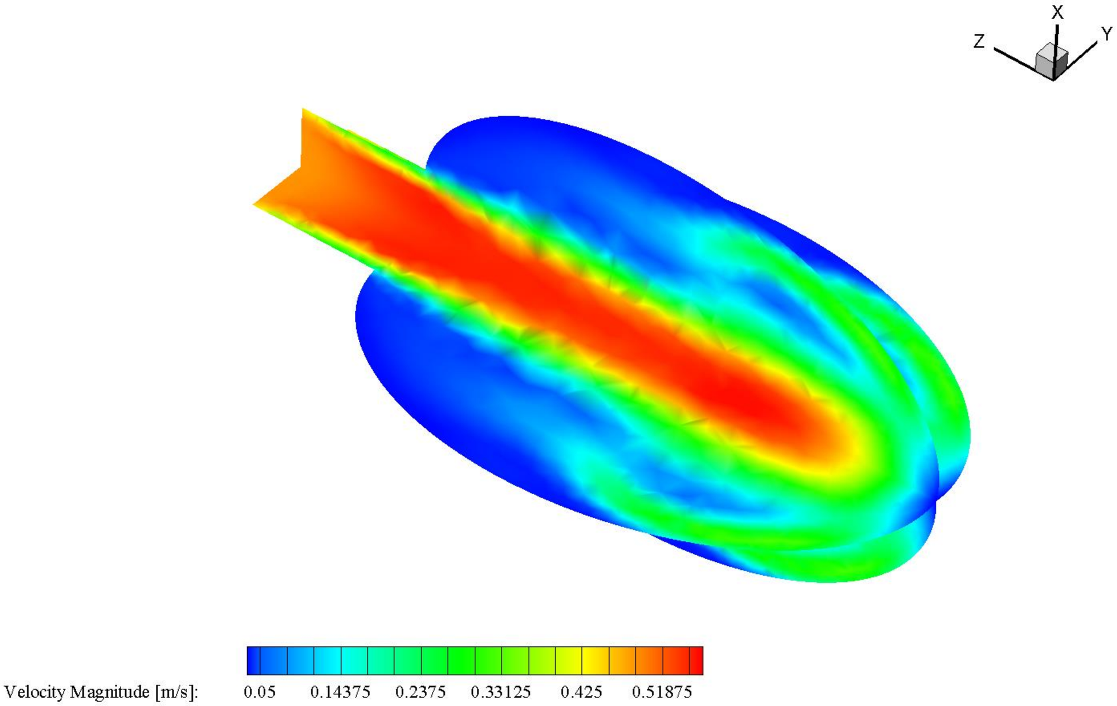

Figure B.30: Velocity magnitude contour at t = 0.9 second

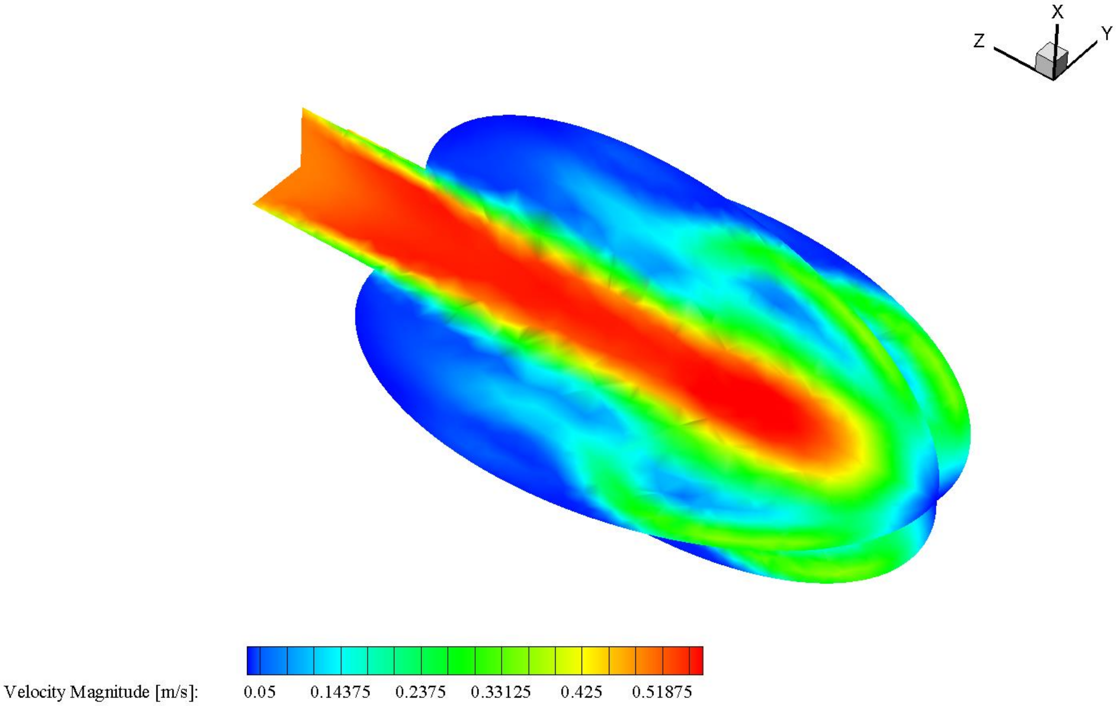

Figure B.31: Velocity magnitude contour at t = 1 second

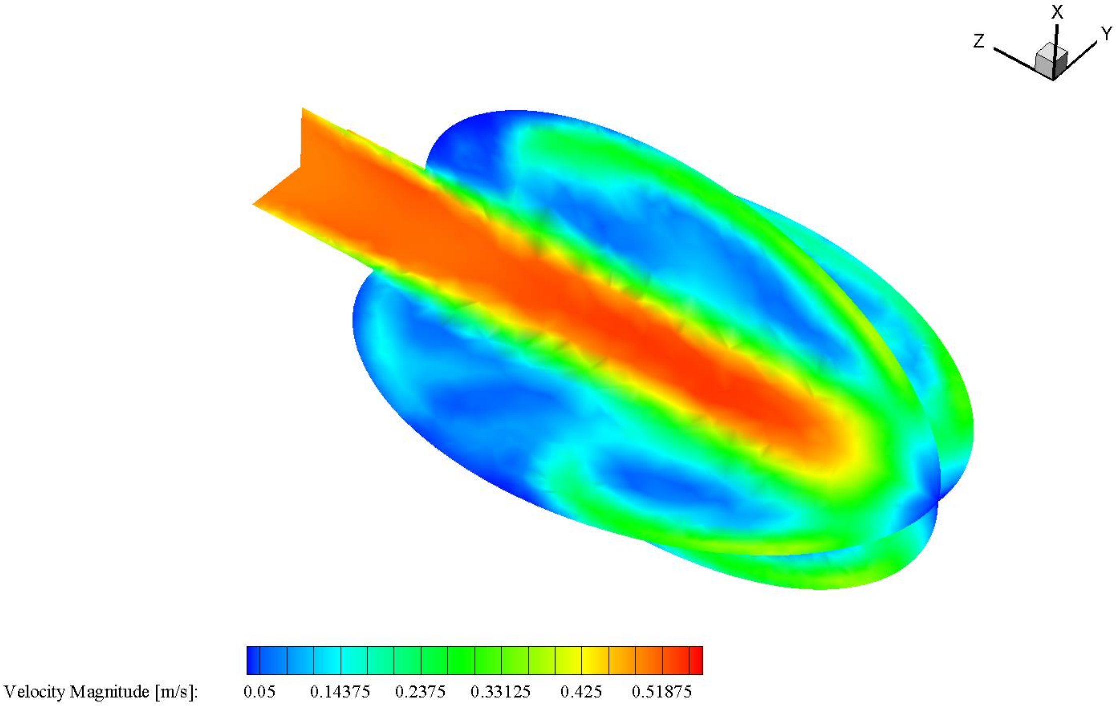

Figure B.32: Velocity magnitude contour at t = 1.5 seconds

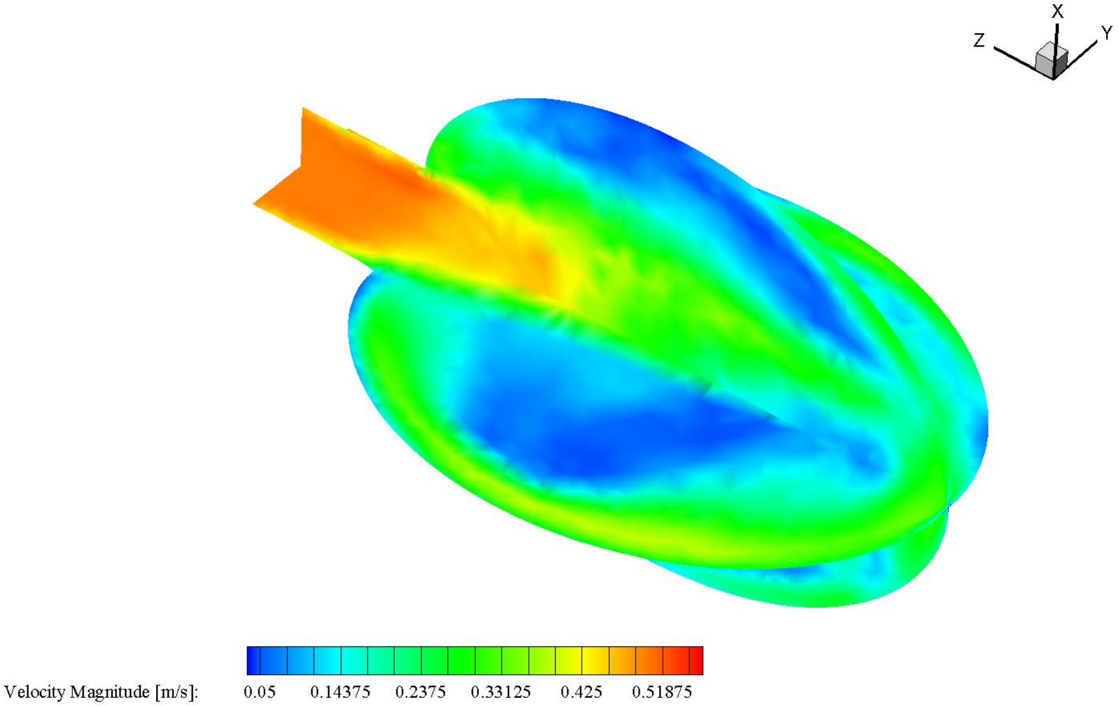

Figure B.33: Velocity magnitude contour at t = 2 seconds

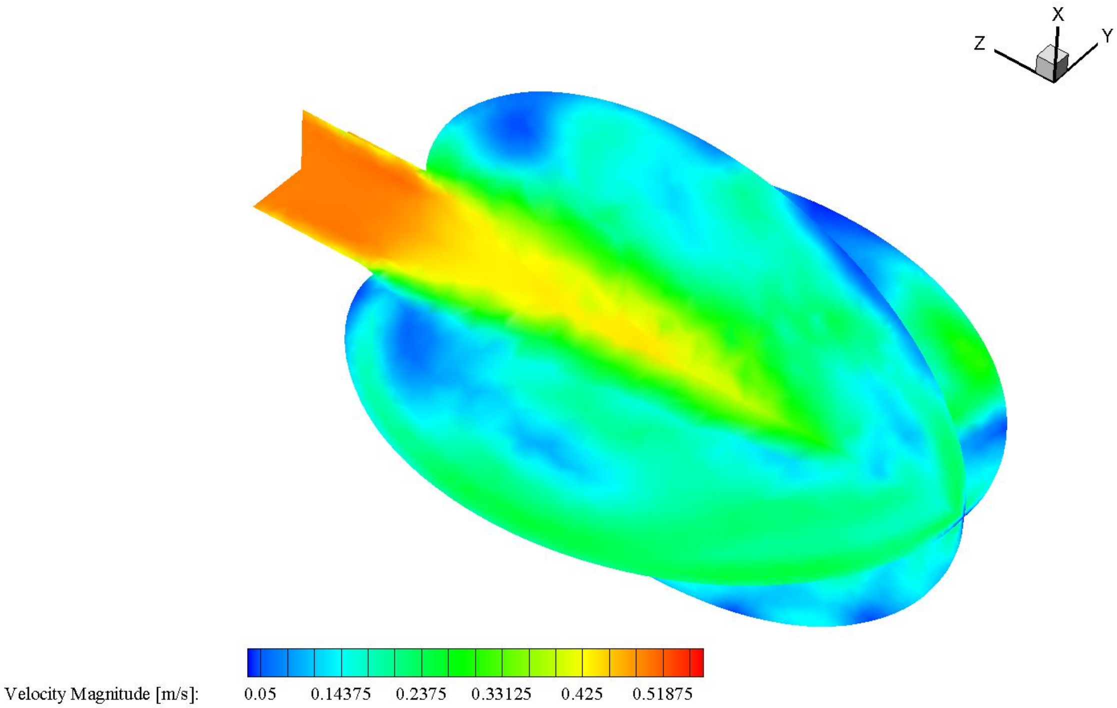

Figure B.34: Velocity magnitude contour at t = 2.26 seconds

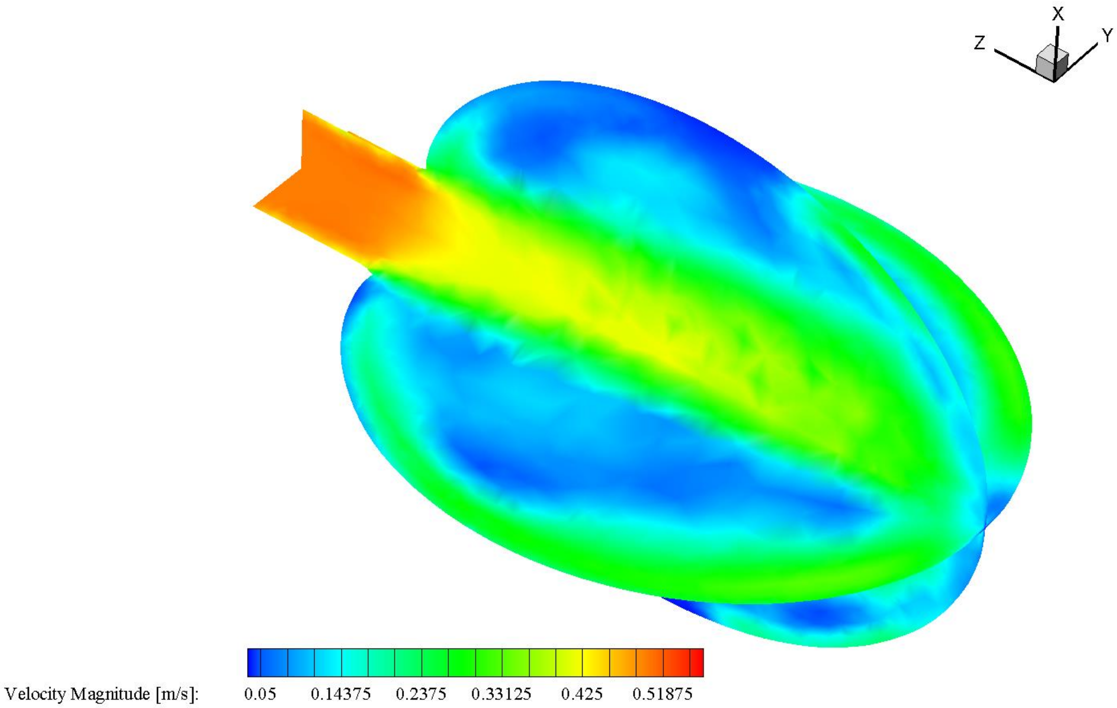

Figure B.35: Velocity magnitude contour at t = 2.5 seconds

3D Balloon Fluid Region: Velocity Vector

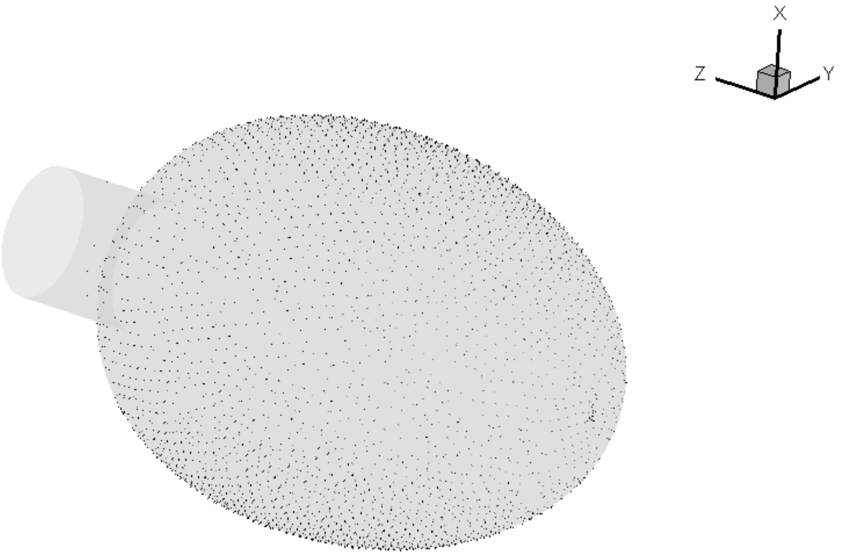

Figure B.36: Velocity Vectors at t = 0.5 second

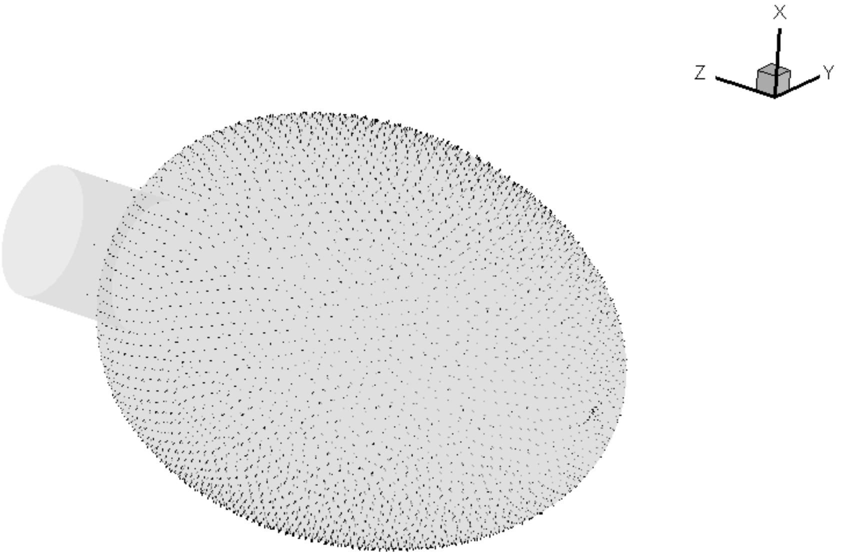

Figure B.37: Velocity Vectors at t = 0.7 second

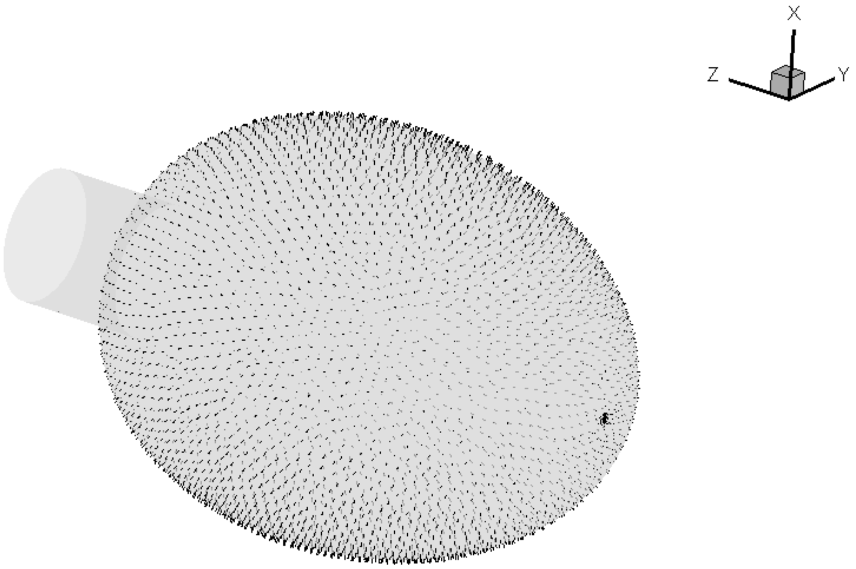

Figure B.38: Velocity Vectors at t = 0.9 second

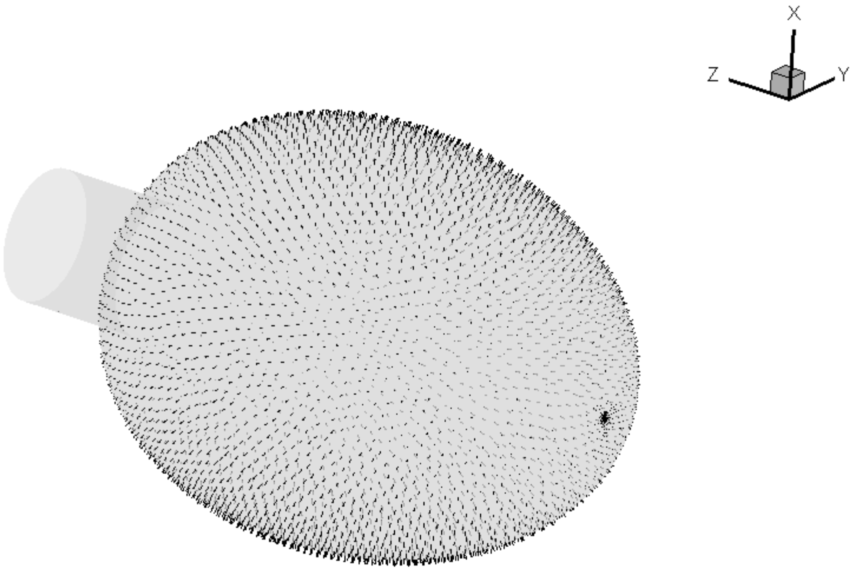

Figure B.39: Velocity Vectors at t = 1 second

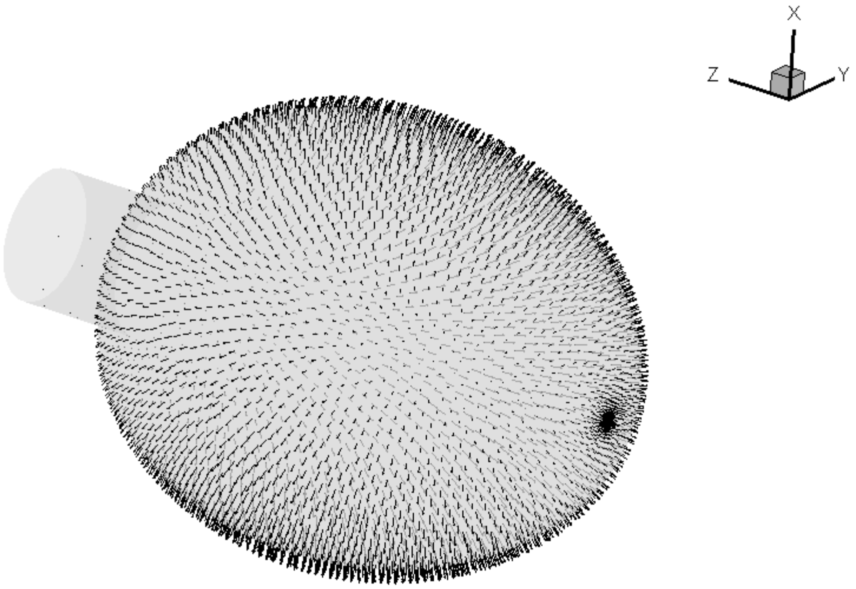

Figure B.40: Velocity Vectors at t = 1.5 seconds

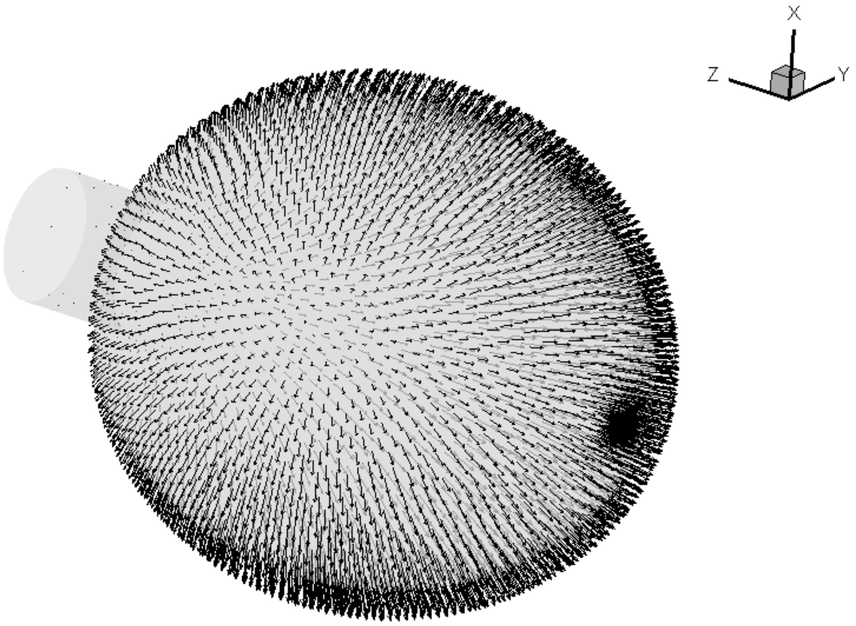

Figure B.41: Velocity Vectors at t = 2 seconds

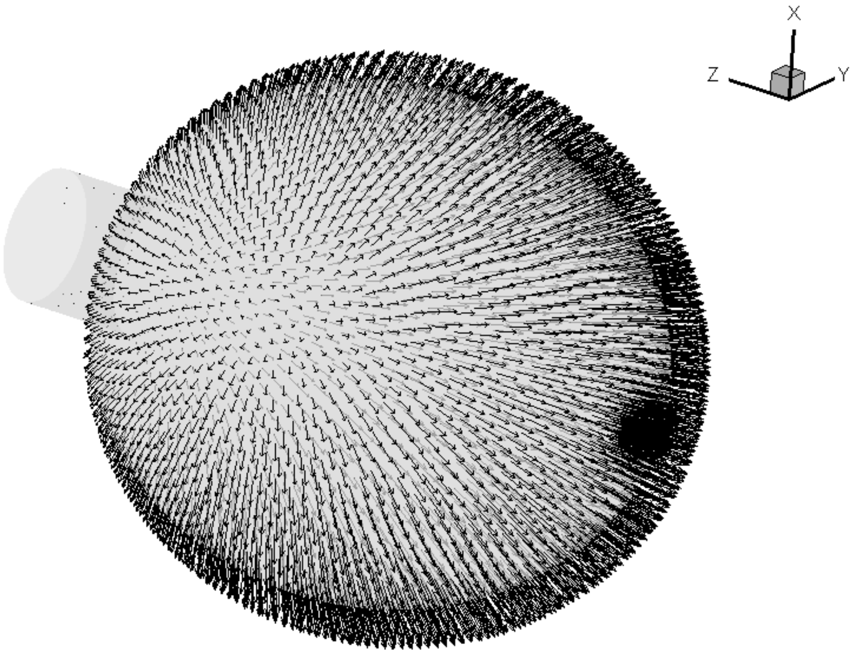

Figure B.42: Velocity Vectors at t = 2.26 seconds

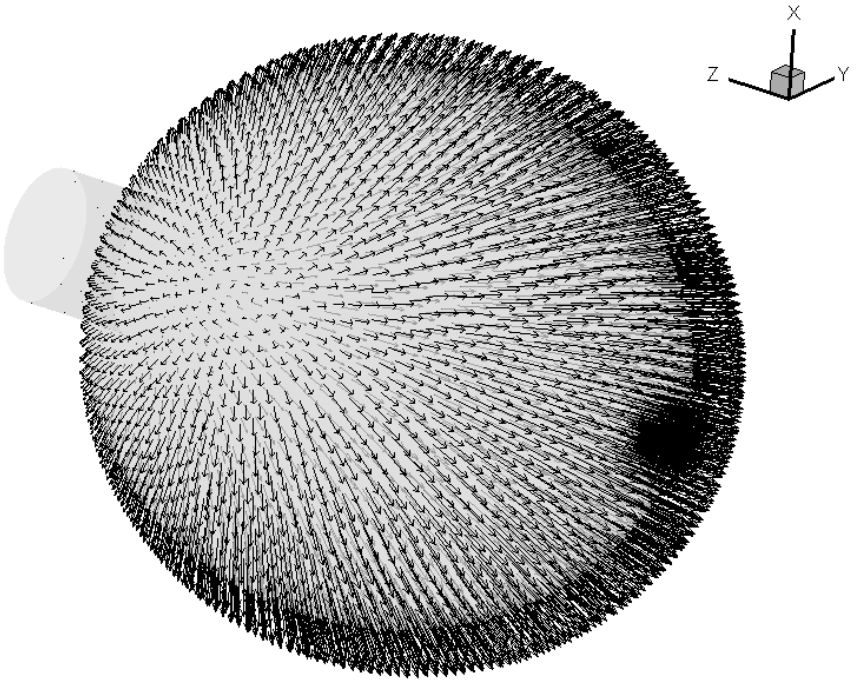

Figure B.43: Velocity Vectors at t = 2.5 seconds

3D Balloon Velocity Inlet Profile Code

```
/*********************************************************************
UDF for specifying parabolic sinusoidal velocity profile boundary condition
*********************************************************************/
#include "udf.h"

DEFINE_PROFILE(ThreeDim_Balloon_velocity, thread, position)
{
	real x[ND_ND];
	real y;
	real umax;
	face_t f;
	real t = CURRENT_TIME;

	begin_f_loop(f, thread)
	{
		F_CENTROID(x, f, thread);
		y = x[1];
		if (t < 1.)
		{
			umax = (sin(3.1412*(t + 1.5)) + 1) / 4;
		}
		else
		{
			umax = 0.5;
		}

		F_PROFILE(f, thread, position) = umax - y*y / (0.5*0.5)*umax;
	}
	end_f_loop(f, thread)
}
```

APPENDIX C – Chapter 4: Porcine Tracheal Material Properties

The following are supplemental materials for Chapter 4: Porcine Tracheal Material Properties.

Summary of Figures	**Page**
Calculations for Preliminary Strain Rate	182
MATLAB code for Trimming Data	184
MATLAB code for Ogden Model Curve Fitting for an Individual Dataset	186
Examples of Location and Data Measurements	189
2nd Order Ogden Material Model Derivation	191

Calculations for Preliminary Strain Rate

Table C.1: Known/measured properties of porcine trachea

Fluid Pressure of Human Airway, *P* (cmH_2O) Fluid Pressure of Human Airway, *P* (MPa)	30 0.00294
Diameter of Trachea, *d* (mm)	20
Thickness of Tracheal Wall, *t* (mm)	4
Breathing Rate, *BR* (s)	2

Table C.2: Initial sample properties to determine strain rate

Thickness, *t* (mm)	4
Width, *w* (mm)	9
Area, *A* (mm^2)	36
Length, *l* (mm)	22

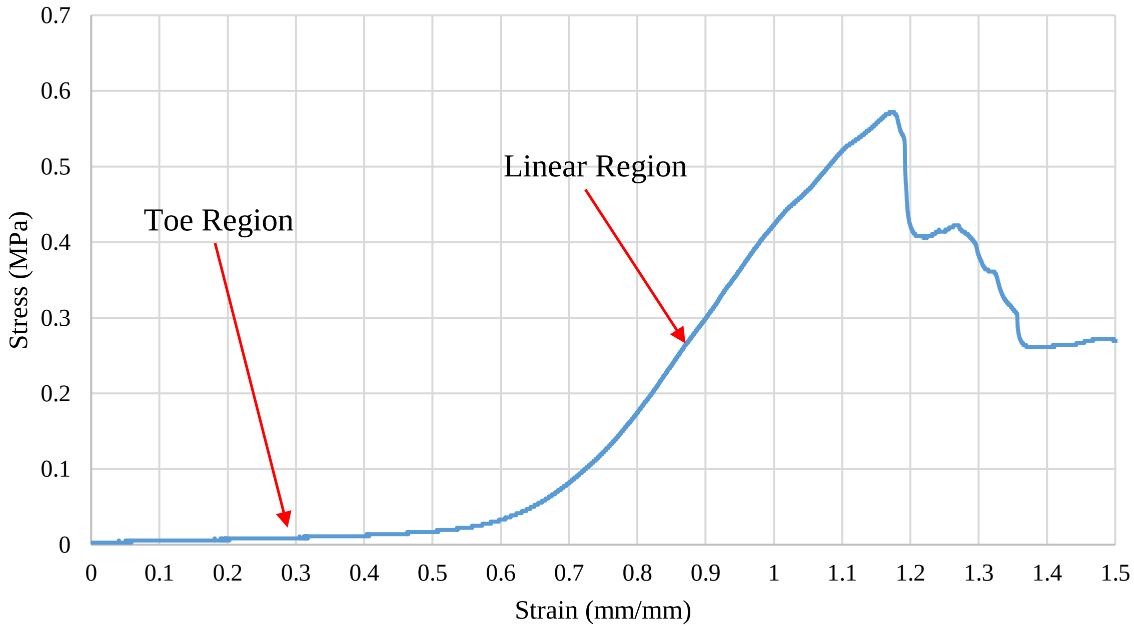

Figure C.1: Stress-Strain curve of a sample

Table C.3: Stress and strain values for toe region

Strain (mm/mm)	Stress (MPa)
0.3	0.008
0.4	0.011

Elastic Modulus Calculation for Linear Toe Region:

$$E = \frac{\sigma_2 - \sigma_1}{\varepsilon_2 - \varepsilon_1} = 0.028(MPa) \tag{C.1}$$

Longitudinal Stress Calculation for Linear Toe Region

$$\sigma_{long} = \frac{pd}{4t} = 0.0037(MPa) \tag{C.2}$$

Hoop Stress Calculation for Linear Toe Region

$$\sigma_{hoop} = \frac{pd}{2t} = 0.0098(MPa) \tag{C.3}$$

Longitudinal Strain calculation for Linear Toe Region

$$\varepsilon_{long} = \frac{1}{E}\left(\sigma_{long} - \nu\sigma_{hoop}\right) = -0.044(mm/mm) \tag{C.4}$$

Strain Rate

$$\dot{\varepsilon} = \frac{BR}{\varepsilon_{long}} = -0.02187(s^{-1}) \tag{C.5}$$

Note, strain rate was calculated based on the toe region because strains that will occur in a healthy (non-diseased) airway are within the toe region.

MATLAB Code for Trimming Data

```
clc
close all
clear all

DataStress = 0;
DataStrain = 0;
Predicted = 0;
Error = 0;
StressData = [];
StrainData = [];

DataFileName = 'AllAxial_Data_EngineeringStrain';   %Excel File Name

for TestNumber = 1
    tic
    Name = strcat('Test',num2str(TestNumber));  %Name of Sheet in Excel
    ExcelName = strcat(DataFileName);
    StressDataTemp = xlsread(ExcelName,Name,'P:P'); %Column for Stress
    StrainDataTemp = xlsread(ExcelName,Name,'O:O'); %Column for Strain
    [MaxNumber,MaxPosition] = max(StressDataTemp);

    for i = 1:MaxPosition
        DataStressTemp(i,1) = StressDataTemp(i,1);
        DataStrainTemp(i,1) = StrainDataTemp(i,1);
    end

    slope = zeros(length(DataStrainTemp),1);

for n = 2:length(DataStrainTemp);
    slope(n,1) = [DataStressTemp(n)-DataStressTemp(n-
1)]/[DataStrainTemp(n)-DataStrainTemp(n-1)];
end

Threshold = 0;
CutPoint = length(DataStrainTemp);

for n = round(length(DataStrainTemp)/2):length(DataStrainTemp);
    if slope(n,1) < Threshold
        CutPoint = (n)-2;
        break
    end
end

for n = 1:CutPoint
    CroppedDataStress(n,1) = DataStressTemp(n);
    CroppedDataStrain(n,1) = DataStrainTemp(n);
end

clear DataStressTemp DataStrainTemp slope

DataStressTemp = CroppedDataStress;
DataStrainTemp = CroppedDataStrain;
```

```
    StressData = [StressData ;DataStressTemp];
    StrainData = [StrainData; DataStrainTemp];
    toc
end
```

MATLAB Code for Ogden Model Curve Fitting for an Individual Dataset

```
clc
close all
clear all

StressData = 0;
StrainData = 0;
DataStress = 0;
DataStrain = 0;
Predicted = 0;
Error = 0;

% Inputs
DataFileName = 'Axial_TestData_20180611_Matlab';    %Excel File Name
GraphTitle = 'June 11, 2018: 2nd Order Ogden Model Test - '; %Title on
Matlab Charts
FileName = '20180611_2ndOrderOgden_Axial_Test_Number_';
% Change lines 17-20
A1 = 18;    %Inital Guess - Ogden Model Constant: Alpha
A2 = 20;
M1 = 1e-3;  %Inital Guess - Ogden Model Constant: Mu
M2 = 1e-3;
% ! ! ! Also change line 23 before running ! ! ! %

%OptimizationCode
for TestNumber = 1:37;
clear StressData StrainData DataStress DataStrain Predicted Error;
%Importing Data
Name = strcat('Test',num2str(TestNumber));
ExcelName = strcat(DataFileName);
StressData = xlsread(ExcelName,Name,'O:O');
StrainData = xlsread(ExcelName,Name,'P:P');
[MaxNumber,MaxPosition] = max(StressData);

for i = 1:MaxPosition
    DataStress(i) = StressData(i);
    DataStrain(i) = StrainData(i);
end

%Setup
S = DataStress;
syms Alpha1 Mu1 Alpha2 Mu2 E real

%Inital Guesses
InitalGuess =[A1;M1;A2;M2];
Ogden = [Alpha1;Mu1;Alpha2;Mu2]; %Optimization Variables

%Strain Energy Density Function - 2nd Order Ogden
Stress = Mu1*(1+E)^(Alpha1-1)-Mu1*(1+E)^(((-Alpha1)/2)-1)+...
    Mu2*(1+E)^(Alpha2-1)-Mu2*(1+E)^(((-Alpha2)/2)-1);
matlabFunction(Stress,'File','Function_Stress','vars',{[Alpha1,Mu1,...
    Alpha2,Mu2,E]});

%Guess-CollectedData
```

```
for n = 1:length(DataStrain)
Error(n)= abs((Function_Stress([Ogden',DataStrain(n)]))-S(n));
end

%RSS of errors (square term-by-term, sum, root)
TheCostFunction = [E]*0; %Initialize cost vector (the symbolic matrix)
for m = 1:length(Error)
    TheCostFunction = TheCostFunction+((Error(m)));
end

TheCostFunction = abs(TheCostFunction);

%Cost Function
matlabFunction(TheCostFunction,'File','FunctionCost','vars',{[Alpha1,Mu1,Al
pha2,Mu2]'});
FunctionCost(InitalGuess) %Used for testing evaluate the initial cost (at
the guess)

%Options = optimoptions('fmincon','Display','iter','Algorithm','interior-
point','MaxIterations',100);
Options = optimoptions('fminunc','Display','iter','Algorithm','trust-
region','MaxFunctionEvaluations',1000,'MaxIterations',3000,'StepTolerance',
1e-8);
OgdenOutput = fminunc(@FunctionCost,InitalGuess,Options);

for i = 1:length(DataStrain)
    Predicted(i) = Function_Stress([OgdenOutput;DataStrain(i)]');
end

%Chart Naming
ChartTitle = strcat(GraphTitle,num2str(TestNumber));
plot(DataStrain,DataStress)
grid on
hold on
plot(DataStrain,Predicted,'--')
legend('Data','Curve Fit')
title(ChartTitle)
xlabel('Strain [mm/mm]')
ylabel('Stress [MPa]')

%Saving
PlotFileTitle = strcat(FileName,num2str(TestNumber),'.jpg');
saveas(figure(1),PlotFileTitle,'jpg')
close all
FileTitle = strcat(FileName,num2str(TestNumber),'.txt');
fileID = fopen(FileTitle,'wt');
fprintf(fileID,'2nd Order Ogden Model Constants \n\n Alpha1 = ');
fileID = fopen(FileTitle,'at');
fprintf(fileID,'%f', OgdenOutput(1));
fprintf(fileID,'\n\n Mu1 = ');
fprintf(fileID,'%f', OgdenOutput(2));
fprintf(fileID,'\n\n Alpha2 = ');
fprintf(fileID,'%f', OgdenOutput(3));
fprintf(fileID,'\n\n Mu2 = ');
fprintf(fileID,'%f', OgdenOutput(4));
```

```
fclose(fileID);
end
```

Examples of Location and Data Measurements

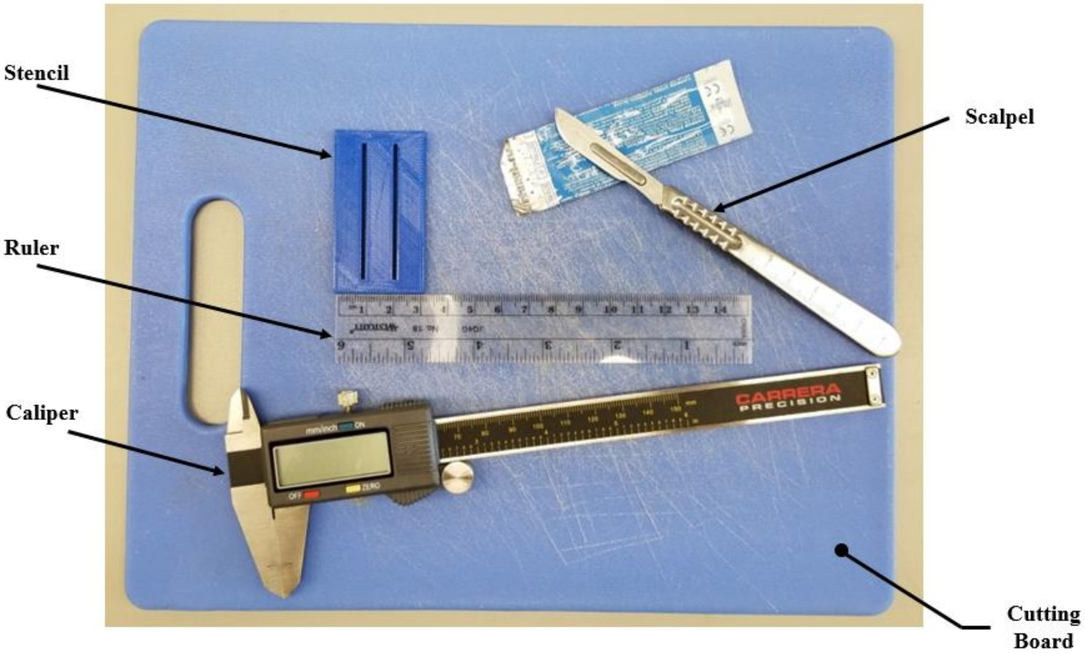

Figure C.2: Tools used for specimen preparation

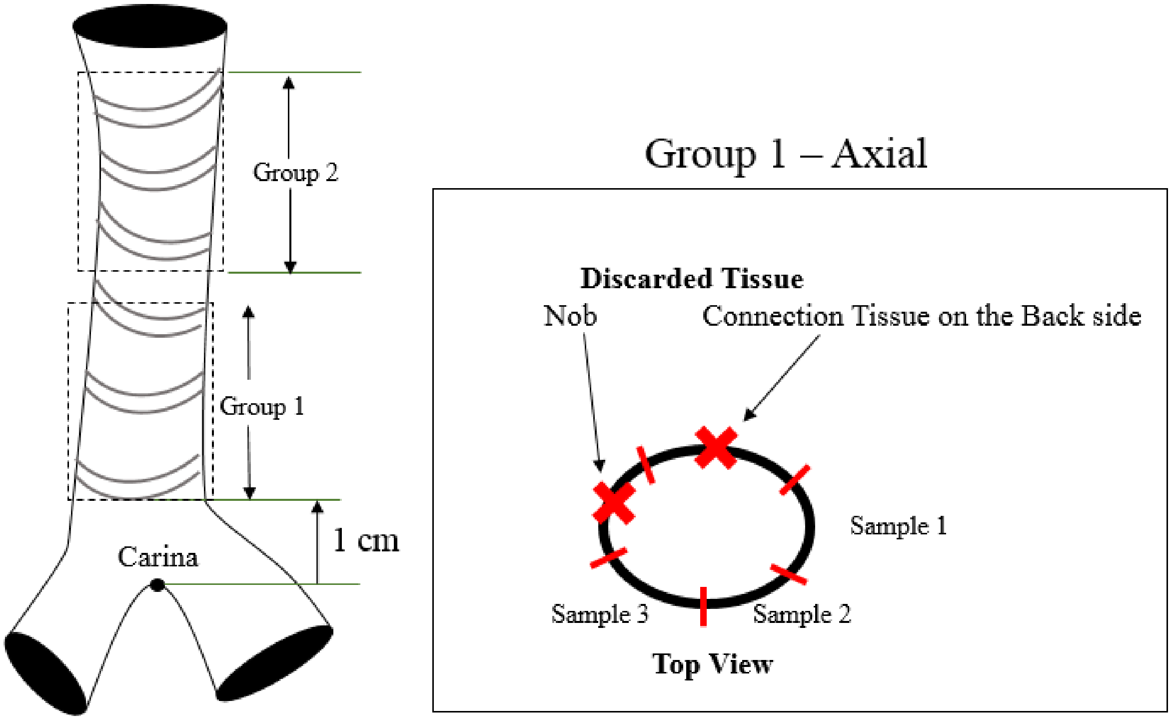

Figure C.3: Location of samples recorded for the axial direction

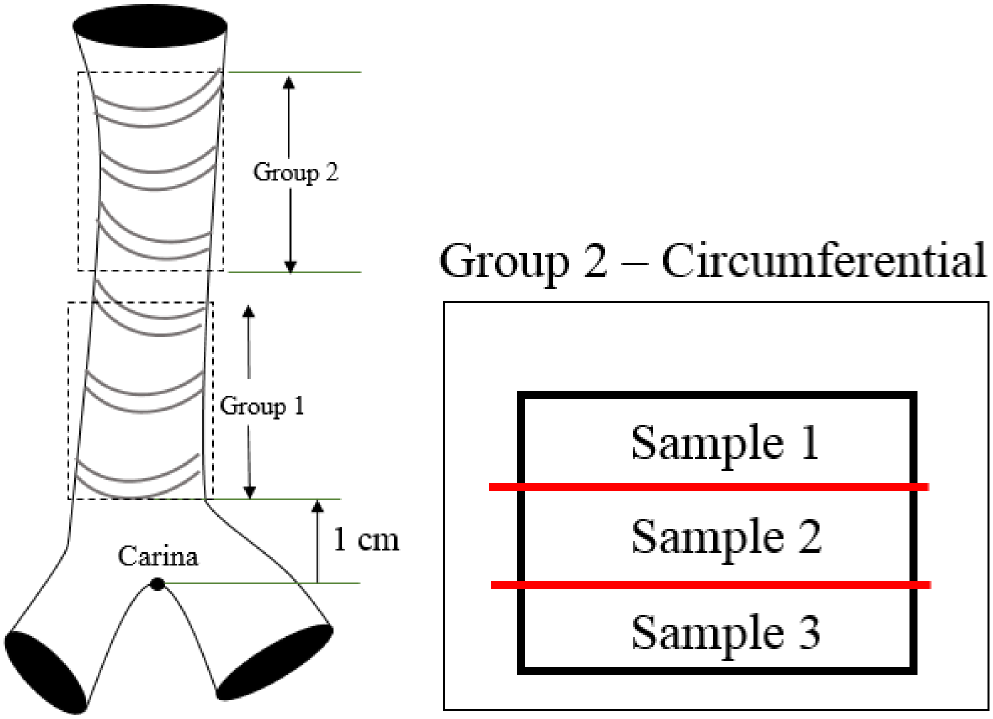

Figure C.4: Location of samples recorded for the axial direction

2nd Order Ogden Material Model Derivation

Ogden Material Model Equation:

$$W\left(\lambda_1,\lambda_2,\lambda_3\right)=\sum_{i=1}^{N}\frac{\mu}{\alpha_i}\left(\lambda_1^{\alpha_i}+\lambda_2^{\alpha_i}+\lambda_3^{\alpha_i}-3\right)+\sum_{k=1}^{N}\frac{1}{d_k}\left(J-1\right)^{2k} \qquad \text{(C.6)}$$

Where μ, α, and d are constants and λ are the stretches. J is the determinant of the deformation gradient, F.

Assuming incompressible material, the Ogden Material Model equation becomes:

$$W\left(\lambda_1,\lambda_2,\lambda_3\right)=\sum_{i=1}^{N}\frac{\mu}{\alpha_i}\left(\lambda_1^{\alpha_i}+\lambda_2^{\alpha_i}+\lambda_3^{\alpha_i}-3\right) \qquad \text{(C.7)}$$

In addition, by assuming incompressibility:

$$\lambda_1\lambda_2\lambda_3=1 \qquad \text{(C.8)}$$

$$\lambda_1=\lambda \qquad \text{(C.9)}$$

$$\lambda_2=\lambda_3=\frac{1}{\sqrt{\lambda}} \qquad \text{(C.10)}$$

The final form of the Ogden equation used becomes:

$$W=\frac{\mu}{\alpha_i}\left(\lambda^{\alpha}+2\left(\frac{1}{\sqrt{\lambda}}\right)^{\alpha}-3\right) \qquad \text{(C.11)}$$

To determine the stress from a strain energy density equation:

$$\sigma_i=\frac{\partial W}{\partial\lambda_i} \qquad \text{(C.12)}$$

After taking partial derivative twice (2nd Order):

$$\sigma=\mu_1\lambda^{\alpha_1-1}-\mu_1\lambda^{-\frac{\alpha_1}{2}-1}+\mu_2\lambda^{\alpha_2-1}-\mu_2\lambda^{-\frac{\alpha_2}{2}-1} \qquad \text{(C.13)}$$

To get the equation in terms of strain:

$$\lambda=1+\varepsilon \qquad \text{(C.14)}$$

Final form of the 2nd Order Ogden Material Model used:

$$\sigma=\mu_1\left(1+\varepsilon\right)^{\alpha_1-1}-\mu_1\left(1+\varepsilon\right)^{-\frac{\alpha_1}{2}-1}+\mu_2\left(1+\varepsilon\right)^{\alpha_2-1}-\mu_2\left(1+\varepsilon\right)^{-\frac{\alpha_2}{2}-1} \qquad \text{(C.15)}$$

APPENDIX D – Chapter 5: FSI Human Upper Airway Simulation

The following are supplemental materials for Chapter 5: FSI Human Upper Airway Simulation.

Summary of Figures	**Page**
Pressure Contour Plots for the Human Lung Model	193
UDF: Velocity Inlet Profile Code for PCV (Fourier Approximation)	198
UDF: Velocity Inlet Profile Code for PCV (Fourier Approximation Halved)	199

Pressure Contour Plots for the Human Lung Model

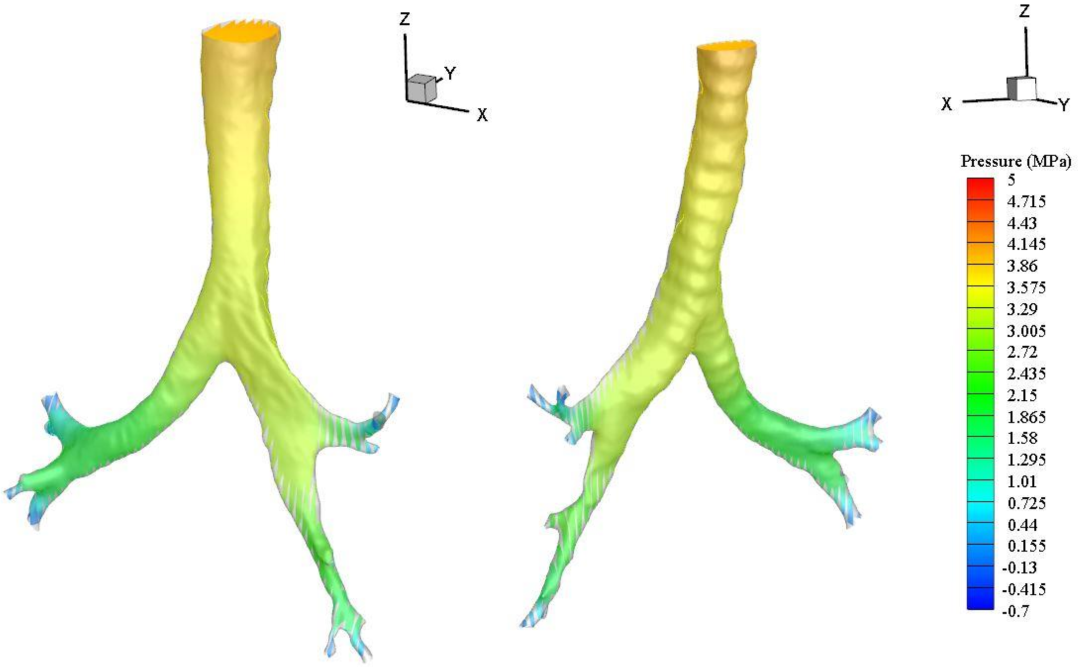

Figure D.1: Fluid pressure contour at t = 0.15 second

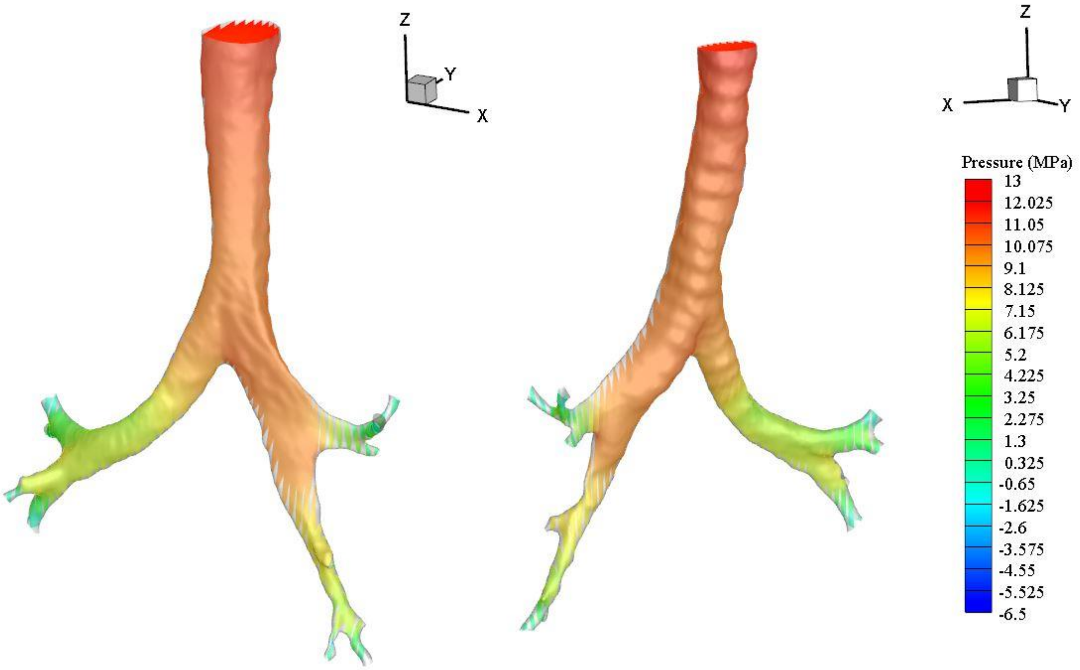

Figure D.2: Fluid pressure contour at t = 0.25 second

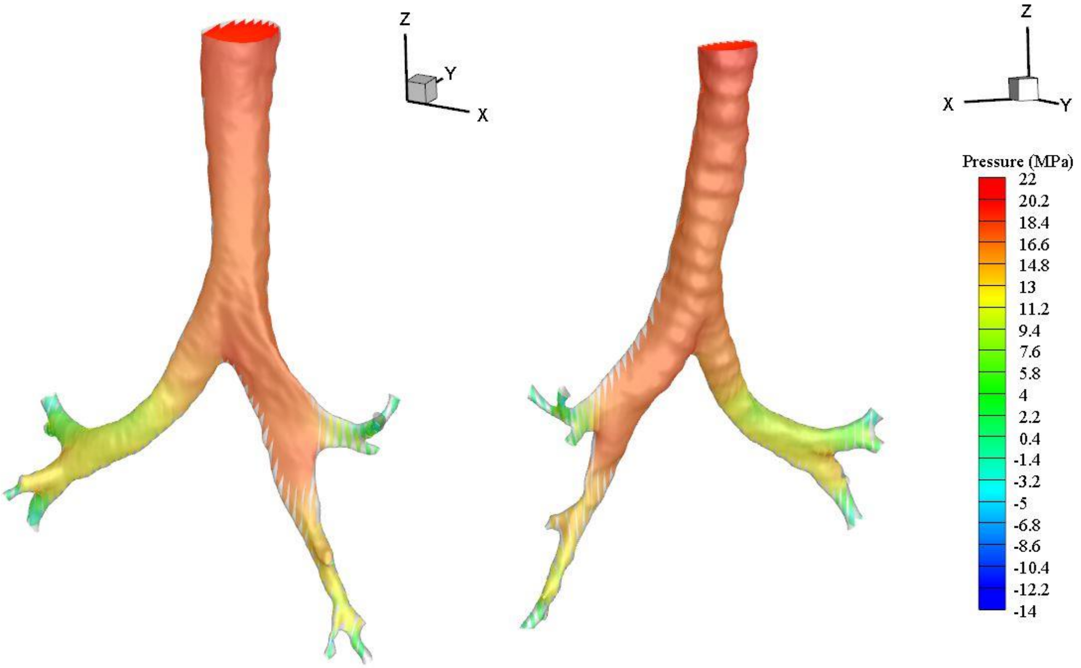

Figure D.3: Fluid pressure contour at t = 0.4 second

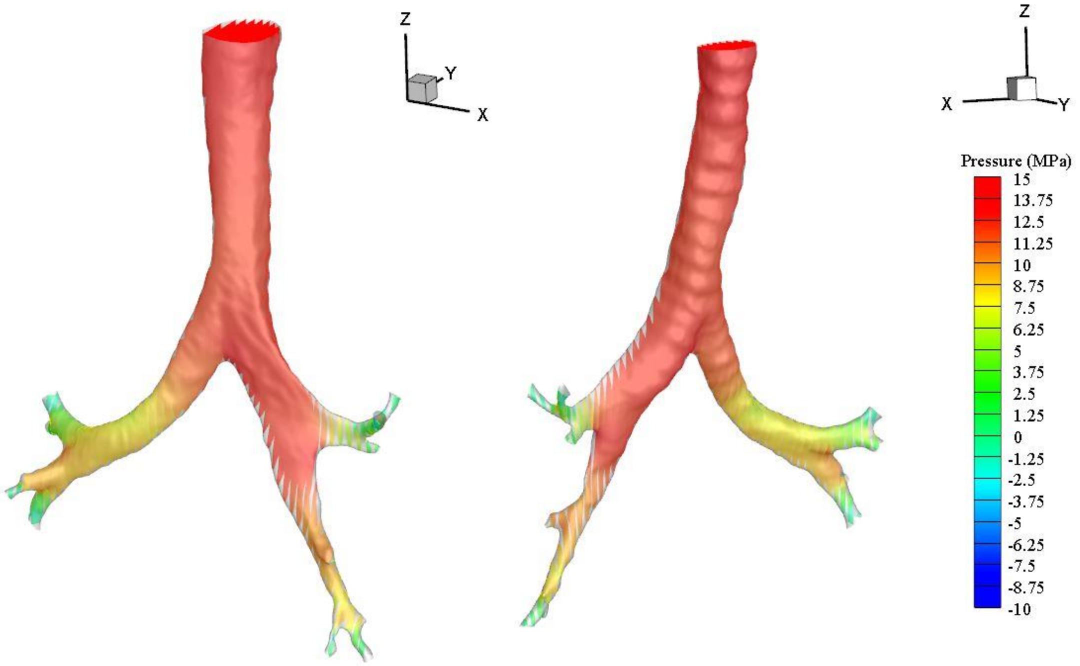

Figure D.4: Fluid pressure contour at t = 0.5 second

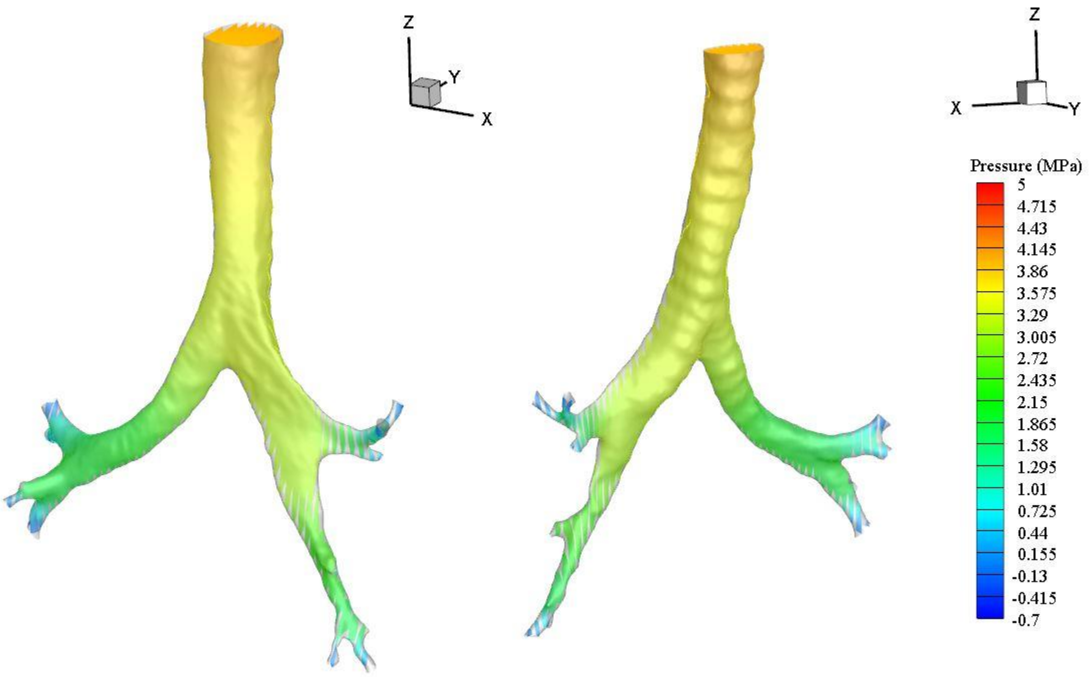

Figure D.5: Fluid pressure contour at t = 0.7 second

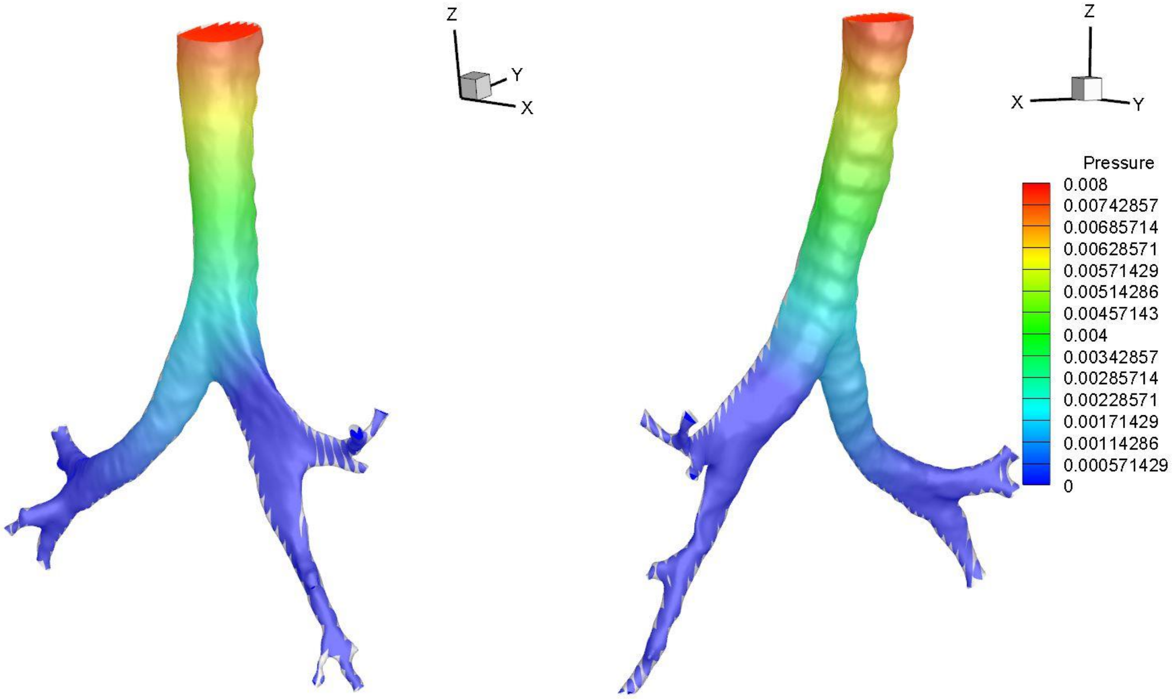

Figure D.6: Fluid pressure contour at t = 1.5 seconds

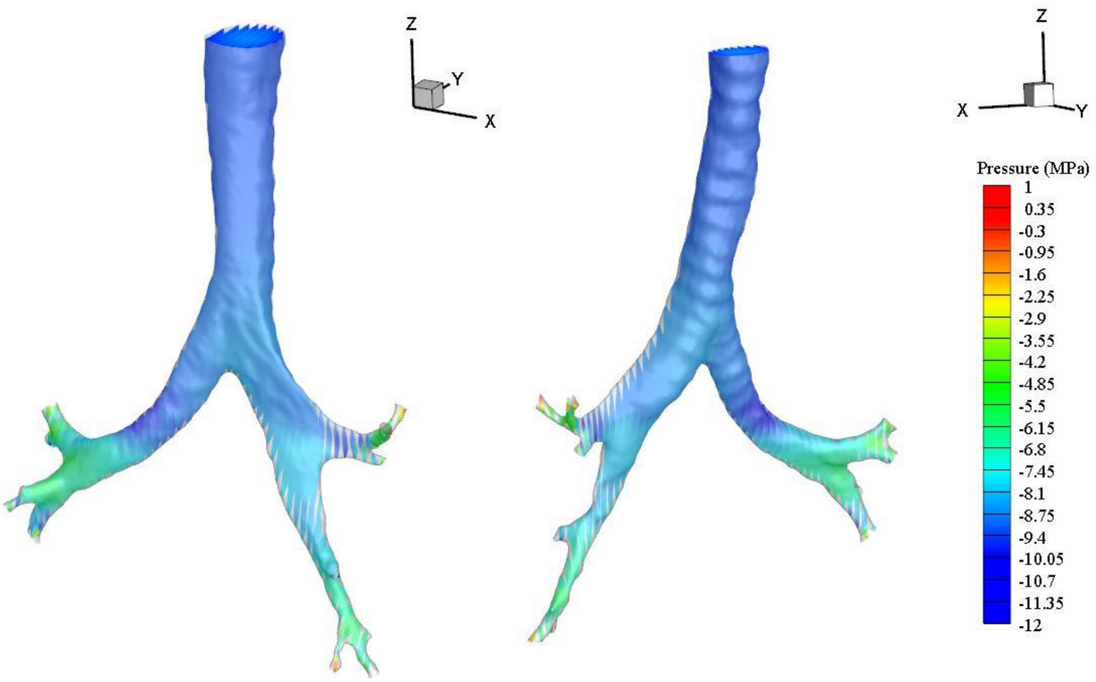

Figure D.7: Fluid pressure contour at t = 1.9 seconds

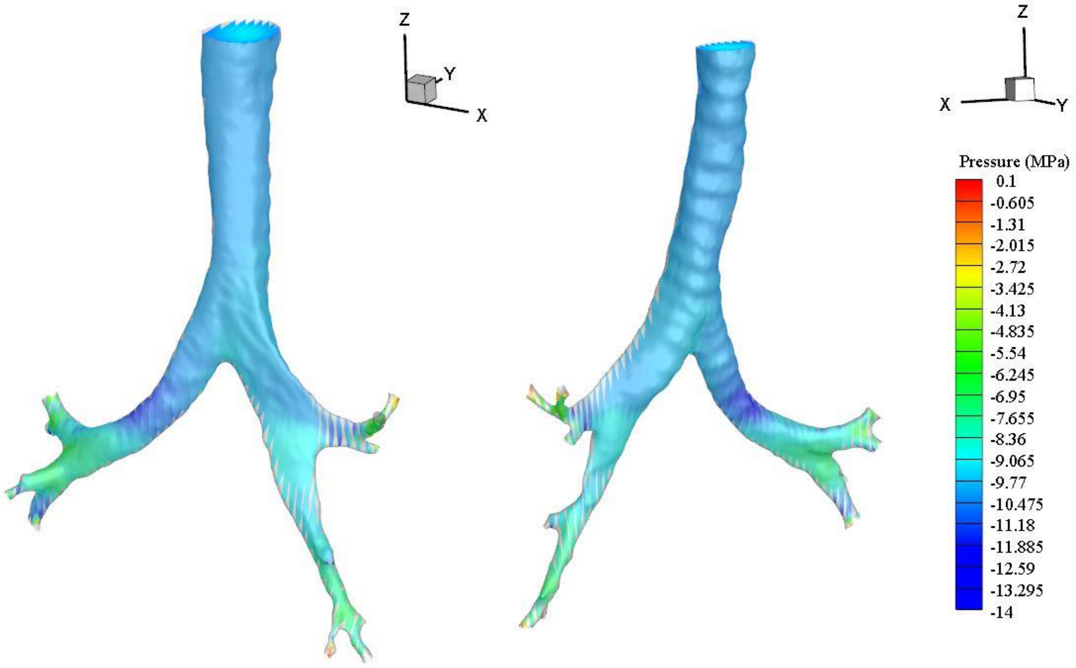

Figure D.8: Fluid pressure contour at t = 2 seconds

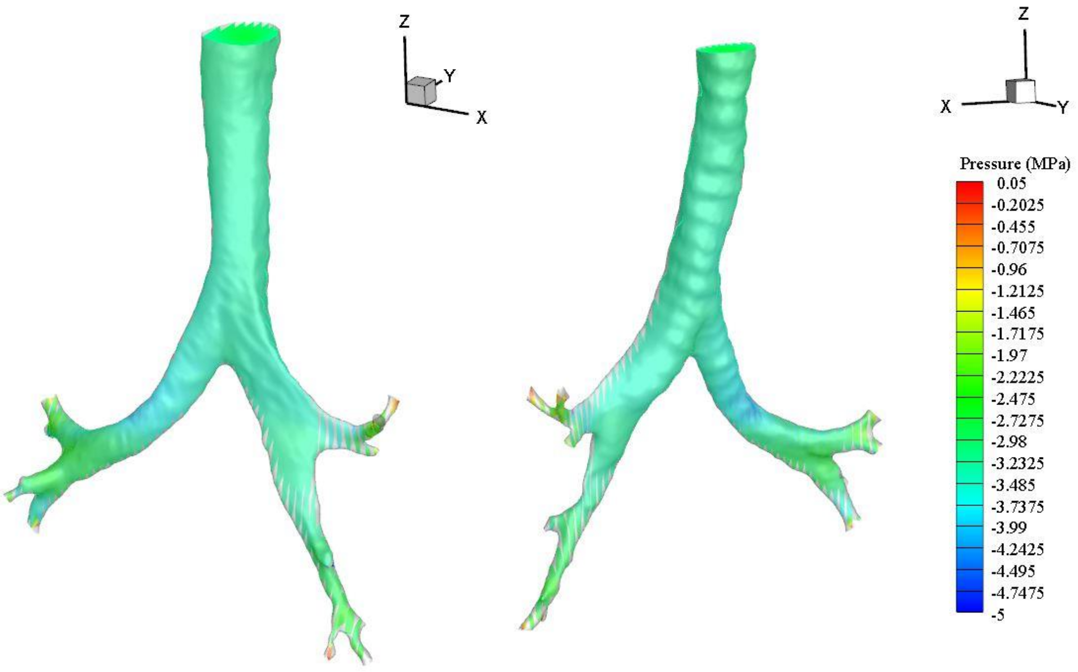

Figure D.9: Fluid pressure contour at t = 2.15 seconds

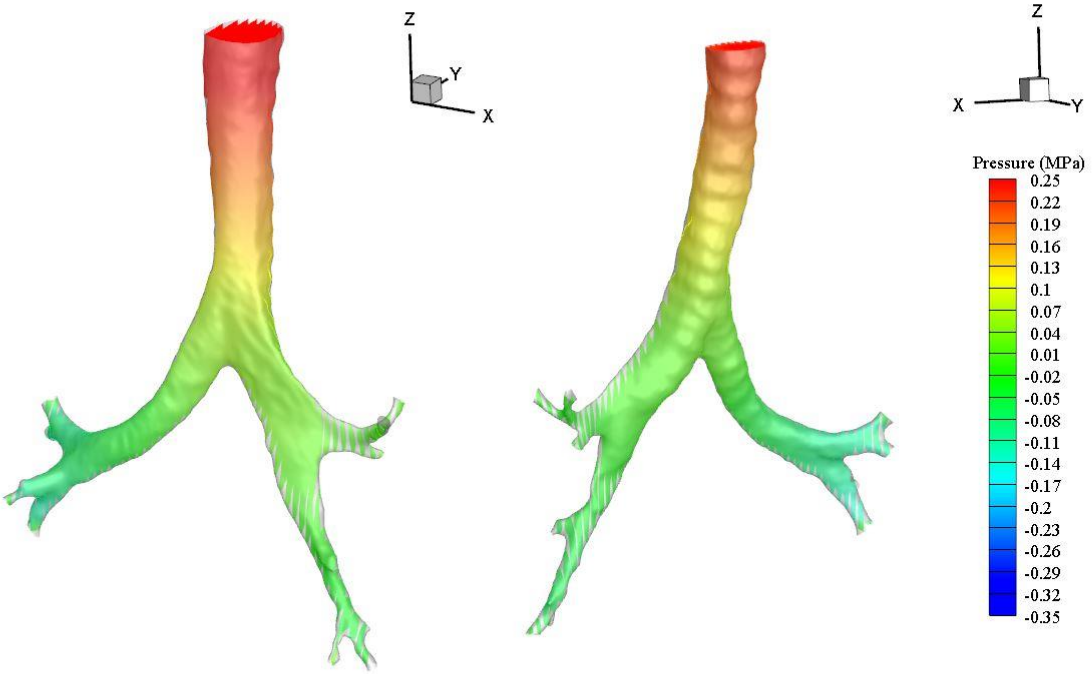

Figure D.10: Fluid pressure contour at t = 2.3 seconds

UDF: Velocity Inlet Profile Code for PCV (Fourier Approximation)

```
/**************************************************************************/
/* unsteady.c                                                             */
/* UDF for specifying a transient velocity profile boundary condition */
/**************************************************************************/

#include "udf.h"

DEFINE_PROFILE(PCV_Fourier, thread, position)
{
  face_t f;

  begin_f_loop(f, thread)
    {
      real t = RP_Get_Real("flow-time");
      F_PROFILE(f, thread, position) = -(((-0.08878) + (-0.5299)*cos(t*1.757+.235) + (-
0.6037)*sin(t*1.757+.235) + 0.2958*cos(2*t*1.757+.235*2) + (-
0.07053)*sin(2*t*1.757+.235*2) + 0.3301*cos(3*t*1.757+.235*3) + (-
0.348)*sin(3*t*1.757+.235*3) + 0.06015*cos(4*t*1.757+.235*4) +
0.2963*sin(4*t*1.757+.235*4) + 0.1689*cos(5*t*1.757+.235*5) +
0.1301*sin(5*t*1.757+.235*5) + (-0.1878)*cos(6*t*1.757+.235*6) +
(0.04543)*sin(6*t*1.757+.235*6) + (-0.0195)*cos(7*t*1.757+.235*7) +
0.05028*sin(7*t*1.757+.235*7) + (-0.03108)*cos(8*t*1.757+.235*8) + (-
0.06483)*sin(8*t*1.757+.235*8)));
    }
  end_f_loop(f, thread)
}
```

UDF: Velocity Inlet Profile Code for PCV (Fourier Approximation Halved)

```
/**********************************************************************/
/* unsteady.c                                                         */
/* UDF for specifying a transient velocity profile boundary condition */
/**********************************************************************/

#include "udf.h"

DEFINE_PROFILE(PCV_Fourier_Halved, thread, position)
{
  face_t f;

  begin_f_loop(f, thread)
    {
      real t = RP_Get_Real("flow-time");
      F_PROFILE(f, thread, position) = (-(((-0.08878) + (-0.5299)*cos(t*1.757+.235) + (-
0.6037)*sin(t*1.757+.235) + 0.2958*cos(2*t*1.757+.235*2) + (-
0.07053)*sin(2*t*1.757+.235*2) + 0.3301*cos(3*t*1.757+.235*3) + (-
0.348)*sin(3*t*1.757+.235*3) + 0.06015*cos(4*t*1.757+.235*4) +
0.2963*sin(4*t*1.757+.235*4) + 0.1689*cos(5*t*1.757+.235*5) +
0.1301*sin(5*t*1.757+.235*5) + (-0.1878)*cos(6*t*1.757+.235*6) +
(0.04543)*sin(6*t*1.757+.235*6) + (-0.0195)*cos(7*t*1.757+.235*7) +
0.05028*sin(7*t*1.757+.235*7) + (-0.03108)*cos(8*t*1.757+.235*8) + (-
0.06483)*sin(8*t*1.757+.235*8)))/2);
    }
  end_f_loop(f, thread)
}
```